Dynamics of Epidermal Innervation

Role of the peptidergic and non-peptidergic nerve fibers in relation to peripheral nerve pathology

Shoista Kambiz

Dynamics of Epidermal Innervation

Role of the peptidergic and non-peptidergic nerve fibers
in relation to peripheral nerve pathology

Shoista Kambiz

Part of studies in this thesis were founded by a grant from Stichting Nuts-Ohra.

Publication of this thesis was financially supported by:
- Stichting Esser Course
- Nederlandse Vereniging voor Plastische Chirurgie
- Erasmus University Rotterdam
- Van Wijngaarden Medical
- Astellas B.V.
- Sigma-tau B.V.

Lay-out: Sergej Schetselaar - Shirokuroart
Printed by: Ridderprint B.V.
ISBN: 978-94-6299-221-4

Dynamics of Epidermal Innervation

role of the peptidergic and non-peptidergic nerve fibers
in relation to peripheral nerve pathology

Dynamiek van Epidermale Innervatie

de rol van de peptiderge en non-peptiderge zenuwvezels
in relatie tot perifere zenuwpathologie

Proefschrift

ter verkrijging van de graad van doctor aan de
Erasmus Universiteit Rotterdam
op gezag van de
rector magnificus

Prof.dr. H.A.P. Pols

en volgens besluit van het College voor Promoties.

De openbare verdediging zal plaatsvinden op
woensdag 25 november 2015 om 9:30 uur

door

Shoista Kambiz
geboren te Kabul, Afghanistan

PROMOTIECOMMISSIE:

Promotor:	Prof.dr. S.E.R. Hovius
Overige leden:	Prof.dr. P.A. van Doorn Prof.dr. F.J.P.M. Huygen Prof.dr. A. Dahan
Copromotoren:	Dr. E.T. Walbeehm Dr. T.J.H. Ruigrok

Paranimfen:	Dr. S.M. Habib Dr. L.S. Duraku

For my parents who taught me to read

باسپاس ازمحبت وحمایت بیشاییهء مادروپدرم
این کتاب را به آنها اهدأ میکنم.

بـــنی آدم اعضـــای یکدیگرنـــد
کـــه درآفـــرینش زیـــک گوهرنـــد
چوعضـــوی بـــدرد آوردروزگـــار
دیگـــر عضـــوهارانماندقرار
توکزمحنـــت دیگـــران بـــی غمـــی
نشـــایدکه نامـــت نهنـــد آدمـــی

Of One Essence is the Human Race,
Thusly has Creation put the Base.
One Limb impacted is sufficient,
For all Others to feel the Mace.
The Unconcern'd with Others' Plight,
Are but Brutes with Human Face.

Saadi Shirazi

Table of contents

Chapter 1

Introduction

1.1.0. Epidermal innervation by nociceptive nerve fibers

The skin is the largest human organ covering a surface of 1.5 m^2 to 2 m^2 and accounts for about 16 percent of a person's total body weight (1). It is composed of multiple layers of ectodermal tissue in which the outermost layer of the skin, the epidermis, consists for 95% of keratinocytes. Other resident cells include melanocytes, Langerhans cells and Merkel cells. The epidermis is a five-layered structure consisting of: stratum corneum, stratum lucidum, stratum granulosum, stratum spinosum and stratum germinativum (basale), superficial to deep layers respectively. The multiple layered epidermis does not only protect the body from the entry of pathogens or allergens, but also serves as a sensor to warn us for tissue injury by means of an extensive innervation of the epidermis that allows pain sensation. Pain information, also known as nociception, is transmitted by Aδ and C fibers, both of which terminate as free nerve endings in the epidermis (Figure 1).

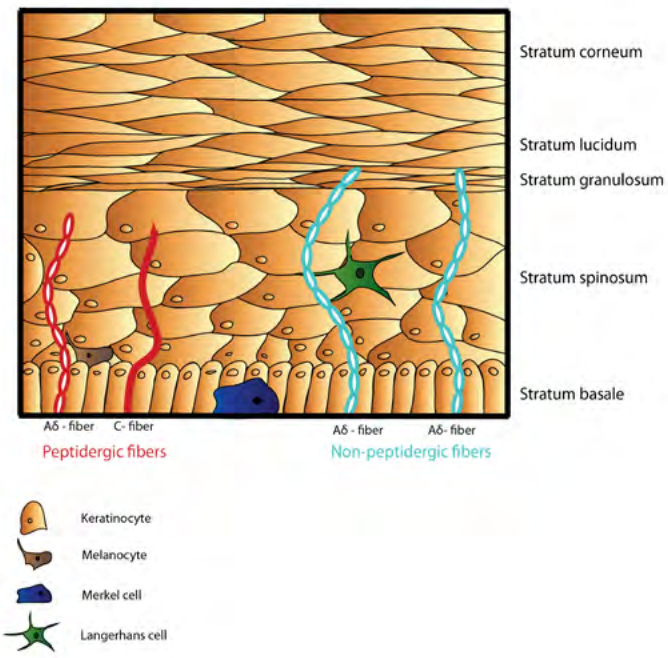

Figure 1. Schematic draw of different layers of the epidermis and its innervation by subgroup of epidermal nerve fibers

These sensory nerve fibers have different conduction properties according to the outside diameter of the fiber and their degree of myelination. Aδ fibers are thinly myelinated and have a diameter of 2 to 5 μm. These fibers conduct at 5-30 meters per second are involved in the detection of temperature, pressure and sharp, short lasting pain that is sensed directly after painful stimulus (2, 3). In contrast, C-fibers are non-myelinated and have a smaller diameter ranging between 0.2 and 1.5 μm. C-fibers conduct signals at velocities of less than 1 meter per second and are considered polymodal because they can react to various stimuli. They react to stimuli that are thermal, mechanical or chemical in nature. Whereas Aδ fibers are responsible for the sensation of quick shallow pain, C-fibers become active in slow pain that persists for longer (3, 4). As neurofilament 200 (NF200) is exclusively expressed in myelinated nerve fibers, it is possible to distinguish between these two subtypes of sensory nerve fibers using this marker.

Besides the epidermis, the skin consists of two additional layers: the dermis and hypodermis. The dermis, which is located directly beneath the epidermis, includes autonomic structures such as hair follicles, pilomotor muscles, blood vessels, sebaceous glands, and sweat glands. This layer of the skin is innervated by thickly myelinated Aβ fibers (3). Aβ fibers are fast conducting fibers that respond to signals originating from Pacinian and Ruffini corpuscles, the mechanoreceptors of the skin that transmit information mainly about touch and skin vibration (5). The deeper cutaneous tissue (hypodermis) consists of fat and connective tissue. This layer serves as a shock absorber and heat isolator. In this thesis we will mainly discuss the innervation of the most outer layer of the skin, the epidermis, and therefore focus on Aδ and C fibers.

1.2.0. Peptidergic and non-peptidergic nerve fibers of the epidermis

All Aδ and C fibers use the fast excitatory neurotransmitter glutamate for signaling to other neurons and some of them also contain various other neuropeptides. Sensory nerve fibers are divided into two subgroups based on their neuropeptide expression: peptidergic (Aδ and C fibers) and non-peptidergic (exclusively Aδ) fibers. Peptidergic fibers contain Calcitonin Gene-Related Peptide (CGRP) and many also express Substance P (SubP) (Figure 2). The remaining sensory nerve fibers, characterized as non-peptidergic fibers, express the plant lectin isolectin B4 (IB4) (6). In addition, more than 90% of IB4-positive nerve fibers co-express the Purinogenic 2X3 (P2X3) receptor. Since the immunohistochemistry for the latter protein results in less non-specific background staining when compared to IB4, the P2X3 receptor is a more suitable alternative marker to determine non-peptidergic fibers in the epidermis.

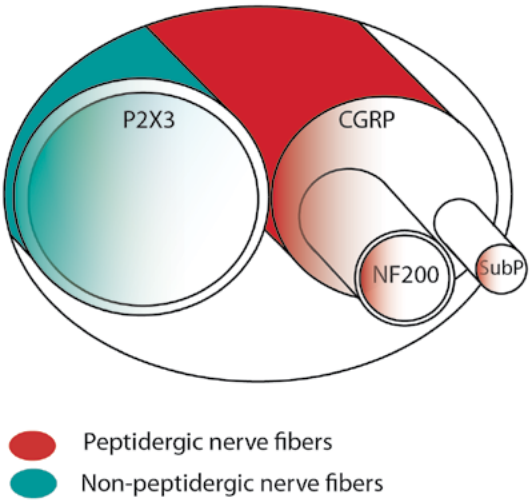

Figure 2. Subtypes of sensory epidermal nerve fibers. Peptidergic nerve fibers contain CGRP and many olso express SubP and NF200. The remaining sensory nerve fibers, characterized as non-peptidergic nerve fibers exrpress P2X3 receptor.

The peptidergic and non-peptidergic nerve fibers respond to different neurotrophic factors; nerve growth factor (NGF) induces outgrowth and regeneration of peptidergic fibers, whereas non-peptidergic fibers are promoted by glial cell-line derived neurotrophic factor (GDNF) (7, 8). Furthermore, the two subgroups of nociceptive nerve fibers have a distinct topographic innervation pattern in the skin: peptidergic nerve fibers terminate in the stratum spinosum while the non-peptidergic nerve fibers terminate more superficially in the stratum granulosum (9). The non-peptidergic nerve fibers, which are exclusively involved in pain sensation directly after painful stimuli may therefore be evolutionary more suitable to innervate the superficial epidermis and the peptidergic nerve fibers also involved in slow pain the deeper layer of the epidermis. After detecting stimuli in these different layers of the skin, the information from Aδ and C-fibers is further conducted to the dorsal horn or the spinal cord. A distinct topographic innervation pattern has also been seen in the spinal cord: peptidergic fibers terminate predominantly in lamina I and outer lamina II of the dorsal horn, whereas the non-peptidergic population terminates in inner lamina II (10) (Figure 3).

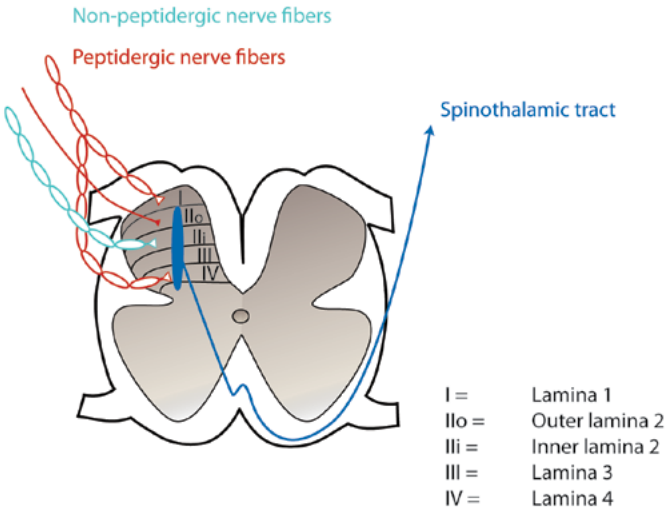

Figure 3. Schematic draw of the spinal cord with the termination of the peptidergic and the non peptidergic nerve fiebrs. The peptidergic nerve fibers terminate in lamina I, the outer lamina II and lamina IV of the dorsal horn in the spinal cord. The non-peptidergic nerve fiebrs terminate exclusively in inner lamina II. The signal is transducted to second-order neurons dat give rise to ascending spinothalamic tract.

Paradoxically, approximately 10% of non-peptidergic fibers is shown to be intertwined with peptidergic fibers in the epidermis (9). While the non-overlapping termination suggests that the two fiber types make use of two separate signaling pathways in the central nervous system (CNS), the intertwined nerve fibers may have the capacity to cross activate, sensitize or desensitize each other under certain conditions. However, their specific role in nociception is unknown.

Among the mechanisms used by epidermal nerve fibers for detection of external stimuli, six temperature-sensitive receptors namely transient receptor potential (TRP) channels are involved in temperature signaling. These TRP channels are shown to be expressed on Aδ and C-fibers; TRPV (Transient Receptor Potential Vanilloid) 1, 2, 3, and 4 channels, TRPM (Transient Receptor Potential Melastatin) 8 channel, and TRPA (Transient Receptor Potential Ankyrin) 1 channel. These TRP channels have a specific range of sensitivity for temperature from noxious hot to noxious cold and almost all innocuous temperatures in-between (11-13). Some thermo-sensitive TRP channels are also sensitive to exogenous components such as capsaicin, the hot pepper ingredient, which activates TRPV1 channels leading to a sense of noxious hot temperature. Another example is menthol, which is sensed as cold due to TRPM8 channel activation (Abe et al. 2002). More recently, evidence was found for the expression of these thermo-sensitive TRP channels on keratinocytes (14), revealing a new role for keratinocytes in thermal signaling.

1.3.0. Nerve damage may result in neuropathic pain

Peripheral nerve injury, which may occur as a result of trauma or iatrogenic, is a significant cause of morbidity and disability. Data taken from a trauma population in Spain and in USA revealed that 1.12% and 1,64% of patients had peripheral nerve injury, respectively (15). The majority of peripheral nerve injuries occurs in the upper limbs (16). In the Netherlands, 29% of all trauma cases include hand injury (17), which leads to substantial disability in daily socio-economic activities (18). The sensibility of the hand is shown to be one of the best prognostic factors for functional recovery after peripheral nerve injury (19). In response to transection of sensory peripheral nerves, early Wallerian degeneration ensues in the distal stump with fragmentation of axons and myelin. Retrograde transport of transcription factors induces changes in the dorsal root ganglion (DRG). Changes in then DRG together with ongoing interactions between peripheral nerve fibers and proliferating Schwann cells enable regeneration. Each step in the regeneration process has important and unique features that have a substantial contribution to later regenerative success. Changes in expression of transcription factors on the uninjured contralateral side are reported.

The current surgical standard therapy is an epineurial primary end-to-end repair of the transected nerve. However, when excessive tension disables primary repair, grafts using nerve, vein and tubes are applied to bridge the gap. Primary repair is shown to result in better outcomes compared to grafts (20). Nevertheless, the overall outcome of peripheral nerve injuries are often unsatisfactory, also due to one of the disabling consequences of peripheral nerve injury: neuropathic pain. Neuropathic pain is defined by the International Association for the Study of Pain (IASP) as 'pain caused by a lesion or disease of the somatosensory nervous system' (21). Neuropathic pain includes three main symptoms 1) spontaneous pain, 2) allodynia, defined as pain in response to a normally non-painful stimulus (e.g., contact of clothing on skin), and 3) hyperalgesia, defined as increased pain in response to a normally painful stimulus (22). These symptoms imply an important role of sensory testing in classifying a pain syndrome as neuropathic. The clinical need for widespread use of sensory testing is increasing due to the high incidence of neuropathic pain and small fiber neuropathies. Therefore, protocols have been developed for Quantitative Sensory Testing (QST) in which Aβ-fiber-related sensitivity is characterized by the assessment of the mechanical detection threshold and the vibration detection threshold, while the small-fiber function is assessed by thermal detection and pain thresholds (23). QST results, together with electrophysiological test procedures and assessment of epidermal nerve fibers density, is considered to be a non-invasive diagnostic test to confirm neuropathies and neuropathic pain (24) in humans.

Neuropathic pain features are also reported on the uninjured contralateral side of the body after unilateral nerve injury. This phenomenon is known as 'mirror image pain' and has been described both in humans and various models of neuropathic and inflammatory pain in rats. Although the pathogenesis of mirror image pain is not exactly known, two different pathways are described in an attempt to explain this phenomenon (25). The humoral pathway includes activation of immune cells and immunomodulatory cytokines after peripheral nerve injury. This hypothesis states that immunomodulatory factors are transported to the contralateral body part via blood and cerebral fluid affecting the contralateral spinal roots, DRG and peripheral nerves (26, 27). The neuronal pathway is described with signals that travel transneuronally to the contralateral side of the body. Electrophysiological and morphological studies have shown that commissural interneurons connect both dorsal horns within the spinal cord (28, 29). These functional connections in the spinal cord coordinate the two body halves. Ultimately, this pathway affects contralateral homonymous neurons after unilateral nerve injury explaining the mirror-image pain phenomenon.

1.4.0. Skin biopsies as a diagnostic tool

The density of epidermal innervation can be assessed by neurodiagnostic skin biopsies to determine both neuropathic pain as well as small fiber neuropathies (30). Diabetes mellitus is the most frequent underlying cause of small fiber neuropathy (31). Other causes include toxic (e.g., alcohol), metabolic, immune-mediated, infectious, and hereditary causes. A small fiber neuropathy whose incidence is increasing alarmingly is diabetic peripheral neuropathy. It affects the most distal nerves that innervate the upper and lower extremities first. Clinical and neurophysiologic investigation of patients with diabetic peripheral neuropathy do not show involvement of large myelinated nerve fibers, making the diagnosis challenging in clinical practice. The earliest signs of diabetic peripheral neuropathy manifest in the epidermal small unmyelinated nerve fibers as assessed by skin biopsies (32). Therefore, diabetic peripheral neuropathy is diagnosed by determining the epidermal innervation using a skin biopsy from affected skin areas (33). This technique has overcome the limitations of routine neurophysiologic tests to detect the damage of small nerve fibers. The skin samples harvested from biopsy are usually histologically examined using a pan-neuronal marker, Protein Gene Product 9.5 (PGP 9.5), which stains all nerve fibers in the skin. The density of epidermal nerve fibers is then used as a parameter for the presence and severity of neuropathies and neuropathic pain symptoms. A lower density of epidermal nerve fibers are associated with more severe neuropathy. Technical procedures and methods to assess the innervation density of epidermal nerve fibers are reported in the guidelines of the European Federation of the Neurological Societies and Peripheral Nerve Society (34). In summary, assessment of cutaneous innervation by skin punch biopsies is nowadays an accepted diagnostic tool to determine both diabetic peripheral neuropathies as well as neuropathic pain.

1.5.0. Nerves and their cutaneous terminal fields

Since skin biopsies cover only a small area, a well-defined cutaneous innervation of the rat hind paw is very important in order to better evaluate and understand the various processes that take place during degeneration and regeneration of cutaneous nerves after peripheral nerve injury. The Evans Blue extravasation is a well-established technique to study cutaneous innervation pattern in animal models (35-48). After intravenous injection of the Evans Blue dye followed by electrically stimulation, the peripheral nerve of interest causes vasodilatation mostly due to the stimulation-induced release of CGRP on arterioles. This results in Evans Blue extravasation and thereby blue coloring of the skin representing the extent of the innervation by the stimulated nerve (49). Using this technique it has been shown that the plantar hind paw of the rat, which is mostly examined when studying nerve regeneration (50, 51), could be divided in medial, central and lateral areas based on their cutaneous innervation by different nerve fibers. The medial glabrous skin is shown to be innervated by the saphenous nerve that originates from the femoral nerve (52). The central and lateral part of the glabrous skin are innervated by the tibial and sural nerve, respectively (48). These nerve fibers originate from the sciatic nerve. However, the anatomical variation between the animals is not taken into account in the analysis of the extravasation areas. The analysis is performed subjectively or may be based on photospectrometrical studies, which overestimate the innervation area since electrical stimulation causes vasodilatation and therefore increased amount of blue staining (38, 40). Furthermore, this technique lacks a full 360° analysis of the extravasation areas in the skin. Although the Evans Blue technique is considered to be a useful method to visualize the cutaneous innervation of individual bundle of nerve fibers in animal models, the objective analysis needs to be improved.

1.6.0. Experimental neuropathic pain models

As neuropathic pain is shown to respond poorly to standard therapies, future therapeutic advancements in the treatment of neuropathic pain are likely to benefit from an improved understanding of nerve regeneration in experimental neuropathic pain models. Therefore, several neuropathic pain models such as chronic constructive injury (CCI) (53), partial nerve injury (PNI), spinal nerve ligation (SNL) (54) and spared nerve injury (SNI) (55) have been introduced in order to study neuropathic pain features in an experimental setting. Neuropathic pain features are more difficult to obtain in animal studies when considering, for example, spontaneous pain. Therefore, different techniques are developed to quantify neuropathic pain features in mammals. Spontaneous pain is measured by the number of flinches and flutters of the affected paw during a period in the absence of any applied external noxious stimuli (56). However, the reliability of this method is questioned by many scientists. Mechanical hypersensitivity (allodynia

and hyperalgesia) is quantified by a decreased mechanical withdrawal threshold as a response to application of von Frey monofilament in the glabrous skin of rats' hind paw: smaller monofilaments are sensed as more painful. Thermal hypersensitivity (allodynia and hyperalgesia) is determined by decreased withdrawal time of the hind paw after placement of the animal on a hot/cold plate (57, 58).

Experimental studies commonly use skin biopsies from the hind paw of the rat to study the underlying mechanism of neuropathic pain, posttraumatic nerve regeneration and neuropathies (50, 51). In addition to PGP9.5 staining used as diagnostic tool in clinical practice, Duraku et al. 2013 recently showed the importance of distinguishing between subgroups of epidermal nerve fibers by demonstrating extensive collateral sprouting of peptidergic fibers from uninjured nerves compared to the non-peptidergic fibers in an experimental neuropathic pain (Spared Nerve Injury) model.

A discrepancy is seen in the appearance of neuropathic pain in human subjects following end-to-end reconstruction of the nerve. Since there are no long-term studies following in detail the events that occur after peripheral nerve injury, it is currently unclear whether it is the actual end-to-end reconstruction or the response of adjacent nerve fibers that lead to the neuropathic pain symptoms. Neuropathic pain features are shown to be present in rats following end-to-end reconstruction of the sciatic nerve after 9 weeks follow up (59), however, in human subjects, improvement of clinical signs may be seen up to two years after nerve reconstruction. Therefore, a longer follow up of neuropathic pain features is necessary to support the previously found epidermal innervation was followed by re-innervation of the skin (59). The origin of these re-innervated nerve fibers, the composition of the subgroups of epidermal nerve fibers and their relation to neuropathic pain features are unclear. In summary, skin biopsies are widely used in experimental models when studying the mechanism of nerve pathology. However, there is a general lack of data covering the changes in composition of different subtypes of epidermal nerve fibers with long-term follow up following peripheral nerve injury and reconstruction.

1.7.0. Experimental diabetic peripheral neuropathy model

Animal models for diabetes are obtained by subcutaneous or intramuscular injection with Streptozotocin (STZ) (60, 61). STZ is a chemical product that is toxic to the insulin producing beta cells of the pancreas in mammals. Type 1 diabetes is induced by injecting a large dose of STZ, whereas multiple low doses injection of STZ combined with high-fat diet is considered to induce type 2 diabetes (62). As diabetic peripheral neuropathy may frequently lead to foot ulcers and can lead to amputations, early diagnosis of diabetic related small fiber neuropathy is crucial (63). Besides skin biopsies a less invasive early diagnostic tool can be used in diabetic subjects: the rewarming rate of the skin (64). However, the relation between microvascular changes in the skin and changes in epidermal innervation

in STZ-induced diabetic rats is unclear. Therefore, it is not known to what extent the diabetic animal resembles human diabetes in this matter. Since STZ-induced diabetic rats are widely used to study peripheral neuropathies (65), it is crucial to validate this rodent model as mimicking faithfully human diabetes in relation to diabetic peripheral neuropathy and its early diagnosis in respect to future therapies.

Despite the attention given to early diagnosis of diabetic peripheral neuropathy, it currently affects 10% of the diabetic population identified by screening. (66). Therefore, in addition to early diagnosis, an effective therapeutic approach for diabetic peripheral neuropathy is necessary. At present, the aim of diabetes treatment is to keep the blood glucose levels as near to normal as possible to prevent complications caused by hyperglycemia such as microvascular deformities (67). Unfortunately, besides blood glucose controlling medicaments, no additional therapy is available for the prevention or treatment of diabetic peripheral neuropathy. Previous experimental studies found decreased levels of L-carnitine, a dietary supplement that is synthesized in the liver and kidney, in rats with diabetic peripheral neuropathy (68, 69). From these findings, a correlation is suggested between the imbalance in carnitine and functional abnormalities associated with diabetic peripheral neuropathy. In agreement with this finding, pain relief and improvement of nerve conduction velocity have been demonstrated in both diabetic rats and humans after supplementation of acetylated L-carnitine (ALCAR) (68, 70). The positive effect of ALCAR has also been observed on peripheral nerve regeneration (71, 72). In summary, ALCAR seems to have a neuro-protective effect on both nerve regeneration and diabetic peripheral nerve regeneration. However, the effect of ALCAR on small fiber neuropathy is unknown.

1.8.0. The aim of this thesis

The aim of this thesis is to study the dynamics of epidermal innervation in rats' hind paw and their role in neuropathic pain after the most common peripheral nerve pathologies: peripheral nerve injury and peripheral neuropathy. In order to do so, additional knowledge about normal skin innervation is required. Therefore, this thesis is divided in three parts. In the first part (chapter 2) we re-designed the Evans Blue extravasation methodology, which enables us to map the detailed 3D skin innervation in rats' hind paw. In the second part (chapter 3 and 4), we focus on skin re-innervation following end-to-end reconstruction of the nerve, which is the golden standard therapy for transected nerves.

Skin innervation is evaluated in the operated hind paw (chapter 3) as well as in the uninjured contralateral side (chapter 4) to study the correlation between thermal hypersensitivity and the subtype of sensory nerve fibers in the epidermis. In addition, we reviewed in chapter 5 the role of thermo-sensitive channels expressed on sensory nerve fibers in the skin after nerve injury to better understand the mechanism involved in temperature sensation. Finally, in the third part of the present thesis we examined the changes in skin innervation following diabetic peripheral neuropathy (Chapter 6) and analyzed the neuro-protective role of ALCAR by evaluation of skin innervation in diabetic rats (Chapter 7). The overall results and their potential for further studies are discussed in chapter 8.

1.9.0. References

1. Martini FH, Nath HG. Fundamentals of Anatomy and Physiology Benjamin Cummings; 2009.
2. Naka D, Kakigi R. Simple and novel method for measuring conduction velocity of A delta fibers in humans. J Clin Neurophysiol. 1998 Mar;15(2):150-3.
3. Kandel ER, Schwartz JH, Jessell TM. Principles of neural science Fourth ed2000.
4. Baba H, Doubell TP, Woolf CJ. Peripheral inflammation facilitates Abeta fiber-mediated synaptic input to the substantia gelatinosa of the adult rat spinal cord. J Neurosci. 1999 Jan 15;19(2):859-67.
5. McGlone F, Reilly D. The cutaneous sensory system. Neurosci Biobehav Rev. 2010 Feb;34(2):148-59.
6. Ruscheweyh R, Forsthuber L, Schoffnegger D, Sandkuhler J. Modification of classical neurochemical markers in identified primary afferent neurons with Abeta-, Adelta-, and C-fibers after chronic constriction injury in mice. J Comp Neurol. 2007 May 10;502(2):325-36.
7. Forrest SL, Keast JR. Expression of receptors for glial cell line-derived neurotrophic factor family ligands in sacral spinal cord reveals separate targets of pelvic afferent fibers. J Comp Neurol. 2008 Feb 20;506(6):989-1002.
8. Stucky CL, Lewin GR. Isolectin B(4)-positive and -negative nociceptors are functionally distinct. J Neurosci. 1999 Aug 1;19(15):6497-505.
9. Zylka MJ, Rice FL, Anderson DJ. Topographically distinct epidermal nociceptive circuits revealed by axonal tracers targeted to Mrgprd. Neuron. 2005 Jan 6;45(1):17-25.
10. Bradbury EJ, Burnstock G, McMahon SB. The expression of P2X3 purinoreceptors in sensory neurons: effects of axotomy and glial-derived neurotrophic factor. Mol Cell Neurosci. 1998 Nov;12(4-5):256-68.
11. Caterina MJ, Schumacher MA, Tominaga M, Rosen TA, Levine JD, Julius D. The capsaicin receptor: a heat-activated ion channel in the pain pathway. Nature. 1997 Oct 23;389(6653):816-24.
12. Guler AD, Lee H, Iida T, Shimizu I, Tominaga M, Caterina M. Heat-evoked activation of the ion channel, TRPV4. J Neurosci. 2002 Aug 1;22(15):6408-14.
13. Peier AM, Moqrich A, Hergarden AC, Reeve AJ, Andersson DA, Story GM, et al. A TRP channel that senses cold stimuli and menthol. Cell. 2002 Mar 8;108(5):705-15.
14. Story GM, Peier AM, Reeve AJ, Eid SR, Mosbacher J, Hricik TR, et al. ANKTM1, a TRP-like channel expressed in nociceptive neurons, is activated by cold temperatures. Cell. 2003 Mar 21;112(6):819-29.
15. Castillo-Galvan ML, Martinez-Ruiz FM, de la Garza-Castro O, Elizondo-Omana RE, Guzman-Lopez S. [Study of peripheral nerve injury in trauma patients] Estudio de la lesion nerviosa periferica en pacientes atendidos por traumatismos. Gac Med Mex. 2014 Nov-Dec;150(6):527-32.
16. Kouyoumdjian JA. Peripheral nerve injuries: a retrospective survey of 456 cases. Muscle Nerve. 2006 Dec;34(6):785-8.

17. Larsen CF, Mulder S, Johansen AM, Stam C. The epidemiology of hand injuries in The Netherlands and Denmark. Eur J Epidemiol. 2004;19(4):323-7.
18. Ring D. Symptoms and disability after major peripheral nerve injury. Hand Clin. 2013 Aug;29(3):421-5.
19. Hundepool CA, Ultee J, Nijhuis TH, Houpt P, Research Group Z, Hovius SE. Prognostic factors for outcome after median, ulnar, and combined median-ulnar nerve injuries: a prospective study. J Plast Reconstr Aesthet Surg. 2015 Jan;68(1):1-8.
20. Varitimidis SE, Sotereanos DG. Partial nerve injuries in the upper extremity. Hand Clin. 2000 Feb;16(1):141-9.
21. Treede RD, Jensen TS, Campbell JN, Cruccu G, Dostrovsky JO, Griffin JW, et al. Neuropathic pain: redefinition and a grading system for clinical and research purposes. Neurology. [Consensus Development Conference Research Support, Non-U.S. Gov't]. 2008 Apr 29;70(18):1630-5.
22. Gilron I, Watson CP, Cahill CM, Moulin DE. Neuropathic pain: a practical guide for the clinician. CMAJ. 2006 Aug 1;175(3):265-75.
23. Rolke R, Magerl W, Campbell KA, Schalber C, Caspari S, Birklein F, et al. Quantitative sensory testing: a comprehensive protocol for clinical trials. Eur J Pain. 2006 Jan;10(1):77-88.
24. Haanpaa M, Attal N, Backonja M, Baron R, Bennett M, Bouhassira D, et al. NeuPSIG guidelines on neuropathic pain assessment. Pain. [Research Support, Non-U.S. Gov't Review]. 2011 Jan;152(1):14-27.
25. Jancalek R. Signaling mechanisms in mirror image pain pathogenesis. Ann Neurosci. [Review]. 2011 Jul;18(3):123-7.
26. Hatashita S, Sekiguchi M, Kobayashi H, Konno S, Kikuchi S. Contralateral neuropathic pain and neuropathology in dorsal root ganglion and spinal cord following hemilateral nerve injury in rats. Spine (Phila Pa 1976). 2008 May 20;33(12):1344-51.
27. Schafers M, Geis C, Brors D, Yaksh TL, Sommer C. Anterograde transport of tumor necrosis factor-alpha in the intact and injured rat sciatic nerve. J Neurosci. [Research Support, Non-U.S. Gov't]. 2002 Jan 15;22(2):536-45.
28. Fitzgerald M. The contralateral input to the dorsal horn of the spinal cord in the decerebrate spinal rat. Brain Res. 1982 Mar 25;236(2):275-87.
29. Fitzgerald M. Influences of contralateral nerve and skin stimulation on neurones in the substantia gelatinosa of the rat spinal cord. Neurosci Lett. 1983 Apr 11;36(2):139-43.
30. Buonocore M. Unilateral peripheral neuropathic pain: The role of neurodiagnostic skin biopsy. World J Clin Cases. 2014 Feb 16;2(2):27-31.
31. Tavee J, Zhou L. Small fiber neuropathy: A burning problem. Cleve Clin J Med. 2009 May;76(5):297-305.
32. Lauria G, Lombardi R, Camozzi F, Devigili G. Skin biopsy for the diagnosis of peripheral neuropathy. Histopathology. [Review]. 2009 Feb;54(3):273-85.
33. Narayanaswamy H, Facer P, Misra VP, Timmers M, Byttebier G, Meert T,

et al. A longitudinal study of sensory biomarkers of progression in patients with diabetic peripheral neuropathy using skin biopsies. J Clin Neurosci. 2012 Nov;19(11):1490-6.
34. Lauria G, Hsieh ST, Johansson O, Kennedy WR, Leger JM, Mellgren SI, et al. European Federation of Neurological Societies/Peripheral Nerve Society Guideline on the use of skin biopsy in the diagnosis of small fiber neuropathy. Report of a joint task force of the European Federation of Neurological Societies and the Peripheral Nerve Society. Eur J Neurol. 2010 Jul;17(7):903-12, e44-9.
35. Baranowski AP, Priestley JV, McMahon S. Substance P in cutaneous primary sensory neurons--a comparison of models of nerve injury that allow varying degrees of regeneration. Neuroscience. 1993 Aug;55(4):1025-36.
36. Bester H, Allchorne AJ, Woolf CJ. Recovery of C-fiber-induced extravasation following peripheral nerve injury in the rat. Exp Neurol. 1998 Dec;154(2):628-36.
37. Brenan A. Collateral reinnervation of skin by C-fibres following nerve injury in the rat. Brain Res. 1986 Oct 15;385(1):152-5.
38. Brenan A, Jones L, Owain NR. The demonstration of the cutaneous distribution of saphenous nerve C-fibres using a plasma extravasation technique in the normal rat and following nerve injury. J Anat. 1988 Apr;157:57-66.
39. Carmichael NM, Dostrovsky JO, Charlton MP. Enhanced vascular permeability in rat skin induced by sensory nerve stimulation: evaluation of the time course and appropriate stimulation parameters. Neuroscience. 2008 May 15;153(3):832-41.
40. Gonzalez HL, Carmichael N, Dostrovsky JO, Charlton MP. Evaluation of the time course of plasma extravasation in the skin by digital image analysis. J Pain. 2005 Oct;6(10):681-8.
41. Hansson T, Povlsen B. Functional regeneration of C-fibres inside a silicone tube after sciatic neurotomy in rats. Scand J Plast Reconstr Surg Hand Surg. 1997 Mar;31(1):7-11.
42. Jancso N, Jancso-Gabor A, Szolcsanyi J. Direct evidence for neurogenic inflammation and its prevention by denervation and by pretreatment with capsaicin. Br J Pharmacol Chemother. 1967 Sep;31(1):138-51.
43. Kingery WS, Guo TZ, Poree LR, Maze M. Colchicine treatment of the sciatic nerve reduces neurogenic extravasation, but does not affect nociceptive thresholds or collateral sprouting in neuropathic or normal rats. Pain. 1998 Jan;74(1):11-20.
44. Povlsen B, Hildebrand C, Stankovic N. Functional projection of sensory lateral plantar and superficial peroneal nerve axons to glabrous and hairy skin of the rat hindfoot after sciatic nerve lesions. Exp Neurol. 1994 Jul;128(1):129-35.
45. Povlsen B, Hildebrand C, Wiesenfeld-Hallin Z, Stankovic N. Functional projection of regenerated rat sural nerve axons to the hindpaw skin after sciatic nerve lesions. Exp Neurol. 1993 Jan;119(1):99-106.
46. Wiesenfeld-Hallin Z. Partially overlapping territories of nerves to hindlimb foot

skin demonstrated by plasma extravasation to antidromic C-fiber stimulation in the rat. Neurosci Lett. 1988 Feb 3;84(3):261-5.
47. Wiesenfeld-Hallin Z, Kinnman E, Aldskogius H. Expansion of innervation territory by afferents involved in plasma extravasation after nerve regeneration in adult and neonatal rats. Exp Brain Res. 1989;76(1):88-96.
48. Dux M, Jancso G. A new technique for the direct demonstration of overlapping cutaneous innervation territories of peptidergic C-fibre afferents of rat hindlimb nerves. J Neurosci Methods. 1994 Nov;55(1):47-52.
49. Gee MD, Lynn B, Cotsell B. The relationship between cutaneous C fibre type and antidromic vasodilatation in the rabbit and the rat. J Physiol. 1997 Aug 15;503 (Pt 1):31-44.
50. Peleshok JC, Ribeiro-da-Silva A. Delayed reinnervation by nonpeptidergic nociceptive afferents of the glabrous skin of the rat hindpaw in a neuropathic pain model. J Comp Neurol. 2011 Jan 1;519(1):49-63.
51. Duraku LS, Hossaini M, Schuttenhelm BN, Holstege JC, Baas M, Ruigrok TJ, et al. Re-innervation patterns by peptidergic Substance-P, non-peptidergic P2X3, and myelinated NF-200 nerve fibers in epidermis and dermis of rats with neuropathic pain. Exp Neurol. 2013 Mar;241:13-24.
52. Pertovaara A. Collateral sprouting of nociceptive C-fibers after cut or capsaicin treatment of the sciatic nerve in adult rats. Neurosci Lett. 1988 Aug 1;90(3):248-53.
53. Lindenlaub T, Sommer C. Epidermal innervation density after partial sciatic nerve lesion and pain-related behavior in the rat. Acta Neuropathol. 2002 Aug;104(2):137-43.
54. Kim SH, Chung JM. An experimental model for peripheral neuropathy produced by segmental spinal nerve ligation in the rat. Pain. [Research Support, Non-U.S. Gov't Research Support, U.S. Gov't, P.H.S.]. 1992 Sep;50(3):355-63.
55. Decosterd I, Woolf CJ. Spared nerve injury: an animal model of persistent peripheral neuropathic pain. Pain. [Research Support, Non-U.S. Gov't
Research Support, U.S. Gov't, P.H.S.]. 2000 Aug;87(2):149-58.
56. Ren LY, Lu ZM, Liu MG, Yu YQ, Li Z, Shang GW, et al. Distinct roles of the anterior cingulate cortex in spinal and supraspinal bee venom-induced pain behaviors. Neuroscience. 2008 Apr 22;153(1):268-78.
57. Jasmin L, Kohan L, Franssen M, Janni G, Goff JR. The cold plate as a test of nociceptive behaviors: description and application to the study of chronic neuropathic and inflammatory pain models. Pain. 1998 Apr;75(2-3):367-82.
58. Eddy NB, Leimbach D. Synthetic analgesics. II. Dithienylbutenyl- and dithienylbutylamines. J Pharmacol Exp Ther. 1953 Mar;107(3):385-93.
59. Cobianchi S, de Cruz J, Navarro X. Assessment of sensory thresholds and nociceptive fiber growth after sciatic nerve injury reveals the differential contribution of collateral reinnervation and nerve regeneration to neuropathic pain. Exp Neurol. 2014 May;255:1-11.
60. Tong M, Tuk B, Shang P, Hekking IM, Fijneman EM, Guijt M, et al. Diabetes-

impaired wound healing is improved by matrix therapy with heparan sulfate glycosaminoglycan mimetic OTR4120 in rats. Diabetes. 2012 Oct;61(10):2633-41.
61. Zangiabadi N, Mohtashami H, Hojatipour M, Jafari M, Asadi-Shekaari M, Shabani M. The effect of Angipars on diabetic neuropathy in STZ-induced diabetic male rats: a study on behavioral, electrophysiological, sciatic histological and ultrastructural indices. ScientificWorldJournal. 2014;2014:721547.
62. Zhang M, Lv XY, Li J, Xu ZG, Chen L. The characterization of high-fat diet and multiple low-dose streptozotocin induced type 2 diabetes rat model. Exp Diabetes Res. 2008;2008:704045.
63. Ramsey SD, Newton K, Blough D, McCulloch DK, Sandhu N, Reiber GE, et al. Incidence, outcomes, and cost of foot ulcers in patients with diabetes. Diabetes Care. 1999 Mar;22(3):382-7.
64. Balbinot LF, Canani LH, Robinson CC, Achaval M, Zaro MA. Plantar thermography is useful in the early diagnosis of diabetic neuropathy. Clinics (Sao Paulo). 2012 Dec;67(12):1419-25.
65. Becker M, Benromano T, Shahar A, Nevo Z, Pick CG. Changes in the basal membrane of dorsal root ganglia Schwann cells explain the biphasic pattern of the peripheral neuropathy in streptozotocin-induced diabetic rats. J Mol Neurosci. 2014 Dec;54(4):704-13.
66. Ziegler D, Papanas N, Vinik AI, Shaw JE. Epidemiology of polyneuropathy in diabetes and prediabetes. Handb Clin Neurol. 2014;126:3-22.
67. Nadkarni GN, Yacoub R, Coca SG. Update on glycemic control for the treatment of diabetic kidney disease. Curr Diab Rep. 2015 Jul;15(7):612.
68. Ido Y, McHowat J, Chang KC, Arrigoni-Martelli E, Orfalian Z, Kilo C, et al. Neural dysfunction and metabolic imbalances in diabetic rats. Prevention by acetyl-L-carnitine. Diabetes. [Research Support, Non-U.S. Gov't Research Support, U.S. Gov't, P.H.S.]. 1994 Dec;43(12):1469-77.
69. Lowitt S, Malone JI, Salem A, Kozak WM, Orfalian Z. Acetyl-L-carnitine corrects electroretinographic deficits in experimental diabetes. Diabetes. [Research Support, Non-U.S. Gov't]. 1993 Aug;42(8):1115-8.
70. Sima AA, Ristic H, Merry A, Kamijo M, Lattimer SA, Stevens MJ, et al. Primary preventive and secondary interventionary effects of acetyl-L-carnitine on diabetic neuropathy in the bio-breeding Worcester rat. J Clin Invest. 1996 Apr 15;97(8):1900-7.
71. Fernandez E, Pallini R, Gangitano C, Del Fa A, Sangiacomo CO, Sbriccoli A, et al. Effects of L-carnitine, L-acetylcarnitine and gangliosides on the regeneration of the transected sciatic nerve in rats. Neurol Res. 1989 Mar;11(1):57-62.
72. Wilson AD, Hart A, Brannstrom T, Wiberg M, Terenghi G. Delayed acetyl-L-carnitine administration and its effect on sensory neuronal rescue after peripheral nerve injury. J Plast Reconstr Aesthet Surg. 2007;60(2):114-8.

Chapter 2

Innervation mapping of the hind paw of the rat using Evans Blue extravasation, Optical Surface Mapping and CASAM

Shoista Kambiz, Martijn Baas, Liron S. Duraku, Anton L. Kerver, Anton H.J. Koning, Erik T. Walbeehm, Tom J.H. Ruigrok

Journal of Neuroscience Methods 2014; (229):15-27

2.1.0. Abstract

Although numerous studies investigate sensory regeneration and re-innervation of the hind paw of the rat after nerve damage, no comprehensive overview of its normal innervation is present in literature. The Evans Blue extravasation technique is a well-known technique to study patterns of skin innervation. This technique has been performed differently by various groups but was never used to study the entire skin innervation in rats' hind paw including all three branches of the sciatic nerve and the saphenous nerve in detail.

In this paper, we have used the Evans Blue extravasation technique to chart the skin areas innervated by the sural, peroneal, tibial and/or saphenous nerves, which together innervate the entire hind paw of the rat, and use a new technique to analyze the distribution, overlap and variability of the results. The technique is based on analysis of whole hind paws using Optical Surface Mapping (OSM) in combination with the Computer Assisted Surgical Anatomy Mapping (CASAM) technology.

While the plantar hind paw is mainly innervated by the tibial nerve, the dorsal hind paw is supplied by the sural, peroneal and the saphenous nerve.

Although our results basically concur with the general nerve-specific innervation of the rat hind paw, they show considerable detail in their areas of overlap as well as in the amount of variability between animals. As such, these results will be invaluable to study and evaluate patterns of innervation and re-innervation of intact and damaged nerve fibers.

2.2.0. Introduction

The past decade has seen an increased interest in the patterns of skin innervation by individual nerves in both naïve and pathological situations, such as neuropathic pain and itch in humans as well as in animal models. The reason for this growing interest is the possibility to analyze different classes of sensory skin fibers for diagnostic purposes (1, 2). The glabrous skin of rat's hind paw has become a commonly used tissue to investigate the pathological changes of sensory skin fibers, especially when examining sensory denervation and re-innervation after peripheral nerve injury (3-6).

In order to properly evaluate these studies it is crucial to understand the pattern of innervation by individual nerves and the areas of overlap found between separate nerves as well as to the intra-individual variability in these patterns, as they might vary in different pathological conditions.

Previous studies have mapped the innervation of rats' hind paw by a recognized technique called 'Evans Blue extravasation' (7-20). After intravenous injection of the Evans Blue dye the peripheral nerve of interest is electrically stimulated to cause plasma extravasation, which will be visible as blue staining on the skin. Since plasma extravasation is caused by primary sensory fibers, mostly

C-fibers (21, 22), this technique offers a valuable approach to study the innervation areas of primary afferents in the skin. Indeed, both in normal and pathologic conditions the areas with extravasated dye have been shown to correspond with the cutaneous innevation area of the investigated nerve (23). Although plasma extravasation has been used in multiple studies, it is mostly evaluated by either a translation of the staining pattern to a diagram or extraction of the dye from the skin sample. The translating technique is sufficient for a general localization of the extravasation, but as size and anatomy varies between rats and interpretations may vary between individuals, the translation to a diagram is always based on subjective interpretation, which may cause high variability in results (8, 13, 16). Extracting the Evans Blue dye for photospectrometry is used when studying quantity of the dye (10, 12). However, apart from increased vascular permeability, electric stimulation eventually may also cause vasodilatation, which enhances the blood flow and thereby increases the Evans Blue extravasation in the skin after electrical stimulation. Therefore, the results of innervation areas by extracting the dye could be overestimated. Moreover, when extracting the dye from the skin the localization of the dye is lost. This prevents a description of the overlap between extravasation areas or to provide an overview of the entire pattern of extravasation areas. Yet, although the Evans Blue extravasation is known to be a valid method for visualizing skin innervation areas, there is no comprehensive study describing and quantifying the detailed innervation areas, overlap areas and variability of innervation patterns by the nerves that innervate the rat's hind paw.

The aim of the present study is to use a novel technique to describe and analyze the cutaneous region of the hind paw that is innervated by a particular nerve. This technique enables a merging of measures of localization, quantity, and overlap. This is accomplished by combining a standardized Evans Blue extravasation technique, optical surface mapping (OSM) and computer-assisted surgical anatomy mapping (CASAM) technologies (24-26).

2.3.0. Materials and Methods

2.3.1. Animals and anesthesia

Experiments were performed on adult female Lewis rats (n=40). All experiments were approved by the Dutch Ethical Committee at Erasmus Medical Center Rotterdam on Animal Welfare (DEC) and all procedures adhered to the European guidelines for the care and use of laboratory animals (Council Directive 86/6009/EEC). During the experiments 3 animals were excluded due to lack of extravasation after 10 minutes of stimulation. Possible reasons for the lack of extravasation could have been a potential break of the anodal or cathodal wire of the stimulation cuff. The final experimental group contained 28 rats, which were subjected to stimulation of either the tibial (n=7), sural (n=7), peroneal (n=7) or saphenous nerve (n=7). Nine additional animals were used in a control study.

The animals were anesthetized with 3% isoflurane, weighted and subsequently the paw was depilated using depilatory-crème 'Veet' to acquire a clear image of the skin.

2.3.2. Surgical procedure

An incision was made on the lateral or medial side of the hind limb depending on the choice of nerve to be investigated. The sciatic branches were approached by a 4 cm incision over the intramuscular septum between the vastus lateralis and the biceps femoris muscles, whereas the saphenous nerve was exposed by a 5 cm incision over the inner thigh. Subsequently, the nerve of interest was microsurgically dissected from its environment and crushed proximal to the stimulation site in order to prevent central propagation of the stimulus (11, 16). The surgical procedure and placement of the stimulation cuffs were performed under microscopic guidance (Zeiss OP-MI 6-SD; Carl Zeiss, Goettingen, Germany) to prevent damage to the nerve of interest and adjacent tissue.

2.3.3. Evans Blue extravasation procedure

The nerve was inserted into a handmade silicone stimulation cuff (3 mm in diameter, 6 mm in length) in which the anodal and cathodal electrode were embedded (Figure 1). These cuffs were developed to restrict stimulation of surrounding tissue. A solution of Evans Blue (2% EB solved in 0.9% saline, 4ml/kg body mass) was injected slowly into the tongue vein of the rat. Because of discrepancies noted in literature (11, 16, 20), we determined the optimal EB concentration in several trial experiments using subjective evaluation of the extravasation contrast.

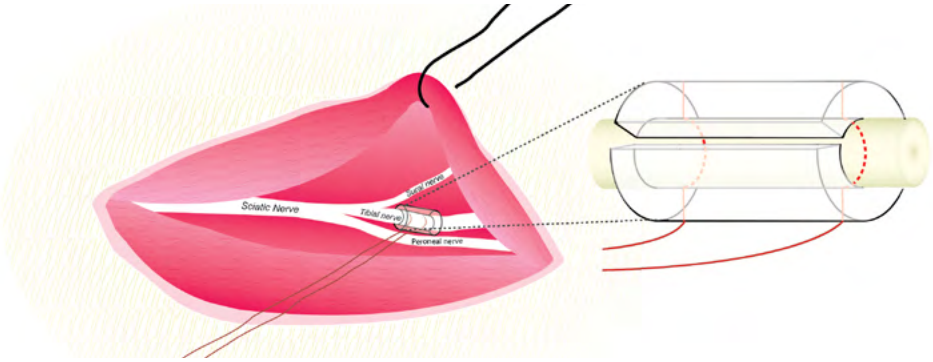

Figure 1. Cuff stimulation of the sciatic nerves and its branches (n. suralis, n. tibialis, n. peroneous). The cuff is made of a silicone tube with both anodal (+) and cathodal (-) wires (visible in red) placed in the cuff. The wire's insulation is removed in the cuff but remains intact outside the cuff to avoid stimulation of the surrounding structures.

Stimulation of the nerves started 5 minutes after the Evans Blue injection and lasted for 10 minutes using a continuous 10Hz, 0.5ms pulse width and 12mA current stimulation (Viking stimulator, Nicolet Biomedical IES405-2). Parameters were chosen based on trials and resembled those in literature (11, 12, 14). During stimulation a slow blue coloring of a part of the hind paw was observed which was attributed to extravasation of the dye. Often, additional extravasation was seen for several minutes after terminating the stimulation (12). Therefore, a 6-minute interval in which the animals were not handled was incorporated before sacrificing the animals by an overdose of pentobarbital (100mg/kg ip). Subsequently, the hind paws of all animals were cut at the level of the heel joint. Then the hind paws were fixed in an identical position using insect needles. Both the tendons and the skin was pulled back to obtain a neutral hind paw position in animals; without flexion of the toes and enough web space between the toes for further imaging of the paw.

2.3.4. Control experiments

In three additional rats the correlation between the Evans Blue extravasation in the skin and the epidermal innervation was verified. In these animals the sciatic nerve was transected and ligated proximally to prevent regeneration of this nerve. Five weeks later, to ensure complete degeneration of the sciatic nerve, the Evans Blue experiment (see section 2.3) was performed by stimulation of the unaffected saphenous nerve, which resulted in extravasation of the medial side of the paw. After sacrificing the animal the paw was photographed. Using microscopical guidance, a superficial epidermal cut was made with a scalpel at the border of the extravasated and non-extravasated skin. A subsequent large skin biopsy of the transition area was taken, fixated in 2% paraformaldehyde-lysin-periodate (PLP) for 24 hours at 4˚C. The skin was embedded in 10% gelatine, hardened and sectioned at 40 µm with a freezing microtome. Sections were processed to visualize nerve fibers using PGP9.5 immunohistochemistry according to Duraku et al. (4, 5). Briefly, free-floating sections were rinsed in phosphate-buffered saline (PBS), pre-treated with hydrogen peroxide to reduce background, heated to 80˚C in citrate buffer (pH 8.75) to unmask antigen sites, incubated in rabbit anti-PGP9.5 (48 h at 4˚C in PBS with 0.5% Triton X-100; dilution 1/10.000: Enzo). After subsequent incubations with biotinylated goat-anti rabbit (1.5h at room temperature, RT; dilution 1/200: Biotine) and Vectastain ABC-Elite™ (1.5h at RT: Vector, Burlingame, CA) followed by additional signal amplification using biotin tyramide (27) for 12 minutes, the antigenic sites were revealed by diaminobenzidine (DAB) histochemistry. Sections were counterstained with thionine, which faded the epidermis blue as a result clear border between epidermis and dermis was visible. Finally, the slides were dehydrated and coverslipped with Permount (Fisher, Hampton, NH). The labelled nerve fiber terminals within the epidermial region of 64 mm^2 (400µm x 160µm) at the level of the epidermal cut were quantified using an Olympus BH microscope equipped with a Lucivid™ miniature monitor and Neurolucida™ software (MicroBrightField).

2.3.5. OSM and CASAM

An optical projection tomography (OPT) scanner (28, 29), which is a commonly used technique for investigating small specimens to visualize aspects of anatomy and gene expression, was used to produce a 3D image of the surface of rats' hind paw in a novel procedure called Optical Surface Mapping (OSM). This method allows an accurate quantification of the paw in which even the areas between the toes can be taken in consideration in contrast to a mere 2D-analysis. Furthermore, we have developed a systematic way of recording and quantifying extravasation making use of a 360 degrees view of the paw by combining the UV sensitive quality of the Evans Blue dye and the UV Filter in the Bioptics OPT scanner (28, 29). Subsequently, the variability in nerve innervations patterns between various individuals was assessed by applying the CASAM technology (30), which is a new anatomy mapping tool used in clinic to improve description of the variability of complex anatomical regions. Using the combination of Evans Blue extravasation, OSM and CASAM allows us to present, for the first time, an anatomically correct impression of the average innervations pattern and indication of intra-animal variability as well as assessment of the areas of overlap between the innervation territories of different nerves.

2.3.6. Analysis

The Bioptronics OSM Scanner 3001 was set up as described in the manual. However, the scan medium was changed from benzyl alcohol benzyl benzoate to demineralised water to avoid unwanted interaction with the specimen or the dye. The scans were made using UV light and a Cys3 filter (Cys3 fluorescence, 545nm/30nm exciter, 610/75nm emitter) (31, 32). In our experiments bright-field images were used. Every specimen was scanned using a 1.8 degree angle increase per frame, resulting in 200 frames per scan. Every paw was recorded in two series because their sizes exceeded the 21 mm frame of the OSM scanner in the vertical position. Both series were merged whilst overlap between recordings was digitally excluded using based on the vertical position of the specimen in the scanner. Quantification of the extravasation was performed using a custom-developed labVIEW™ (National Instruments) application. The percentage of staining per view was calculated using different thresholds to distinguish between background, unstained skin and stained skin. The thresholds were adjusted every 18 degrees (10 frames) to compensate for the varying lightning due to the irregular surface of the paw. The 0 degree point was determined as the largest surface area (as measured by the total number of stained plus unstained pixels containing skin) on the plantar side of the paw.

The extent of extravasated skin area and the overlap between areas innervated by different nerves were determined using the CASAM technology (30). Four frames in total, at 0 degree (plantar view), 90 degrees (lateral view), 180 degrees (dorsal view) and 270º (medial view) were selected to show the average extravasation, intra-animal variability of extravasation per nerve and overlap of extravasation for the studied nerves. Matching frames were selected from every scan and characteristic landmarks of five pixels each were placed, resulting in 30 to 50 landmarks per frame depending on the shape and variability of the paws for that specific frame. To ensure reproducibility of placing identical landmarks for all hind paws, we placed five times all the landmarks on the same hind paw and only the landmarks that showed overlap in all five cases were selected. From these landmarks an average size and shape of the hind paw was computed and all paws were morphed to match this average. Then, the area of extravasation for each animal was manually selected onto these average paws. Finally, merging and comparing the resulting images in Adobe Photoshop enabled determination and quantification of both intra-animal variability of extravasation area per nerve as well as of the areas of overlap between two nerves.

2.3.7. Statistical analysis

For determining statistical differences of the surface areas, the one way-ANOVA with a Tukey post hoc test was used for intergroup comparisons to calculate the average staining in each group. Errors in variations were determined as standard error of the mean (SEM), and $p < 0.05$ was taken as significant.
In the CASAM analysis single pixels within the circumference of the landmarks were either assigned the label "stained" or "non-stained". Pixels with identical incidences (ranging from stained in 1 animal to stained in all 7 cases) were grouped and two way t-test with a Tukey post hoc test was used to determine the threshold for significance ($p<0.05$) between groups. Subsequently overlap was divined as groups of individual significantly "stained" pixels with no significant difference between the compared nerves.

2.4.0. Results

All nerve stimulations resulted in a blue coloring of a part of the skin of the hind paw. Several controls were conducted to verify that Evans Blue extravasation was positively correlated with the innervation of the skin innervated by the stimulated nerve. First, in three animals lesion of the nerve distal to stimulation site 10 weeks prior to the Evans Blue experiment failed to result in blue coloring of any part of the skin (not shown). In addition, in other three rats a lesion of the sciatic nerve was performed five week previous to stimulation of the saphenous nerve which resulted in a blue colored extravasation of the medial part of the paw (Figure 2). The transition area was indicated by a shallow epidermal cut, which was subsequently excised and processed for PGP9.5 immuohistochemistry.

Although the Evans Blue coloring disappeared during the immunohistochemical procedure, the results clearly demonstrate that at the formerly extravasated side of the transition line (i.e. medial of the cut) PGP9.5-positive fibers of the stimulated saphenous nerve are present (Figure 2C). These nerve fibers could not be discerned at the formerly non-extravasated area (Figure 2D), lateral of the cut, which had been denervated by the sciatic lesion. Quantification of the epidermal nerve fibers was performed in all three animals. Average of 980 ± 16 PGP9.5 positive epidermal nerve fibers per milimeter-squared were counted on the formerly extravasated side. The few (28 ± 7 per mm^2) remaining fibers, which are mainly present in the upper dermis, at the non-extravasated area are very thin (arrows in Figure 2D) and could reflect sprouting fibers.

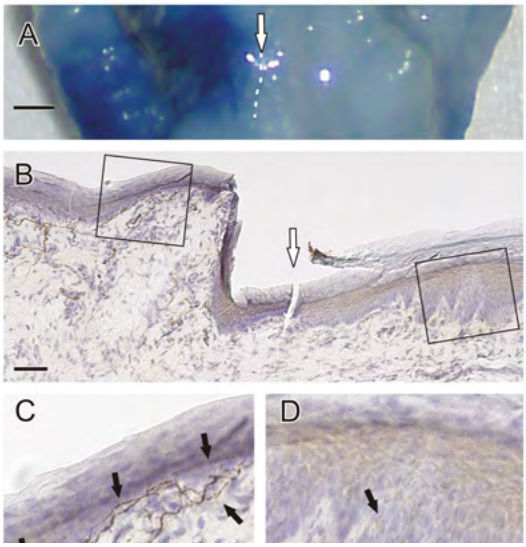

Figure 2. Correlation between Evans Blue extravasation and the innervation of the skin. A) Macroscopic iew of a part of the left plantar hind paw of the rat. After ligation of the sciatic nerve, stimulation of the healthy saphenous nerve showed blue coloring of the medial part of the plantar hind paw. B) PGP9.5 staining of the glabrous skin of rats' hind paw, in which an epidermal cut (white arrow) is made to localize the border between extravasated (left) side and non-extravasated (right) side. PGP9.5-positive nerve fibers are observed in the extravasated area medial to the incision. C) Magnification of the Evans Blue extravasated side of the skin. The black arrows show the brown PGP9.5 positive nerve fibers. D) Magnification of the non-extravasated side of the skin. The black arrows show some light staining in the upper dermis of the skin. These thin fiber-like structures could reflect sprouting fibers. Scale bar = 1mm in A and 50μm in B-D, E = epidermis, UD = upper dermis.

These results exclude any possible blue staining of the skin due to diffusion of the dye and show a positive correlation between the extravasation by Evans Blue and the innervation of the epidermis.

Finally, three control animals were transcardially perfused with saline followed by 4% paraformaldehyde in order to determine if the wash-out of Evans Blue from the blood vessels interfered with the OSM measurements. Because no difference was observed between the perfused and non-perfused animals we chose to standardly use non-perfused animals in the current study.

2.4.1. Evans Blue extravasation areas of the individual nerves

Stimulation of the four selected nerves resulted invariably in characteristic patterns of extravasation as evidenced by a dark blue staining of the skin. Stained areas always formed a consistent and continuous region with well-defined borders. Remarkably, no staining was observed on the footpads while less staining was seen on the callosities of the toes in all cases (Figure 3).

The extravasation of the innervated areas by individual nerves were quantified and are represented by different colors (i.e. tibial nerve pink, sural nerve red, peroneal nerve green and saphenous nerve blue)(Figure 3). In addition, different shadings of of the colors pink, red, green and blue from bright to dark were used to represents the incidence of extravasation (i.e. one to seven) resulting from the stimulation of a particular nerve in the group of 7 animals (Figure 3).

The percentage of staining per individual case was calculated from the 200 degrees views in which the unstained hind paw from the most proximal footpad until the tip of the toes (including the footpads and the callosities) was automatically determined as 100% of the area that was analyzed by labVIEW. Subsequently, the average overall staining of the hind paw for the individual nerves and in each view of the 360 degrees rotation was calculated over all 7 cases in each group (Figure 4). A general description of the 3D staining pattern and the average percentage staining for the individual nerves is given in figure 4.

2.4.2.Tibial nerve

Stimulation of the tibial nerve typically caused staining of the glabrous skin, extending to both the lateral and the medial sides of the paw (Figure 3). Maximal coverage of the hind paw with extravasated skin (up to 66,7% ± 5.0) after tibial nerve stimulation was seen on the plantar side of the hind paw at 0-45 degrees and 315-360 degrees (Figure 4A). Note that the cycle starts with the full plantar view. Since the footpads, that do not show extravasation, are included in this view a lower than maximal percentage of extravasation was obtained. The average overall extravasation area of the skin of the rats' hind paw after tibial nerve stimulation is 44.4% (±2,3) (Figure 4E).

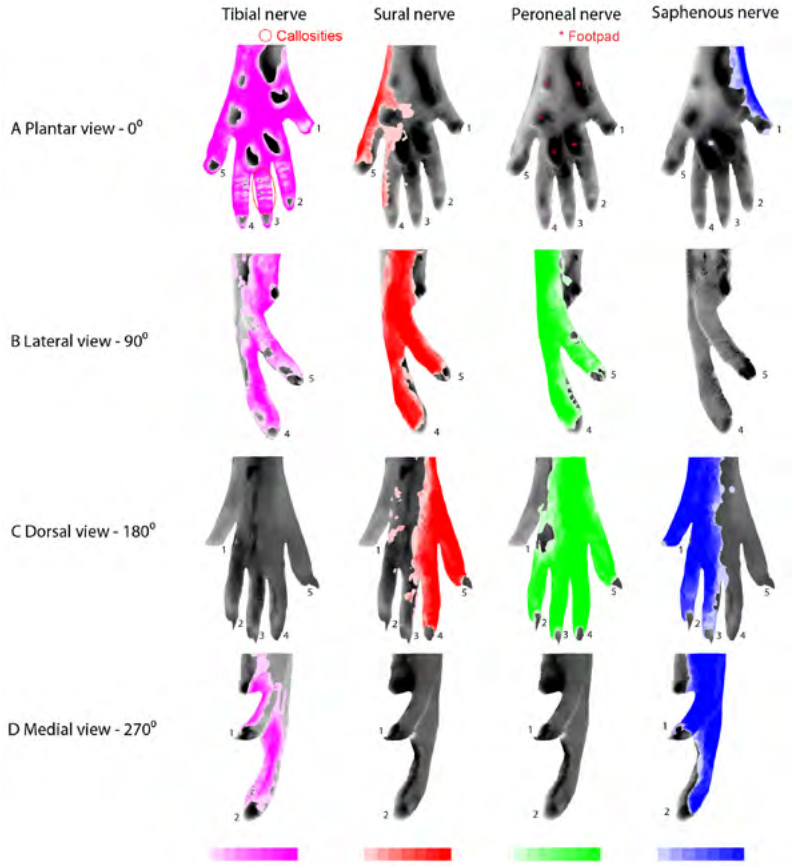

Figure 3. Intra-animal variability in nerve specific extravasation patterns.
The figure shows examples of the nerve specific extravasation pattern results from CASAM protocol after stimulation of the tibial, sural, peroneal and saphenous nerve in four views: A) 0 degree *for the plantar view, B) 90* degrees *for the lateral view, C) 180 degrees for the dorsal view and D) 270* degrees *for the medial view. All grey-black colored hind paws represent the area without extravasation. The pink (tibial nerve), red (sural nerve), green (peroneal nerve) and blue (saphenous nerve) colors indicate nerve specific extravasation ranging in incidence from light (1 animal) to dark (all 7 animals) as shown in the color legend at the bottom of the figure. Footpads are visible as red asterisks and callosities as red circles in the plantar view.*

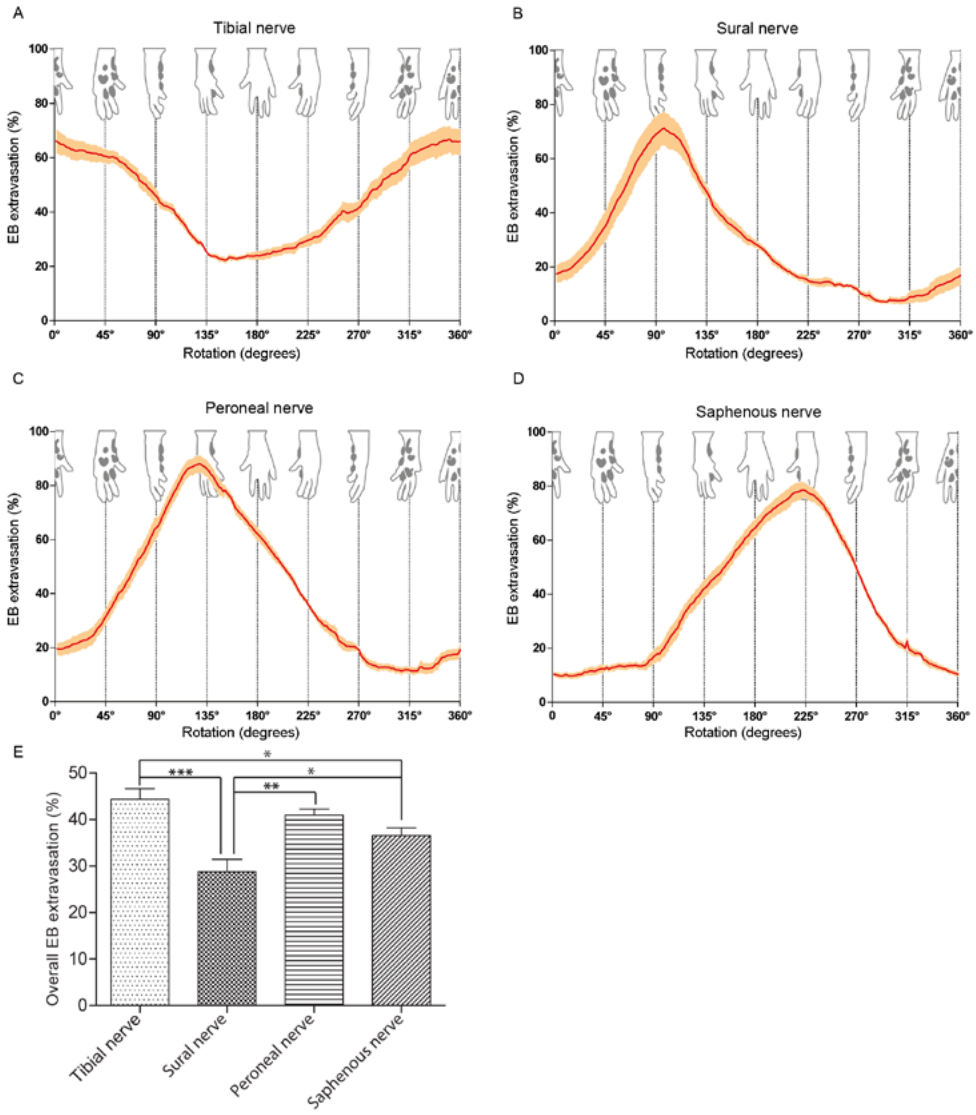

Figure 4. Percentage average extravasation in 360 degrees rotation per nerve.
*Figures A-D show the average extravasation as a function of rotation after stimulation of the tibial nerve (A), the sural nerve (B), the peroneal nerve (C) and the saphenous nerve (D). The yellow band around the red line indicates SEM's in figures. Figure E shows the average extravasation calculated for tibial, sural, peroneal and saphenous nerve over all 200 frames made by the OSM-scanner. In this figure the location is not taken into consideration. Note the significant differences in average percentage extravasation between the different nerves and that these percentages add up to 155%. Analysis by two-tailed t-test. *p<0.05; **p<0.01); ***p<0.001.*

2.4.3. Sural nerve

Stimulation of the sural nerve resulted in a dark blue staining on the lateral side of the hind paw, extending to the 4th and 5th digit on the dorsal side and partially the 4th and 5th digit on the plantar side (Figure 3). Although the sural nerve extravasation area is narrow proximally, it becomes wider towards the toes (Figure 3). This typical narrow elongated band of staining on the lateral part of the hind paw is represented by the low rather narrow peak that was present around 100 degrees reaching 71.3% ± 6.3 (Figure 4B). Lowest coverage (7.1%± 0.1) is seen in the medioplantar view of the paw between 270 and 315 degrees (Figure 4B). Stimulation of the sural nerve caused an overall extravasation of 28.8% (±2.7) in rats' hind paw, which represents the lowest overall Evans Blue extravasation of the four nerves supplying the hind paw (Figure 4E).

2.4.4. Peroneal nerve

The skin area colored by peroneal nerve stimulation shows remarkable correspondence with the proximal part of the area of extravasation by sural nerve stimulation. However, peroneal nerve-induced extravasation extends wider than the sural nerve and covers all digits except digit 1 (Figure 3) with a wide high peak of 88.0% (± 3.3) in the dorsolateral view of the hind paw at 131 degrees (Figure 4C). Note that both slopes of the peroneal nerve and the sural nerve are initially very much alike (Figure 4B and C). Like the sural nerve, the least amount of extravasation after peroneal nerve stimulation was found in the medioplantar view of the paw between 270 and 315 degrees reaching a minimum of 11,4% (±1.5) (Figure 4). The average extravasation after peroneal nerve stimulation is 40,9% (±1.3) (Figure 4E).

2.4.5. Saphenous nerve

Saphenous nerve stimulation typically resulted in extravasation of the most medial side of the hind paw, covering the best part of the 1st, 2nd and 3rd digit and extending till the medial footpads on the plantar side of the paw (Figure 3). Similar to the stimulation of the peroneal nerve, the saphenous nerve has a broad extravasation area causing a high wide peak covering 78.6% (±3.0) of the dorsomedial paw at 225 degrees (Figure 4D). Minimal extravasation (9.7% ± 1.2) was found on the plantar view of the paw. Overall, stimulation of the sapheneous nerve caused 36.6% (±1.7) of the skin to demonstrate extravasation (Figure 4E).

In summary, the average extravasation area of the skin in rats' hind paw after tibial nerve stimulation is 44.4% (±2.3), whereas the sural nerve shows 28.8% (±2.7) extravasation, the peroneal nerve 40.9% (±1.3) and the saphenous nerve 36.6% (±1.7) extravasation (Figure 4E). From this first analysis, which is based on

the summed projections of individual frames, it is determined that the sum of all averaged extravasation areas in the skin of rats' hind paw contributed to 150.7% (±16.0), which indicates a considerable overlap of the extravasation areas induced by stimulation of the individual nerves.

2.4.6. Analysis of variability and overlap

Although stimulation of a particular nerve generally resulted in extravasation of a specific part of the skin, small differences were observed between animals. As these differences may reflect intra-animal variability in the extent of the areas innervated by a single nerve, we have analyzed the intra-animal variability further using the CASAM technique (24), which entails superimposing the extravasated areas on an averaged hind paw (Figure 3). In addition, the staining areas of two adjacent nerves were merged to gain a better understanding of the location of the considerable overlap areas as found in our previous average staining calculations (Figures 5-9). The intra-animal variability within the four groups of seven animals has been taken into account by using different shades of the color that represents the specific cutaneous nerve extravasation ranging from bright to dark as described previously. After merging the stained areas for two nerves, it was possible to create a new 49 (7x7) grid of color combinations that represents the incidence that a particular surface area is extravasated by stimulation of either or both of the nerves (Fig. 5B, 6B, 7B, 8B). Subsequently, the areas that showed significant overlap in extravasation by both nerves (i.e. at least four of the seven animals showed extravasation in this area in both groups) were extracted (Fig. 5C, 6C, 7C, 8C). Using this analysis we can now describe which skin areas show systematic overlap in extravasation due to stimulation of different nerves.

2.4.7. Plantar View

As shown in figure 3A and visible in figure 5, parts of the plantar aspect of the hind paw are extravasated by the stimulation of the saphenous, tibial and sural nerves. The plantar skin of the hind paw shows most consistent staining after stimulation of the tibial nerve (Figure 5A). Color coding indicates the consistency of the results. Dark pink indicates that all seven studied animals showed extravasation of the tibial nerve in the same region whereas bright pink to white regions depict areas with extravasation in only one of the rats. Note that in all animals the footpads appear as black islands since they never show extravasation of the skin (Figure 5). Variety in shape and position of footpads caused some lower densities around the footpad areas. The callosities on the plantar side of the toes also demonstrate a lower incidence of coloring.

Both the sural and the saphenous nerves have a minimal area of extravasation in the plantar view as compared to the dorsal view. Moreover, these small plantar areas also show some variability as indicated by the amount of bright

colours (i.e. bright red in case of the sural nerve in figure 5A.3). Intra-animal variability in the extent of extravasation area for the saphenous nerve is further represented by the white shade proximal to the first digit next to the first proximal footpad (Figure 5A.1).

In addition, Figure 5C shows the consistency in areas of overlap between the tibial and saphenous nerve (Figure 5C-1.2) and between the tibial and sural nerves (Figure 5C-2.3). Indeed, small regions of consistent overlap in extravasation by these nerves are noted. The overlap region of the saphenous nerve and the tibial nerve starts at the medial base of the most proximal footpad and ends on the 1st digit (Figure 5C-1.2). The overlap between the tibial and the sural nerve covers almost the entire lateral edge of the hind paw including the 4th digit (Figure 5C-2.3: fuchsia area). However, it should be noted that this overlap region is more consistently involved after tibial nerve stimulation as compared to sural nerve stimulation.

2.4.8. Lateral view

The lateral view of the hind paw incorporates a view of both the 4th and 5th digit and the separation of dorsal and glabrous skin on the lateral side of the paw (Figure 3B). The saphenous nerve is the only nerve that does not contribute to the extravasation of this view while the sural nerve provide the most consistent extravasation (Figure 3B). Extravasation by the peroneal and the tibial nerve results in considerable overlap with the territory of the sural nerve (Figure 6A, B). However, note that, in contrast to the tibial nerve, both sural and peroneal nerve stimulation predominantly resulted in extravasation of the dorsal edge of the paw.

Although, the extravasation area by the peroneal nerve shows overlap with extravasation areas of tibial as well as sural nerves, more prominent interaction is seen with the latter. This is illustrated by figure 6C-1.2 where the large dark red/dark green areas indicate consistency of overlap in the extravasation areas between the peroneal and the sural nerve without any dominance for either nerve in this area. Fewer overlap is seen between the sural and the tibial nerve (fuchsia area in Figure 6C-2.3), which were mostly restricted to the border between the glabrous skin and non-glabrous skin at the lateral view. However, least overlap was found between the peroneal and the tibial nerve (Figure 6-C3.4).

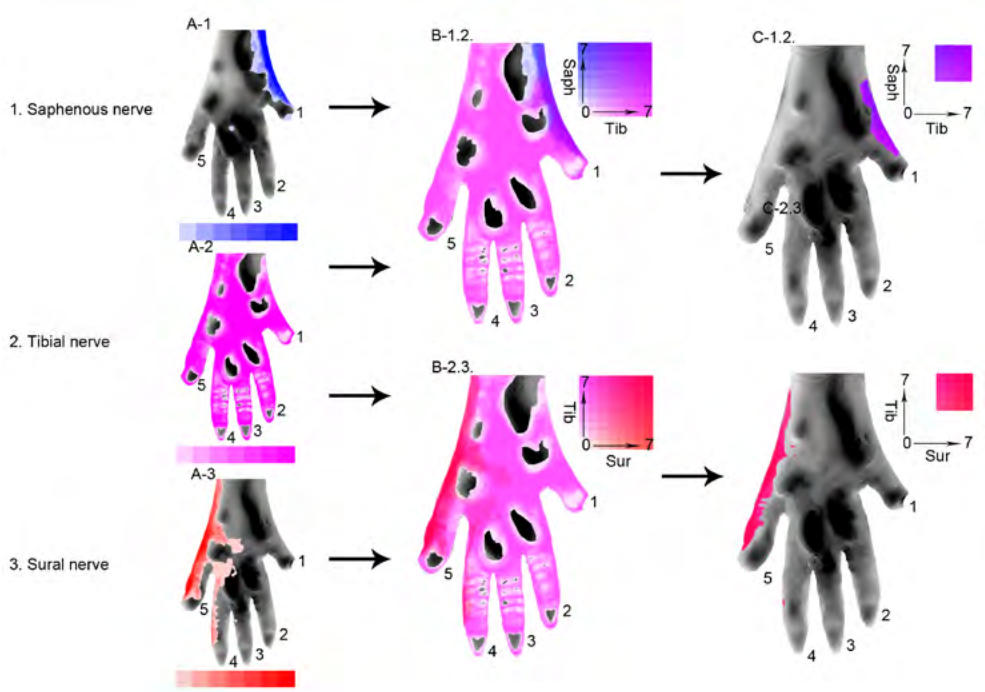

Figure 5. Analysis of the plantar overal areas.
A) The intra-animal variability of the extravasation is shown individually for the saphenous (blue), tibial (pink) and sural (red) nerve on the plantar side of the paw ranging in incidence from light (1 animal) to dark (all 7 animals) as shown in the color legend below the hind paws. Note the lack of extravasation by the peroneal nerve on the plantar view B) Combined extravasation areas showing overlap. The combined figures of the saphenous and the tibial nerve (B-1.2) as well as the combined figures of the tibial and the sural nerve (B-2.3) shows a small blue area on the medial and red area on the lateral part of the hind paw showing overlap with tibial nerve extravasation. The 7x7 grid of color combinations is represented to show the incidence that a particular surface area is extravasated by stimulation of either or both of the nerves as given in the x and the y axis. C) Extraction of significant overlap areas between the saphenous and the tibial nerve (C-1.2) shows a small area of overlap on the medioproximal part of the plantar side while the overlap between tibial and the sural nerve (C-2.3) is seen on the lateral part of the hind paw. 4x4 grid of color in overlap areas of two nerves in at least four of the seven animals in each group. Saph= saphenous nerve, Tib= tibial nerve, Sur = sural nerve.

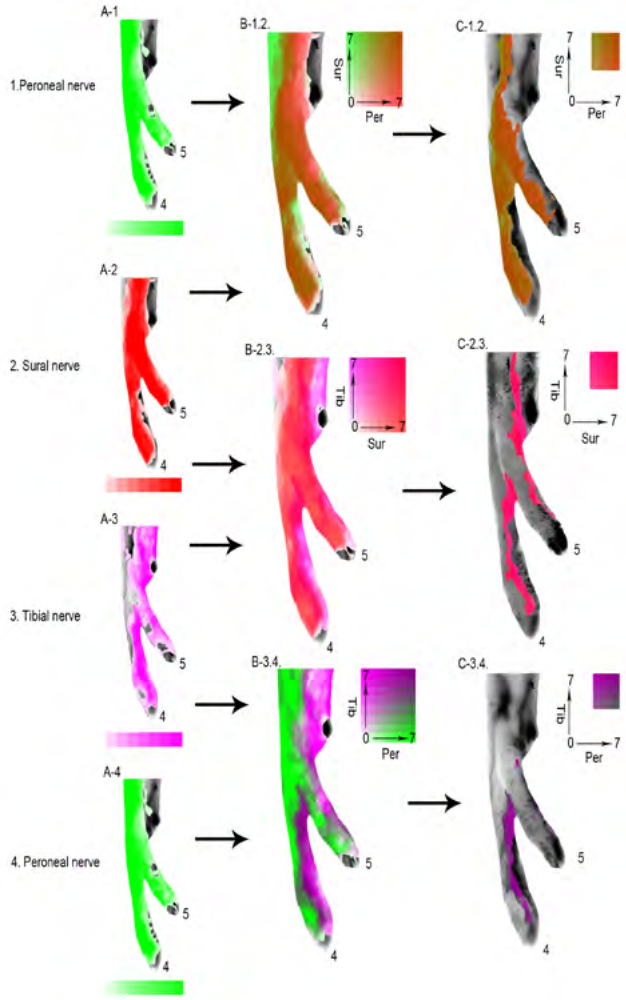

Figure 6. Analysis of the lateral overlap areas.
A) The intra-animal variability of the extravasation is shown individually for the peroneal (green), sural (red) en tibial (pink) nerve on the lateral side of the paw ranging in incidence from light (1 animal) to dark (all 7 animals) as shown in the color legend below the hind paws. In the lateral view there is overlap between three nerves, therefore in (A) the peroneal nerve was displayed twice. B) Combined extravasation figures show comparable extravasation areas while after correction for anatomical variety three different overlapping areas ia seen. The 7x7 grid of color combinations is represented to show the incidence that a particular surface area is extravasated by stimulation of either or both of the nerves as given in the x and the y axis. I (C). Relatively large significant overlap is seen between the peroneal and sural nerve (C-1.2), whereas the tibial and the sural nerves show typically overlap in a vertical line on the lateral border between the glabrous and hairy skin (C-2.3). The peroneal and the tibial nerve present overlap mostly on the 4th digit of the lateral hind paw (C-3.4). 4x4 grid of colour in overlap areas of two nerves in at least four of the seven animals in each group. Sur = sural nerve, Per= peroneal, Tib= tibial nerve.

2.4.9. Dorsal view

All animals showed extravasation of at least some parts of the skin at the dorsal aspect of the hind paw after stimulation of either the saphenous, the peroneal or the sural nerve. Tibial nerve stimulation resulted only in some animals in small spots of extravasation between the digits. Since these spots did not represent a significant overlap they were excluded in the analysis of overlap with other nerves.

Stimulation of the sural nerve caused extravasation of the dorsolateral part of the paw, covering the 5th and the 4th digit and in 3 out of 7 cases some spots were noticeable on the 3rd digit as well (Figures 3C, 7A). Saphenous stimulation, on the other hand, resulted in coloring of the dorsomedial aspect of the paw, usually including the 3rd digit. Peroneal-induced extravasation is located centrolaterally at the dorsal view of the paw and incorporating the 2nd -5th digit in all 7 cases. As such, some overlap with both the sural nerve laterally and the saphenous nerve medially exists (Figures 3C, 7A).

From the dorsal extravasation figures it can be appreciated that the territories extravasated by the saphenous and peroneal nerve stimulation cover almost the entire dorsal aspect of the paw (Figure 7B-2.3). Both areas meet each other proximally in the centre of the hind paw and generally demonstrated a shared extravasation of the skin of the 2nd and 3rd digit. Comparing the extravasation representations of the peroneal and sural nerve in the lateral view indicates that the sural nerve area is systematically and almost completely overlapped by that of the peroneal nerve. The overlap area is mostly dark red showing an even administration of the extravasation with a dark green line at the centre of the hind paw due to dominance of the peroneal nerve in this overlap area (Figure 7C-1.2).

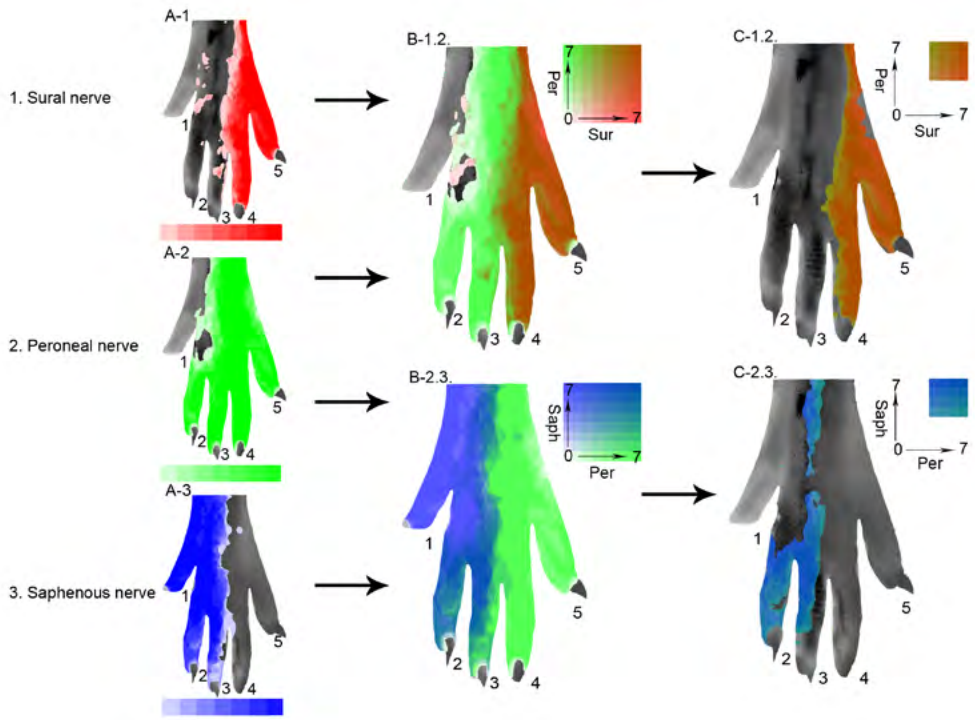

Figure 7. Analysis of the dorsal overlap areas.
A) The intra-animal variability of the extravasation is shown individually for the sural (red), peroneal (green) and saphenous (blue) nerves on the dorsal side of the hind paw ranging in incidence from light (1 animal) to dark (all 7 animals) as shown in the color legend below the hind paws. B) Combined extravasation areas showing overlap (B-1.2.) in which 7x7 grid of color combinations is represented to show the incidence that a particular surface area is extravasated by stimulation of either or both of the nerves as given in the x and the y axis. Note that the area of combined overlap of the peroneal and the sural nerve is very alike the extravasation figure of peroneal nerve (A-2) (B-2.3) The combined extravasation areas of the saphenous and the peroneal nerve show a complete innervation of the dorsal skin of the hind paw. C) The significant overlap between the saphenous and the peroneal nerve (C-1.2) and between the peroneal and sural nerve (C-2.3) are shown. The 4x4 grid of color in overlap areas of two nerves in at least four of the seven animals in each group. Per= peroneal, Sur = sural nerve, Saph= saphenous nerve.

2.4.10. Medial view

The medial view specifically incorporated the 1st and the 2nd digit and the separation of dorsal and glabrous skin at the medial side of the hind paw (Figures 3D, 8A). The saphenous nerve caused extravasation of almost the entire medial view of the hind paw while extravasation by the tibial nerve was observed at the medioplantar side of the hind paw (Figure 8A). Stimulation of the tibial nerve resulted in coloring of more selective and rather variable spots while extravasation by the saphenous nerve showed more consistent and elaborate staining. Note again that also in this view no extravasation of the footpads was noted (Figure 8). Furthermore, the saphenous nerve (blue) dominates the mediodorsal side, while the tibial nerve (pink) dominates the medioplantar side (Figures 3D, 8A). Similar to the lateral view of overlap (Figure 6C-2.3), the overlap at the medial aspect is mostly restricted to the border between the glabrous skin and the non-glabrous skin at the medial view (Figure 8C-1.2).

All significant extravasation areas by individual nerves and all significant overlap areas are summarized in the four views shown in Figure 9. This figure clearly illustrates the dominant appearance of the tibial nerve at the plantar side of the paw, whereas the dorsal side is covered by the saphenous, the peroneal and the sural nerve and demonstrates the significant overlap in innervation areas of these nerves.

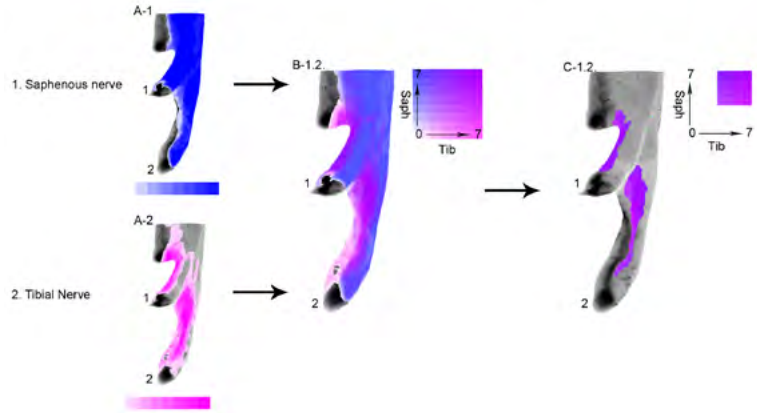

Figure 8. Analysis of the medial overlap areas.
A) The intra-animal variability of the extravasation is shown individually for the saphenous and tibial nerves on the medial side of the paw ranging in incidence from light (1 animal) to dark (all 7 animals) as shown in the color legend below the hind paws: 7x7 grid of color combinations is represented to show the incidence that a particular surface area is extravasated by stimulation of either or both of the nerves as given in the x and the y axis. B) The combined extravasation areas of the saphenous and tibial nerves shows extravasation of all skin areas of the medial view except the footpads. This area consist mostly of the colours blue (saphenous nerve) on the dorsal side and and pink (tibial nerve) on the plantar side of the medial view, suggesting little overlap. C) Indeed the overlap figure shows a small area of significant overlap between saphenous and tibial nerve. The 4x4 grid of color in overlap areas of two nerves in at least four of the seven animals in each group. Saph= saphenous nerve, Tib= tibial nerve.

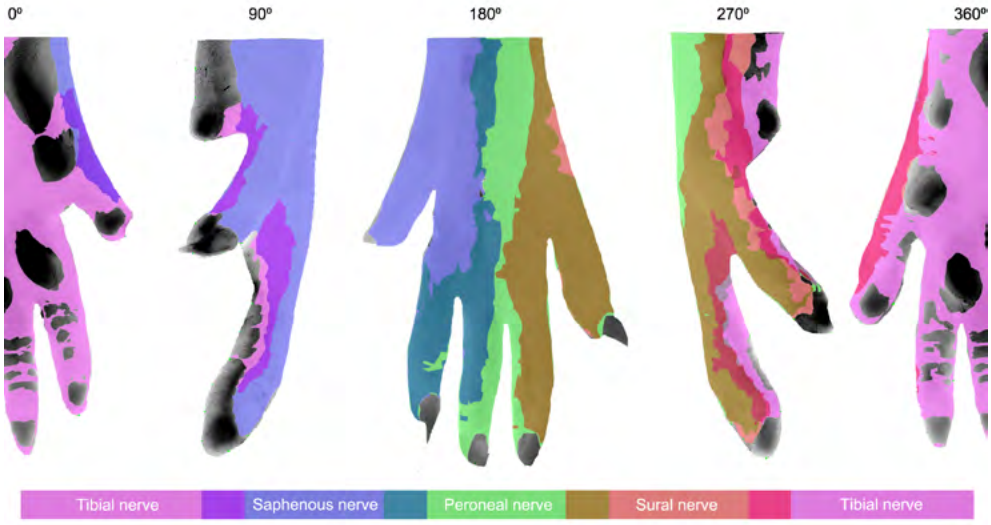

Figure 9. Complete extravasation areas of rats' hind paw.
All extravasation areas of rats' hind paw are shown in plantar (0 degree), lateral (90 degrees), dorsal (180 degrees) and medial (270 degrees) view by tibial (pink), saphenous (blue), peroneal (green) and sural (orange) nerve. Each significant overlap area between the two nerves is indicated by different coulours: overlap between tibial and saphenous nerve is dark purple, between saphenous and peroneal nerve dark green, between peroneal and sural nerve brown and between sural and tibial nerve fuchsia. This figure serves as a summary of both individual extravasation as well as overlap in extravasation areas of rats' hind paw.

2.5.0. Discussion

2.5.1. Methodological considerations combining Evans Blue extravasation, OSM scanner and CASAM technology

Sensory nerve fibers are important in perception of the environmental stimuli in order to allow interaction but also to avoid traumatic forces and extreme thermal exposure (33). Individual fibers are characterized by well-defined receptive fields, which may partly overlap with that of other fibers. Many studies have been devoted to the analysis of changes in sensory skin fibers after peripheral nerve injury. The hind paw of the rat has become a commonly used model in studying these changes resulting from different kinds of trauma (3, 5).

In order to better evaluate and understand the various processes that take place during degeneration and regeneration of cutaneous nerves we have noted that a more precise description of the innervation areas of the hind paw would be in-valuable. Although several studies have used the well-known technique based

on vascular labeling in order to examine the cutaneous regions of innervation by particular nerves, (7-20), their results are prone to subjective interpretations or are very cumbersome to obtain; i.e. subjective translation of staining patterns and extraction of dye from skin samples, respectively . The OSM scanning technique enabled a new and objective analysis of the area of extravasation by using a full 360 degrees circle of views. Furthermore, it should be noted that the results of extraction studies are based on the assumption that the extracted amount of the extravasated dye is proportional to the number of nerve endings present in the skin (10). However, this assumption seems less reliable since studies indicated that the extent of plasma extravasation depends on stimulation parameters such as frequency and time (11, 12). These parameters have been used differently in literature, which makes comparison of evaluated dye extraction between studies difficult.

The stimulation parameters used in the present study were chosen with utmost care. Our stimulation frequency of 10 Hz was based on that of earlier results from which it could be deduced that changing stimulation frequency from 4 to 8 Hz (for 10 min) resulted in a more prominent plasma extravasation in the event of 8 Hz (11, 12, 14). Furthermore, a trial study was performed from which the stimulation parameters were determined to ensure an optimal plasma extravasation without loss of information. Although some studies have used guanethidine (a vasodilator), at varying concentrations in order to enhance both blood flow and extravasation (12, 13, 16), this was not deemed necessary in the present study , as we have used isoflurane as an anesthetic, which has been demonstrated to also have a vasodilatory action (34).

After Evans Blue experiment the hind paw was morphed to an average size using CASAM technology. However, the heel was excluded in these calculations since no anatomic landmarks, which are required to morph the hind paw, are present in the heel. In addition, the heel is partly innervated by the gastrocnemius nerve, which is not included in this manuscript. Therefore, the hind paw from the most proximal footpad until the tip of the toes was chosen as the area of interest to maintain consistent and accurate CASAM measurements for each hind paw and to show the innervation areas of the four (tibial, sural, peroneal, and saphenous) nerves supplying this area of the hind paw. The glabrous skin containing footpads is an important area in nerve regeneration and neuropathic pain studies in animals; behavioral studies to determine mechanical sensitivity using von Frey filaments is performed between the footpads (36-38), while thermal sensitivity (cold- and hot plate) (39, 40) is measured in the footpads. Furthermore, the four nerves that supply this area are stained in immunohistochemical studies, in which the sensory nerves in the footpads and/or in between the footpads are visualized and quantified (3, 41, 42).

Knowledge about the extent of overlap of innervation areas is crucial when studying the short and long-term effects of peripheral nerve injury. In addition, collateral sprouting of undamaged fibers following nerve injury may induce or enlarge areas of overlap in innervation area, which may be important when

evaluating the behavior of regenerating nerves. Although accurate and exact results were obtained by combining the Evans Blue extravasation technique and the 360 degrees imaging using OSM scanning technique, it was not possible to determine the overlap between the extravasation areas of different nerves within the same animal.

Using extravasation of two different dyes (Evans Blue and colloid silver) Dux et al. (20) already used the plasma extravasation technique in order to study the overlap areas of cutaneous innervation. Staining of the skin by both dyes visualized skin areas with Evans Blue, areas with colloid silver and areas with both Evans Blue and colloid silver staining that indicates for the overlap territory. However, these authors used an interval of 60 minutes between the stimulation of the two nerves in the same specimen to exclude any skin staining by the previous dye and waited another 30 minutes after the last nerve stimulation. It is known that Evans Blue is a fluorescent dye (43), which faded in time in our trial study (data not shown). In our view, this may have caused an underrepresentation of the Evans Blue extravasation areas in the study by Dux et al. (20), which could explain the smaller overlap in extravasation areas in comparison to our results. Moreover, the intra-animal variability of the individual extravasation areas was not taken in consideration in their translation studies. As the CASAM technology employed in our study uses many landmarks in order to determine an average hind paw, an accurate representation and subsequent comparison of the individual extravasation areas was possible (24). Subsequently, the individual representations were marked and an overlay was made to quantify the area of overlap between two adjacent extravasation areas. It is important to note that in order to prevent dispersion in average paw size calculation, all animals had to be from the same strain, sex and of a comparable body weight. Although the hind paws were scanned and analyzed in 200 frames to cover 360 degrees to determine the extravasation and overlap areas, only four views are shown in the present study as they cover the complete hind paw (apart from the 3rd inter-digital space).

2.5.2. Results of extravasation in comparison with previous studies

Previously it has been shown that antidromic stimulation of the autonomic nervous system can lead to an increase in skin blood flow due to activation of Aδ-fibers (21), whereas the C-fiber activation causes both vasodilatation and plasma extravasation of Evans Blue by release of neuropeptides (22). Therefore, the interpretation of the results from Evans Blue extravasation is based on the assumption that the stained skin corresponds with the afferent C-fiber and to some extent Aδ-fiber innervation areas of the stimulated nerve, as could be verified with electrophysiological techniques (23). Consistent with this evidence, preliminary results from our laboratory using the pan-neuronal marker PGP9.5 confirmed that the extravasation areas correspond exactly to the innervation area of the stimulated nerve (see section 2.8.0.). From these findings we can conclude that the Evans Blue extravasation

results in an indirect but accurate representation of skin regions innervated by primary afferents of a particular nerve.

Swett and Woolf were one of the first to describe the size and location of cutaneous innervation of rats' hind paw by electrophysiological recording techniques and labeling (44). Consistent with our findings, they show that the plantar side of the hind paw is mainly innervated by the tibial nerve (Figures 5, 9). Moreover, the boundaries between the sural and the saphenous nerve with the tibial nerve corresponded closely with the hair line margin of the plantar skin, which is similar to our results (Figure 5B). Interestingly, over time different groups studying nerve regeneration have been referring to the classic work of Swett and Woolf when considering the plantar innervation area of rats' hind paw (45, 46). It seems however that these studies described the plantar innervation of the hind paw differently: in three equal parts in which the medial part (including the entire 1st and parts of the 2nd digit) would be innervated by the saphenous nerve, the central part by the tibial nerve and the lateral part (including parts of the 4th digit and the entire 5th digit) by the sural nerve. In the light of the present findings and the initial paper of Swett and Woolf we think that this representation is incorrect and should be interpreted attentively and with caution.

The results from this study indicated that the intra-animal variability in extravasation areas for individual nerves is rather low (Figure 3). This is visible by small areas of bright-discolored (low incidence) hind paws (Figure 3) and small SEM values for average extravasation calculation (Figure 4). Hence, the stained areas were consistent and continuous in all animals showing characteristic patterns of extravasation. As described by other studies, the skin of the footpads never showed any sign of extravasation (Figures 3 and 9)(13, 18), while it is shown that the footpads are innervated (47). These findings are previously ascribed to the thickening of the skin in the footpads. However, recent studies in our lab by Duraku et al.(4), showed that the density of peptidergic nerve fibers in the epidermis of the footpads was considerably lower in comparison to the surrounding non-footpad area of rats' hind paw. After stimulation of the nerve, peptidergic neuropeptides are excreted and cause the extravasation of the dye (12, 48). Moreover, the epidermis of the footpads is almost three times as thick as the surrounding skin. Taken together, these properties, at least partly, could explain the generally poor extravasation results of the foot pads.

Although our extravasation areas are highly consistent, they are generally somewhat larger than those observed in other studies (8, 9, 18) . A control experiment was performed to exclude that possible diffusion of the Evans Blue dye could cause the larger extravasation area. The results of this control experiment showed a positive correlation between the Evans Blue extravasation and the innervation of the skin by PGP9.6 positive nerve fibers (Figure 2). In our view the smaller extravasation area shown by other studies can be ascribed to the usage of the hook electrodes that could keep the nerve under tension and may cause damage to the nerve. Although mineral oil and liquid paraffin was used, relatively long

stimulation time (ranging from 5 to 90 minutes) might have caused drying of the nerve (8, 9, 18) and the fluorescent character of the dye might not been taken into account. Furthermore, some studies have mapped the innervation of the hind paw of the rat in which both hind paws (ipsi- and contralateral) were simultaneously stimulated causing smaller extravasation areas. This assumption is confirmed by a study in which subsequently two nerves are stimulated to show overlap areas: when saphenous nerve is stimulated first followed by the peroneal nerve the dorsal 5th digit, which is stained completely in the recent study due to peroneal nerve stimulation (Figure 7A-2), does not show any extravasation. However, when the condition is reversed and the peroneal nerve is stimulated first almost the entire 5th digit shows extravasation (18). From these findings we can conclude that bilateral or subsequent stimulation of two or more nerves shows less plasma extravasation, which, apparently, may result in incomplete extravasation areas. In addition, it seems possible that by allowing central transmission, stimulation of a nerve also influence extravasation not only of the contralateral paw but potentially in the ipsilateral paw as well. Therefore, in the present study unilateral stimulation was performed with a crush lesion proximal from the stimulation site to obtain a complete and detailed extravasation.

One of the most remarkable findings from this study is the dorsal innervation of the paw by the peroneal and saphenous nerve. These nerves intersect at the center of the dorsal hind paw causing a complete extravasation of the skin with a small area of overlap (Figure 7B-2.3). In contrast, the combination of the sural and peroneal nerve extravasation areas showed exclusively overlap of the entire area of the sural nerve on the dorsal view (Figure 7B-2.3). Moreover, it is interesting to note that larger areas of overlap were seen on the dorsal part of the hind paw, whereas the overlap on the plantar side was minimal (18). In our view these differences in overlap between the dorsal and the plantar surface could have implications for regeneration processes of the relevant nerves.

Results from this study could be used as control to compare the denervation and re-innervation areas of specific nerves in the skin after nerve injury. Since sprouting plays a major role once denervation takes place, it is important to acknowledge the correct and detailed innervation areas and the amount of overlap in healthy skin when studying nerve regeneration. In our view the use of the Evans Blue technology in combination with OSM and CASAM analysis represents an excellent tool to examine the origin of the nerves that sprout and contribute to the hypersensitivity in neuropathic pain animals. This could help answering the question why and where neuropathic pain syndromes occur.

2.6.0. References

1. Narayanaswamy H, Facer P, Misra VP, Timmers M, Byttebier G, Meert T, et al. A longitudinal study of sensory biomarkers of progression in patients with diabetic peripheral neuropathy using skin biopsies. J Clin Neurosci. 2012 Nov;19(11):1490-6.
2. McCarthy BG, Hsieh ST, Stocks A, Hauer P, Macko C, Cornblath DR, et al. Cutaneous innervation in sensory neuropathies: evaluation by skin biopsy. Neurology. 1995 Oct;45(10):1848-55.
3. Peleshok JC, Ribeiro-da-Silva A. Delayed reinnervation by nonpeptidergic nociceptive afferents of the glabrous skin of the rat hindpaw in a neuropathic pain model. J Comp Neurol. 2011 Jan 1;519(1):49-63.
4. Duraku LS, Hossaini M, Hoendervangers S, Falke LL, Kambiz S, Mudera VC, et al. Spatiotemporal dynamics of re-innervation and hyperinnervation patterns by uninjured CGRP fibers in the rat foot sole epidermis after nerve injury. Mol Pain. 2012;8:61.
5. Duraku LS, Hossaini M, Schuttenhelm BN, Holstege JC, Baas M, Ruigrok TJ, et al. Re-innervation patterns by peptidergic Substance-P, non-peptidergic P2X3, and myelinated NF-200 nerve fibers in epidermis and dermis of rats with neuropathic pain. Exp Neurol. 2013 Mar;241:13-24.
6. Hsieh CH, Jeng SF, Lu TH, Yang JC, Hsieh MW, Chen YC, et al. Correlation between skin biopsy with quantification of intraepidermal nerve fiber and the severity of sciatic nerve traction injury in rats. J Trauma. 2009 Mar;66(3):737-42.
7. Baranowski AP, Priestley JV, McMahon S. Substance P in cutaneous primary sensory neurons--a comparison of models of nerve injury that allow varying degrees of regeneration. Neuroscience. 1993 Aug;55(4):1025-36.
8. Bester H, Allchorne AJ, Woolf CJ. Recovery of C-fiber-induced extravasation following peripheral nerve injury in the rat. Exp Neurol. 1998 Dec;154(2):628-36.
9. Brenan A. Collateral reinnervation of skin by C-fibres following nerve injury in the rat. Brain Res. 1986 Oct 15;385(1):152-5.
10. Brenan A, Jones L, Owain NR. The demonstration of the cutaneous distribution of saphenous nerve C-fibres using a plasma extravasation technique in the normal rat and following nerve injury. J Anat. 1988 Apr;157:57-66.
11. Carmichael NM, Dostrovsky JO, Charlton MP. Enhanced vascular permeability in rat skin induced by sensory nerve stimulation: evaluation of the time course and appropriate stimulation parameters. Neuroscience. 2008 May 15;153(3):832-41.
12. Gonzalez HL, Carmichael N, Dostrovsky JO, Charlton MP. Evaluation of the time course of plasma extravasation in the skin by digital image analysis. J Pain. 2005 Oct;6(10):681-8.
13. Hansson T, Povlsen B. Functional regeneration of C-fibres inside a silicone tube after sciatic neurotomy in rats. Scand J Plast Reconstr Surg Hand Surg. 1997 Hand Surg. 1997 Mar;31(1):7-11.

14. Jancso N, Jancso-Gabor A, Szolcsanyi J. Direct evidence for neurogenic inflammation and its prevention by denervation and by pretreatment with capsaicin. Br J Pharmacol Chemother. 1967 Sep;31(1):138-51.
15. Kingery WS, Guo TZ, Poree LR, Maze M. Colchicine treatment of the sciatic nerve reduces neurogenic extravasation, but does not affect nociceptive thresholds or collateral sprouting in neuropathic or normal rats. Pain. 1998 Jan;74(1):11-20.
16. Povlsen B, Hildebrand C, Stankovic N. Functional projection of sensory lateral plantar and superficial peroneal nerve axons to glabrous and hairy skin of the rat hindfoot after sciatic nerve lesions. Exp Neurol. 1994 Jul;128(1):129-35.
17. Povlsen B, Hildebrand C, Wiesenfeld-Hallin Z, Stankovic N. Functional projection of regenerated rat sural nerve axons to the hindpaw skin after sciatic nerve lesions. Exp Neurol. 1993 Jan;119(1):99-106.
18. Wiesenfeld-Hallin Z. Partially overlapping territories of nerves to hindlimb foot skin demonstrated by plasma extravasation to antidromic C-fiber stimulation in the rat. Neurosci Lett. 1988 Feb 3;84(3):261-5.
19. Wiesenfeld-Hallin Z, Kinnman E, Aldskogius H. Expansion of innervation territory by afferents involved in plasma extravasation after nerve regeneration in adult and neonatal rats. Exp Brain Res. 1989;76(1):88-96.
20. Dux M, Jancso G. A new technique for the direct demonstration of overlapping cutaneous innervation territories of peptidergic C-fibre afferents of rat hindlimb nerves. J Neurosci Methods. 1994 Nov;55(1):47-52.
21. Janig W, Lisney SJ. Small diameter myelinated afferents produce vasodilatation but not plasma extravasation in rat skin. J Physiol. 1989 Aug;415:477-86.
22. Gee MD, Lynn B, Cotsell B. The relationship between cutaneous C fibre type and antidromic vasodilatation in the rabbit and the rat. J Physiol. 1997 Aug 15;503 (Pt 1):31-44.
23. Pertovaara A. Collateral sprouting of nociceptive C-fibers after cut or capsaicin treatment of the sciatic nerve in adult rats. Neurosci Lett. 1988 Aug 1;90(3):248-53.
24. Kerver AL, van der Ham AC, Theeuwes HP, Eilers PH, Poublon AR, Kerver AJ, et al. The surgical anatomy of the small saphenous vein and adjacent nerves in relation to endovenous thermal ablation. J Vasc Surg. 2012 Jul;56(1):181-8.
25. Kerver AL, Carati L, Eilers PH, Langezaal AC, Kleinrensink GJ, Walbeehm ET. An anatomical study of the ECRL and ECRB: feasibility of developing a preoperative test for evaluating the strength of the individual wrist extensors. J Plast Reconstr Aesthet Surg. 2013 Apr;66(4):543-50.
26. van der Graaf T, Verhagen PC, Kerver AL, Kleinrensink GJ. Surgical anatomy of the 10th and 11th intercostal, and subcostal nerves: prevention of damage during lumbotomy. J Urol. 2011 Aug;186(2):579-83.
27. Hopman AH, Ramaekers FC, Speel EJ. Rapid synthesis of biotin-, digoxigenin-, trinitrophenyl-, and fluorochrome-labeled tyramides and their applicationfor In situ hybridization using CARD amplification. J Histochem Cytochem. 1998 Jun;46(6):771-7.

28. Sharpe J, Ahlgren U, Perry P, Hill B, Ross A, Hecksher-Sorensen J, et al. Optical projection tomography as a tool for 3D microscopy and gene expression studies. Science. 2002 Apr 19;296(5567):541-5.
29. Sharpe J. Optical projection tomography as a new tool for studying embryo anatomy. J Anat. 2003 Feb;202(2):175-81.
30. Kerver AL, van der Ham AC, Theeuwes HP, Eilers PH, Poublon AR, Kerver AJ, et al. The surgical anatomy of the small saphenous vein and adjacent nerves in relation to endovenous thermal ablation. J Vasc Surg. 2012 Apr 11.
31. Rossner W, Tempel K. [Quantitative determination of the permeability of the so-called blood-brain barrier of Evans blue (T 1824)]
Quantitative Bestimmung der Permeabilitat der sogenannten Blut-Hirnschranke fur Evans-Blau (T 1824). Med Pharmacol Exp Int J Exp Med. 1966;14(2):169-82.
32. Hed J, Dahlgren C, Rundquist I. A simple fluorescence technique to stain the plasma membrane of human neutrophils. Histochemistry. 1983;79(1):105-10.
33. Weddell G, Miller S. Cutaneous sensibility. Annu Rev Physiol. 1962;24:199-222.
34. Kirstetter P, Lagneau F, Le Corre F, Cailmail S, Moreau R, Lebrec D, et al. Vascular properties of isoflurane: comparison between normal and cirrhotic rats. Br J Anaesth. 1998 Dec;81(6):968-9.
35. Apps R, Garwicz M. Anatomical and physiological foundations of cerebellar information processing. Nat Rev Neurosci. 2005 Apr;6(4):297-311.
36. Chaplan SR, Bach FW, Pogrel JW, Chung JM, Yaksh TL. Quantitative assessment of tactile allodynia in the rat paw. J Neurosci Methods. 1994 Jul;53(1):55-63.
37. Smits ES, Duraku LS, Niehof SP, Daanen HAM, Hovius SER, Selles RW, et al. Cold-induced vasodilatation in cold-intolerant rats after nerve injury. J Plast Reconstr Aes. 2013 Sep;66(9):1279-86.
38. Castel A, Helie P, Beaudry F, Vachon P. Bilateral central pain sensitization in rats following a unilateral thalamic lesion may be treated with high doses of ketamine. BMC Vet Res. 2013;9:59.
39. Carter RB. Differentiating analgesic and non-analgesic drug activities on rat hot plate: effect of behavioral endpoint. Pain. 1991 Nov;47(2):211-20.
40. Jasmin L, Kohan L, Franssen M, Janni G, Goff JR. The cold plate as a test of nociceptive behaviors: description and application to the study of chronic neuropathic and inflammatory pain models. Pain. 1998 Apr;75(2-3):367-82.
41. Oaklander AL, Brown JM. Unilateral nerve injury produces bilateral loss of distal innervation. Ann Neurol. 2004 May;55(5):639-44.
42. Yen LD, Bennett GJ, Ribeiro-da-Silva A. Sympathetic sprouting and changes in nociceptive sensory innervation in the glabrous skin of the rat hind paw following partial peripheral nerve injury. J Comp Neurol. 2006 Apr 20;495(6):679-90.
43. Saria A, Lundberg JM. Evans blue fluorescence: quantitative and morphological evaluation of vascular permeability in animal tissues. J Neurosci Methods. 1983 May;8(1):41-9.

44. Swett JE, Woolf CJ. The somatotopic organization of primary afferent terminals in the superficial laminae of the dorsal horn of the rat spinal cord. J Comp Neurol. 1985 Jan 1;231(1):66-77.
45. Decosterd I, Woolf CJ. Spared nerve injury: an animal model of persistent peripheral neuropathic pain. Pain. 2000 Aug;87(2):149-58.
46. Smits ES, Duraku LS, Niehof SP, Daanen HA, Hovius SE, Selles RW, et al. Cold-induced vasodilatation in cold-intolerant rats after nerve injury. J Plast Reconstr Aesthet Surg. 2013 May 6.
47. Lauria G, Lombardi R, Borgna M, Penza P, Bianchi R, Savino C, et al. Intraepidermal nerve fiber density in rat foot pad: neuropathologic-neurophysiologic correlation. J Peripher Nerv Syst. 2005 Jun;10(2):202-8.
48. Louis SM, Jamieson A, Russell NJ, Dockray GJ. The role of substance P and calcitonin gene-related peptide in neurogenic plasma extravasation and vasodilatation in the rat. Neuroscience. 1989;32(3):581-6.

Chapter 3

Long term follow-up of peptidergic and non-peptidergic re-innervation of the epidermis following sciatic nerve reconstruction in rats

Shoista Kambiz, Liron S. Duraku, Tim H.J. Nijhuis, Saniye G. Cosgun, Steven E.R. Hovius, Tom J.H. Ruigrok, Erik T. Walbeehm

Journal of Neurosurgery 2015; 123(1):254-269

3.1.0. Abstract

Peripheral nerve injuries are a commonly encountered clinical problem and often result in long-term functional deficits. The current golden standard for transected nerves is an end-to-end reconstruction, which results in intermittent appearance of neuropathic pain. In order to improve our understanding of the relation between this type of reconstruction and neuropathic pain, we transected and immediately end-to-end reconstructed the sciatic nerve in rats. The effect of this procedure on neuropathic pain, as measured by thermal and mechanical hypersensitivity at four different time points (5, 10, 20 and 30 weeks post reconstruction) was related to the density of the peptidergic and non-peptidergic fiber innervation in the glabrous skin of rats' hind paw.

Thermal hypersensitivity occurring 20 weeks after reconstruction was accompanied by a significant increase in peptidergic epidermal fibers. However, the lesion-induced reduction in the density of non-peptidergic epidermal fibers remained decreased at all experimental time points. Moreover, temporal collateral sprouting by undamaged saphenous nerve was visualized using the recently revised Evans Blue extravasation technique. Strikingly, as the sciatic nerve repopulated rats' hind paw, the saphenous nerve withdraw to its original territory.

We conclude that the transient thermal hypersensitivity is related to increased density of epidermal peptidergic fibers, which are mainly originating from regenerating fibers. Furthermore, changed composition in the peptidergic and non-peptidergic epidermal fibers is demonstrated following end-to-end reconstruction of the sciatic nerve.

3.2.0. Introduction

Peripheral nerve injury often results in sensory and motor impairments of the affected body parts (1). However, one of the very disabling consequences of nerve injury is neuropathic pain, which is defined by International Association for the Study of Pain (IASP) as "pain arising as a direct consequence of a lesion or disease affecting the somatosensory system" (2). Neuropathic pain responds poorly to standard pain therapies and therefore, may have a major impact on the quality of patients' lives (3, 4). Future therapeutic advancement in neuropathic pain therapies are likely to benefit from improved understanding of nerve regeneration after nerve injury. Recently, it has been shown that changes in the epidermal innervation may play a pivotal role in neuropathic pain features (5-7).

The epidermis is innervated by Aδ and C-fiber nociceptors, which can be divided into two functionally distinct sensory nerve population: peptidergic and non-peptidergic fibers. Peptidergic nerve fibers are sensitive for nerve growth factor (NGF) while the non-peptidergic fibers respond to glial cell line-derived neurotrophic factor (GDNF). The peptidergic and non-peptidergic fibers can be further divided by their expression of different neurotrophic receptors. The

peptidergic fibers express neuropeptide calcitonin gene-related peptide (CGRP), and many of them also express substance P (SubP), whereas the non-peptidergic fibers are characterized by expression of the plant lectin isolectine B4 (IB4). The myelinated Aδ fibers express neurofilament 200 (NF200) (8). The most common staining technique currently used for staining skin biopsies in a clinical setting is PGP9.5 (9). This is a non-discriminant pan-neuronal cytoplasmic marker and is predominantly used to diagnose peripheral neuropathies. Duraku et al. recently showed the importance of the distinction between subgroup of intra-epidermal nerve fibers (IENFs) by extensive collateral sprouting of peptidergic fibers from uninjured nerves, compared with the non-peptidergic fibers following a spared nerve injury lesion (7, 10). However, regeneration of the different subgroups of IENFs has not yet been described following end-to-end reconstruction, which provides the best outcome compared to nerve graft repair (11). It is also unclear if these fibers play a role in the pathogenesis of neuropathic pain similar to the spared nerve injury model (7). While Stankovic et al. (1996) showed a decrease in density of IENFs 12 weeks after end-to-end reconstruction of the sciatic nerve in rats (12), the authors of a more recent study demonstrated return of the density of IENFs to control in less than 9 weeks after reconstruction (13). However, in humans, improvement of clinical signs can be seen up to 2 years after nerve reconstruction (personal communication). In the present study, we describe for the first time a longer and more complete follow up of the re-innervation pattern of both peptidergic and non-peptidergic IENFs in the glabrous skin of rats' hind paw following end-to-end reconstruction of the sciatic nerve. Together with analysis of collateral sprouting, our results provide more insights into the mechanism of both peripheral nerve regeneration and neuropathic pain.

3.3.0. Materials and Methods

3.3.1. Animals and anesthesia

Experiments were performed on adult female Lewis rats (n=60), weighing 180-200 gram. Animals were pair-housed in hooded cages at room temperature on a 12-hour light/dark schedule, and were given water and food ad libitum. All experiments were approved by the Dutch Ethical Committee on Animal Welfare (DEC) according to the European guidelines for the care and use of laboratory animals (Council Directive 86/6009/EEC).

3.3.2. Surgical procedure

Under isoflurane (3%) anesthesia, the left sciatic nerve of all 60 animals was exposed through a gluteal muscle-splitting approach using a surgical microscope (Zeiss OP-MI 6-SD; Carl Zeiss, Goettingen, Germany). Subsequently, in 48 animals the sciatic nerve was transected by cutting the nerve with a sharp scissor proximal

to its trifurcation. Transection was immediately followed by an epineural end-to-end reconstruction in which we used six 10/0 Ethilon sutures (Ethicon). The remaining 12 animals served as control in which the sciatic nerve was only exposed without transection. The split muscle and skin of all animals were closed using Vicryl Rapide sutures (Ethicon). In all cases, postoperative analgesia was provided by subcutaneous administration of buprenorphine (0.05-0.1 mg/kg; Temgesic). Animals were monitored daily for signs of stress or discomfort.

3.3.3. Experimental groups

The 48 operated animals were randomly divided into four groups consisting of 12 rats each that had a 5, 10, 20 and 30 weeks survival time. Of each group, 6 rats were used to determine the effect of lesion and its recovery by various behavioral and physiological experiments and immunohistochemistry. In the remaining 6 rats the Evans Blue technique was performed to identify collateral innervation of the skin by the saphenous nerve. The 12 sham-operated animals consisted of the control animals. The end-point of 12 sham-operated animals was determined at 5 weeks.

All rats were habituated by exposing them to the stimuli and the environment in the week prior to performing functional tests.

3.3.4. Pin-prick test

The pin-prick test was used to estimate the advancement of the area demonstrating recovery of nociception (14, 15) The lateral and medial skin of the hind paw was pinched with a fine forceps starting distally at the toes and ascending up towards the ankle. The spot on the skin with the positive pinch test (the animal's reflex withdrawal response) was marked and indicated on a standardized drawing of the hind paw (Adobe Illustrator, CS5.1). The position with a positive pinprick results nearest to the toe was determined and indicated in cm. The drawings with positive pinpricks were used as a measure of the average skin sensitivity in the hind paw and served to assemble a 'sensory regeneration map' of the hind paw.

3.3.5. Von Frey test

The von Frey test was performed to determine the mechanical sensitivity threshold of the hind paws using a set of von Frey hairs ranging from 2 - 300 g in a set of 16 filament steps. The rat was placed in a chamber with a mesh metal floor and each filament was indented for 4 seconds in the lateral and medial plantar skin at its max force (i.e. until it just bent). This stimulus was repeated 5 times, and was scored positive when a minimum of 3 paw flicks (the animal's reflex withdrawal response) was observed. The thresholds for withdrawal responses were compared between the operated hind paw and the sham (control) hind paw for both the medial and the

lateral side of the hind paw. The group animals that underwent reconstruction was considered to be hypersensitive to mechanical stimuli when a significant decrease of withdrawal threshold was noted in comparison to the control animals.

3.3.6. Hot and cold plate test

To determine the occurrence of thermal hypersensitivity, cold (16) and hot plate testing (17) was performed. Rats were placed in an open-ended chamber with clear walls and a surface temperature of 5°C (cold plate) or 50°C (hot plate) on separate days to prevent interference. The time until hind paw withdrawal or licking was observed. Significant differences between the reconstruction and the control group served as an indication of thermal hypersensitivity.

3.3.7. Electromyography

Regeneration and re-innervation of motor axons was evaluated by recording evoked Compound Muscle Action Potentials (CMAPs) of the gastrocnemius muscles (18). Under anesthesia a monopolar needle stimulation electrode was placed 6-7 mm proximally from the nerve injury close to the sciatic nerve at the level of trochanter major using an ultrasound image as guide. This is a reliable minimally invasive method for selectively eliciting CMAPs (19). For recordings, an active electrode was positioned over the midpoint of the medial gastrocnemius muscle with the reference electrode at the later distal end of this muscle. CMAP peak-to-peak amplitude was recorded and averaged over a batch of 20 responses. The average amplitude in each group was compared with the control group.

3.3.8. Gastrocnemius muscle index

After termination of the rat by pentobarbital overdose, we routinely determined gastrocnemius muscle weight to measure muscle atrophy. This is an indirect indication for muscle re-innervation after nerve reconstruction (20). Both ipsilateral and contralateral gastrocnemius muscles were excised. Consequently, the gastrocnemius muscle index (GMI) was calculated; muscle weight from the operated side divided by the muscle weight from the contralateral side.

3.3.9. Evans blue-test

The distribution of afferent fibers from the intact saphenous nerve was tested through stimulation-induced extravasation of Evans blue albumin in the hind paw of 6 rats in each reconstructed group to visualize collateral sprouting (21). The Evans Blue extravasation technique was performed as described previously (22).

Animals were anesthetized with 3% isofluraan. Subsequently, the saphenous nerve was carefully dissected from its environment under microscopic guidance (Zeiss OP-MI 6-SD; Carl Zeiss, Goettingen, Germany). The nerve was inserted in a handmade silicone stimulation cuff (3 mm in diameter, 6 mm in length) in which anodal and cathodal electrodes are embedded. Stimulation was started 5 minutes after the Evans Blue (2%, 4ml/kg) injection in the tongue vein and lasted for 10 minutes using 10Hz, 0.5ms and 12 mA positive pulses (Viking stimulator, IES405-2, Nicolet Biomedical). The skin area of the hind paw innervated by the stimulated nerve exhibited the characteristic deep blue coloration indicating local extravasation of Evans Blue. After stimulation, each rat received an overdose of pentobarbital and the hind paw was removed for subsequent analysis. The 360° view of extravasation areas was recorded and quantified using optical projection tomography (OPT) scanner, computer assisted surgical anatomy mapping (CASAM) technology (23) and Adobe Photoshop. Moreover, the intra-animal difference in extravasation areas are shown in different shades of blue representing the incidence (i.e. 1-6) of extravasation resulting from the stimulation of the saphenous nerve.

3.3.10. Tissue preparation

At the appropriate survival time, animals were sacrificed by an overdose pentobarbital (100mg/kg intraperitoneally). Subsequently, the glabrous skin of the operated hind paw was dissected and immersion-fixed in 2% paraformaldehyde-lysin-periodate (PLP) for 24 hours at 4˚C. The skin was then embedded in 10% gelatin, which was hardened in 10% formaldehyde for 2 hours, stored overnight in 30% sucrose, and subsequently sectioned at 40-µm with a freezing microtome and collected in glycerol for long-term storage at –20 °C.

3.3.11. Immunohistochemistry

Immunohistochemistry was performed to evaluate the density of nerve fibers innervating the skin as described by Duraku et al. in 2013. The sections were washed five times 10 minutes in phosphate buffered saline. Thereafter, the sections were pre-treated with 30% hydrogen peroxide solution at room temperature for 10 min to ensure minimal background. Subsequently, the sections were heated at 80˚C in 2.5 mM sodium citrate (pH 8.75) for 40 minutes to break protein cross links and therefore unmask antigen sites. The sections were then pre-incubated 90 minutes

at room temperature in a blocking solution containing bovine serum albumin (2%) diluted in phosphate buffered saline (pH 7,4) with 0.5% Triton X-100 (Fraction V, Roche). After rinsing, the sections were incubated for 48 hours in a cocktail of 2% bovine serum albumine or milk powder containing the diluted antibody at 4 ˚C. The primary antibodies were PGP9.5 (1/10.000, anti-rabbit, Enzo), SubP (1/500, anti-rabbit, made by R.M. Buijs, department of Neuroscience ErasmusMC, Rotterdam, The Netherlands), P2X3 (1/25.000, anti-guinea pig, Neuromics) and NF-200 (1/15.000, anti-rabbit, Chemicon). Subsequently, sections where incubated with the appropriate secondary biotinylated antibody (1/200, Biotine) for 90 minutes at room temperature. Sections were further processed using a Vectastain Elite ABC kit (Vector, Burlingame, CA) (90 minutes at room temperature) and additional signal amplification was achieved by treating the sections with self-made biotin tyramide (24) for 12 minutes. The 3, -3' diaminobenzidine reaction (25) was then used to reveal the antigenic sites. Thereafter, the sections were mounted on slides and stained with 0.05% thionin for 4 minutes, which discolored the epidermis blue, and as a result a clear border between the epidermis and dermis was visible. Finally, the slides were dehydrated using absolute ethanol (< 0.01% methanol), transferred to xylene and coverslipped with Permount (Fisher, Hampton, NH).

3.3.12. Analysis

All slides were scanned in multiple layers (3 layers of each 8 μm) into digital slides by Nanozoomer 2.0 series system (Hamamatzu). Areas of interest were quantified using digital microscope ImageScope software (Aperio ImageScope v11.1.2.760) using a x 20 objective in a 80-mm^2 region in medial, central and lateral side and the footpad area of the glabrous skin of rats' hind paw. For each rat, the nerve fiber terminals within the epidermis and labeled NF200-immunoreactive (IR) fibers in the upper dermis were counted in 4 sections of the proximal and 4 sections of the distal foot sole area. In addition, the number of Langerhans cells was quantified (26, 27). From these counts the average number of labeled nerve fibers per milimeter squared was calculated for each rat. Finally, the results per group were averaged and compared to the results in the control group.

3.3.13. Statistical analysis

For determining statistical differences, the one way-ANOVA with a Tukey post hoc test was used for intergroup comparisons. Errors in variations were determined as standard error of the mean (SEM), and $p < 0.05$ was taken as significant.

3.4.0. Results

No animals were excluded in this study. All surgical operations were performed successfully, without any signs of postoperative infection, loss of weight, or auto-mutilation. As expected, directly after surgery, lesioned animals dragged their operated hind paw, which completely recovered at about 8 weeks postoperatively. Sham-operated animals used their hind limb normally.

3.4.1. Recovery of sensory function

Pin-prick test
Positive responses, as indicated by paw withdrawal, were seen at all experimental time points for the sham-operated hind paws and at the medial side of the operated hind paws. However, the lateral part of the operated paws did not exhibit any response to the pin-pricks attempted distal to the lateral ankle 3 weeks following end-to-end reconstruction. This indicates that the lateral part of the hind paw, which is known to be exclusively innervated by the sciatic nerve, was completely denervated. Therefore, the lateral part of the hind paw was used to gain information about recovery of nociception of the sciatic nerve following end-to-end reconstruction. At 5 weeks postoperatively an average positive response was observed at the level of the ankle (mean 3,2 cm ± 0,1 from the toe) (Figure 1). Two and a half weeks later, the positive response reached the middle of the plantar hind paw (mean1,9 cm ± 0,1 from the toe). Regeneration of nociceptive fibers was completed 10 weeks after end-to-end reconstruction resulting is positive responses at all levels from the ankle to toe, which equals a nerve growth rate of 0.9 ± 0,01 mm/day.

Mechanical hypersensitivity
The mechanical withdrawal thresholds determined with von Frey monofilaments did not show any significant differences in the medial and the lateral area of the sham-operated hind paw (Figure 2). Confirming the results of the pin-prick test, no reaction was seen in the lateral part of the operated hind paw after applying von Frey filaments up to 300 g at 2, 3, and 5 weeks postoperatively ($p<0,001$). The medial part of the operated hind paw showed loss of sensation at 2 weeks postoperatively. In contrast to the lateral part of the hind paw, the medial part demonstrated similar mechanical sensitivity as sham-operated animals 3 and 5 weeks, suggesting an initiation of collateral sprouting by undamaged saphenous nerve at 3 weeks postoperatively. However, at 10 weeks, a significant decrease in mechanical withdrawal threshold was noted in both medial and lateral areas of the operated hind paw ($p<0,01$; $p<0,001$) demonstrating mechanical hypersensitivity. Mechanical withdrawal thresholds reached control values 20 weeks postoperatively showing no significant difference in von Frey test between the reconstructed and the sham-operated hind paws at this time point (Figure 2).

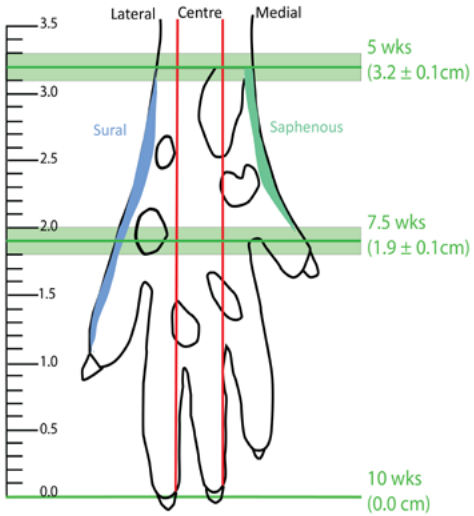

Figure 1. Average sensory nociceptive regeneration map of lateral hind paw after end-to-end reconstruction determined by the pin-prick test. The sensory regeneration map shows the average positive response in green lines (± SEM in light green) at different time intervals (5, 7.5, and 10 weeks) after end-to-end reconstruction in specific portions of the hind paw. While a 5 week positive response was seen distal from the most proximal footpad, all animals showed complete regeneration of sensory nociceptive fibers at 10 weeks.

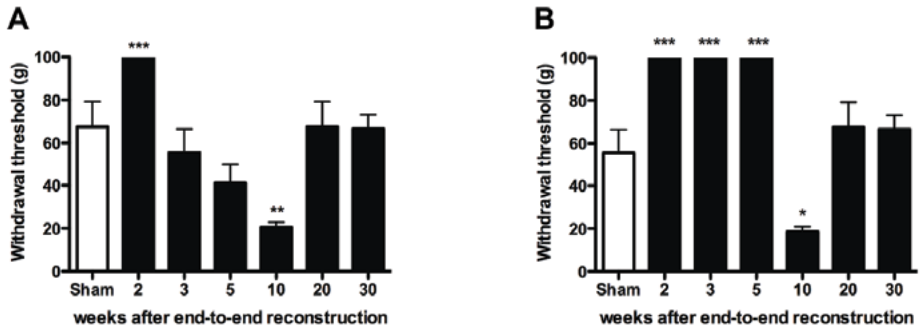

Figure 2. Mechanical withdrawal threshold.
*Histograms showing the mechanical withdrawal thresholds in grams (± SEM) in (A) the medial and (B) the lateral areas in the foot sole of the operated hind paws determined with von Frey monofilaments. No positive response was measured using up to 300 gram filaments in the lateral part of the operated hind paw 2,3, and 5 weeks postoperatively and in the medial aspect of the hind paw until week 3, suggesting mechanical hyposensitivity due to denervation of the skin. A significantly decreased mechanical withdrawal threshold was seen in both the lateral and medial glabrous skin 10 weeks in comparison to sham-operated rats. However, the mechanical hypersensitivity diminished 20 and 30 weeks PO. (*p < 0.05; **p <0.01; ***p <0.001; One-way ANOVA).*

Thermal hypersensitivity
A non significant increase in withdrawal time is observed in cold plate testing at 5 and 10 weeks and in hotplate testing at 5 weeks postoperatively (Figure 3B). Remarkably, a significantly shorter withdrawal latency of the operated hind paws, when compared with sham-operated hind paws, was found for both hot and cold plate tests at 20 weeks postoperatively ($p < 0,05$), indicating hypersensitivity to cold and hot temperatures at this time point. However, withdrawal latencies returned to control values at 30 weeks postoperatively (Figure 3).

In contrast to the neuropathic pain models, end-to-end reconstruction eventually resulted in recovery of both mechanical and thermal hypersensitivity to control levels.

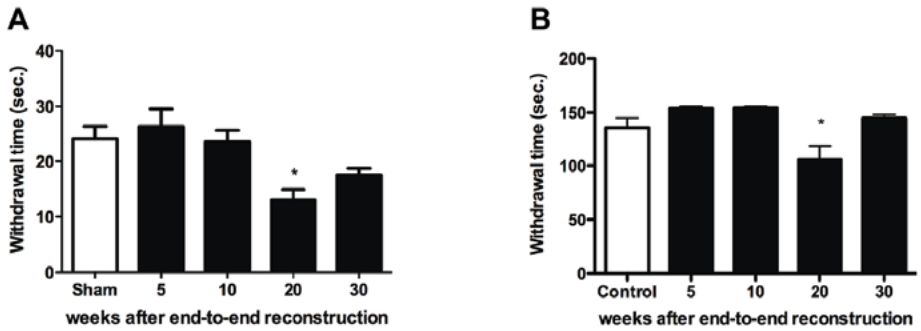

Figure 3. Hot and cold plate testing.
Histograms showing the withdrawal latency in seconds (± SEM) of the operated hind paws in (A) the hot plate test (50 ºC) and (B) the cold plate test (5 ºC) for sham-operated and end-to-end reconstructed hind paws. Although not significant, an increase is seen in the withdrawal time at 50°C (5 weeks postoperatively*) and 5°C (5 and 10 weeks* postoperatively*). Note that in both the hot and cold plate tests a significant shorter withdrawal latency was seen at 20 weeks compared with sham-operated rats. (*p < 0.05; One-way ANOVA).*

3.4.2. Recovery of motor function

Electromyography
CMAPs amplitude provides an indirect estimate of the number of functional axonal fibers in the stimulated nerve. As expected, the amplitude of evoked g CMAPs in the gastrocnemius muscle was considerably decreased in the operated hind paw at 5 weeks ($p<0,001$) compared with respect to sham-operated animals. A gradual functional recovery was evidenced by the ongoing increase in CMAPs measured at the subsequent postoperative times. At 30 weeks postoperative reached values that were similar to those of sham-operated rats (Figure 4A).

Gastrocnemius muscle weight
Sham-operated rats showed a ratio of 1.0 between the ipsilateral and contralateral gastrocnemius muscle weight. Five weeks after end-to-end reconstruction a significant decrease, to less than 0.5 was seen ($p<0.001$) (Figure 4B). Although a subsequent gradual increase is seen at longer survival times, the average GMI leveled out at 0.7 while the CMAPs amplitude recovers to control values. This could be explained by disuse of the formerly denervated gastrocnemius muscle and in the course of time resulting in irreversible damage to the muscles.

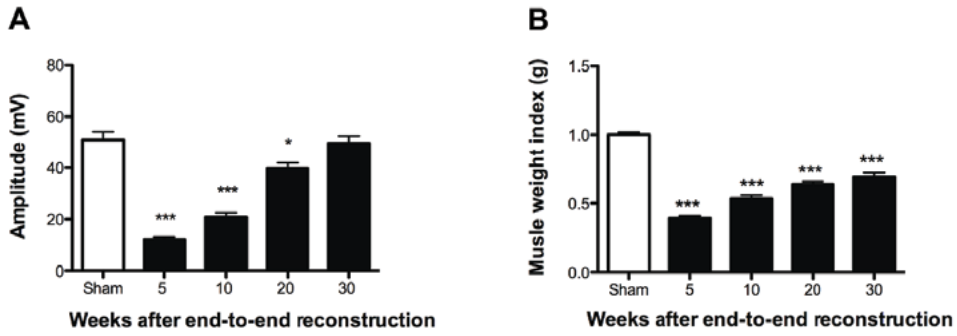

Figure 4. Compound muscle action potentials and Gastrocnemius Muscle Index.
A) Histograms showing the evoked CMAPs in mV (± SEM) in the gastrocnemius muscle of the operated side of the hind paw. A significant decrease is seen at 5, 10, and 20 weeks postoperatively as compared with sham-operated rats. Note the gradual increase that reaches sham values 30 weeks.
*B) Histogram showing the GMI (the ration between affected and contralateral wet gastrocnemius muscle weight). Sham-operated rats show a ratio of about 1.0, whereas rats after end-to-end reconstruction show a significant decrease in GMI at all time points postoperatively. (*p <0.05; ***p <0.001; One-way ANOVA).*

3.4.3. Saphenous nerve participation in regeneration process as determined by Evans Blue extravasation

The Evans Blue technique was applied on the intact saphenous nerve and showed a characteristic blue staining on the medial hair-line margin of the plantar skin of the hind paws of sham-operated animals. However, at 5 weeks postoperatively the area of blue staining was significantly ($p<0.001$) increased and extended to the center part of the operated hind paw (Figures 5A,B). This was interpreted as being due to an extensive collateral sprouting from the adjacent, undamaged, saphenous nerve that invaded the denervated area. This finding, furthermore, is in accordance with the positive withdrawal reaction in the von Frey test on the plantar medial portion of the operated hind paw 5 weeks after surgery. Sprouting of the saphenous nerve

was temporary, as the Evans Blue extravasated skin area returned to control values at 20 and 30 weeks (p=0.221; p=0.297) (Figure 5B), which suggest a withdrawal of the collateral sprouting. This decrease could be explained by re-innervation of the operated sciatic nerve, which is visible in the greatly increased density of epidermal sensory nerve endings 20 and 30 weeks postoperatively in the center and lateral skin area that remained non-extravasated after stimulation of the saphenous nerve. Based on these results, we can conclude that initially there is sprouting of the saphenous nerve to the denervated skin area 5 weeks after surgery that seems to draw back once the regenerating sciatic axons reach their target areas.

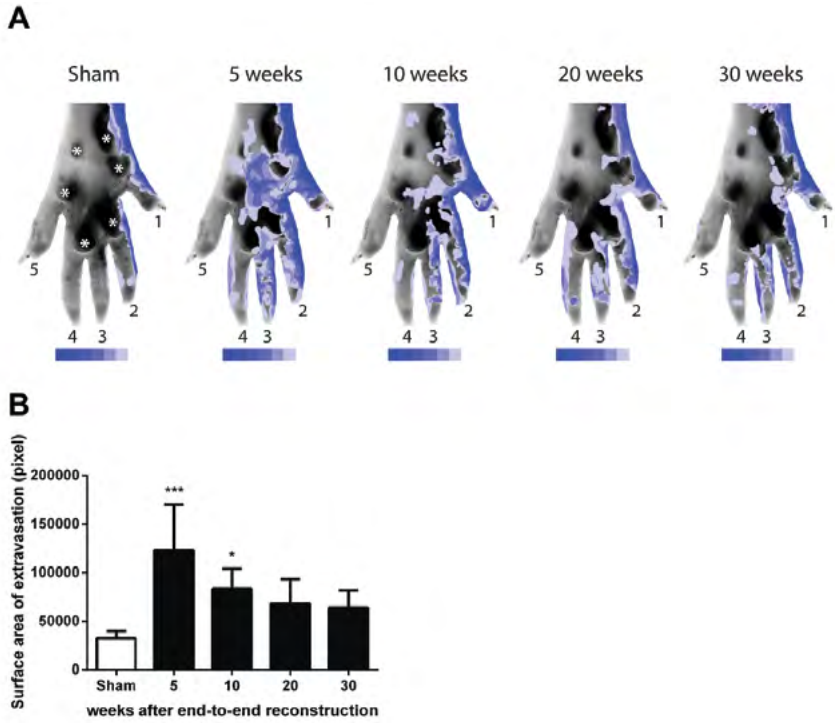

Figure 5. Plantar view of sham and end-to-end operated hind paw following Evans Blue extravasation experiment.
A) Different shadings of the blue color is used to represent the incidence of extravasation resulting from the stimulation of the saphenous nerve. Dark blue is the area of the skin in which 100% of the rats (6 of 6) showed extravasation, whereas the light blue color indicates extravasation in 33%. Note that the area of Evans Blue extravasation increases the most at 5 weeks postoperatively and gradually decreases in time. (1=first index; 2=second index; 3=third index; 4:=orth index; 5=fifth index; and asterics=footpad).
B) Histogram showing the surface calculation of Evans Blue extravasation in pixels (± SEM) of the operated plantar hind paw. A significant increase in the surface of extravasated skin is seen 5 and 10 weeks postoperatively, which decreases to sham values over time (:p <0.05; ***p <0.001; One-way ANOVA).*

3.4.4. Denervation and re-innervation of intra-epidermal nerve fibers

The peripheral nociceptive sensory system can be divided into 3 classes; the unmyelinated peptidergic (CGRP-IR, SubP-IR), the unmyelinated non-peptidergic (P2X3-IR), and the myelinated peptidergic (NF200-IR) nerve fibers. These fibers all terminate with free nerve endings in the epidermis and constitute the IENFs.

The density of the IENFs was quantified in selected regions of the medial, central and lateral part of the glabrous skin of non-footpad and footpad at both proximal and distal planes of the hind paw. Furthermore, the density of nerve fibers in the upper dermis were quantified. However, these data is not shown as no significant changes were obtained when compared to the IENFs.

The results of our immunohistochemical testing provide, for the first time, a complete overview of the time course of sensory nerve fiber regeneration in large skin biopsies of the operated hind paw following end-to-end reconstruction.

3.4.5. PGP9.5 immunoreactive fibers

As a pan-neuronal marker, PGP9.5 stains all nerve fibers in the skin without any distinction in the various subgroups of sensory nerve fibers. No significant difference in the density of PGP9.5-immunoreactive (IR) nerve endings was observed between the epidermis of the non-footpad area and the lateral footpad in the sham-operated rats. Five weeks after lesion and subsequent reconstruction, a serious depletion of IENFs had occurred at all investigated regions ($p<0.001$). Density of fibers was highest at the medial aspects of the glabrous skin (Figure 6). Whereas an increase in density of all regions was noted at longer postoperative times, the density did not reach control values in the non-footpad areas. In contrast, the significant decrease in density of IENFs in the lateral footpad was only noted 5 and 10 weeks postoperatively, but these values returned to control levels at 20 and 30 weeks (Figures 6A,B).

The largest expansion in the number of epidermal PGP9.5-IR nerve fibers was seen between 5 and 10 weeks postoperatively ($p<0,001$) in both non-footpad and footpad areas, while only a slight, non-significant, additional increase was seen between weeks 20 and 30. This finding shows an early and fast-velocity re-innervation process of PGP9.5-IR nerve fibers taking place between 5 and 10 weeks, with a slower and less pronounced addition of fibers that reach the epidermis at later stages.

Previous studies have shown that epidermal nerve fibers affect the skin cells such as the keratinocytes, which have been suggested to communicate with epidermal nerve fibers (28, 29) We quantified the epidermal thickness of both the non-footpad and the footpad area to see if the observed changes in the regeneration of IENFs after end-to-end reconstruction correlate with the thickness of the epidermis. Because we found significantly greater epidermal thickness in the footpad area (±130µm) than in the non-footpad areas (±50µm) of sham-operated

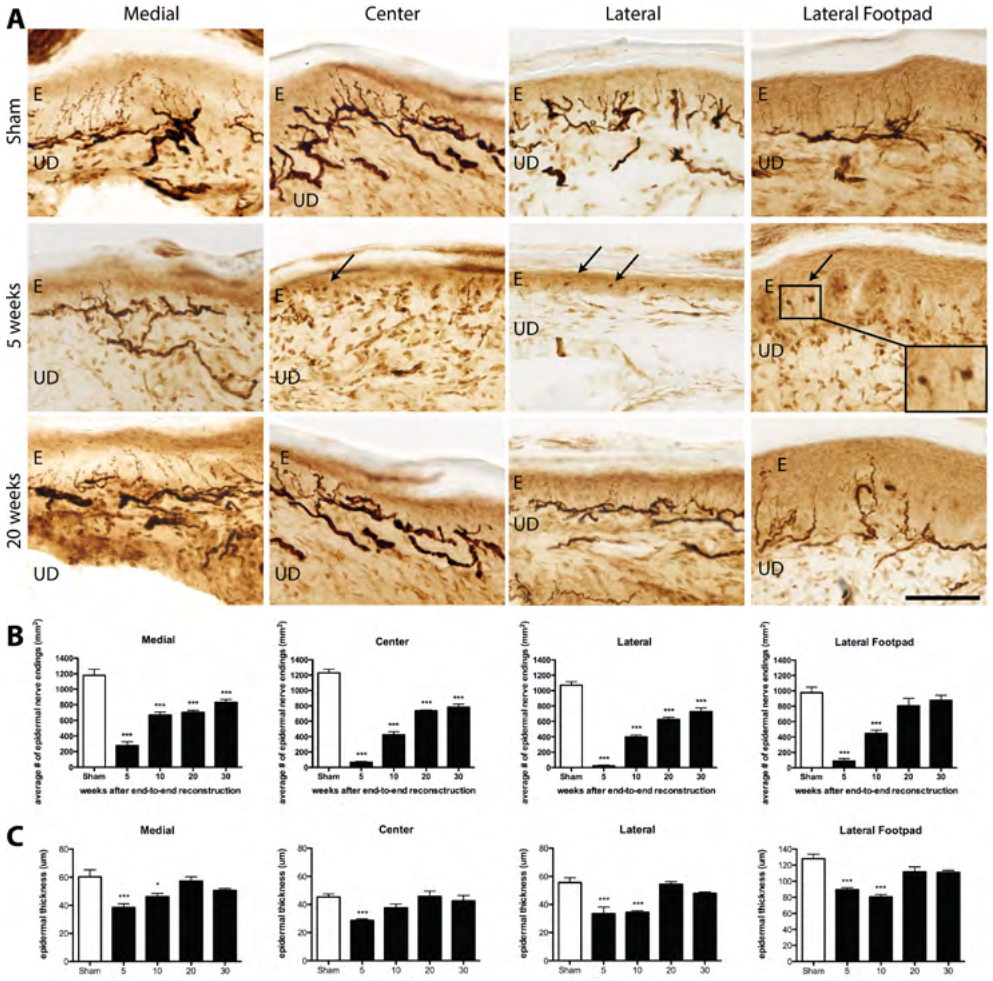

Figure 6. Histologic analysis of PGP9.5-IR nerve fibers, LCs and epidermal thickness of the operated plantar hind paw. Analysis was performed of samples obtained from the medial, center and lateral non-footpad areas and the lateral footpad area of the plantar hind paw.
A) Multilayered scans labeled for PGP9.5-IR nerve fibers of the epidermis and the upper dermis. Fewer nerve fibers are visible in the center and lateral epidermis and the upper dermis 5 weeks postoperatively in comparison with the sham-operated group. However, this diminishment is less clear at 20 weeks. The black arrows indicate LCs, which were incresed twofold in the lateral part of the skin 5 weeks postoperatively. E=epidermis; UD=upper dermis; Scale bar =100µm.
B) Histograms showing the average number of epidermal PGP9.5-IR fibers in all experimental groups. Note the significant decrease in PGP9.5-IR fibers in the non-footpad area at all time points postoperatively as compared with sham-operated rats. The footpad areas showed a significant decreased at 5 and 10 weeks, which recovered to sham levels 20 and 30 weeks.
C) Histograms showing the average epidermal thickness of the operated plantar hind paw. It is evident at 5 weeks that all the regions have a significantly thinner epidermis than that of the sham-operated group, which returns to sham levels at 20 and 30 weeks. Although not significant, a slight increase is seen at 20 weeks.

rats but no significant difference in the number of IENFs, a correlation between the density of nerve innervation and epidermal thickness could not be established (Figure 6C). However, after end-to-end reconstruction, the epidermal thickness was significantly reduced at 5 weeks of examination ($p<0,001$), and it increased to control values after 20 weeks, as the epidermis was re-innervated.

In addition to the effect of IENFs on epidermal thickness, denervation of the skin also affected the epithelial Langerhans cells (LCs). These cells can be recognized by their positive staining for PGP9.5 (20). Consistent with previous studies, LCs were rarely seen in sham-operated animals. However, after lesion induction and reconstruction, the decrease in epidermal nerve fibers was associated with the up regulation of LCs. Epithelial LCs increased significantly in the epidermis of the denervated center and lateral areas of the non-footpad area and even more in the footpads. As the skin was re-innervated, the number of LCs decreased and reached control values for the non-footpad area and remains up regulated for in the footpads (Figure 6D).

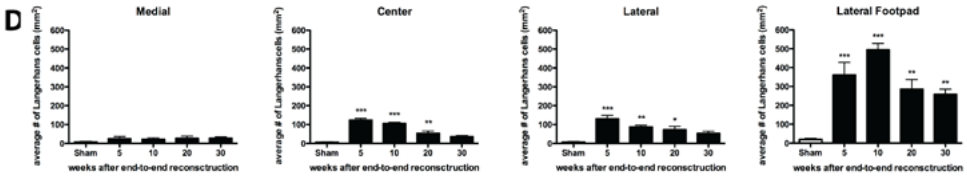

*Figure 6D. Histograms showing the average number of LCs in the epidermis. A significant increase in the number of LCs in the center and lateral parts of the plantar hind paw is seen up to 20 weeks postoperatively in comparison with sham-operated rats. However, at all time points after end-to-end reconstruction, the LCs remained significantly increased. *p < 0.05; **p < 0.01; and ***p < 0.001; One-way ANOVA).*

3.4.6. Peptidergic fibers

Although not significant, the density of epidermal CGRP-IR nerve fibers in the footpad area was smaller than it was in the non-footpad area in sham-operated rats. Five weeks postoperatively, a decrease in CGRP-IR nerve fibers was seen in all quantified parts of the hind paw of surgically treated rats compared with controls. However, the decrease was significant only in the lateral part of the hind paw ($p < 0.001$) (Figure 7). This would be in accordance with potential collateral sprouting of the intact saphenous nerve to the medial and center hind paw regions as suggested by the Evans Blue extravasation experiments (Figures 5A,B).

Striking results are seen 20 weeks postoperatively: all areas of the glabrous skin, except the medial area, showed a significant increase in the density of CGRP-IR nerve fibers (reaching densities of over 600 terminal fibers/mm^2) in the epidermis not only in comparison with 5- and 10-week results, but also with results observed in controls. However, at 30 weeks postoperatively, the density of CGRP-IR epidermal fibers recovered to a level that was comparable to that seen in sham-operated rats (400 /mm2) (Figure 7).

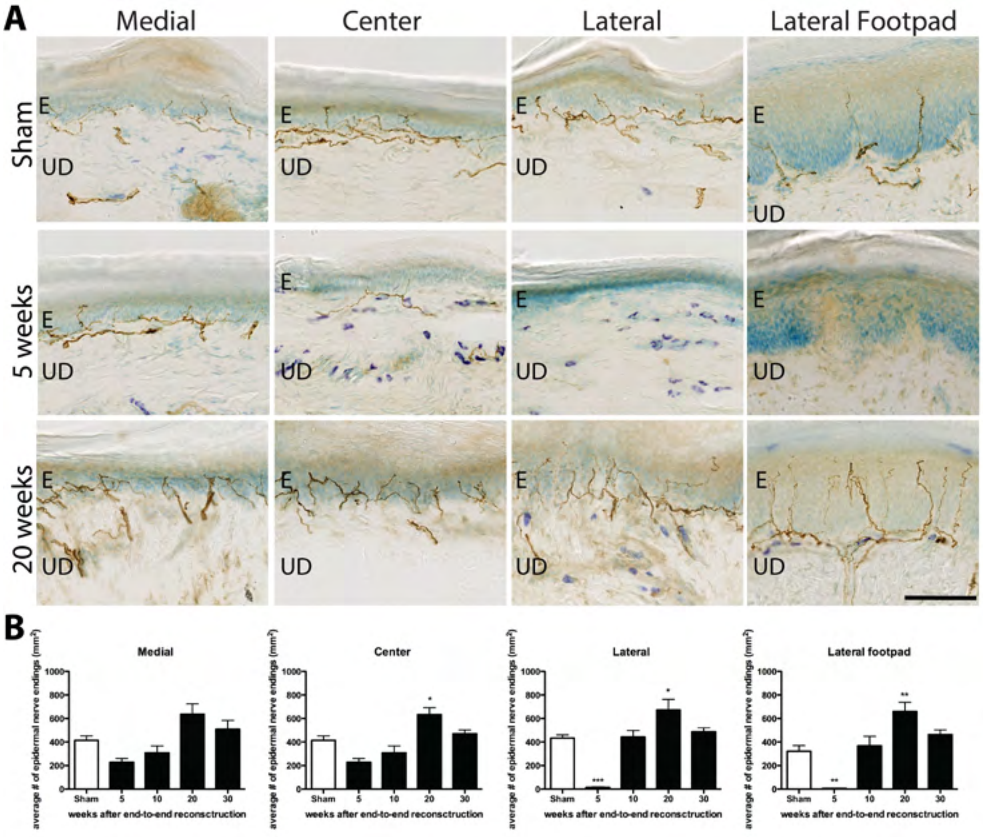

Figure 7. Histological analysis of CGRP-IR nerve fibers. Analysis was performed of samples obtained from the medial, center, and lateral non-footpad areas and the lateral footpad area of the plantar hind paw.
A) Multilayered scans labeled for CGRP-IR fibers in the epidermis and the upper dermis of the plantar hind paw showing almost no fibers in the center and lateral part of the skin 5 weeks PO. At 20 weeks PO a larger quantity of CGRP-IR nerve fibers is visible in comparison with sham-operated animals. E = epidermis; UD = upper dermis. Scale bar = 100 μm.
*B) Histograms showing the number of epidermal peptidergic CGRP-IR fibers in all experimental groups. A significant decrease in CGRP-IR fiber density was exclusively seen in the lateral part of both the footpad and non-footpad 5 weeks postoperatively compared with sham-operated rats. However, the epidermal CGRP-IR fiber density reached its peak at 20 weeks and returned to sham values at 30 weeks. *p < 0.05; **p < 0.01; and ***p < 0.001; One-way ANOVA).*

The epidermal SubP-IR fiber density was significantly lower in the footpad area than in the non-footpad areas in the sham-operated rats ($p < 0.05$). A decrease in epidermal SubP-IR nerve fibers was seen in all areas of the plantar hind paw at 5 weeks postoperatively. Similar to CGRP-IR fibers, a conspicuous increase in epidermal SubP-IR fibers was documented at 20 weeks, which reached control levels at 30 weeks (Figure 8).

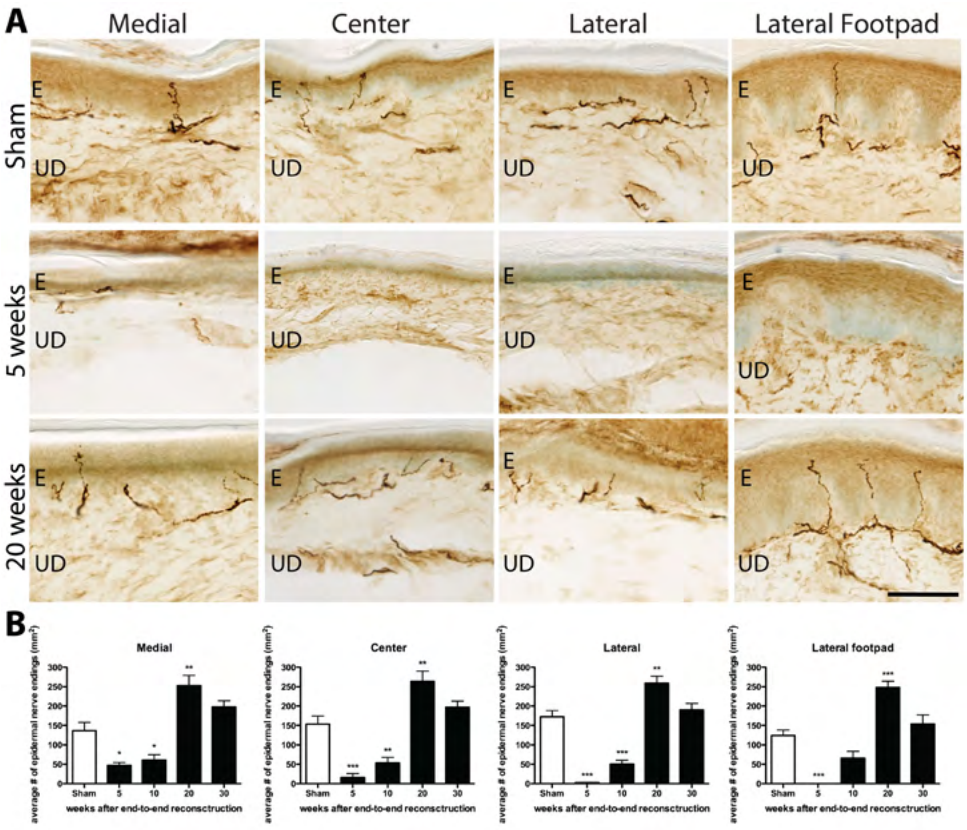

Figure 8. Histological analysis of SubP-IR nerve fibers. Analysis was performed of samples obtained from the medial, center, and lateral non-footpad areas and the lateral footpad area of the plantar hind paw. A: Multilayered scans labeled for SubP-IR fibers in the epidermis and the upper dermis of the hind paw showing an almost empty epidermis and upper dermis 5 weeks postoperatively, which is reinnervated at 20 weeks. E = epidermis UD = upper dermis. Scale bar = 100 μm.

*B) Histograms showing the number of epidermal peptidergic SubP-IR fibers in all experimental groups. Note the significant decrease in epidermal SubP-IR fiber density in the entire plantar hind paw 5 weeks postoperatively compared with sham-operated rats. After reaching a peak at 20 weeks, the SubP-IR fiber density recovers to sham-operated levels. *p < 0.05; **p < 0.01; and ***p < 0.001; One-way ANOVA).*

NF200 stains both the nociceptive and non-nociceptive myelinated fibers (8). As such, NF200 staining is not specific for nociception only. In addition, myelinated fibers lose their myelin and Schwann cell sheets when they penetrate the epidermis. Therefore, NF200-IR nerve fibers could only be determined in the upper dermis (27, 30).

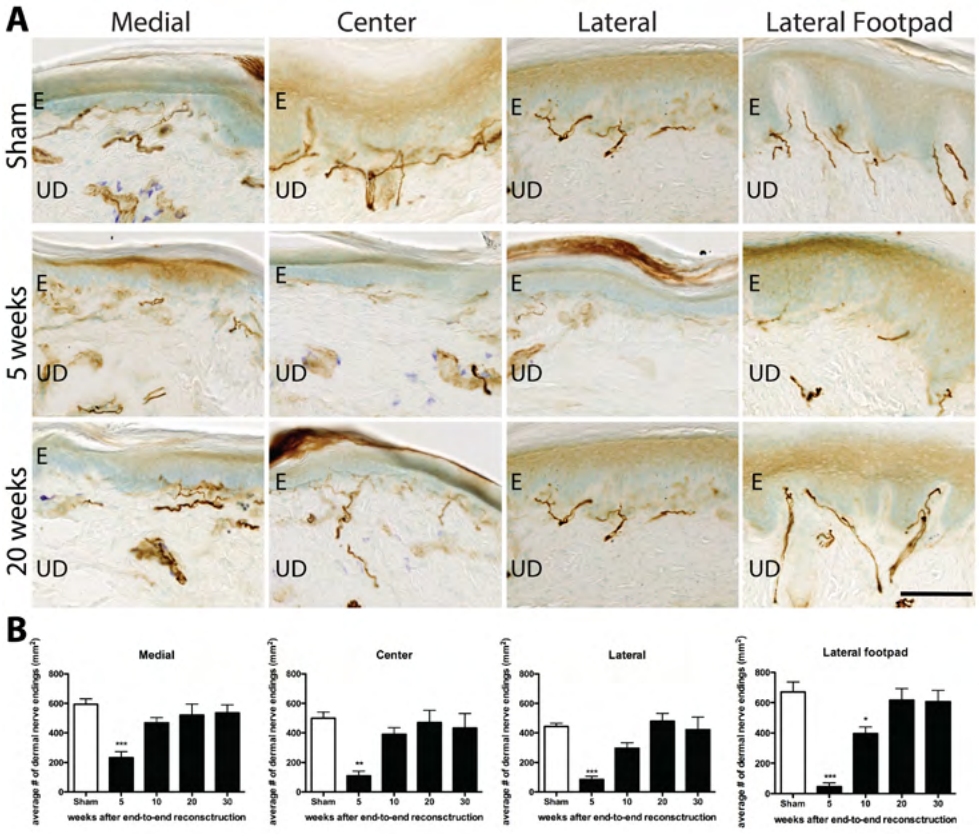

Figure 9. Histological analysis of NF200-IR nerve fibers. Analysis was performed of samples obtained from the medial, center, and lateral non-footpad areas and the lateral footpad area of the plantar hind paw.
A) Multilayered scans labeled for NF200-IR fibers in the epidermis and the upper dermis of the foot sole showing that NF200-IR fibers are exclusively visible in the upper dermis. Fewer NF200-IR fibers are visible in all regions of the hind paw 5 weeks postoperatively, while these fibers are clearly apparent at 20 weeks. E = epidermis; UD = upper dermis. Scale bar = 100 μm.
*B) Histograms showing the number of epidermal peptidergic NF200-IR fibers of all experimental groups. A significant decrease in epidermal NF200-IR fiber density is seen in the entire glabrous foot sole 5 weeks postoperatively as compared with sham-operated rats. The NF200-IR fiber density reaches sham values in the non-footpad areas at 10 weeks and in the lateral footpad at 20 weeks. *p < 0.05; **p < 0.01; and ***p < 0.001; One-way ANOVA).*

Despite the inability to quantify fibers in the epidermis, dermal NF-200-IR fibers were significantly diminished 5 weeks postoperatively in medial, central, and lateral regions of the hind paw ($p < 0.001$; $p < 0.0001$) (Figure 9). Similar to the peptidergic CGRP-IR and SubP-IR fiber densities, NF200-IR fiber density followed a gradual increase and reached the control value at 10 weeks in the non-footpad area and at 20 weeks in the lateral footpad (Figure 9)

3.4.7. Non-peptidergic fibers

The epidermis of sham-operated rats was predominantly innervated by nonpeptidergic P2X 3–IR nerve fibers (± 800 /mm2). Non-footpad areas contained a significantly ($p < 0.001$) higher density of nonpeptidergic epidermal P2X3–IR nerve fibers than did the footpad area.9 Although the number of epidermal P2X3–IR nerve fibers increased after 5 weeks postoperatively, it never reached control levels ($p < 0.001$); indeed, it never exceeded more than half the density of that of sham-operated rats (Figure 10).

3.5.0. Discussion

The main aim of the present study was twofold: to describe the long-term spatial changes in epidermal innervation following sectioning and immediate end-toend reconstruction of the sciatic nerve and to relate these changes to the development of neuropathic pain. The following key observations were made: 1) the initial denervation of the glabrous skin of the hind paw was followed by a transient innervation by sprouting fibers from the undamaged saphenous nerve; and 2) a thermal hypersensitivity noted at 20 weeks postoperatively coincided with a transiently increased density of peptidergic fibers, which mainly originate from newly arriving fibers from the reconstructed nerve.

Since previous studies showed no significant age-related differences in withdrawal latency to hot temperatures (31) and mechanical stimuli (32) in adult rats, the end point of sham-operated rats was determined at 5 weeks postoperatively. In addition, as part of unpublished experiments, we have examined 3 sham-operated rats for behavioral but mainly for possible age-related changes in histological data at 30 weeks postoperatively. Consistent with pervious findings, no differences were found in behavioral data. Although a study showed changes in withdrawal latency for cold plate test using aging rats of 35 months old (33), we could not find any significant differences in sham-operated animals between 5 and 30 weeks of follow-up. This discrepancy may be ascribed to the shorter follow-up in the present study. Moreover, we could not find any age-related differences in the density of IENFs nor in the CMAP amplitude when compared with sham-operated rats at 5 weeks (data not shown). Therefore, behavioral and histological data as presented in the current study contain 5-week follow-up data of sham-operated rats.

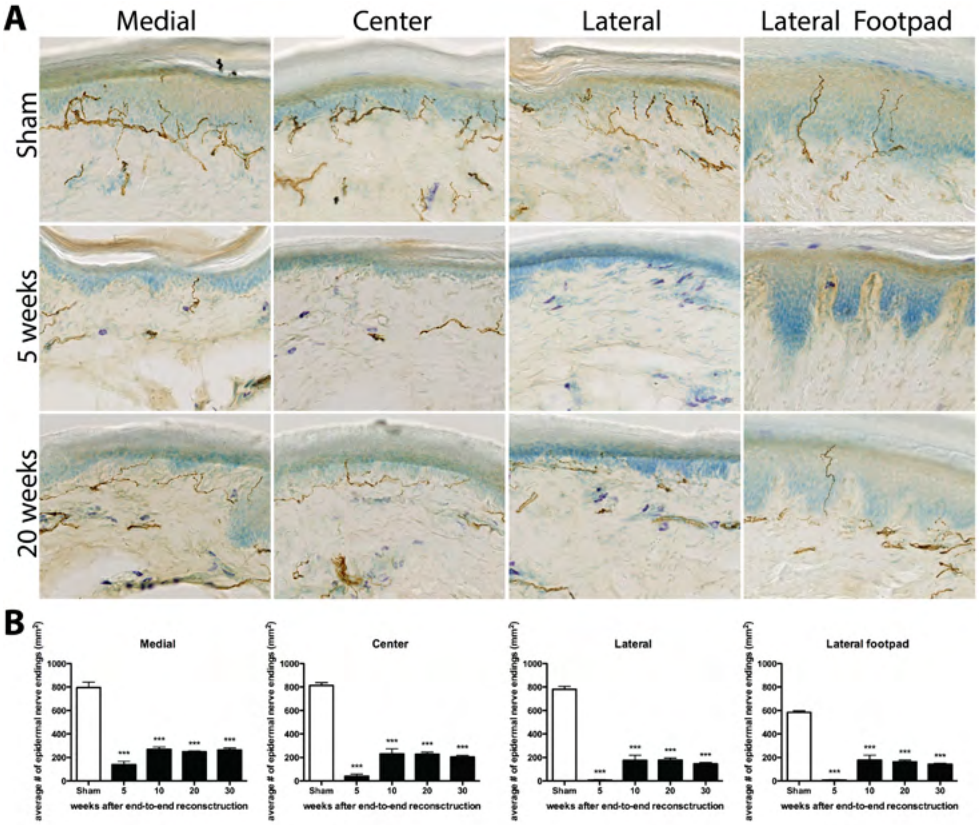

Figure 10. Histologic analysis of P2X3-IR nerve fibers. Analysis was performed of samples obtained from the medial, center, and lateral non-footpad areas area and the lateral footpad area of the plantar hind paw.
*A) Multilayered scans labeled for P2X3–IR fibers in the epidermis and the upper dermis of the foot sole showing evidently less nerve fibers 5 and 20 weeks postoperatively as compared with sham-operated rats. E = epidermis; UD = upper dermis. Scale bar = 100 µm. B: Histograms showing the number of epidermal nonpeptidergic P2X3–IR fibers of all experimental groups. Note that the dramatic and permanent decrease in epidermal P2X3–IR fiber density at all time points after end-to-end reconstruction compared with sham-operated rats. ***p < 0.001; One-way ANOVA).*

3.5.1. Dynamic innervation of the hind paw by undamaged nerve fibers

A response failure to both the pinprick test and von Frey test was demonstrated in the lateral glabrous skin at 2, 3, and 5 weeks postoperatively. This finding, along with the near absence of nerve fibers in the skin biopsies of the lateral operated hind paw 5 weeks postoperatively, indicates the denervation of the glabrous skin. The medial part of the glabrous hind paw was initially (at 2 weeks postoperatively) not responsive to mechanical stimuli due to denervation of the skin. At 3 and 5 weeks, von Frey responses at the medial region of the glabrous skin were comparable to

those in controls, suggesting initiation of collateral sprouting by the undamaged saphenous nerve. In favor of this latter observation, the glabrous skin on the medial and, to some extent, central aspects of the hind paw, normally also supplied by the sciatic nerve, contained many nerve fibers 5 weeks postoperatively. A similar conclusion, drawn from using a nociceptive pinprick test, was made in a recent study by Cobianchi et al (13). However, we were able to demonstrate that these fibers were derived from the nonlesioned saphenous nerve by using a newly adapted Evans blue extravasation technique (34). The collateral sprouting of nerve fibers toward the center of the hind paw predominantly involved peptidergic fibers as was demonstrated by the 5-weeks histological results of the skin biopsies.

Collateral sprouting has often been correlated with neuropathic pain in other peripheral nerve injury models (27, 35-37). In contrast to these studies, no obvious features of neuropathic pain could be observed in the present end-to-end reconstruction model at 5 weeks postoperatively, when collateral innervation was most prominent. This is in accordance with the clinical dogma that immediate and careful reconstruction of transected nerve, despite the invasion of fibers from undamaged neighboring nerves, can prevent persistent neuropathic pain of the affected skin. Presently, however, it is unclear how this mechanism works.

Moreover, using the Evans blue technique, we showed a withdrawal of the extraterritorial saphenous nerve as the sciatic nerve regeneration proceeded throughout the longer follow-up period (i.e., 20 and 30 weeks postoperatively). In addition, in the current study with it longer follow-up, the greatest increase in the density of IENFs was observed between 10 and 20 weeks. These insights have important implications for future research in the regeneration of the sciatic nerve, underscoring the importance of a minimum follow-up of at least 20 weeks.

Based on these results, we conclude that end-to-end reconstruction can successfully prevent the occurrence of neuropathic pain but also that it reduces the chance that alien fibers can obtain a permanent foothold in the denervated skin.

3.5.2. Thermal hypersensitivity correlated to peptidergic epidermal nerve fibers

As the sciatic nerve regenerated, mechanical and thermal hypersensitivity of the affected skin was observed at 10 and 20 weeks postoperatively, respectively. The different time points for mechanical hypersensitivity and thermal hypersensitivity after nerve injury could be related to differences in threshold, or speed of nerve outgrowth of the regenerating sensory fibers. Although we did not observe a correlation between mechanical hypersensitivity and the density of reinnervated fibers by specific subgroups of sensory nerve fibers, such a correlation was established in a recent study by Duraku et al (7). This discrepancy can be ascribed to differences in the experimental model that was applied. While Duraku et al. ligated the nerve proximal from the nerve injury, thereby preventing nerve regeneration (7), we examined actively regenerating axons following end-to-end reconstruction of the nerve.

Remarkably, some disparity is shown between the density of skin innervation and behavioral data 5 weeks postoperatively. Even with the contribution of the saphenous nerve afferent sprouting, as shown using the Evans blue extravasation technique, a 75% loss of innervation was demonstrated at the medial aspect of the glabrous skin (PGP9.5-IR positive fibers), yet no sensory deficits were observed. However, a more than 90% decrease in IENFs was seen on the lateral aspect of the glabrous hind paw. The more pronounced decrease in skin innervation corresponds with mechanical hyposensitivity. Based on these findings, we suggest that a possible threshold for the density of IENFs needs to be reached to cause changes in sensitivity. This phenomenon was in part shown by Verdu and Navarro (38).

Another explanation would be that the collateral sprouted nerve fibers have different features than regenerating nerve fibers. This notion is supported by the observation of normal responses to the von Frey test, while decreased IENF density was demonstrated in the collateral sprouted skin area compared with sham-operated rats in the spared nerve injury model (7). Therefore, we believe that after withdrawal of collateral sprouted nerve fibers (after 5 weeks postoperatively), the relation between behavioral and histological data is more evident. This is confirmed by the finding of thermal hypersensitivity, which correlated well with the hyperinnervation by peptidergic epidermal nerve fibers noted at 20 weeks postoperatively. A time point in which the sciatic nerve is regenerated—as shown by increased density of IENFs in the skin and the collateral sprouting—is absent, as demonstrated by withdrawal of Evans blue extravasation area. Moreover, it has been demonstrated that specific temperature-sensitive transient receptor potential (TRP) channels are expressed on peptidergic fibers. These TRP channels were shown to become active at temperatures on the hot (50°C) and cold (5°C) plate tests, as performed in the present study (39, 40). Therefore, we propose that the increased density of epidermal peptidergic fibers results in thermal hypersensitivity. However, further research quantifying TRP channels by immunostaining or electrophysiological determination of activated TRP channels at 20 weeks postoperatively will be required to support our proposition.

These increased peptidergic fibers are likely to be derived from regenerating sciatic nerve fibers as the sprouting fibers from the saphenous nerve have retracted at 20 weeks postoperatively, when thermal hypersensitivity and enhanced density of peptidergic fibers are demonstrated. Because the innervation density of the myelinated peptidergic fibers was not enhanced with respect to control levels, we suggest that the thermal hypersensitivity was specifically related to the increased density of the unmyelinated peptidergic fibers seen at 20 weeks. It should be noted that the density of myelinated peptidergic fibers could be assessed in the upper dermis.

Because of the long follow-up period in the present study in contrast to that in other studies (12, 13), our results suggest that a complete recovery of both the mechanical and thermal hypersensitivity, as well as of the density of

epidermal peptidergic fibers to control levels, is eventually achieved. We conclude that no features of neuropathic pain can be observed 30 weeks after end-to-end reconstruction of the sciatic nerve, nor are they expected to appear at longer survival times.

3.5.3. Changed composition in IENFs following end-to-end reconstruction

It was remarkable to note the contrasting regeneration pattern in the two populations of epidermal nerve fibers: The peptidergic epidermal fibers gradually increased and recovered to control levels 30 weeks postoperatively, whereas the nonpeptidergic epidermal nerve fibers, as assessed by P2X3-IR (27), remained significantly diminished at all experimental time points after end-to-end reconstruction. The anatomical and functional differences of these two subtypes of sensory fibers in the dorsal root ganglion suggest separate regeneration pathways and possibly, therefore, a slower regeneration of nonpeptidergic fibers compared with peptidergic fibers. The peptidergic fibers terminate predominantly in lamina I and outer lamina II of the dorsal horn, whereas the nonpeptidergic population terminates in inner lamina II (41). Moreover, the peptidergic and the non-peptidergic fibers are promoted by different neurotrophic factors: NGF induces peptidergic outgrowth whereas GDNF promotes non-peptidergic regeneration (42, 43). These findings, along with the demonstrated shift from mainly non-peptidergic epidermal fibers in sham-operated footpad to predominately peptidergic fibers in end-to-end reconstructed footpad, supports our proposition of separate regeneration pathways. Although an increased expression of GDNF is demonstrated at the site of peripheral nerve injury (44), the epidermal non-peptidergic fibers remain diminished in the present study. It is has been shown that local administration of GDNF after peripheral nerve injury vanquishes the features of neuropathic pain (45) and results in an increased expression of non-peptidergic fibers in the DRG (46). These observations could suggest that the released GDNF in the periphery might be affected after injury of the nerve. However, we have not been able to find any previously published data on the regeneration pattern of epidermal nonpeptidergic fibers after local GDNF application. Thus, although a relation between GDNF and nonpeptidergic fibers seems obvious, the nature of this relation is unclear.

Because previous studies have shown no significant age-related differences in withdrawal latency to thermal (47) and mechanical (48) stimuli in adult rats, the end-point of sham-operated rats was determined at 5 weeks postoperatively. In addition, as part of unpublished experiments, we examined 3 sham-operated rats mainly for possible age-related changes in histological data, as well as behavioral changes, at 30 weeks postoperatively. Consistent with previous findings, we found no differences in behavioral data. Moreover, we found no age-related differences in the density of IENFs or in the CMAP amplitudes when comparing experimental sham-operated rats at 5 weeks (data not shown). Therefore, behavioral and histological data as presented in the current study reflect 5-week follow-up findings of sham-operated rats.

3.5.4. Langerhans Cells

Behavioral studies using various models of nerve injury-induced neuropathic pain suggest a relation between the density of PGP9.5-positive LCs and the occurrence of neuropathic pain (7, 49). However, these models cold not distinguish between regeneration of nerve fibers and the expression of neuropathic pain. Thus, the present study in which transient neuropathic pain features were present after end-to-end reconstruction might offer a more promising model with which to study this correlation. Although we found an enhanced LC density, a correlation with the period of hypersensitivity could not be established. Furthermore, enhanced density of LCs was demonstrated only at the central and lateral plantar hind paw, areas that showed more dramatic denervation compared with the medial portion of the hind paw. Combining these findings with the observation that LC density decreased once the skin was reinnervated at 30 weeks suggests a role for LCs in regeneration rather than pain. It should be noted that although a slight decrease in density was seen at 30 weeks, the density of LCs in the footpad remained increased compared with sham-operated animals. This may possibly involve increased of LCs migrating to the epidermis from deeper parts of the skin in reaction to nerve injury (50). The twofold thicker epidermis of the footpad, as compared to non-footpad areas, may result in longer migration time and therefore increased expression of LCs in the epidermal footpad up to 30 weeks postoperatively. The precise role of LCs in nerve regeneration remains to be determined.

3.5.5. Motor recovery

To compare the speed of recovery of skin sensitivity by myelinated and nonmyelinated fibers with that of the heavily myelinated Type 1α motor fibers, we studied the rate of recovery of motor function. We observed a gradual increase in CMAP amplitude, showing the effect of the ongoing regenerative process, which recovered to control levels 30 weeks postoperatively. These results are in agreement with previous electromyography findings reported by Korte et al., who suggested that a progressive and full functional motor recovery is possible after a correctly performed end-to-end reconstruction (51).

3.6.0. Conclusions

Peripheral nerve injury followed by end-to-end reconstruction results in a dynamic reinnervation of the denervated skin. Transiently invading fibers from the adjacent undamaged nerve are gradually replaced by an ingrowth of fibers from the reconstructed nerve. Moreover, the regenerative process results in a nonhomogeneous reinnervation of the epidermis by different subgroups of IENFs after end-to-end reconstruction, which does not cause long-lasting neuropathic pain. Furthermore, the present study demonstrated a role for epidermal peptidergic nerve fibers in thermal hypersensitivity following end-to-end reconstruction, and therefore these nerve fibers seem to be a suitable target for analgesics.

3.7.0. References

1. Siemionow M, Brzezicki G. Chapter 8: Current techniques and concepts in peripheral nerve repair. Int Rev Neurobiol. 2009;87:141-72.
2. Treede RD, Jensen TS, Campbell JN, Cruccu G, Dostrovsky JO, Griffin JW, et al. Neuropathic pain: redefinition and a grading system for clinical and research purposes. Neurology. 2008 Apr 29;70(18):1630-5.
3. Novak CB, Anastakis DJ, Beaton DE, Mackinnon SE, Katz J. Biomedical and psychosocial factors associated with disability after peripheral nerve injury. J Bone Joint Surg Am. 2011 May 18;93(10):929-36.
4. Dubuisson AS, Kline DG. Brachial plexus injury: a survey of 100 consecutive cases from a single service. Neurosurgery. 2002 Sep;51(3):673-82; discussion 82-3.
5. Oaklander AL, Siegel SM. Cutaneous innervation: form and function. J Am Acad Dermatol. 2005 Dec;53(6):1027-37.
6. Lauria G, Lombardi R, Camozzi F, Devigili G. Skin biopsy for the diagnosis of peripheral neuropathy. Histopathology. 2009 Feb;54(3):273-85.
7. Duraku LS, Hossaini M, Schuttenhelm BN, Holstege JC, Baas M, Ruigrok TJ, et al. Re-innervation patterns by peptidergic Substance-P, non-peptidergic P2X3, and myelinated NF-200 nerve fibers in epidermis and dermis of rats with neuropathic pain. Exp Neurol. 2013 Mar;241:13-24.
8. Ruscheweyh R, Forsthuber L, Schoffnegger D, Sandkuhler J. Modification of classical neurochemical markers in identified primary afferent neurons with Abeta-, Adelta-, and C-fibers after chronic constriction injury in mice. J Comp Neurol. 2007 May 10;502(2):325-36.
9. Mellgren SI, Nolano M, Sommer C. The cutaneous nerve biopsy: technical aspects, indications, and contribution. Handb Clin Neurol. 2013;115:171-88.
10. Duraku LS, Hossaini M, Hoendervangers S, Falke LL, Kambiz S, Mudera VC, et al. Spatiotemporal dynamics of re-innervation and hyperinnervation patterns by uninjured CGRP fibers in the rat foot sole epidermis after nerve injury. Mol Pain. 2012;8:61.
11. Varitimidis SE, Sotereanos DG. Partial nerve injuries in the upper extremity. Hand Clin. 2000 Feb;16(1):141-9.
12. Stankovic N, Johansson O, Hildebrand C. Occurrence of epidermal nerve endings in glabrous and hairy skin of the rat foot after sciatic nerve regeneration. Cell Tissue Res. 1996 Apr;284(1):161-6.
13. Cobianchi S, de Cruz J, Navarro X. Assessment of sensory thresholds and nociceptive fiber growth after sciatic nerve injury reveals the differential contribution of collateral reinnervation and nerve regeneration to neuropathic pain. Exp Neurol. 2014 Feb 16;255C:1-11.
14. Nixon BJ, Doucette R, Jackson PC, Diamond J. Impulse activity evokes precocious sprouting of nociceptive nerves into denervated skin. Somatosens Res. 1984;2(2):97-126.

15. Kovacic U, Sketelj J, Bajrovic FF. Sex-related difference in collateral sprouting of nociceptive axons after peripheral nerve injury in the rat. Exp Neurol. 2003 Nov;184(1):479-88.
16. Jasmin L, Kohan L, Franssen M, Janni G, Goff JR. The cold plate as a test of nociceptive behaviors: description and application to the study of chronic neuropathic and inflammatory pain models. Pain. 1998 Apr;75(2-3):367-82.
17. Eddy NB, Leimbach D. Synthetic analgesics. II. Dithienylbutenyl- and dithienylbutylamines. J Pharmacol Exp Ther. 1953 Mar;107(3):385-93.
18. Werdin F, Grussinger H, Jaminet P, Kraus A, Manoli T, Danker T, et al. An improved electrophysiological method to study peripheral nerve regeneration in rats. J Neurosci Methods. 2009 Aug 30;182(1):71-7.
19. Nijhuis TH, Smits ES, van Neck JW, Visser GH, Walbeehm ET, Blok JH, et al. Ultrasound-guided needle positioning near the sciatic nerve to elicit compound muscle action potentials from the gastrocnemius muscle of the rat. J Neurosci Methods. 2011 Jan 15;194(2):283-6.
20. Shin RH, Vathana T, Giessler GA, Friedrich PF, Bishop AT, Shin AY. Isometric tetanic force measurement method of the tibialis anterior in the rat. Microsurgery. 2008;28(6):452-7.
21. Gonzalez HL, Carmichael N, Dostrovsky JO, Charlton MP. Evaluation of the time course of plasma extravasation in the skin by digital image analysis. J Pain. 2005 Oct;6(10):681-8.
22. Kambiz S, Baas M, Duraku LS, Kerver AL, Koning AH, Walbeehm ET, et al. Innervation mapping of the hind paw of the rat using Evans Blue extravasation, Optical Surface Mapping and CASAM. J Neurosci Methods. 2014 May 30;229:15-27.
23. Kerver AL, van der Ham AC, Theeuwes HP, Eilers PH, Poublon AR, Kerver AJ, et al. The surgical anatomy of the small saphenous vein and adjacent nerves in relation to endovenous thermal ablation. J Vasc Surg. 2012 Jul;56(1):181-8.
24. Hopman AH, Ramaekers FC, Speel EJ. Rapid synthesis of biotin-, digoxigenin-, trinitrophenyl-, and fluorochrome-labeled tyramides and their application for In situ hybridization using CARD amplification. J Histochem Cytochem. 1998 Jun;46(6):771-7.
25. Kuhlmann WD, Peschke P. Glucose oxidase as label in histological immunoassays with enzyme-amplification in a two-step technique: coimmobilized horseradish peroxidase as secondary system enzyme for chromogen oxidation. Histochemistry. 1986;85(1):13-7.
26. Zylka MJ, Rice FL, Anderson DJ. Topographically distinct epidermal nociceptive circuits revealed by axonal tracers targeted to Mrgprd. Neuron. 2005 Jan 6;45(1):17-25.
27. Peleshok JC, Ribeiro-da-Silva A. Delayed reinnervation by nonpeptidergic nociceptive afferents of the glabrous skin of the rat hindpaw in a neuropathic pain model. J Comp Neurol. 2011 Jan 1;519(1):49-63.
28. Li Y, Hsieh ST, Chien HF, Zhang X, McArthur JC, Griffin JW. Sensory and

denervation influence epidermal thickness in rat foot glabrous skin. Exp Neurol. 1997 Oct;147(2):452-62.
29. Chiang HY, Huang IT, Chen WP, Chien HF, Shun CT, Chang YC, et al. Regional difference in epidermal thinning after skin denervation. Exp Neurol. 1998 Nov;154(1):137-45.
30. Lauria G, Borgna M, Morbin M, Lombardi R, Mazzoleni G, Sghirlanzoni A, et al. Tubule and neurofilament immunoreactivity in human hairy skin: markers for intraepidermal nerve fibers. Muscle Nerve. 2004 Sep;30(3):310-6.
31. Rowe WB, Spreekmeester E, Meaney MJ, Quirion R, Rochford J. Reactivity to novelty in cognitively-impaired and cognitively-unimpaired aged rats and young rats. Neuroscience. 1998 Apr;83(3):669-80.
32. Taguchi T, Ota H, Matsuda T, Murase S, Mizumura K. Cutaneous C-fiber nociceptor responses and nociceptive behaviors in aged Sprague-Dawley rats. Pain. 2010 Dec;151(3):771-82.
33. Yezierski RP, King CD, Morgan D, Carter CS, Vierck CJ. Effects of age on thermal sensitivity in the rat. J Gerontol A Biol Sci Med Sci. 2010 Apr;65(4):353-62.
34. Kambiz S, Baas M, Duraku LS, Kerver AL, Koning AH, Walbeehm ET, et al. Innervation mapping of the hind paw of the rat using Evans Blue extravasation, Optical Surface Mapping and CASAM. J Neurosci Methods. 2014 Apr 8;229C:15-27.
35. Kim HJ, Na HS, Sung B, Nam HJ, Chung YJ, Hong SK. Is sympathetic sprouting in the dorsal root ganglia responsible for the production of neuropathic pain in a rat model? Neurosci Lett. 1999 Jul 9;269(2):103-6.
36. Shinder V, Govrin-Lippmann R, Cohen S, Belenky M, Ilin P, Fried K, et al. Structural basis of sympathetic-sensory coupling in rat and human dorsal root ganglia following peripheral nerve injury. J Neurocytol. 1999 Sep;28(9):743-61.
37. Zhang JM, Strong JA. Recent evidence for activity-dependent initiation of sympathetic sprouting and neuropathic pain. Sheng Li Xue Bao. 2008 Oct 25;60(5):617-27.
38. Verdu E, Navarro X. Comparison of immunohistochemical and functional reinnervation of skin and muscle after peripheral nerve injury. Exp Neurol. 1997 Jul;146(1):187-98.
39. Alenmyr L, Herrmann A, Hogestatt ED, Greiff L, Zygmunt PM. TRPV1 and TRPA1 stimulation induces MUC5B secretion in the human nasal airway in vivo. Clin Physiol Funct Imaging. 2011 Nov;31(6):435-44.
40. Cavanaugh DJ, Chesler AT, Braz JM, Shah NM, Julius D, Basbaum AI. Restriction of transient receptor potential vanilloid-1 to the peptidergic subset of primary afferent neurons follows its developmental downregulation in nonpeptidergic neurons. J Neurosci. 2011 Jul 13;31(28):10119-27.
41. Bradbury EJ, Burnstock G, McMahon SB. The expression of P2X3 purinoreceptors in sensory neurons: effects of axotomy and glial-derived neurotrophic factor. Mol Cell Neurosci. 1998 Nov;12(4-5):256-68.

42. Forrest SL, Keast JR. Expression of receptors for glial cell line-derived neurotrophic factor family ligands in sacral spinal cord reveals separate targets of pelvic afferent fibers. J Comp Neurol. 2008 Feb 20;506(6):989-1002.
43. Stucky CL, Lewin GR. Isolectin B(4)-positive and -negative nociceptors are functionally distinct. J Neurosci. 1999 Aug 1;19(15):6497-505.
44. Shakhbazau A, Martinez JA, Xu QG, Kawasoe J, van Minnen J, Midha R. Evidence for a systemic regulation of neurotrophin synthesis in response to peripheral nerve injury. J Neurochem. 2012 Aug;122(3):501-11.
45. Pezet S, Krzyzanowska A, Wong LF, Grist J, Mazarakis ND, Georgievska B, et al. Reversal of neurochemical changes and pain-related behavior in a model of neuropathic pain using modified lentiviral vectors expressing GDNF. Mol Ther. 2006 Jun;13(6):1101-9.
46. Tannemaat MR, Eggers R, Hendriks WT, de Ruiter GC, van Heerikhuize JJ, Pool CW, et al. Differential effects of lentiviral vector-mediated overexpression of nerve growth factor and glial cell line-derived neurotrophic factor on regenerating sensory and motor axons in the transected peripheral nerve. Eur J Neurosci. 2008 Oct;28(8):1467-79.
47. Sinis N, Horn F, Genchev B, Skouras E, Merkel D, Angelova SK, et al. Electrical stimulation of paralyzed vibrissal muscles reduces endplate reinnervation and does not promote motor recovery after facial nerve repair in rats. Ann Anat. 2009 Oct;191(4):356-70.
48. Sakakima H, Kawamata S, Kai S, Ozawa J, Matsuura N. Effects of short-term denervation and subsequent reinnervation on motor endplates and the soleus muscle in the rat. Arch Histol Cytol. 2000;63(5):495-506.
49. Lindenlaub T, Sommer C. Epidermal innervation density after partial sciatic nerve lesion and pain-related behavior in the rat. Acta Neuropathol. 2002 Aug;104(2):137-43.
50. Demarchez M, Asselineau D, Czernielewski J. Migration of Langerhans cells into human epidermis of "reconstructed" skin, normal skin, or healing skin, after grafting onto the nude mouse. J Invest Dermatol. 1993 May;100(5):648-52.
51. Korte N, Schenk HC, Grothe C, Tipold A, Haastert-Talini K. Evaluation of periodic electrodiagnostic measurements to monitor motor recovery after different peripheral nerve lesions in the rat. Muscle Nerve. 2011 Jul;44(1):63-73.

Chapter 4

Mirror-image pain after nerve reconstruction in rats is related to enhanced density of epidermal peptidergic nerve fibers

Shoista Kambiz, Elise M. Brakkee, Liron S. Duraku,
Steven E.R. Hovius, Tom J.H. Ruigrok, Erik T. Walbeehm

Experimenral Neurology 2015; 267:87-94

4.1.0. Abstract

Mirror-image pain is a phenomenon in which unprovoked pain is detected on the uninjured contralateral side after unilateral nerve injury. Although it has been implicated that enhanced production of nerve growth factor (NGF) in the contralateral dorsal root ganglion (DRG) is important in the development of mirror-image pain, it is not known if this is related to enhanced expression of nociceptive fibers in the contralateral skin.

Mechanical and thermal sensitivity in the contralateral hind paw was measured at four different time points (5, 10, 20 and 30 weeks) after transection and immediate end-to-end reconstruction of the sciatic nerve in rats. These findings were compared to the density of epidermal (peptidergic and non-peptidergic) nerve fibers on the contralateral hind paw.

Mechanical hypersensitivity of the contralateral hind paw was observed at 10 weeks postoperatively, a time point in which both subgroups of epidermal nerve fibers reached control values. Thermal hypersensitivity was observed with simultaneous increase in the density of epidermal peptidergic nerve fibers in the contralateral hind paw at 20 weeks. Both thermal sensitivity and the density of epidermal nerve fibers returned to control values 30 weeks postoperatively.
We conclude that changes in skin innervation and sensitivity are present on the uninjured corresponding side in a transient pain model. Therefore, the contralateral side cannot serve as control. Moreover, the current study confirms the involvement of the peripheral nervous system in the development of mirror-image pain.

4.2.0. Introduction

Contralateral pain, also known as mirror-image pain, is a mysterious phenomenon in which patients with trauma or inflammation of the ipsilateral side also feel pain at the non-injured contralateral side. Mirror-image pain after peripheral nerve injury has been suggested to evoke a time-dependent reorganisation of both the central and peripheral nervous system (1). In literature, central sensitization and spinal glia activation are still playing the leading role in current hypotheses of the potential underlying mechanism of mirror-image pain (1-4). Although these studies favor a mechanism that involves the central nervous system in development of mirror-image pain (5), a recent study has suggested an important role for the peripheral nervous system (6). These authors demonstrated that after peripheral nerve injury, Tumor Necrosis Factor a (TNF-a) produced in the DRG on the injured side diffuses via cerebrospinal fluid to the contralateral DRG where it activates satellite glia to produce NGF, which was supported by others (7, 8). It is one of the possible signaling mechanism, however, we cannot exclude neuronal and/or glial signaling pathways.

NGF is known to promote outgrowth and regeneration of the peptidergic subgroup of sensory nerve fibers (9). While these peptidergic nerve fibers contain

calcitonin gene-related peptide (CGRP), the remaining epidermal non-peptidergic sensory nerve fibers express the plant lectin isolectin B4 (IB4) and are promoted by glial cell line-derived neurotrophic factor (GDNF) (10).

Although mirror-image pain has been described as a persistent pain syndrome detected by nerve fibers in the skin (11), no data is available about contralateral changes in the two subgroups of epidermal sensory nerve fibers. The importance of distinction between subgroups of epidermal nerve fibers was demonstrated in an experimental peripheral nerve injury model in which the sciatic nerve was ligated and immediate end-to-end reconstruction was performed (12). This reconstruction is shown to result in transient ipsilateral pain that was related to increased density of epidermal peptidergic nerve fibers. However, as yet, it is unknown if this model also induces mirror-image pain. Therefore, in the current study, mirror-image pain is examined by determining the thermal and mechanical sensitivity in the contralateral hind paw after unilateral end-to-end reconstruction. Moreover, results from behavioral experiments are compared to the density of epidermal peptidergic and non-peptidergic nerve fibers to provide further insight of the correlation between mirror-image pain and subtypes of sensory epidermal nerve fibers.

4.3.0. Materials and methods

4.3.1. Animals and anaesthesia

Experiments were performed on adult female Lewis rats (n= 30), weighing between 180-200 gram. Animals were pair-housed in hooded cages at room temperature on a 12-hour light/dark schedule, and were given food ad libitum. All experiments were approved by the Dutch Ethical Committee on Animal Welfare (DEC) according to the European guidelines for the care and use of laboratory animals (Council Directive 86/6009/EEC).

4.3.2. Surgical procedure

Under isuflurane (3%) anesthesia, the left sciatic nerve of all 30 animals was exposed through a gluteal muscle-splitting approach using a surgical microscope (Zeiss OP-MI 6-SD; Carl Zeiss, Goettingen, Germany) as described previously (12). Subsequently, in 24 animals the sciatic nerve was transected by cutting the nerve with a sharp scissor proximal to its trifurcation. Transection was immediately followed by an epineural end-to-end reconstruction using six 10/0 Ethilon sutures. The remaining 6 animals served as control in which the sciatic nerve was only exposed without transection. The split muscle and skin of all animals were closed using Vicryl Rapide sutures. In all cases, postoperative analgesia was provided by subcutaneous administration of buprenorphine (0.05-0.1 mg/kg; Temgesic). Animals were monitored daily for signs of stress or discomfort.

4.3.3. Experimental groups

All end-to-end reconstructed animals were randomly divided into 4 groups consisting of 6 rats each. Different survival times (5, 10, 20 and 30 weeks after reconstruction) were allowed for each group. The remaining group consisted of the control (sham-operated) animals and was allowed a survival time of 5 weeks. The effect of lesion and its recovery was determined by various behavioral and physiological experiments and immunohistochemistry on the glabrous skin of the contralateral hind paw.
All functional and histological data are obtained from the contralateral hind paw after unilateral end-to-end reconstruction of the sciatic nerve or unilateral sham-operation.

4.3.4. Pin-prick test

The pin-prick test was used to estimate the advancement of the area demonstrating recovery of nociception (13, 14). The lateral and medial skin of the hind paw was pinched with a fine forceps starting distally at the toes and ascending up towards the ankle.

4.3.5. Von Frey test

The von Frey test was performed to determine the mechanical sensitivity threshold of the hind paw using a set of von Frey hairs ranging from 2 gram to 300 gram in a set of 16 filament steps. The rat was placed in a chamber with a mesh metal floor and each filament was indented for 4 seconds in the medial and lateral glabrous skin at its max force (i.e, until it just bent). This stimulus was repeated 5 times, and was scored as positive when 3 paw flicks (the animal's reflex withdrawal response) were observed. The thresholds for withdrawal responses were compared between the hind paw of the end-to-end reconstructed animals and the hind paw of the sham operated animals. The group of animals that underwent reconstruction was considerd to be hypersensitive for mechanical stimuli when a significant decrease of withdrawal threshold was noted in comparison to control animals.

4.3.6. Hot and cold plate

The hot and cold plate test was used to assess thermal hypersensitivity in the hind paw. Rats were placed in an open-ended chamber with clear walls and a surface temperature of 5˚C (cold plate) or 50˚C (hot plate) on separate days to prevent interference. The time until hind paw withdrawal or licking was observed. Significant differences between the ereconstruction and the control group served as an indication of thermal changes in the sensitivity.

4.3.7. Electromyography

Innervation of motor axons was evaluated by recording evoked compound muscle action potentials (CMAPs) of the gastrocnemius muscles (15). Under general anesthesia, the sciatic nerve was exposed through a gluteal muscle-splitting approach using a surgical microscope (Zeiss OP-MI 6-SD; Carl Zeiss, Goettingen, Germany). A monopolar needle stimulation electrode was placed 6-7 mm proximally from the trifurcation of the sciatic nerve (16). For recordings, an active electrode was positioned over the midpoint of the medial gastrocnemius muscle with the reference electrode at the later distal end of this muscle. CMAP peak-to-peak amplitudewas recorded and averaged over a batch of 20 responses. The average amplitude in each group was compared with the control group.

4.3.8. Tissue preparation

At the appropriate survival time, animals were sacrificed by an overdose pentobarbital (100mg/kg ip). Subsequently, the glabrous skin of the contralateral hind paw was dissected and immersion-fixed in 2% paraformaldehyde-lysin-periodate (PLP) for 24 hours at 4˚C. The skin was then embedded in 10% gelatin, which was hardened in 10% formaldehyde for 2 hours, stored overnight in 30% sucrose, and subsequently sectioned at 40-µm sections with a freezing microtome and collected in glycerol for long-term storage at –20 °C.

4.3.9. Immunohistochemistry

Immunohistochemistry was performed to evaluate the density and the length of nerve fibers innervating the skin as described previously (17). In short, sections were rinsed, pre-incubated (90 minutes at room temperature) in a blocking solution containing bovine serum albumin (2%) diluted in phosphate buffered saline (pH 7,4) with 0.5% Triton X-100 (Roche Diagnostics). After rinsing, the sections were incubated for 48 hours in a cocktail of 2% bovine serum albumin or milk powder containing the diluted antibody at 4˚C. The primary antibodies were PGP9.5 (1/10.000, anti-rabbit, BML-PG9500, Enzo Life Sciences, New York, USA), CGRP (1/30.000, anti-rabbit, PC205L, Calbiochem, Germany) and P2X3 (1/200, anti-rabbit, P0121-077K1349, Sigma, USA). Following incubation with the appropriate secondary biotinylated antibody (1/200, Biotine) for 90 minutes at room temperature, sections were further processed using a Vectastain Elite ABC kit (Vector, Burlingame, CA) (90 minutes at room temperature) and additional signal amplification was achieved by treating the sections with self-made biotin tyramide (18) for 12 minutes. The 3, -3' diaminobenzidine reaction (19) was then used to reveal antigenic sites. Thereafter, the sections were mounted on slides and stained for 4 minutes with 0.05% thionin, which colored the epidermis blue to achieve a clear border between epidermis and dermis. Finally, the slides were dehydrated using absolute ethanol (< 0.01% methanol), transferred to xylene and cover slipped.

4.3.10. Analysis

All slides were scanned in multiple layers (3 layers of each 8µm) into digital slides by Nanozoomer 2.0 series system (Hamamatzu). These images were quantified using digital microscope ImageScope software (Aperio ImageScope v11.1.2.760) using a x20 objective in a 80 milimeter squared region in medial, central, lateral side of the glabrous skin of the rats' hind paw. It is important to divide the glabrous hind paw in these three regions with respect to their anatomical innervation; i.e., medial region is innervated by the saphenous nerve, central region by the tibial nerve and the lateral region by the sural nerve.

For each rat, the nerve fiber terminals within the epidermis were counted in four sections of the proximal and four sections of the distal foot sole area. From these counts the average number of labeled nerve fibers per milimeter squared was calculated for each rat. Per operated group, the results were averaged and compared with the results in the control group.

4.3.11. Statistical analysis

For determining statistical differences, the one way-ANOVA with a Tukey post hoc test was used for intergroup comparisons. Errors in variations were determined as standard error of the mean (SEM), and $p < 0.05$ was taken as significant.

4.4.0. Results

All surgical procedures were performed successfully without any exclusion of animals due to postoperative infection, loss of weight or auto-mutilation. As expected and previously described (12), directly after surgery, lesioned animals dragged their operated hind paw directly after surgery, which completely recovered at about 8 weeks postoperatively. No abnormalities were seen at the contralateral hind paws. Likewise, sham-operated animals used both their hind paws normally. All results in the present study concern the contralateral hind paw after unilateral end-to-end reconstruction of the sciatic nerve. Results concerning ipsilateral hind paw of the same animals are reported elsewhere (12).

4.4.1. Functional sensitivity

Pinprick test showed positive responses, as indicated by hind paw withdrawal, at the medial and lateral region of the hind paw in sham-operated and in the group of animals that underwent reconstruction at all examined time points (data not shown). This indicated that the hind paw remained innervated by nociceptive nerve fibers. In addition, a set of von Frey hairs was used to test the extent of mechanical sensitivity. This resulted in a non-significant decreased response to mechanical stimuli at the medial and lateral region of the hind paw at 5 weeks postoperatively.

However, at 10 weeks, a significantly lower mechanical withdrawal threshold (i.e. signifying an enhanced response with respect to the sham-operated animals) in both medial and lateral areas of the hind paw was noted (p<0,001) suggesting transient mechanical hypersensitivity (Figure 1). Mechanical withdrawal threshold thresholds reached control values at 20 and 30 weeks postopeatively.

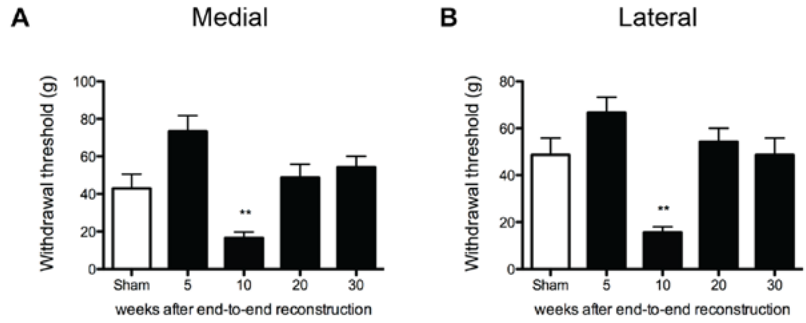

*Figure 1. Contralateral mechanical hypersensitivity. Histograms showing the mechanical withdrawal thresholds in grams (± SEM) in (A) the medial and (B) the lateral region of the contralateral plantar hind paw following unilateral end-to-end reconstruction determined with von Frey monofilaments. A significantly decreased mechanical withdrawal threshold was seen in both the lateral and medial glabrous skin 10 weeks postoperatively in comparison with sham-operated rats. However, the mechanical hypersensitivity diminished at 20 and 30 weeks. (**p <0.01; One-way ANOVA).*

4.4.2. Thermal sensitivity

Hot and cold plate testing was performed to measure the thermal sensitivity of the hind paw. At 5 and 10 weeks, no significant differences were found in withdrawal time between end-to-end reconstructed animals and sham-operated animals (Figure 2). A significant decrease in withdrawal time is found at 20 weeks postoperatively in both the hot and cold plate tests. Similar to mechanical sensitivity, responses to thermal stimuli returned to control values at 30 weeks.

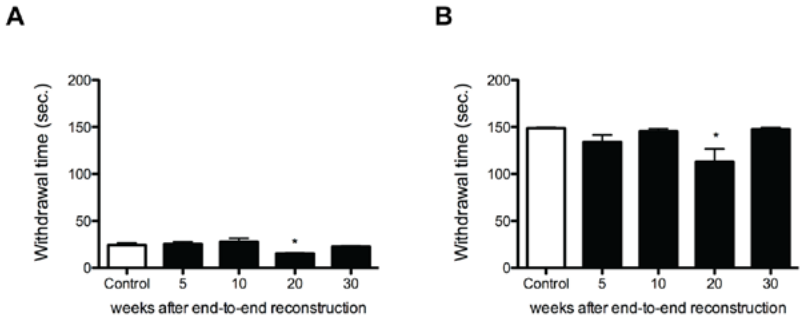

*Figure 2. Contralateral thermal hypersensitivity. Histograms showing the withdrawal latency in seconds (± SEM) of contralateral hind paw in (A) the hot plate test (50 ºC) and (B) the cold plate test (5 ºC) for sham-operated and end-to-end reconstructed hind paw. Note that in both the hot and cold plate testing a significant shorter withdrawal latency was seen 20 weeks postoperatively as compared with sham-operated rats. (*p < 0.05; One-way ANOVA).*

4.4.3. Recovery of functional motor axons

CMAPs amplitude measured at the contralateral gastrocnemius muscle provides an indirect estimate of the number of functional axonal fibers in the stimulated nerve. No significant difference in CMAPs amplitude was seen on the hind paw at all time-points (Figure 3).

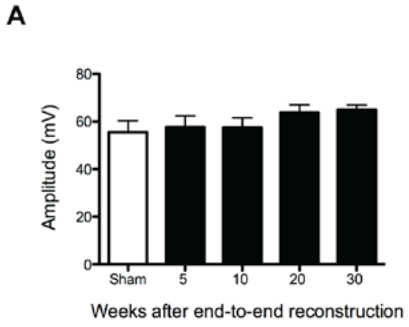

Figure 3. Compound muscle action potentials. A) Histograms showing the evoked CMAPs (± SEM) in the gastrocnemius muscle of the contralateral hind paw. No significant difference is seen in the CMAP amplitudes between the contralateral operated hind paw and contralateral sham operated hind paw at all experimental time points (One-way ANOVA).

4.4.4. Intra-epidermal nerve fibers

PGP9.5 is a pan-neuronal marker that labels both subgroups of epidermal nerve fibers; i.e., the peptidergic (CGRP-immunoreactive: IR) and the non-peptidergic (IB4-IR) fibers. At 5 and 10 weeks, a significant decrease of epidermal PGP9.5-IR nerve fibers was noted at the central and lateral region of the hind paw (Figure 4). At 20 and 30 weeks postoperatively this change in density had returned to control values in all examined regions of the glabrous skin. However, the medial region recovered to control value already at 10 weeks.

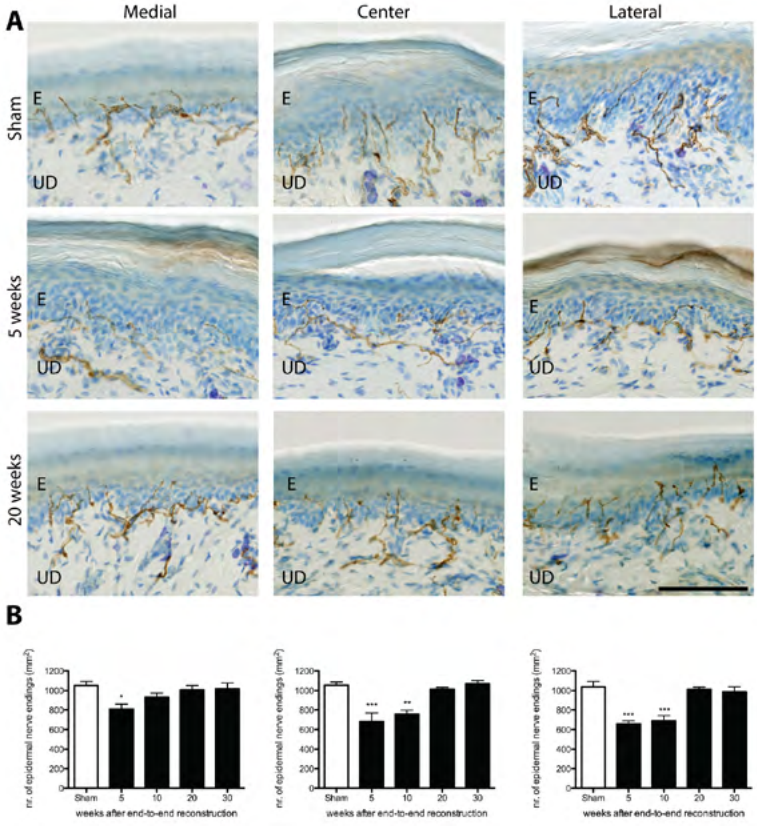

Figure 4. Histological analysis of PGP9.5-IR nerve fibers. Analysis was performed of samples obtained from the medial, center, and lateral regions of the contralateral plantar hind paw.
A) Multilayered scans labeled for PGP9.5-IR nerve fibers in the epidermis and the upper dermis. Fewer nerve fibers are visible in the medial, center and lateral epidermis and the upper dermis of the hind paw at 5 weeks in comparison to sham-operated group. However, this decrease not visible at 20 weeks. E=epidermis, UD=upper dermis. Scale bar=100µm.
B) Histograms showing the average number of epidermal PGP9.5-IR fibers in all experimental groups. Note that the density of PGP9.5-IR fibers on the medial region reached control values already at 10 weeks postoperatively while the central and lateral foot sole regions showed control values at 20 weeks. (: p <0.05**: p <0.01, ***: p <0.001, One-way ANOVA).*

The density of the CGRP-IR fibers diminished significantly in all examined regions of the glabrous skin at 5 weeks. However, values returned to control at 10 weeks postoperatively, and showed a significant increase in the central and lateral region of the skin at 20 weeks. Control values were reached in the medial region at 20 weeks while the central and lateral regions of the glabrous skin recovered to control at 30 weeks postoperatively (Figure 5).

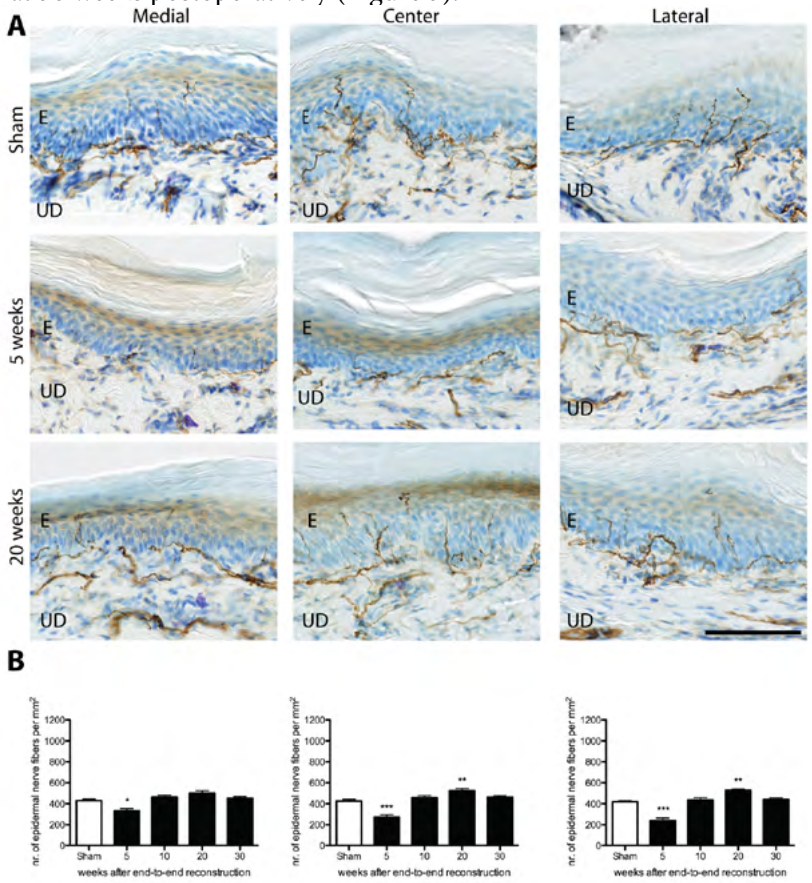

Figure 5. Histological analysis of CGRP-IR nerve fibers. Analysis was performed of samples obtained from the medial, center, and lateral regions of the contralateral plantar hind paw.

A) Multilayered scans labeled for CGRP-IR fibers in the epidermis and the upper dermis of the foot sole shows decreased densities in all examined foot sole regions at 5 weeks. 20 weeks postoperatively a larger quantity of CGRP-IR nerve fibers is visible in comparison with sham-operated animals in the central and lateral foot sole region. E=epidermis, UD=upper dermis. Scale bar=100μm.

*B) Histograms showing the number of epidermal peptidergic CGRP-IR fibers in all experimental groups. A significant decrease in CGRP-IR fiber density is shown at 5 weeks PO as compared to sham-operated rats. However, the epidermal CGRP-IR fiber density reached its peak in the central and lateral region at 20 weeks and returned to sham values 30 weeks postoperatively. (*p <0.05; **p <0.01; ***p <0.001; One-way ANOVA).*

In the present study, the density of the non-peptidergic fibers was determined by P2X3-IR fibers. P2X3 has been shown to co-localize for more than 90% with IB4 positive nerve fibers. Moreover, fewer non-specific binding was seen using P2X3 staining when compared with IB4. Therefore, P2X3 staining is considered to be a more suitable alternative to determine non-peptidergic fibers (20, 21).

The density of non-peptidergic fibers was significantly decreased at the central and lateral regions of the glabrous skin at 5 weeks (Figure 6). The density of the non-peptidergic fibers returned to control value at 10, 20, and 30 weeks. Notably, no significant changes were seen on the medial region of the glabrous skin at all examined time points. This was in accordance with the fewer decrease in the density of PGP9.5-IR fibers on the medial region of the glabrous skin at 5 weeks.

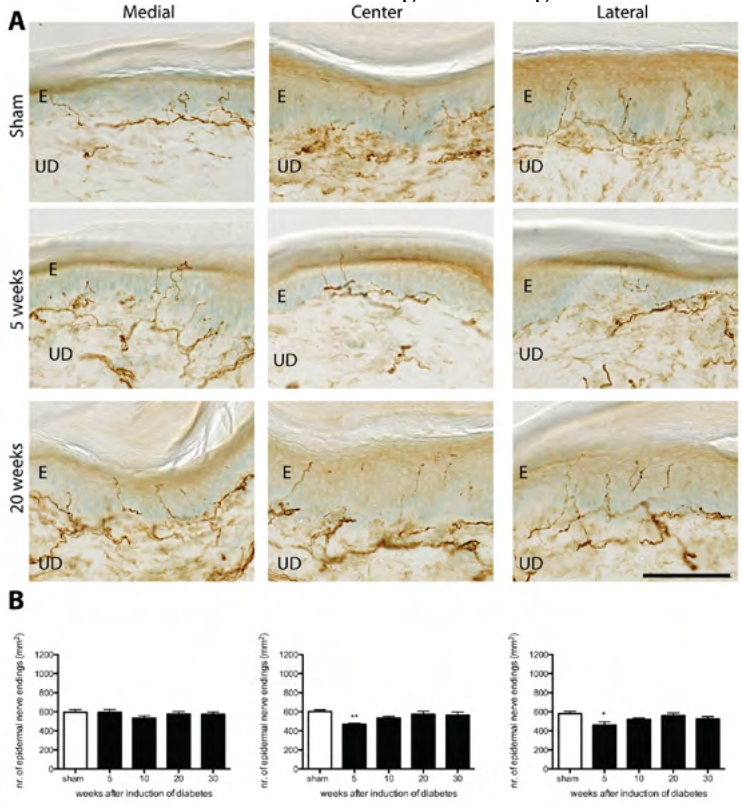

Figure 6. Histological analysis of P2X3-IR nerve fibers. Analysis was performed of samples obtained from the medial, center, and lateral regions of the contralateral plantar hind paw. A) Multilayered scans labeled for P2X3-IR fibers in the epidermis and the upper dermis of the hind paw showed evidently fewer nerve fibers in the central and medial region of the foot sole at 5 weeks as compared to sham-operated rats. E=epidermis, UD=upper dermis. Scale bar=100μm.
B) Histograms showing the number of epidermal non-peptidergic P2X3-IR fibers in all experimental groups. Note the significant decreased density of P2X3-IR fibers on the central and lateral region at 5 week postoperatively. The remaining examined time points show control values (: $p < 0.05$, ANOVA).*

4.5.0. Discussion

The aim of this study was to show possible mirror-image pain and its relation to changes in epidermal innervation following unilateral lesion and end-to-end reconstruction of the sciatic nerve. Mirror-image pain is demonstrated in various animal models of chronic neuropathic pain, such as the chronic constriction injury (CCI) (22), the spared nerve injury (SNI) (23), and the spinal nerve ligation (SNL) (24). As yet, current findings demonstrate mirror-image pain after end-to-end reconstruction of the sciatic nerve.

Although hyposensitivity may be expected when decreased skin innervation is observed, the present study shows reduction in the contralateral epidermal innervation without changes in mechanical or thermal sensitivity 5 weeks after unilateral end-to-end reconstruction of the sciatic nerve. In fact, comparable to previous study, at 10 weeks postoperatively the significant decreased total density of sensory nerve fibers was accompanied by mechanical hypersensitivity (25). However, Oaklander and Brown did not distinguish between the subgroups of intra-epidermal nerve fibers. The importance of this distinction is shown in the present study by demonstrating normal densities for the subgroups of epidermal nerve fibers while reduction was observed in the total density of epidermal nerve fibers. This discrepancy could be explained by an increase in the previously described intertwinning between the peptidergic and the non-peptidergic nerve fibers at 10 weeks postoperatively. However, double labeling for both CGRP-IR and P2X3-IR nerve fibers in combination with recordings of concomitant changes in excitability of these fibers would be required to confirm this proposition.

The importance of the distinction between subgroups of epidermal nerve was shown by significant increase in the density of the epidermal peptidergic nerve fibers when the total density of epidermal nerve fibers reached control values at 20 weeks postoperatively. The increased density of epidermal peptidergic nerve fibers was accompanied by thermal hypersensitivity. This correlation could be explained by expression of thermo-sensitive transient receptor potential (TRP) channels on peptidergic nerve fibers. These TRP channels become active when exposed to temperatures of the hot plate (> 42°C) and cold plate (< 17°C) test (26). Therefore, thermal hypersensitivity seems to be specifically related to the increased density of epidermal peptidergic nerve fibers.

Based on our results, we suggest that firstly, the density of epidermal nerve fibers need to drop below a certain threshold to cause hyposensitivity: a phenomenon previously described in peripheral nerve injury studies on the ipsilateral side (12, 27). Secondly, intertwinning between the peptidergic and non-peptidergic nerve fibers is related to mechanical hypersensitivity while increased innervation of specifically the peptidergic nerve fibers is correlated to thermal hypersensitivity, suggesting two different pathophysiological mechanisms. This is emphasized by the presence of mechanical and thermal hypersensitivity at different

time points as shown in the present study and by Duraku et al. 2013. Finally, increased contralateral peptidergic epidermal nerve fiber outgrowth supports the peripheral mirror-image pain pathway described by Cheng and collaborators in which increased NGF production in the contralateral DRG following unilateral nerve lesion is shown to play a role in the development of mirror image pain (Figure 7).

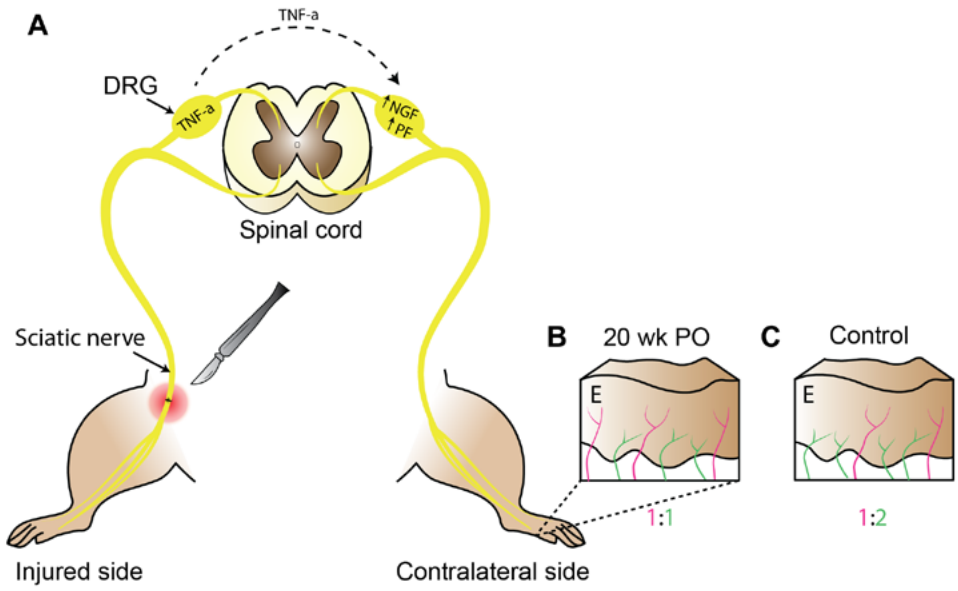

Figure 7. Schematic illustration of peripheral nervous system in the development of mirror-image pain.
A) Unilateral peripheral nerve injury induces TNF-a production in the DRG on the injured side. TNF-a diffuses via cerebrospinal fluid to the contralateral DRG where it activates satellite glia to produce NGF, which promotes the outgrowth of the peptidergic sensory nerve fibers in the contralateral DRG.
B) Illustration of the contralateral skin innervation after 20 weeks of unilateral end-to-end reconstruction. Increased epidermal peptidergic (green) nerve fibers are seen resulting in 1:1 composition of the peptidergic and the non-peptidergic (pink) nerve fibers in the epidermis, respectively.
C) Illustration of the contralateral skin innervation in sham (control) animals showing 1:2 composition of the peptidergic and the non-peptidergic nerve fibers, respectively. DRG = dorsal root ganglion, TNF-a = tumor necrose factor a, NGF = nerve growth factor, PF = peptidergic fibers, E = epidermis.

Mechanical sensitivity, thermal sensitivity and density of epidermal nerve fibers return to control values at 30 weeks postoperatively. Therefore, we suggest that pain on the uninjured corresponding side can be present in transient pain states after unilateral nerve injury. This contrasts a recent other study on unilateral end-to-end reconstruction where pain or changes in skin innervation were not observed at the uninjured contralateral side (28). First, this could be ascribed to the minor differences in experimental techniques and setup. Second, contralateral changes frequently have a more delayed and restricted temporal profile (29). They might have failed to reach statistical significance due to short follow up time as in the present study thermal mirror-image pain and increased density of epidermal peptidergic nerve fibers were observed at 20 weeks. Therefore, the current study demonstrates the necessity for more prolonged follow-up of the time course when examining mirror-image pain. Third, it is shown that genetic background has major impact on pain perception (30) and therefore differences in rat strains may be the cause of the discrepancy in results when studying mirror-image pain. These factors should be taken into account when comparing different peripheral nerve injury induced animal models. Moreover, different laboratories using techniques such as gene expression, in situ hybridization, immunohistochemistry and electrophysiology were able to observe contralateral changes after unilateral nerve injury (31-35). Therefore, it is unlikely that mirror-image pain is an artifact of measurements.

Similar to ipsilateral hind paw (12), less dramatic changes were observed in the density of intra-epidermal nerve fibers on the medial region of the glabrous skin of the contralateral side when compared to the central and lateral areas after unilateral end-to-end reconstruction of the sciatic nerve. This could be explained by collateral sprouting on the contralateral hind paw by the uninjured saphenous nerve, which normally innervates the medio-dorsal hind paw (36). However, collateral sprouting should be confirmed using Evans Blue extravasation technique.

Changes in contralateral skin innervation in the current study were smaller compared to the ipsilateral side as reported previously (37), while contralateral pain intensity measured by von Frey monofilaments and the hot and cold plate tests was observed to be similar to the ipsilateral side. Although we emphasize the importance of the peripheral nervous system in the development of mirror-image pain, the present results do not exclude the involvement of the central nervous system in pain perception on the uninjured corresponding side following unilateral nerve injury (1-5).

4.6.0. Conclusions

The current study confirms the involvement of the peripheral nervous system in the development of mirror-image pain by temporal alterations in the composition of peptidergic and non-peptidergic subgroups of intra-epidermal nerve fibers in the contralateral hind paw. Therefore, the contralateral side cannot serve as the appropriate control to compare with lesion effects at the ipsilateral hind paw. Furthermore, the current study demonstrates a potential relation between the peptidergic nerve fibers and thermal hypersensitivity.

4.7.0. References

1. Obata H, Sakurazawa S, Kimura M, Saito S. Activation of astrocytes in the spinal cord contributes to the development of bilateral allodynia after peripheral nerve injury in rats. Brain Res. 2010 Dec 2;1363:72-80.
2. Jaggi AS, Singh N. Role of different brain areas in peripheral nerve injury-induced neuropathic pain. Brain Res. 2011 Mar 24;1381:187-201.
3. Milligan ED, Twining C, Chacur M, Biedenkapp J, O'Connor K, Poole S, et al. Spinal glia and proinflammatory cytokines mediate mirror-image neuropathic pain in rats. The Journal of neuroscience : the official journal of the Society for Neuroscience. 2003 Feb 1;23(3):1026-40.
4. Racz I, Nadal X, Alferink J, Banos JE, Rehnelt J, Martin M, et al. Crucial role of CB(2) cannabinoid receptor in the regulation of central immune responses during neuropathic pain. J Neurosci. 2008 Nov 12;28(46):12125-35.
5. Hatashita S, Sekiguchi M, Kobayashi H, Konno S, Kikuchi S. Contralateral neuropathic pain and neuropathology in dorsal root ganglion and spinal cord following hemilateral nerve injury in rats. Spine (Phila Pa 1976). 2008 May 20;33(12):1344-51.
6. Cheng CF, Cheng JK, Chen CY, Lien CC, Chu D, Wang SY, et al. Mirror-image pain is mediated by nerve growth factor produced from tumor necrosis factor alpha-activated satellite glia after peripheral nerve injury. Pain. 2014 May;155(5):906-20.
7. Carcamo CR. Mirror-image pain is mediated by nerve growth factor produced from tumor necrosis factor-alpha-activated satellite glia after peripheral nerve injury. Pain. 2014 Aug;155(8):1675.
8. Jancalek R, Dubovy P, Svizenska I, Klusakova I. Bilateral changes of TNF-alpha and IL-10 protein in the lumbar and cervical dorsal root ganglia following a unilateral chronic constriction injury of the sciatic nerve. Journal of neuroinflammation. 2010;7:11.
9. Forrest SL, Keast JR. Expression of receptors for glial cell line-derived neurotrophic factor family ligands in sacral spinal cord reveals separate targets of pelvic afferent fibers. J Comp Neurol. 2008 Feb 20;506(6):989-1002.
10. Stucky CL, Lewin GR. Isolectin B(4)-positive and -negative nociceptors are functionally distinct. J Neurosci. 1999 Aug 1;19(15):6497-505.
11. Seltzer Z, Dubner R, Shir Y. A novel behavioral model of neuropathic pain disorders produced in rats by partial sciatic nerve injury. Pain. 1990 Nov;43(2):205-18.
12. Kambiz S, Duraku LS, Baas M, Nijhuis TH, Cosgun SG, Hovius SE, et al. Long-term follow-up of peptidergic and nonpeptidergic reinnervation of the epidermis following sciatic nerve reconstruction in rats. J Neurosurg. 2015 Jul;123(1):254-69.
13. Nixon BJ, Doucette R, Jackson PC, Diamond J. Impulse activity evokes precocious sprouting of nociceptive nerves into denervated skin. Somatosens Res. 1984;2(2):97-126.

14. Kovacic U, Sketelj J, Bajrovic FF. Sex-related difference in collateral sprouting of nociceptive axons after peripheral nerve injury in the rat. Exp Neurol. 2003 Nov;184(1):479-88.
15. Werdin F, Grussinger H, Jaminet P, Kraus A, Manoli T, Danker T, et al. An improved electrophysiological method to study peripheral nerve regeneration in rats. J Neurosci Methods. 2009 Aug 30;182(1):71-7.
16. Nijhuis TH, Smits ES, van Neck JW, Visser GH, Walbeehm ET, Blok JH, et al. Ultrasound-guided needle positioning near the sciatic nerve to elicit compound muscle action potentials from the gastrocnemius muscle of the rat. J Neurosci Methods. 2011 Jan 15;194(2):283-6.
17. Duraku LS, Hossaini M, Schuttenhelm BN, Holstege JC, Baas M, Ruigrok TJ, et al. Re-innervation patterns by peptidergic Substance-P, non-peptidergic P2X3, and myelinated NF-200 nerve fibers in epidermis and dermis of rats with neuropathic pain. Exp Neurol. 2013 Mar;241:13-24.
18. Hopman AH, Ramaekers FC, Speel EJ. Rapid synthesis of biotin-, digoxigenin-, trinitrophenyl-, and fluorochrome-labeled tyramides and their application for In situ hybridization using CARD amplification. J Histochem Cytochem. 1998 Jun;46(6):771-7.
19. Kuhlmann WD, Peschke P. Glucose oxidase as label in histological immunoassays with enzyme-amplification in a two-step technique: coimmobilized horseradish peroxidase as secondary system enzyme for chromogen oxidation. Histochemistry. 1986;85(1):13-7.
20. Peleshok JC, Ribeiro-da-Silva A. Delayed Reinnervation by Nonpeptidergic Nociceptive Afferents of the Glabrous Skin of the Rat Hindpaw in a Neuropathic Pain Model. J Comp Neurol. 2011 Jan 1;519(1):49-63.
21. Taylor AMW, Peleshok JC, Ribeiro-Da-Silva A. Distribution of P2X(3)-Immunoreactive Fibers in Hairy and Glabrous Skin of the Rat. J Comp Neurol. 2009 Jun 20;514(6):555-66.
22. Paulson PE, Morrow TJ, Casey KL. Bilateral behavioral and regional cerebral blood flow changes during painful peripheral mononeuropathy in the rat. Pain. 2000 Feb;84(2-3):233-45.
23. Li D, Yang H, Meyerson BA, Linderoth B. Response to spinal cord stimulation in variants of the spared nerve injury pain model. Neurosci Lett. 2006 May 29;400(1-2):115-20.
24. Kim SH, Chung JM. An experimental model for peripheral neuropathy produced by segmental spinal nerve ligation in the rat. Pain. 1992 Sep;50(3):355-63.
25. Oaklander AL, Brown JM. Unilateral nerve injury produces bilateral loss of distal innervation. Ann Neurol. 2004 May;55(5):639-44.
26. Kambiz S, Duraku LS, Holstege JC, Hovius SE, Ruigrok TJ, Walbeehm ET. Thermo-sensitive TRP channels in peripheral nerve injury: a review of their role in cold intolerance. J Plast Reconstr Aesthet Surg. 2014 May;67(5):591-9.
27. Verdu E, Navarro X. Comparison of immunohistochemical and functional

reinnervation of skin and muscle after peripheral nerve injury. Exp Neurol. 1997 Jul;146(1):187-98.
28. Cobianchi S, de Cruz J, Navarro X. Assessment of sensory thresholds and nociceptive fiber growth after sciatic nerve injury reveals the differential contribution of collateral reinnervation and nerve regeneration to neuropathic pain. Exp Neurol. 2014 Feb 16;255C:1-11.
29. Koltzenburg M, Wall PD, McMahon SB. Does the right side know what the left is doing? Trends Neurosci. 1999 Mar;22(3):122-7.
30. Rode F, Thomsen M, Brolos T, Jensen DG, Blackburn-Munro G, Bjerrum OJ. The importance of genetic background on pain behaviours and pharmacological sensitivity in the rat spared serve injury model of peripheral neuropathic pain. Eur J Pharmacol. 2007 Jun 14;564(1-3):103-11.
31. Brazda V, Klusakova I, Svizenska IH, Dubovy P. Dynamic response to peripheral nerve injury detected by in situ hybridization of IL-6 and its receptor mRNAs in the dorsal root ganglia is not strictly correlated with signs of neuropathic pain. Mol Pain. 2013 Aug 16;9.
32. Jancalek R, Dubovy P, Svizenska I, Klusakova I. Bilateral changes of TNF-alpha and IL-10 protein in the lumbar and cervical dorsal root ganglia following a unilateral chronic constriction injury of the sciatic nerve. J Neuroinflamm. 2010 Feb 10;7.
33. Bhangoo S, Ren D, Miller RJ, Henry KJ, Lineswala J, Hamdouchi C, et al. Delayed functional expression of neuronal chemokine receptors following focal nerve demyelination in the rat: a mechanism for the development of chronic sensitization of peripheral nociceptors. Mol Pain. 2007 Dec 12;3.
34. Kleinschnitz C, Brinkhoff J, Sommer C, Stoll G. Contralateral cytokine gene induction after peripheral nerve lesions: Dependence on the mode of injury and NMDA receptor signaling. Mol Brain Res. 2005 May 20;136(1-2):23-8.
35. Han Y, Li N, Zeiler SR, Pelled G. Peripheral Nerve Injury Induces Immediate Increases in Layer V Neuronal Activity. Neurorehab Neural Re. 2013 Sep;27(7):664-72.
36. Kambiz S, Baas M, Duraku LS, Kerver AL, Koning AH, Walbeehm ET, et al. Innervation mapping of the hind paw of the rat using Evans Blue extravasation, Optical Surface Mapping and CASAM. J Neurosci Methods. 2014 May 30;229:15-27.
37. Kambiz S, Duraku LS, Baas M, Nijhuis THJ, Cosgun SG, Hovius SER, et al. Long term follow up of peptidergic and non-peptidergic re-innervation of the epidermis following sciatic nerve reconstruction in rats. Journal of Neurosurgery. 2014.

Chapter 5

Thermo-sensitive TRP channels in peripheral nerve injury: a review of their role in cold intolerance

Shoista Kambiz, Liron S. Duraku, Jan C. Holstege, Steven E.R. Hovius, Tom J.H. Ruigrok, Erik T. Walbeehm

Journal of Plastic, Reconstructive & Aesthetic Surgery 2014; 67(5):591-599

5.1.0. Abstract

One of the sensory complications of traumatic peripheral nerve injury is thermal intolerance, which manifests in humans mainly as cold intolerance. It has a major effect on the quality of life, and adequate therapy is not yet available. In order to better understand the pathophysiological background of thermal intolerance, we focus first on the various transient receptor potential (TRP) channels that are involved in temperature sensation, including their presence in peripheral nerves and in keratinocytes. Second, the role of thermo-sensitive TRP channels in cold and heat intolerance is described showing three different mechanisms that contribute to thermal intolerance in the skin: (a) an increased expression of TRP channels on nerve fibres and on keratinocytes, (b) a lower activation threshold of TRP channels and (c) the sprouting of non-injured nerve fibres. Finally, the data that are available on the effects of TRP channel agonists and antagonists and their clinical use are discussed.

In conclusion, TRP channels play a major role in temperature sensation and in cold and heat intolerance. Unfortunately, the available pharmaceutical agents that successfully target TRP channels and counteract thermal intolerance are still very limited. Yet, our focus should remain on TRP channels since it is difficult to imagine a reliable treatment for thermal intolerance that will not involve TRP channels.

5.2.0. Introduction

Traumatic peripheral nerve injury in humans leads to a variety of motor and sensory deficits, depending on the severity of the lesion. Initially, functional (motor) recovery is of primary concern to patients and physicians, while sensory recovery receives less attention. However, at a later stage, attention may shift to sensory complications, such as thermal intolerance, also known as cold intolerance, which are often highly disabling and difficult to treat (1). To clinicians, cold intolerance is the most common manifestation of neuropathic pain. Cold intolerance has been defined as "an exaggerated or abnormal reaction to cold exposure of the injured part causing discomfort or the avoidance of cold" (2). The highest incidence of cold intolerance is found in patients after peripheral nerve injury in the upper extremities (91%) (3). Cold intolerance is a ubiquitous problem in moderate to cold climates but, despite its high prevalence, its pathophysiology is largely unknown. In order to have a better understanding of the mechanism underlying thermal intolerance, we review the present data about temperature signalling under normal and pathologic conditions, with a focus on the thermal transducers called transient receptor potential (TRP) channels.

5.2.1. Temperature sensation

The sensation of temperature is transmitted by Aδ and C-fibers, which terminate as free nerve endings in the skin (4, 5). Aδ fibers are thinly myelinated, relatively fast conducting fibers with an average conduction velocity of about 12 meter per second (6), whereas C-fibers are non-myelinated, slowly conducting fibers with a conduction velocity of less than 0.8 meter per second (7). Aδ and C-fibers are commonly referred to nociceptive fibers as they are involved in conveying nociceptive information leading to pain, although non-nociceptive temperatures are also sensed by some of these fibers. All Aδ and C-fibers terminate on neurons in the dorsal horn of the spinal cord, and some of these neurons in turn project to various brainstem nuclei and the thalamus. Three cortical areas are important for temperature sensation: the insula and the cingulate cortex for emotional processing and the somatosensory cortex for assessing the intensity and localization of the stimulus (8, 9) (Figure 1).

5.2.2. Temperature transduction

The receptors in the free nerve endings of Aδ and C-fibers that are involved in temperature signaling were only recently discovered. They are TRP channels, which were named on basis of their diminishing transient response to continuous light in mutant fruit flies (Drosophila) (10). Several subfamilies, defined by specific domains of the receptor have been identified. The currently known subfamilies are TRPV (vanilloid), TRPM (melastin), TRPA (acyrin), TRPN (no mechanoreceptor potential C), TRPP (polycystic), TRPML (mucolipin) and TRPC (canonical) (11). Most TRP receptors are polymodal, that is, sensitive to more than one modality (temperature, chemical, mechanical stimuli, etc.) (12). In the present review, we only discuss the thermo-sensitive TRP channels, namely the TRPV, TRPM, and TRPA members.

Each thermo-sensitive TRP channel has a specific range of sensitivity for temperature (e.g., TRPV3: ≥34-38°C, TRPM8: 25-28°C, etc.), and together they are able to perceive all temperatures from noxious hot to noxious cold (Table 1) except for temperatures between 17 and 26°C. The latter range of temperatures is covered by mechano-gated potassium channels (TWIK-related potassium channel-1 (TREK1) and TWIK-related arachidonic acid-stimulated potassium channel protein (TRAAK)), also expressed on sensory neurons, that become increasingly active when the temperature rises from 17 to 40 °C (13). In thermo-sensitive TRP channels an influx of sodium and calcium initiates the generation of action potentials (12)(Figure 1A). Some thermo-sensitive TRP channels are also sensitive to exogeneous components such as capsaicin, the hot pepper ingredient, which activates TRPV1 channels leading to a sense of noxious hot temperature. Another example is menthol, which is sensed as cold due to TRPM8 channel activation (14).

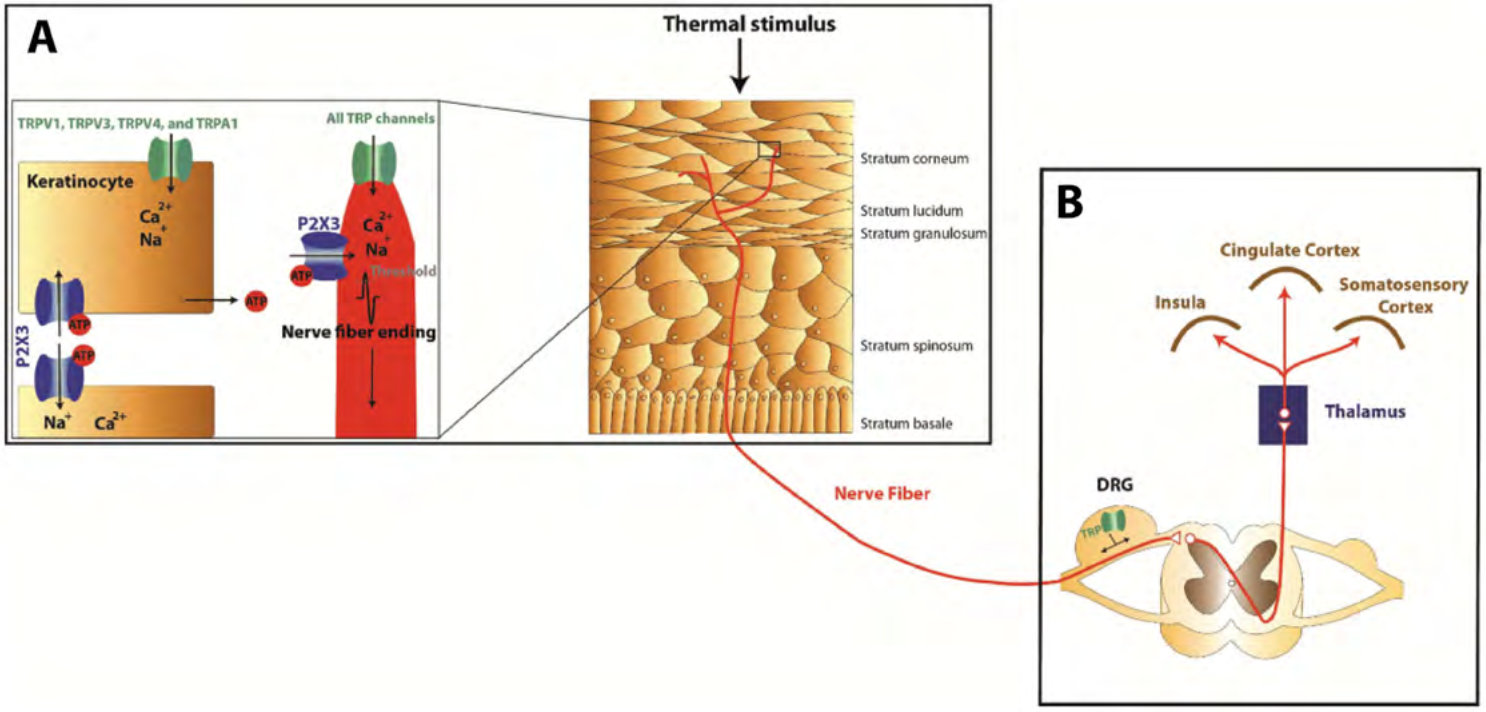

Figure 1. Thermal detection in the skin and transmission to the somatosensory cortex via the spinal cord.
A) Epidermis: temperature is detected by the activation of TRP channels on keratinocytes and Aδ- and C-fibers in the skin. These channels allow an influx of sodium and calcium ions that initiates the generation of action potentials in the Aδ- and C-fibers. Keratinocytes communicate with adjacent nerve fibers by secreting ATP, which binds on P2X3 receptors. Expression of the P2X3 receptor on keratinocytes also enables an autocrine interaction between keratinocytes.
B) The action potential from the Aδ- and C-fibers is transferred, via the dorsal root ganglion (DRG), where TRP channels are phosphorylated, to the cingulate cortex, the insula, and the somatosensory cortex with branches to other brainstem areas.

In the present review, various characteristics of the thermo-sensitive TRP channels will be discussed with a special attention to their characteristics and their role in nerve injury induced thermal intolerance.

5.3.0. Characteristics of thermo-sensitive TRP channels

5.3.1. TRPV1 channels

TRPV1 was the first temperature-sensitive channel to be discovered in 1997 (12). This channel was identified due to its responsiveness to capsaicin, the pungent compound derived from chili peppers, which causes a burning sensation (12, 15). In the initial report of its discovery, the investigators showed that aside from being sensitive to capsaicin, the TRPV1 channel is also activated by noxious heat (>42°C). In addition, the TRPV1 channel, which is expressed by both Aδ and C-fibers (16, 17), functions as a sensor for several non-thermal agents such as endocannabinoids and H+ ions, that is, acidic conditions below a pH of 6.6 (12, 15) (Table 1).

More recently, evidence was found that thermal signaling is also transduced by keratinocytes in the epidermis, which express thermo-sensitive TRP channels (18, 19). TRPV1 channels are expressed on keratinocytes throughout the epidermis, with the highest expression in the granular layer (20) where they may be involved in thermal sensation. Activation of these epidermal TRPV1 channels by high temperature (44°C) or by capsaicin causes an increase in the intracellular calcium levels (21). Calcium influx in keratinocytes activates signaling pathways (22, 23) leading to secretion of ATP, which binds to P2X3-receptors on Aδ and C-fibers (24, 25). This was confirmed in electron microscopy studies showing synapse-like structures between nerve endings in the epidermis and keratinocytes (26, 27). Since keratinocytes also express P2X3 receptors (28), they will respond to ATP by other keratinocytes leading to paracrine and autocrine communication (18, 19, 29) (Figure 1A) that may further enhance thermal signaling. These findings show the importance of keratinocytes in thermosensation next to the thermo-sensitive nerve fibers.

5.3.2. TRPV2 channels

TRPV2 channels are activated by temperatures above 52°C. In TRPV1-knockout mice, a small population of heat-sensitive fibers, only reacting to temperatures above 52°C, was still present (30). This finding led to the discovery of a second TRPV heat-gated channel, by the Julius group in 1999 (30), now termed TRPV2. It is 50% homologous to TRPV1, it becomes active only by temperatures above 52°C and lacks sensitivity for capsaicin (30). In addition, TRPV2 channels are responsive to hypo-osmolarity and cell stretch (31), suggesting roles in mechano-transduction as well. The TRPV2 channel is expressed by Aδ-fibers (30, 32)(Table 1), which are important for relative fast neural transmission, as needed for the fast initiation

of reflexes that serve as a protective defense mechanism against tissue-damaging temperatures, that is, over 52°C. In contrast to TRPV1, TRPV2 is not expressed by keratinocytes.

5.3.3. TRPV3 channels

Three research groups independently identified the TRPV3 channel in 2002 (18, 33, 34). This channel is the third member of the TRPV subfamily, and is expressed more prominently by keratinocytes than by nerve fibers (18). TRPV3 becomes active at innoxious warm temperatures (≥34–38°C) and is also activated by exogenous plant-derived chemicals, which act as skin sensitizers, such as camphor and 2 amino-ethoxydiphenyl borate (2-APB) (35, 36)(Table 1). Camphor activates cultured keratinocytes but not sensory neurons, making camphor a specific activator of TRPV3 channels in keratinocytes (36). Furthermore, it suggests that TRPV3 channels in nerve fibers and keratinocytes are not identical. Co-cultures with keratinocytes from TRPV3-deficient mice were created, in which 10 times less ATP release was found after heat-activation in comparison to wild type cultures (37). These findings further emphasize the importance of TRP channels and ATP in temperature sensation.

5.3.4. TRPV4 channels

The fourth TRPV channel (TRPV4) is active at temperatures between 27 and 35 °C, and is also responsive to osmotic pressure (38-40). This channel was discovered in 2000 and is expressed by C- and Aδ- fibers and by keratinocytes (39, 41, 42). While TRPV3 channels are expressed by cells in the stratum basale (the proliferating layer) of the epidermis (18, 33), TRPV4 channels are confined to keratinocytes in the stratum spinosum (the differentiating layer) (38) (Table 1). This is an interesting finding since the two subpopulations of nociceptive fibers terminate in different layers of the skin: peptidergic fibers ascend to the basal layer and terminate in the stratum spinosum, whereas the nonpeptidergic fibers terminate more superficially, in the stratum granulosum (43).

5.3.5. TRPM8 channels

The TRPM subfamily has only one member called TRPM8 and is activated by innoxious cold temperatures ranging between 25 and 28°C (44, 45). This TRP channel was originally reported in 2003 and called the cold and menthol receptor 1 (CMRl), later renamed TRPM8 channel. The cool sensation that results from the application of menthol to the skin is due to the activation of this channel, which is expressed by both Aδ and C fibres. In addition to menthol, a number of other cooling agents, including icilin, eucalyptol and winsense/N-Ethyl-5-methyl-2-(1-methylethyl)cyclohexanecarboxamide (WS-3), also activate TRPM8 in vitro (45) (Table 1).

Table 1. A summary of the properties of all six thermo-sensitive TRP channels.
Thermal threshold of activation, non-thermal agonists and expression of thermo-sensitive TRP channels are summarized.

TRP-channel	Sensitive for temperature	Non-thermal agonists	Expression in	Reference
TRPV1	>42°C	PH<6.6, capsaicin, or endocannabinoids	Aδ, C-fibers, keratinocytes	(11,26,27)
TRPV2	>52°C	Hypo-osmolarity, growth-factor signaling	Aδ-fibers, DRG	(11,33,34,66)
TRPV3	≥34-38°C	Camphor, 2-APB	Human brain, spinal cord, DRG, and C-fibers	(37,38)
TRPV4	≥27-35°C	Hypo-osmolarity, arachidonic acid metabolites, or 4α-phorbol dibutyryl didecanoate	Aδ, C-fibers, keratinocytes, and DRG	(15,37, 42,13, 81)
TRPM8	≥25-28°C	Mentol, icilin, eucalyptol, WS-3, pungent isothiocyanates	Aδ, and C-fibers	(49, 82)
TRPA1	<17°C	Mentol, pungent natural compound in cinnamon oil (cinnamaldehyde-CA), mustard oil, wintergreen oil (methyl salicylate), clove oil (isoeugenol-IE), icilin and ginger	Aδ, and C-fibers, keratinocytres, dermis and in the epithelium of the hair follicle	(16,45,46,49)

5.3.6. TRPA1

TRPA1 channel is the single member of the TRPA subfamily and is expressed by both Aδ and C-fibers. This channel is activated by noxious cold temperatures (<17°C) (46), and by pungent-natural compounds that are used in cooking, including wasabi, mustard, cinnamon oil (cinnamaldehyde-CA) (46), wintergreen oil (methyl salicylate), clove oil (Isoeugenol-IE), icilin, and ginger (zingerone) to produce a burning pain sensation (47), comparable to nociceptive cold (Table 1). TRPA1 is found in a subset of TRPV1 expressing nerve fibers (47, 48), which may explain the paradoxical heat sensation that is sometimes experienced on exposure to a very cold stimulus.

TRPA1, along with TRPV1, TRPV3 and TRPV4, is also expressed by keratinocytes (19). Gene expression analysis revealed that activation of TRPA1 by TRPA1 agonists modulates the delicate proliferation and differentiation program of keratinocytes (49). In addition, TRPA1 channels affect the keratinocyte-specific inflammatory response; this was shown by the finding (19) that activation by a TRPA1 agonist resulted in an increase in expression of pro-inflammatory cytokines in the epidermis. Thus, TRPA1 channels are important not only for detecting noxious cold temperatures but also for the promotion of cutaneous inflammation by keratinocytes.

5.4.0. Changes following (traumatic) peripheral nerve injury

Peripheral nerve injury, with severely lesioned nerves, leads to immediate and irreversible interruption of nerve conduction followed by (Wallerian) degeneration of the axons distal to the injury, while ganglion cells start up the regeneration process from the proximal stump (50). At the same time, the Schwann cells in the distal segment initiate a response, such as the release of nerve growth factor (NGF) and glial cell line-derived neurotrophic factor (GDNF) (51), that further stimulates regeneration. NGF, produced at the axonal injury site, binds to tyrosine kinase receptor A (TrkA) and is retrogradely transported to the dorsal root ganglion (DRG) somata after nerve injury (52). At the DRG somata, NGF causes a series of morphologic and biochemical changes in the neuronal cell body (53, 54), including increased expression of TRP channel messenger RNAs (mRNAs) (55). Furthermore, the expression of TRP channels in the sensory nerve endings and in the skin increases, a phenomenon also seen in inflammatory states (56). At the same time, increased NGF in the skin leads to collateral sprouting: new nerve fibers braching off from existing undamaged ones (57-59), which leads to an increase in the number of nerve fibers that express TRP channels (Figure 2a). Finally, other inflammatory mediators, such as bradykinin (60) and prostaglandins (61) are released in the skin and bind to their cognate receptors. This causes a decrease in the threshold of TRP channel activation, for example, TRPV1 channels become active at temperatures below 42 °C causing a burning pain sensation as

if the temperature is above 42 °C, which makes TRPV1 channel a contributor to heat intolerance (15) (Figure 2A). Thus, nerve injury-induced thermal intolerance, which includes thermal allodynia (i.e., the situation in which normally non-painful temperatures have become painful) and thermal hyperalgesia (i.e., painful temperatures that have become even more painful), is elicited due to one or more of the following mechanisms that take place in the skin: (a) an increased expression of TRP channels on nerve fibres and on keratinocytes (56), (b) a lower activation-threshold of TRP channels, and (c) sprouting of non-injured nerve fibers (57) (Figure 2). Central changes that contribute to the development and maintenance of thermal intolerance, and may also involve TRP channels (62), are not discussed here.

5.4.1. Cold intolerance

After nerve injury, some patients develop cold intolerance, which makes them hypersensitive for innoxious and/or noxious cold temperatures. One of the definitions of cold intolerance is 'an icy cold feeling that can progress to pain' (63), which is often a prominent symptom in neuropathic pain, and currently it is an essential topic in pain management. The incidence of cold intolerance has been reported to vary between 35% and 91% after upper extremity injury by different groups (64-67). Several lines of evidence have shown that the TRP channels are likely involved in the development of cold intolerance (68). Knocking out the TRPA1 gene in mice eliminated avoidance of temperatures below 17 °C (69). By contrast, the presence of a TRPA1 channel agonist caused increased TRPA1 channel activation and subsequently cold intolerance during mild cooling. These results suggest that TRPA1 is a key mediator of cold intolerance after nerve injury. By contrast, the TRPM8 channel's role in thermal intolerance is controversial. Remarkably, TRPM8-knockout mice were deficient in detecting noxious cold even though the TRPM8 is activated only at innoxious temperatures. This would suggest that TRPM8 is involved in cold intolerance (70-73). However, in neuropathic pain models, in which cold intolerance is present, a decrease instead of an increase in TRPM8 expression is seen in the affected DRGs (55, 74), while the expression in the nearby uninjured DRGs did not change. In addition, decreasing TRPM8 channel expression, using application of anti-sense oligodeoxynucleotides, did not diminish cold intolerance in cold-intolerant animals (74) while administration of TRPM8 antagonists such as vinylcycloalkyl-substituted benzimidazole (75) and capsazepine (70) showed significant less cold intolerance in animal studies. More investigation is essential in which analysis of TRPM8/TRPA1 double-mutant animals are required, as the presence of TRPM8 might be masking any subtle phenotype present in TRPA1-deficient mice. Despite the large number of animal studies with cold intolerance, its mechanism is still not revealed and neither the pharmacological nor the surgical treatments have shown any satisfactory results yet (67). Therefore, cold intolerance is a major challenge for both the clinicians and the scientists.

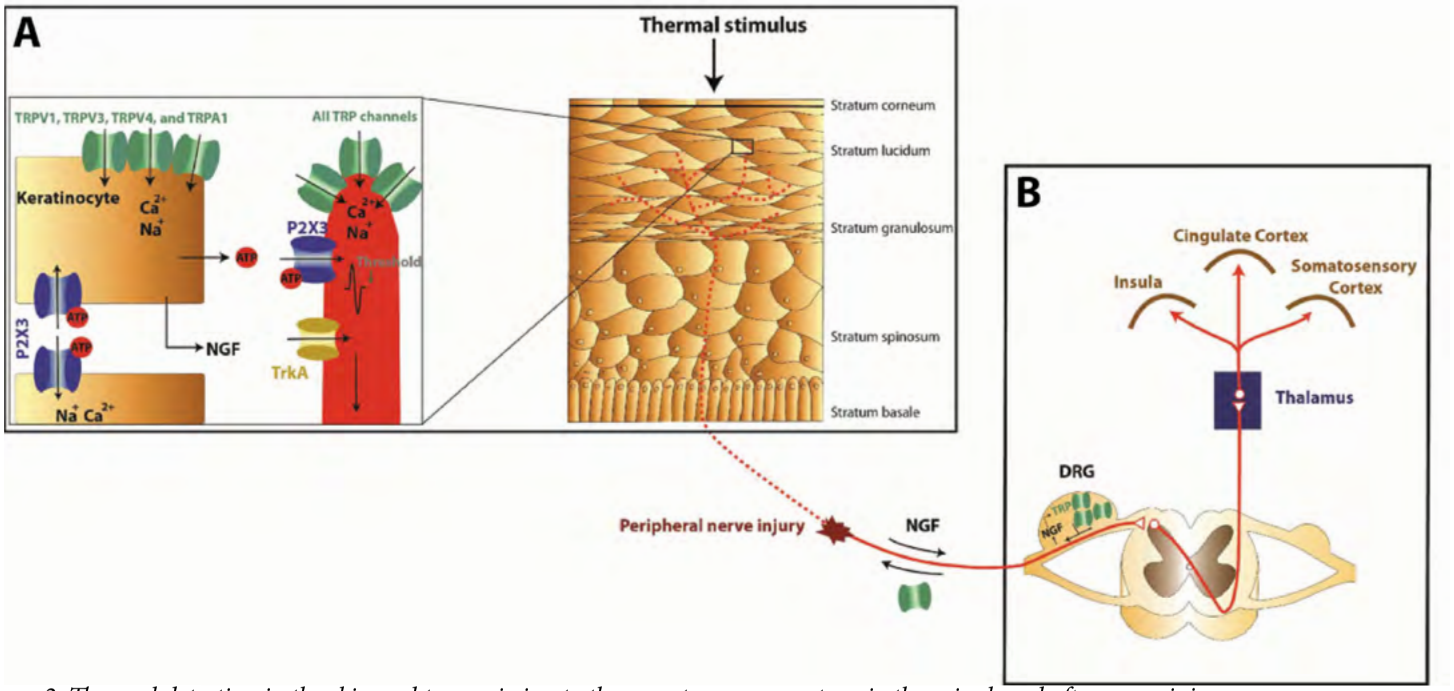

Figure 2. Thermal detection in the skin and transmission to the somatosensory cortex via the spinal cord after nerve injury.
A) Epidermis: most of the TRP channels, which are phosphorylated in the DRG, are subsequently transferred to the periphery and expressed on nerve fiber endings and keratinocytes in the skin. After nerve injury an increased number of TRP channels are expressed on both keratinocytes and adjacent nerve fibers that allow a higher influx of sodium- and calcium ions. In addition, a decrease in the activation threshold is demonstrated in nerve fibers. Both changes cause hypersensitivity to thermal stimuli after nerve injury. In addition, NGF, which is transported from the skin to the DRG elicits excessive nerve fiber growth in the epidermis after nerve regeneration. This leads to an increase in the number of nerve fibers that express TRP channels and causes more interaction sites between keratinocytes and nerve fibers.
B) After nerve injury inflammatory mediators such as NGF are released, which binds to its receptor (TrkA) and mediates increased phosphorylation of TRP channels in the dorsal root ganglion.

5.4.2. Heat intolerance

A less common symptom of neuropathic pain is heat intolerance, which is better known as heat allodynia and hyperalgesia (76). With the discovery of the first thermo-sensitive TRP channel (TRPV1), it was found that overexpression of the TRPV1 channel will lead to heat intolerance (15). This was confirmed in a human study, which also showed an increase in TRPV3 channel expression after nerve injury, while the TRPV4 channel remained unchanged (77). Data about changes in the expression of the remaining thermo-sensitive TRPV2 channel after nerve injury are lacking.

5.4.3. Keratinocytes and thermal intolerance

Apart from nerve fibres, keratinocytes also play a role in thermal intolerance. Increased quantities of ATP were secreted by keratinocytes upon heating in a co-culture study. Subsequently, ATP activated P2X3 receptors on both keratinocytes and nerve fibres, further contributing to thermal intolerance. The secretion of ATP by keratinocytes was found to be compromised in TRPV3-knockout mice, which suggests that this channel is necessary for heat-induced ATP release, with subsequent activation of adjacent nerve fibres (37). In line with this mechanism, it was found in mice that keratinocyte-specific overexpression of TRPV3 and simultaneous application of a TRPV1 antagonist (to prevent activation of TRPV1 channel at temperatures above 42 °C) induced thermal pain at 42 °C through increased activation of TRPV3 ion channels on keratinocytes (78). In agreement with these findings, the expression of both TRPV3 and TRPV4 channels is significantly increased in keratinocytes of skin sections harvested from painful human breast tissue after breast reconstruction (79). These patients reported burning pain, indicating that overexpression of TRPV3 and TRPV4 may account for the pain and thermal intolerance in these patients. These findings provide further evidence for the participation of keratinocytes in thermal sensory transduction and thermal intolerance. Taken together, the above findings show that increased expression of TRPV1 and TRPV3 by nerve fibres, as well as TRPV3 and TRPV4 by keratinocytes, may well lead to heat intolerance

5.5.0. Clinical importance of thermo-sensitive TRP channels

Severe neuropathic pain is directly associated with an impairment in the quality of life (80-82). This is largely due to a weak response to standard pain therapies such as paracetamol, non-steroidal anti-inflammatory drugs (NSAIDs) and opioids, while tricyclic antidepressants may provide some relief (83). According to European Federation of Neurological Societies (EFNS) guidelines, not only the efficacy/safety ratio and the presence of co-morbidities but also the quality of life should be taken into consideration when selecting pharmacological treatment for neuropathic

pain (84). As described by different groups and summarised in this review, active TRP channels are involved in thermal (cold) intolerance. Therefore, specific TRP antagonists have been developed by pharmaceutical companies to provide pain relief.

Some of the developed TRPV1 antagonists (SB705498 , A425619 (85), AMG-9810 (86), BCTC (87, 88), 6-aryl-7-isopropylquinazolinones (89)) have reverted or inhibited neuropathic pain symptoms such as cold intolerance in preclinical trials. Regrettably, only SB705498 reached phase I clinical trial, whereby it reduced capsaicin-evoked flare and heat-evoked pain (90). However, side effects need to be taken into consideration: TRPV1 channels stimulate the production of the neuropeptides calcitonin gene-related peptide (CGRP) and substance P that serve as cardio-protective components by causing vasodilation (91). Since TRPV1 antagonists prevent this protection, they may produce cardiovascular side effects (92). A clinical trial using AMG517 as a TRPV1 antagonist was terminated prematurely due to side effects like persistent hyperthermia (93). Besides hyperthermia, it is shown that TRPV1 antagonists can induce gastric ulcer formation, hypertension and central nervous system effects (94). At present, there are no TRPV1 channel antagonists available for clinical use and the same holds true for analgesics that target TRPV2, TRPV3 or TRPV4 channels. Paradoxically, multiple applications of the TRPV1 channel agonist, capsaicin, produces an antagonistic effect on the TRPV1 channel. Initial application of capsaicin activates peripheral nerve fibres expressing TRPV1 channels, as expected. However, after continued exposure, the TRPV1 channel becomes defunctionalized (95). As a consequence, pain-relieving single application of high-dose (8%) capsaicin patches and repeated application of low-dose (0.075%) capsaicin creams are used in clinical settings with strict dose boundaries to prevent undesirable effects such as skin reactions (96). For the past 20 years, many clinical trials have been published in which capsaicin patches and creams are used to relieve pain not only in cases of posttraumatic neuropathic pain but also in patients with post-mastectomy pain syndrome, diabetic polyneuropathy, posthepatic neuralgia and neuropathic pain in cancer patients (97). Only two randomised, double-blind, placebo-controlled studies reported substantial levels of pain relief (≥50%) (98, 99) while four studies reported moderate levels of pain relief (≥ 30-40%) (100-102). The remaining studies showed decrease in pain in certain categories or no improvement at all (103, 104). In addition, currently a review is published on different classes of compounds that have been identified as TRPA1 antagonists: AMG2504, AMG7160, AMG9090, CMP1, CMP2 and CMP3 (105). However, so far, only a small number of TRPA1 antagonists have been investigated in preclinical in vivo studies due to their partial block of the TRPA1 channel (106). As described previously, genetic deletion of TRPM8 channels identified that this channel could serve as a potential therapeutic target for cold intolerance. However, the application of a TRPM8 antagonist, anti-sense oligodeoxynucleotides, did not diminish hypersensitivity to cold temperatures (74) while capsazepine, a blocker for both TRPM8 and TRPV1 channels, showed significant attenuate of cold intolerance (70).

Unfortunately, there are no data available on the effects of TRPM8 antagonists in clinical trials. It is often debated whether TRPM8 activation, such as the TRPV1 agonist capsaicin, or TRPM8 antagonists could serve as analgesics for cold intolerance.

Neuropathic pain remains a major problem, especially since there is no effective treatment. Since thermal intolerance is a prominent symptom of neuropathic pain and in view of its high incidence after nerve injury, there is a strong clinical need to develop an effective treatment. Thermo-sensitive TRP channels play a crucial role in thermal intolerance and therefore seem to be a suitable target for analgesics. At present, topically applicable capsaicin, the TRPV1 channel agonist, is the only frequently used analgesic that acts on TRP channels and has a pain-relieving effect in patients with thermal intolerance. TRP channel antagonists that are effective analgesics are still not available for clinical use. Nevertheless, the crucial role of TRP channels in temperature sensing makes it difficult to imagine an effective treatment for thermal intolerance that will not involve TRP channels.

5.6.0. References

1. Irwin MS, Gilbert SE, Terenghi G, Smith RW, Green CJ. Cold intolerance following peripheral nerve injury. Natural history and factors predicting severity of symptoms. Journal of hand surgery. [Research Support, Non-U.S. Gov't]. 1997 Jun;22(3):308-16.
2. Kay S. Venous occlusion plethysmography in patients with cold related symptoms after digital salvage procedures. Journal of hand surgery. 1985 Jun;10(2):151-4.
3. Stokvis A, Ruijs AC, van Neck JW, Coert JH. Cold intolerance in surgically treated neuroma patients: a prospective follow-up study. The Journal of hand surgery. 2009 Nov;34(9):1689-95.
4. Provitera V, Nolano M, Pagano A, Caporaso G, Stancanelli A, Santoro L. Myelinated nerve endings in human skin. Muscle Nerve. 2007 Jun;35(6):767-75.
5. Lumpkin EA, Caterina MJ. Mechanisms of sensory transduction in the skin. Nature. 2007 Feb 22;445(7130):858-65.
6. Naka D, Kakigi R. Simple and novel method for measuring conduction velocity of A delta fibers in humans. J Clin Neurophysiol. 1998 Mar;15(2):150-3.
7. Baba H, Doubell TP, Woolf CJ. Peripheral inflammation facilitates Abeta fiber-mediated synaptic input to the substantia gelatinosa of the adult rat spinal cord. J Neurosci. 1999 Jan 15;19(2):859-67.
8. Coghill RC, Sang CN, Maisog JM, Iadarola MJ. Pain intensity processing within the human brain: a bilateral, distributed mechanism. J Neurophysiol. 1999 Oct;82(4):1934-43.
9. Peltz E, Seifert F, DeCol R, Dorfler A, Schwab S, Maihofner C. Functional connectivity of the human insular cortex during noxious and innocuous thermal stimulation. NeuroImage. [Research Support, Non-U.S. Gov't]. 2011 Jan 15;54(2):1324-35.
10. Minke B. Drosophila mutant with a transducer defect. Biophys Struct Mech. 1977 Apr 21;3(1):59-64.
11. Xiao R, Xu XZ. Function and regulation of TRP family channels in C. elegans. Pflugers Archiv : European journal of physiology. [Research Support, N.I.H., ExtramuralResearch Support, Non-U.S. Gov'tReview]. 2009 Sep;458(5):851-60.
12. Caterina MJ, Schumacher MA, Tominaga M, Rosen TA, Levine JD, Julius D. The capsaicin receptor: a heat-activated ion channel in the pain pathway. Nature. 1997 Oct 23;389(6653):816-24.
13. Noel J, Zimmermann K, Busserolles J, Deval E, Alloui A, Diochot S, et al. The mechano-activated K+ channels TRAAK and TREK-1 control both warm and cold perception. The EMBO journal. [Research Support, Non-U.S. Gov't]. 2009 May 6;28(9):1308-18.
14. Abe R, Tominaga T, Nomizu T, Nomura Y, Takashima S, Koyama H, et al. [CGS20267 (Letrozole), a new aromatase inhibitor: late phase II study for postmenopausal women with advanced or recurrent breast cancer (no. 1)

Clinical TrialClinical Trial, Phase IMulticenter StudyRandomized Controlled Trial]. 2002 May;29(5):729-40.
15. Caterina MJ, Leffler A, Malmberg AB, Martin WJ, Trafton J, Petersen-Zeitz KR, et al. Impaired nociception and pain sensation in mice lacking the capsaicin receptor. Science. 2000 Apr 14;288(5464):306-13.
16. Tominaga M, Caterina MJ, Malmberg AB, Rosen TA, Gilbert H, Skinner K, et al. The cloned capsaicin receptor integrates multiple pain-producing stimuli. Neuron. 1998 Sep;21(3):531-43.
17. Caterina MJ, Julius D. The vanilloid receptor: a molecular gateway to the pain pathway. Annu Rev Neurosci. 2001;24:487-517.
18. Peier AM, Reeve AJ, Andersson DA, Moqrich A, Earley TJ, Hergarden AC, et al. A heat-sensitive TRP channel expressed in keratinocytes. Science. 2002 Jun 14;296(5575):2046-9.
19. Atoyan R, Shander D, Botchkareva NV. Non-neuronal expression of transient receptor potential type A1 (TRPA1) in human skin. J Invest Dermatol. 2009 Sep;129(9):2312-5.
20. Denda M, Fujiwara S, Hibino T. Expression of voltage-gated calcium channel subunit alpha1C in epidermal keratinocytes and effects of agonist and antagonists of the channel on skin barrier homeostasis. Exp Dermatol. 2006 Jun;15(6):455-60.
21. Inoue R, Ito Y, Mori Y. [The TRP proteins, a rapidly expanding Ca2+ entry channel family and a new molecular target for drug development]. Nihon Rinsho. 2002 Jan;60(1):18-24.
22. Smith WL, DeWitt DL, Garavito RM. Cyclooxygenases: structural, cellular, and molecular biology. Annu Rev Biochem. 2000;69:145-82.
23. Funk CD. Prostaglandins and leukotrienes: advances in eicosanoid biology. Science. 2001 Nov 30;294(5548):1871-5.
24. Chen CC, Akopian AN, Sivilotti L, Colquhoun D, Burnstock G, Wood JN. A P2X purinoceptor expressed by a subset of sensory neurons. Nature. 1995 Oct 5;377(6548):428-31.
25. Bardoni R, Goldstein PA, Lee CJ, Gu JG, MacDermott AB. ATP P2X receptors mediate fast synaptic transmission in the dorsal horn of the rat spinal cord. J Neurosci. 1997 Jul 15;17(14):5297-304.
26. Hilliges M, Wang L, Johansson O. Ultrastructural evidence for nerve fibers within all vital layers of the human epidermis. J Invest Dermatol. 1995 Jan;104(1):134-7.
27. Chateau Y, Dorange G, Clement JF, Pennec JP, Gobin E, Griscom L, et al. In vitro reconstruction of neuro-epidermal connections. J Invest Dermatol. 2007 Apr;127(4):979-81.
28. Inoue K, Denda M, Tozaki H, Fujishita K, Koizumi S. Characterization of multiple P2X receptors in cultured normal human epidermal keratinocytes. J Invest Dermatol. 2005 Apr;124(4):756-63.

29. Denda M, Fuziwara S, Inoue K, Denda S, Akamatsu H, Tomitaka A, et al. Immunoreactivity of VR1 on epidermal keratinocyte of human skin. Biochem Biophys Res Commun. 2001 Aug 3;285(5):1250-2.
30. Caterina MJ, Rosen TA, Tominaga M, Brake AJ, Julius D. A capsaicin-receptor homologue with a high threshold for noxious heat. Nature. 1999 Apr 1;398(6726):436-41.
31. Muraki K, Iwata Y, Katanosaka Y, Ito T, Ohya S, Shigekawa M, et al. TRPV2 is a component of osmotically sensitive cation channels in murine aortic myocytes. Circ Res. 2003 Oct 31;93(9):829-38.
32. Benham CD, Gunthorpe MJ, Davis JB. TRPV channels as temperature sensors. Cell Calcium. 2003 May-Jun;33(5-6):479-87.
33. Xu H, Ramsey IS, Kotecha SA, Moran MM, Chong JA, Lawson D, et al. TRPV3 is a calcium-permeable temperature-sensitive cation channel. Nature. 2002 Jul 11;418(6894):181-6.
34. Smith GD, Gunthorpe MJ, Kelsell RE, Hayes PD, Reilly P, Facer P, et al. TRPV3 is a temperature-sensitive vanilloid receptor-like protein. Nature. 2002 Jul 11;418(6894):186-90.
35. Chung MK, Lee H, Mizuno A, Suzuki M, Caterina MJ. 2-aminoethoxydiphenyl borate activates and sensitizes the heat-gated ion channel TRPV3. J Neurosci. 2004 Jun 2;24(22):5177-82.
36. Moqrich A, Hwang SW, Earley TJ, Petrus MJ, Murray AN, Spencer KS, et al. Impaired thermosensation in mice lacking TRPV3, a heat and camphor sensor in the skin. Science. 2005 Mar 4;307(5714):1468-72.
37. Mandadi S, Sokabe T, Shibasaki K, Katanosaka K, Mizuno A, Moqrich A, et al. TRPV3 in keratinocytes transmits temperature information to sensory neurons via ATP. Pflugers Arch. 2009 Oct;458(6):1093-102.
38. Guler AD, Lee H, Iida T, Shimizu I, Tominaga M, Caterina M. Heat-evoked activation of the ion channel, TRPV4. J Neurosci. 2002 Aug 1;22(15):6408-14.
39. Liedtke W, Choe Y, Marti-Renom MA, Bell AM, Denis CS, Sali A, et al. Vanilloid receptor-related osmotically activated channel (VR-OAC), a candidate vertebrate osmoreceptor. Cell. 2000 Oct 27;103(3):525-35.
40. Suzuki M, Mizuno A, Kodaira K, Imai M. Impaired pressure sensation in mice lacking TRPV4. J Biol Chem. 2003 Jun 20;278(25):22664-8.
41. Suzuki M, Watanabe Y, Oyama Y, Mizuno A, Kusano E, Hirao A, et al. Localization of mechanosensitive channel TRPV4 in mouse skin. Neurosci Lett. 2003 Dec 26;353(3):189-92.
42. Chung MK, Lee H, Mizuno A, Suzuki M, Caterina MJ. TRPV3 and TRPV4 mediate warmth-evoked currents in primary mouse keratinocytes. J Biol Chem. 2004 May 14;279(20):21569-75.
43. Zylka MJ, Rice FL, Anderson DJ. Topographically distinct epidermal nociceptive circuits revealed by axonal tracers targeted to Mrgprd. Neuron. 2005 Jan 6;45(1):17-25.
44. Peier AM, Moqrich A, Hergarden AC, Reeve AJ, Andersson DA, Story GM,

et al. A TRP channel that senses cold stimuli and menthol. Cell. 2002 Mar 8;108(5):705-15.
45. McKemy DD, Neuhausser WM, Julius D. Identification of a cold receptor reveals a general role for TRP channels in thermosensation. Nature. 2002 Mar 7;416(6876):52-8.
46. Story GM, Peier AM, Reeve AJ, Eid SR, Mosbacher J, Hricik TR, et al. ANKTM1, a TRP-like channel expressed in nociceptive neurons, is activated by cold temperatures. Cell. 2003 Mar 21;112(6):819-29.
47. Bandell M, Story GM, Hwang SW, Viswanath V, Eid SR, Petrus MJ, et al. Noxious cold ion channel TRPA1 is activated by pungent compounds and bradykinin. Neuron. 2004 Mar 25;41(6):849-57.
48. Anand U, Otto WR, Facer P, Zebda N, Selmer I, Gunthorpe MJ, et al. TRPA1 receptor localisation in the human peripheral nervous system and functional studies in cultured human and rat sensory neurons. Neurosci Lett. 2008 Jun 20;438(2):221-7.
49. Biro T, Kovacs L. An "ice-cold" TR(i)P to skin biology: the role of TRPA1 in human epidermal keratinocytes. The Journal of investigative dermatology. [CommentResearch Support, Non-U.S. Gov't]. 2009 Sep;129(9):2096-9.
50. Guertin AD, Zhang DP, Mak KS, Alberta JA, Kim HA. Microanatomy of axon/glial signaling during Wallerian degeneration. J Neurosci. 2005 Mar 30;25(13):3478-87.
51. Trupp M, Belluardo N, Funakoshi H, Ibanez CF. Complementary and overlapping expression of glial cell line-derived neurotrophic factor (GDNF), c-ret proto-oncogene, and GDNF receptor-alpha indicates multiple mechanisms of trophic actions in the adult rat CNS. The Journal of neuroscience : the official journal of the Society for Neuroscience. [Research Support, Non-U.S. Gov't]. 1997 May 15;17(10):3554-67.
52. Curtis R, Tonra JR, Stark JL, Adryan KM, Park JS, Cliffer KD, et al. Neuronal injury increases retrograde axonal transport of the neurotrophins to spinal sensory neurons and motor neurons via multiple receptor mechanisms. Molecular and cellular neurosciences. 1998 Oct;12(3):105-18.
53. Reichardt LF. Neurotrophin-regulated signalling pathways. Philosophical transactions of the Royal Society of London Series B, Biological sciences. [Research Support, N.I.H., ExtramuralResearch Support, Non-U.S. Gov'tReview]. 2006 Sep 29;361(1473):1545-64.
54. Hanz S, Fainzilber M. Retrograde signaling in injured nerve--the axon reaction revisited. Journal of neurochemistry. [Research Support, Non-U.S. Gov'tReview]. 2006 Oct;99(1):13-9.
55. Frederick J, Buck ME, Matson DJ, Cortright DN. Increased TRPA1, TRPM8, and TRPV2 expression in dorsal root ganglia by nerve injury. Biochem Biophys Res Commun. 2007 Jul 13;358(4):1058-64.
56. Ji RR, Samad TA, Jin SX, Schmoll R, Woolf CJ. p38 MAPK activation by NGF in primary sensory neurons after inflammation increases TRPV1 levels and maintains heat hyperalgesia. Neuron. 2002 Sep 26;36(1):57-68.

57. Duraku LS, Hossaini M, Hoendervangers S, Falke LL, Kambiz S, Mudera VC, et al. Spatiotemporal dynamics of re-innervation and hyperinnervation patterns by uninjured CGRP fibers in the rat foot sole epidermis after nerve injury. Molecular pain. 2012 Aug 30;8(1):61.
58. Diamond J, Holmes M, Coughlin M. Endogenous NGF and nerve impulses regulate the collateral sprouting of sensory axons in the skin of the adult rat. J Neurosci. 1992 Apr;12(4):1454-66.
59. Di Marco E, Marchisio PC, Bondanza S, Franzi AT, Cancedda R, De Luca M. Growth-regulated synthesis and secretion of biologically active nerve growth factor by human keratinocytes. The Journal of biological chemistry. [Research Support, Non-U.S. Gov't]. 1991 Nov 15;266(32):21718-22.
60. Cesare P, Dekker LV, Sardini A, Parker PJ, McNaughton PA. Specific involvement of PKC-epsilon in sensitization of the neuronal response to painful heat. Neuron. 1999 Jul;23(3):617-24.
61. Hu HJ, Bhave G, Gereau RWt. Prostaglandin and protein kinase A-dependent modulation of vanilloid receptor function by metabotropic glutamate receptor 5: potential mechanism for thermal hyperalgesia. J Neurosci. 2002 Sep 1;22(17):7444-52.
62. Kim YH, Back SK, Davies AJ, Jeong H, Jo HJ, Chung G, et al. TRPV1 in GABAergic interneurons mediates neuropathic mechanical allodynia and disinhibition of the nociceptive circuitry in the spinal cord. Neuron. [Research Support, Non-U.S. Gov't]. 2012 May 24;74(4):640-7.
63. Engkvist O, Wahren LK, Wallin G, Torebjrk E, Nystrom B. Effects of regional intravenous guanethidine block in posttraumatic cold intolerance in hand amputees. Journal of hand surgery. [Research Support, Non-U.S. Gov't]. 1985 Jun;10(2):145-50.
64. Ruijs AC, Jaquet JB, van Riel WG, Daanen HA, Hovius SE. Cold intolerance following median and ulnar nerve injuries: prognosis and predictors. J Hand Surg Eur Vol. 2007 Aug;32(4):434-9.
65. Carlsson IK, Rosen B, Dahlin LB. Self-reported cold sensitivity in normal subjects and in patients with traumatic hand injuries or hand-arm vibration syndrome. BMC Musculoskelet Disord. 2010;11:89.
66. Nijhuis TH, Smits ES, Jaquet JB, Van Oosterom FJ, Selles RW, Hovius SE. Prevalence and severity of cold intolerance in patients after hand fracture. J Hand Surg Eur Vol. 2010 May;35(4):306-11.
67. Stokvis A, Ruijs AC, van Neck JW, Coert JH. Cold intolerance in surgically treated neuroma patients: a prospective follow-up study. J Hand Surg Am. 2009 Nov;34(9):1689-95.
68. Obata K, Katsura H, Mizushima T, Yamanaka H, Kobayashi K, Dai Y, et al. TRPA1 induced in sensory neurons contributes to cold hyperalgesia after inflammation and nerve injury. J Clin Invest. 2005 Sep;115(9):2393-401.
69. Rosenzweig M, Brennan KM, Tayler TD, Phelps PO, Patapoutian A, Garrity PA. The Drosophila ortholog of vertebrate TRPA1 regulates thermotaxis. Genes Dev. 2005 Feb 15;19(4):419-24.

70. Xing H, Chen M, Ling J, Tan W, Gu JG. TRPM8 mechanism of cold allodynia after chronic nerve injury. J Neurosci. 2007 Dec 12;27(50):13680-90.
71. Knowlton WM, Bifolck-Fisher A, Bautista DM, McKemy DD. TRPM8, but not TRPA1, is required for neural and behavioral responses to acute noxious cold temperatures and cold-mimetics in vivo. Pain. 2010 Aug;150(2):340-50.
72. Dhaka A, Murray AN, Mathur J, Earley TJ, Petrus MJ, Patapoutian A. TRPM8 is required for cold sensation in mice. Neuron. 2007 May 3;54(3):371-8.
73. Colburn RW, Lubin ML, Stone DJ, Jr., Wang Y, Lawrence D, D'Andrea MR, et al. Attenuated cold sensitivity in TRPM8 null mice. Neuron. 2007 May 3;54(3):379-86.
74. Katsura H, Obata K, Mizushima T, Yamanaka H, Kobayashi K, Dai Y, et al. Antisense knock down of TRPA1, but not TRPM8, alleviates cold hyperalgesia after spinal nerve ligation in rats. Exp Neurol. 2006 Jul;200(1):112-23.
75. Calvo RR, Meegalla SK, Parks DJ, Parsons WH, Ballentine SK, Lubin ML, et al. Discovery of vinylcycloalkyl-substituted benzimidazole TRPM8 antagonists effective in the treatment of cold allodynia. Bioorg Med Chem Lett. 2012 Mar 1;22(5):1903-7.
76. Costigan M, Scholz J, Woolf CJ. Neuropathic pain: a maladaptive response of the nervous system to damage. Annual review of neuroscience. [Research Support, N.I.H., ExtramuralReview]. 2009;32:1-32.
77. Facer P, Casula MA, Smith GD, Benham CD, Chessell IP, Bountra C, et al. Differential expression of the capsaicin receptor TRPV1 and related novel receptors TRPV3, TRPV4 and TRPM8 in normal human tissues and changes in traumatic and diabetic neuropathy. BMC Neurol. 2007;7:11.
78. Huang SM, Lee H, Chung MK, Park U, Yu YY, Bradshaw HB, et al. Overexpressed transient receptor potential vanilloid 3 ion channels in skin keratinocytes modulate pain sensitivity via prostaglandin E2. J Neurosci. 2008 Dec 17;28(51):13727-37.
79. Gopinath P, Wan E, Holdcroft A, Facer P, Davis JB, Smith GD, et al. Increased capsaicin receptor TRPV1 in skin nerve fibres and related vanilloid receptors TRPV3 and TRPV4 in keratinocytes in human breast pain. BMC Womens Health. 2005 Mar 8;5(1):2.
80. Ciaramitaro P, Mondelli M, Logullo F, Grimaldi S, Battiston B, Sard A, et al. Traumatic peripheral nerve injuries: epidemiological findings, neuropathic pain and quality of life in 158 patients. J Peripher Nerv Syst. 2010 Jun;15(2):120-7.
81. Cocito D, Paolasso I, Pazzaglia C, Tavella A, Poglio F, Ciaramitaro P, et al. Pain affects the quality of life of neuropathic patients. Neurol Sci. 2006 Jul;27(3):155-60.
82. Jensen MP, Chodroff MJ, Dworkin RH. The impact of neuropathic pain on health-related quality of life: review and implications. Neurology. 2007 Apr 10;68(15):1178-82.
83. McCleane G. Pharmacological management of neuropathic pain. CNS Drugs. 2003;17(14):1031-43.

84. Attal N, Cruccu G, Baron R, Haanpaa M, Hansson P, Jensen TS, et al. EFNS guidelines on the pharmacological treatment of neuropathic pain: 2010 revision. Eur J Neurol. 2010 Sep;17(9):1113-e88.
85. Honore P, Wismer CT, Mikusa J, Zhu CZ, Zhong C, Gauvin DM, et al. A-425619 [1-isoquinolin-5-yl-3-(4-trifluoromethyl-benzyl)-urea], a novel transient receptor potential type V1 receptor antagonist, relieves pathophysiological pain associated with inflammation and tissue injury in rats. J Pharmacol Exp Ther. 2005 Jul;314(1):410-21.
86. Gavva NR, Tamir R, Qu Y, Klionsky L, Zhang TJ, Immke D, et al. AMG 9810 [(E)-3-(4-t-butylphenyl)-N-(2,3-dihydrobenzo[b][1,4] dioxin-6-yl)acrylamide], a novel vanilloid receptor 1 (TRPV1) antagonist with antihyperalgesic properties. J Pharmacol Exp Ther. 2005 Apr;313(1):474-84.
87. Valenzano KJ, Grant ER, Wu G, Hachicha M, Schmid L, Tafesse L, et al. N-(4-tertiarybutylphenyl)-4-(3-chloropyridin-2-yl)tetrahydropyrazine -1(2H)-carbox-amide (BCTC), a novel, orally effective vanilloid receptor 1 antagonist with analgesic properties: I. in vitro characterization and pharmacokinetic properties. J Pharmacol Exp Ther. 2003 Jul;306(1):377-86.
88. Krause JE, Chenard BL, Cortright DN. Transient receptor potential ion channels as targets for the discovery of pain therapeutics. Curr Opin Investig Drugs. 2005 Jan;6(1):48-57.
89. Culshaw AJ, Bevan S, Christiansen M, Copp P, Davis A, Davis C, et al. Identification and biological characterization of 6-aryl-7-isopropylquinazolinones as novel TRPV1 antagonists that are effective in models of chronic pain. J Med Chem. 2006 Jan 26;49(2):471-4.
90. Rami HK, Thompson M, Stemp G, Fell S, Jerman JC, Stevens AJ, et al. Discovery of SB-705498: a potent, selective and orally bioavailable TRPV1 antagonist suitable for clinical development. Bioorg Med Chem Lett. 2006 Jun 15;16(12):3287-91.
91. Julius D, Basbaum AI. Molecular mechanisms of nociception. Nature. 2001 Sep 13;413(6852):203-10.
92. Wang DH. The vanilloid receptor and hypertension. Acta Pharmacol Sin. 2005 Mar;26(3):286-94.
93. Gavva NR, Bannon AW, Hovland DN, Jr., Lehto SG, Klionsky L, Surapaneni S, et al. Repeated administration of vanilloid receptor TRPV1 antagonists attenuates hyperthermia elicited by TRPV1 blockade. The Journal of pharmacology and experimental therapeutics. 2007 Oct;323(1):128-37.
94. Szallasi A, Appendino G. Vanilloid receptor TRPV1 antagonists as the next generation of painkillers. Are we putting the cart before the horse? J Med Chem. 2004 May 20;47(11):2717-23.
95. Knotkova H, Pappagallo M, Szallasi A. Capsaicin (TRPV1 Agonist) therapy for pain relief: farewell or revival? The Clinical journal of pain. [Review]. 2008 Feb;24(2):142-54.
96. Attal N, Cruccu G, Baron R, Haanpaa M, Hansson P, Jensen TS, et al. EFNS

guidelines on the pharmacological treatment of neuropathic pain: 2010 revision. European journal of neurology : the official journal of the European Federation of Neurological Societies. [Meta-Analysis Practice Guideline Review]. 2010 Sep;17(9):1113-e88.
97. Derry S, Lloyd R, Moore RA, McQuay HJ. Topical capsaicin for chronic neuropathic pain in adults. Cochrane Database Syst Rev. 2009(4):CD007393.
98. Watson CP, Evans RJ. The postmastectomy pain syndrome and topical capsaicin: a randomized trial. Pain. 1992 Dec;51(3):375-9.
99. Ellison N, Loprinzi CL, Kugler J, Hatfield AK, Miser A, Sloan JA, et al. Phase III placebo-controlled trial of capsaicin cream in the management of surgical neuropathic pain in cancer patients. J Clin Oncol. 1997 Aug;15(8):2974-80.
100. Backonja MM, Malan TP, Vanhove GF, Tobias JK, Group CS. NGX-4010, a high-concentration capsaicin patch, for the treatment of postherpetic neuralgia: a randomized, double-blind, controlled study with an open-label extension. Pain Med. 2010 Apr;11(4):600-8.
101. Bernstein JE, Korman NJ, Bickers DR, Dahl MV, Millikan LE. Topical capsaicin treatment of chronic postherpetic neuralgia. J Am Acad Dermatol. 1989 Aug;21(2 Pt 1):265-70.
102. Simpson DM, Gazda S, Brown S, Webster LR, Lu SP, Tobias JK, et al. Long-term safety of NGX-4010, a high-concentration capsaicin patch, in patients with peripheral neuropathic pain. J Pain Symptom Manage. 2010 Jun;39(6):1053-64.
103. Basha KM, Whitehouse FW. Capsaicin: a therapeutic option for painful diabetic neuropathy. Henry Ford Hosp Med J. 1991;39(2):138-40.
104. Low PA, Opfer-Gehrking TL, Dyck PJ, Litchy WJ, O'Brien PC. Double-blind, placebo-controlled study of the application of capsaicin cream in chronic distal painful polyneuropathy. Pain. 1995 Aug;62(2):163-8.
105. Andrade EL, Meotti FC, Calixto JB. TRPA1 antagonists as potential analgesic drugs. Pharmacol Therapeut. 2012 Feb;133(2):189-204.
106. Patapoutian A, Tate S, Woolf CJ. Transient receptor potential channels: targeting pain at the source. Nat Rev Drug Discov. 2009 Jan;8(1):55-68.

Chapter 6

Early changes in epidermal innervation detected by skin rewarming rate

Shoista Kambiz, Johan W. van Neck, Saniye G. Cosgun, Marit H.N. van Velzen, Joop A.M.J.L. Janssen, Naim Avazverdi, Tom J.H. Ruigrok, Erik T. Walbeehm

Based on: An early diagnostic tool for diabetic peripheral neuropathy in rats. PLoS One 2015; 10 (5)

6.1.0. Abstract

The skin's rewarming rate of diabetic patients is used as a diagnostic tool for early diagnosis of diabetic neuropathy. At present, the relationship between microvascular changes in the skin and diabetic neuropathy is unclear in streptozotocin (STZ) diabetic rats. The aim of this study was to investigate whether the skin rewarming rate in diabetic rats is related to microvascular changes and whether this is accompanied by changes observed in classical diagnostic methods for diabetic peripheral neuropathy. Computer-assisted infrared thermography was used to assess the rewarming rate after cold exposure on the plantar skin of STZ diabetic rats' hind paws. Peripheral neuropathy was determined by the density of intra-epidermal nerve fibers (IENFs), mechanical sensitivity, and electrophysiological recordings. Data were obtained in diabetic rats at 4, 6, and 8 weeks after the induction of diabetes and in controls. Four weeks after the induction of diabetes, a delayed rewarming rate, decreased skin blood flow and decreased density of IENFs were observed. However, the mechanical hyposensitivity and decreased motor nerve conduction velocity (MNCV) developed 6 and 8 weeks after the induction of diabetes.

Our study shows that the skin rewarming rate is related to microvascular changes in diabetic rats. Moreover, the skin rewarming rate is a non-invasive method that provides more information for an earlier diagnosis of peripheral neuropathy than the classical monofilament test and MNCV in STZ induced diabetic rats.

6.2.0. Introduction

Diabetic peripheral neuropathy is a common complication of diabetes (1). Assessment of the density of IENFs in a skin biopsy is considered to be a reliable method to measure diabetic peripheral neuropathy in both human diabetes and animal models with diabetes (2, 3). However, taking skin biopsies may be considered a risk factor in a disease where wound healing is prone to be disturbed. Moreover, skin biopsies cover only a small area and are invasive. In contrast, corneal nerve parameters and nerve conduction velocity are non-invasive diagnostic tools to determine diabetic peripheral neuropathy. However, corneal nerve parameters do not directly test the areas that are affected by peripheral neuropathy. Furthermore, nerve conduction is a measure of the degree to which an axon is myelinated and therefore neglects the small unmyelinated fibers (4).

Reduction of nerve conduction velocity in diabetic peripheral neuropathy has been shown to be preceded by impaired vasodilation of the arterioles (5). Consistent with this, thermography studies have reported decreased skin temperatures in diabetic subjects with microvascular disease before other clinical signs of peripheral neuropathy can be identified (6-8). In addition, the rewarming rate of the skin after cooling has been demonstrated to be useful for early diagnosis

of diabetic peripheral neuropathy (9, 10). Taken together, these data suggest that signs of microvascular disease are already present prior to the development of clinically overtdiabetic peripheral neuropathy. Therefore, monitoring changes in skin rewarming rate may enable early diagnosis and management of diabetic peripheral neuropathy, leading to reduction in the development of foot ulcers (11) and infections, which are often followed by amputations.

The STZ induced diabetic rat is one of the most frequently used animal models to study diabetes (12, 13). However, the exact relationships between microvascular changes and diabetic peripheral neuropathy have not been studied in this animal model. Therefore, in the present study, microvascular changes in the plantar skin of STZ diabetic rats were studied and related to the development of diabetic peripheral neuropathy. In addition, the onset of detectable changes by classical diagnostic tools such as sensitivity to the intensity of pressure, the density of IENFs and MNCV were compared to the skin rewarming rate in STZ diabetic rats. With these tools it was investigated whether the skin rewarming rate could serve as an early diagnostic tool for diabetic peripheral neuropathy in STZ diabetic rats as is shown in human diabetes.

6.3.0. Materials and Methods

6.3.1. Animals and anesthesia

WAG/RijHsd female rats (n = 27, 10 weeks old, weighing 130–150 gram) were purchased from Charles River (l'Arbresle, France) (14). The animals were pair-housed in hooded cages at room temperature on a 12-hour light/dark schedule, and were given water and food ad libitum. All experiments were approved by the Dutch Ethical Committee on Animal Welfare according to the European guidelines for the care and use of laboratory animals (Council Directive 86/6009/EEC).

6.3.2. Induction of diabetes

Diabetes was induced in 21 rats by a single intra-peritoneal injection of STZ (Sigma-Aldrich, St. Louis, MO, USA) at a dose of 65 mg/kg body weight in 0.05 mol/L sodium citrate buffer, pH 4.5, as described previously (14). The rats were randomly assigned into 3 groups: A, B and C (n = 7 in each group). Following diabetes induction, group A was killed after 4 weeks, group B after 6 weeks and group C after 8 weeks. The control group consisted of 6 rats who received a single intra-peritoneal injection with an equal volume of vehicle without STZ. Control rats were followed for 8 weeks. Blood glucose was measured from tail vein blood by a glucometer (OneTouch, LifeScan, Milpitas, California, USA). Diabetes was diagnosed in rats, when blood glucose levels were higher than 20 mmol/L during the entire 4 weeks after the induction of diabetes. Insulin treatment was not given.

6.3.3. The blood flow and oxygenation of the plantar hind paws' skin

A combined laser doppler flowmetry and spectrophotometry system (O2C, LEA Medizintechnik, Giessen, Germany), which has been applied in human and animal studies (15, 16), was used to non-invasively measure blood flow and oxygen saturation of the glabrous plantar hind paws. In both diabetic and control rats the percentage oxygen saturation and amount of skin blood flow were assessed at 4, 6, and 8 weeks.

6.3.4. Rewarming rate after cold exposure

The temperature of the skin was assessed using the built-in infrared digital video camera (320 × 240 pixels) by 1 Hz data acquisition system (ThermaCAM Researcher 2001 HS; FLIR Systems, Berchem, Belgium), and all data were continuously collected by a laptop. The distance between the camera and the hind paw was 13 cm ± 2 cm. The pixel size of the temperature recordings was 0.8 × 0.8 mm. The skin temperature of the entire plantar hind paw was recorded while the animal was fixed after placing the animal on a 14°C plate for 5 seconds. The minimum temperature of the plantar hind paws were exported to text files using ThermaCAM Researcher Pro (version 2001-HS; FLIR Systems, Wilsonville, Oregon, USA). The area of interest was selected by drawing a line surrounding the entire plantar hind paws. The average rewarming rate is demonstrated as the increase in skin temperature per 120 seconds.

6.3.5. Thermal sensitivity

In order to determine the occurrence of thermal hypersensitivity, cold and hot plate tests were performed as described previously (17, 18). In short, rats were placed in an open-ended chamber with clear walls with a surface temperature of either 5°C (cold plate) or 50°C (hot plate). These experiments were performed on separate days to prevent interference. The time until hind paw withdrawal or licking was observed.

6.3.6. Von Frey test

In the von Frey test, used to determine the mechanical sensitivity threshold for nociception, each rat was placed in a chamber with a mesh metal floor. Then, von Frey hairs, ranging from 2 to 300 grams, were applied 5 times, and was scored positive when a minimum of 3 paw flicks (the animal's reflex withdrawal response) were observed, as described previously (19). The control group served as the reference group.

6.3.7. Electromyography

Innervation of motor axons in muscles was evaluated by recording the evoked CMAP peak-to-peak amplitudes and latencies of the gastrocnemius muscles (20) in the diabetic groups and control animals as described previously (21). CMAP peak-to-peak amplitudes and latencies were recorded and averaged over a batch of 20 responses. The average amplitudes in each diabetes group were compared to the control group. The MNCV was calculated as the distance of stimulating electrode to recording electrode (mm)/latency (ms).

6.3.8. Tissue preparation

After 4, 6, or 8 weeks, the animals were killed by an overdose of pentobarbital (100mg/kg ip). For each rat, the plantar skin of the hind paw was dissected and directly immersion-fixed in 2% paraformaldehyde-lysin-periodate (PLP) for 24 hours at 4°C. The skin was further processed and embedded in gelatin as described previously (22). Finally, the embedded skin was sectioned at 40 μm with a freezing microtome and collected in glycerol for long-term storage at -20°C.

The pancreas tissue of the rats was harvested, fixed in 10% neutral buffered formalin solution, and embedded in paraffin. Subsequently, these specimens were stained with hematoxylin and eosin (H&E). Each specimen was evaluated by a bright-field microscope and scanned into digital slides (Nanozoomer 2.0 series SYSTEM, Hamamatzu, Japan).

6.3.9. Immunohistochemistry

Immunohistochemistry of the skin sections was performed as previously described to semi quantify the density of sensory nerve fibers innervating the skin (22), and to evaluate the presence of CD-31 positive endothelial cells. The skin sections were incubated for 48 hours in a cocktail of 2% bovine serum albumin containing the diluted primary antibody protein gene product 9.5 (PGP9.5, 1/10.000, anti-rabbit, Enzo Life Sciences, New York, USA), or anti-CD31+ (1/5000, anti-rabbit, Spring Bioscience, California, USA) at 4°C. Subsequently, skin sections where incubated with the appropriate secondary biotinylated antibody labeled with horseradish peroxidase (HRP) (1/200, Biotine, Sigma-Aldrich, St. Louis, MO, USA) for 90 min at RT. The 3, -3' diaminobenzidine (DAB) reaction was then used to reveal the antigenic binding sites of the primary antibodies (23). Thereafter, the sections were mounted on slides and the CD31+ stained sections stained with 0.05% thionin for 4 minutes, which colored the keratinocytes blue. Finally, all skin sections were dehydrated using absolute ethanol (< 0.01% methanol), transferred to xylene, and cover slipped with Permount (Fisher Scientific, Hampton, NH). Each skin section was scanned in 3 layers of 8μm each by Nanozoomer 2.0 series (Nanozoomer 2.0 series, Hamamatzu, Japan). Four proximal and 4 distal skin sections of the plantar

hind paw were quantified for epidermal nerve fibers in the center part of the plantar hind paw (80.000 μm2) using a 40x objective in ImageScope software (Aperio ImageScope v11.1.2.760) (24, 25). The average labeled nerve fibers per mm2 and the average epidermal thickness were calculated for each rat. Percentage CD31-positive cells was calculated by Leica Cell-D (Olympus, Imaging software for life science microscopy, USA) in 4 proximal and 4 distal skin sections over the entire upper dermis of the plantar hind paw.

6.3.10. Statistical analysis

Results were presented as means with standard error of the mean (SEM). An one-way ANOVA with Tukey post hoc test was performed to determine the differences between the experimental groups. In addition, a two-way analysis of variance (ANOVA) with one repeated-measures factor time, with a Bonferroni post-test, was used to determine the overall differences when the test was performed at different examined time points in the same group. The average skin rewarming rate was compared between the diabetic rats and controls at different time intervals using an unpaired Students' t-test. A p-value of 0.05 or less was considered statistically significant. Data were analyzed using Graph Pad Prism software (GraphPad Prism Inc., San Diego, California, USA) version 5.0b for apple MacBook.

6.4.0. Results

Diabetic animals showed more than three times higher blood glucose levels than control animals during the entire study period (Figure 1A). One week after induction of diabetes by STZ, all rats demonstrated polydipsia and polyuria (data not shown). The body weight of the diabetic rats was significantly less compared to controls at all experimental time points studied but did not significantly change across time points (Figure 1B).

Eight weeks after induction of diabetes, no pathological changes were observed in the pancreatic tissue of the control group (Figure 2A). However, in the diabetic group the Islets of Langerhans showed shrinkage and displayed degenerative and necrotic changes due to the toxic effects of STZ already 4 weeks after induction of diabetes (Figure 2 B).

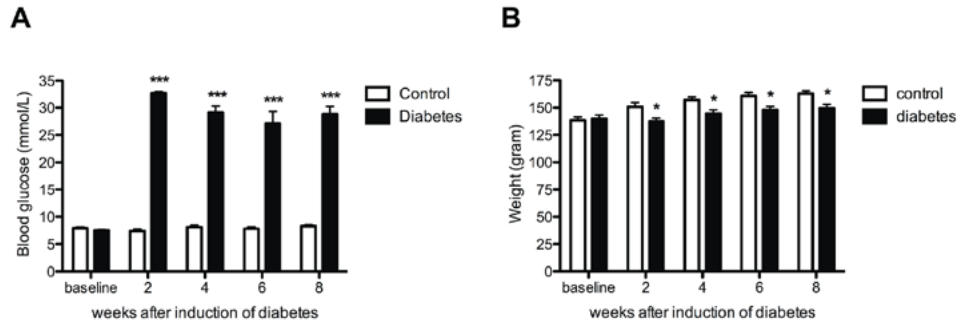

Figure 1. Increased blood glucose and stable body weight in diabetic animals.
*Blood glucose was increased in all diabetic animals (black bars) when compared to controls (white bars) (A). Significantly smaller increase in body weight is demonstrated in the diabetic animals (black bars) when compared with controls (white bars) (B). Each diabetic group consists of 7 animals and control group consists of 6 animals. Data are presented as mean ± SEM. *p <0.05; ***p <0.001 (One-way ANOVA with Tukey post hoc test).*

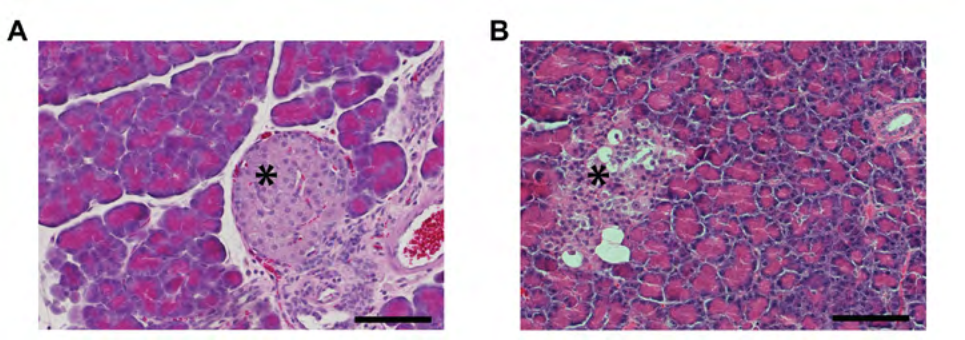

Figure 2. Degeneration of pancreatic tissue in diabetic animals.
Hematoxylin and eosin stained figures of the pancreas (A, B) showing that the cells and the Islets of Langerhans were considerably smaller in the diabetic pancreas (B) compared with control (A). Scale bar=100μm.

6.4.1. Microvascular changes in diabetic rats

Four weeks after the induction of diabetes, the blood flow in the skin of the plantar hind paw was significantly lower in diabetic rats than in controls (Control 4 weeks: 160.8 ± 61.2 AU vs. 4 weeks diabetes: 52.7 ± 11.8 AU; p<0.001) (Figure 3). In contrast, the percentage of CD31-positive endothelial cells in the glabrous skin of the hind paw was significantly higher 4 weeks after induction in diabetic rats than in controls (Control: 6.6 ± 0.7% vs. 4 weeks diabetes: 12.9 ± 1.9%; p < 0.05) (Figure 4B). However, while the blood flow remained low during further follow-up at 6 and 8 weeks after induction of diabetes, no significant difference in the percentage of CD31-positive endothelial cells was seen between diabetic rats and controls at these time points (Figure 4B-F).

Four weeks after induction of diabetes, skin oxygenation was not different between diabetic rats and controls (Figure 4A). However, 6 weeks after induction the skin oxygenation in diabetic rats became significantly lower than in controls (p< 0.05)(Figure 4A).

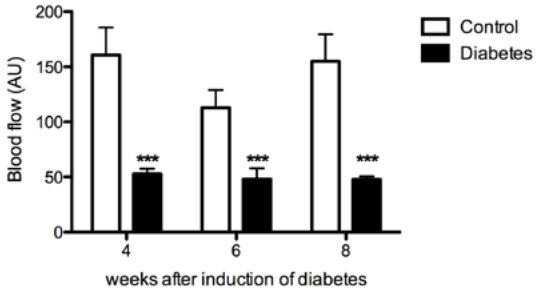

Figure 3. Decreased skin blood flow in diabetic animals.
*Plantar skin blood flow was decreased in all diabetic animals (black bars) when compared with controls (white bars). Data is presented as mean ± SEM. *** p< 0.001 (two-way ANOVA with one repeated-measures factor 'time' with Bonferroni post-test).*

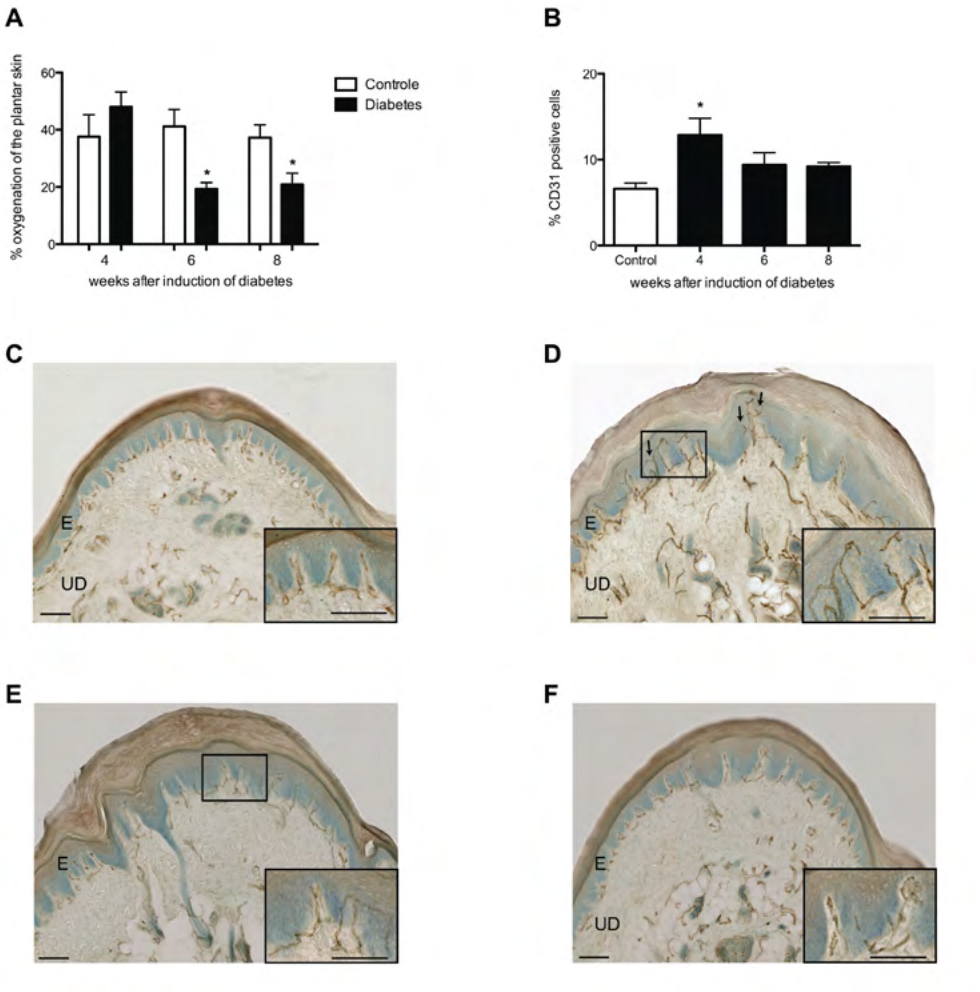

Figure 4. Percentage skin oxygenation and CD31-positive cells in the plantar skin. Decreased percentage in skin oxygenation was observed in diabetic animals (black bars) 6 and 8 weeks after the induction of diabetes when compared with controls (white bars) (A). Four weeks after induction of diabetes (black bar), a significantly increased percentage CD31-positive cells was observed in diabetic rats when compared to controls (white bar) (B), which is illustrated in histological scans of controls (C), 4 (D), 6 (E), and 8 (F) weeks after the induction of diabetes. Arrows indicate sprouting angiogenesis. Scale bars=50μm.

The skin rewarming rate in the controls were not significantly different at 4, 6 and 8 weeks (Figure 5A). Directly after cooling the skin (t = 0 seconds), no significant differences in skin temperature were observed between the controls and the 3 diabetic groups (Figure 5B-D). However, the difference in temperature between controls and diabetic rats becomes significant at earlier time points after cooling, 120 seconds after cooling in rats 4 weeks post induction, 90 seconds after cooling in rats 6 weeks post induction, and after 30 seconds in rats 8 weeks post induction. This indicates that there is a progressively bigger delay in rewarming at later time points after induction of diabetes (Table 1).

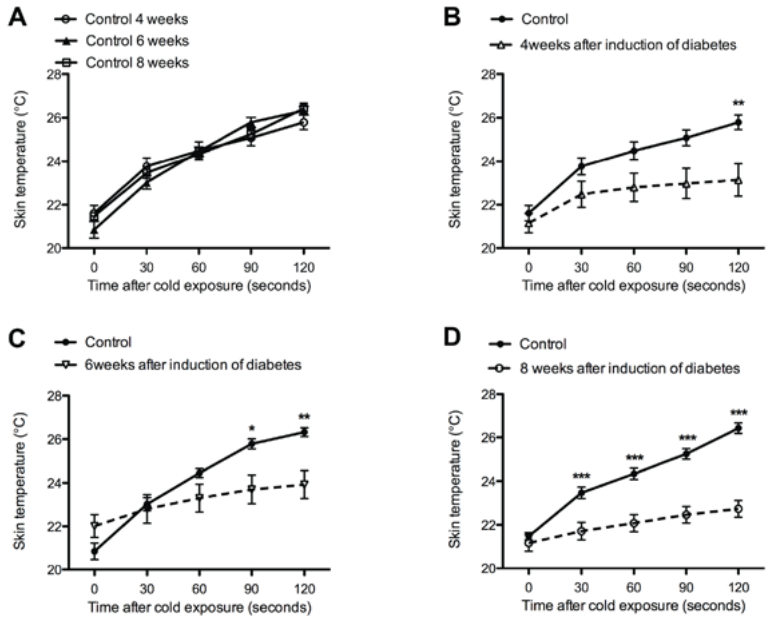

*Figure 5. Decreased skin temperature of the plantar hind paw after cold exposure. Control groups were not significantly different (A). Significant lower skin temperatures were observed in diabetic animals 4 (B), 6 (C), and 8 weeks (D) after the induction of diabetes (dotted line) when compared with controls (continuous line). Data is presented as mean ± SEM. *p < 0.05; **p <0.01; *** p< 0.001 (two-way ANOVA with one repeated-measures factor 'time' with Bonferroni post-test).*

Table 1. Average increase in temperature per 120 seconds ± SEM (°C).*Progressive decrease in the average skin temperature (degrees Celsius) per 120 seconds is shown in diabetic animals when compared to control. Data is presented as mean ± SEM (Unpaired T-test).*

Time (weeks)	Control	Diabetes	p-value
4	4.3 ± 0.04	2.0 ± 0.6	p < 0.01
6	5.5 ± 0.5	1.9 ± 0.3	p < 0.001
8	4.9 ± 0.1	1.6 ± 0.3	p < 0.001

6.4.2. Changes in skin innervations in diabetic rats

Four weeks after the induction of diabetes, no significant difference in the mean withdrawal response to mechanical stimuli were observed between the diabetic rats and the control rats (Figure 6). However, 6 and 8 weeks after the induction of diabetes, a significant increase in the mean withdrawal threshold was observed in diabetic rats (Figure 6).

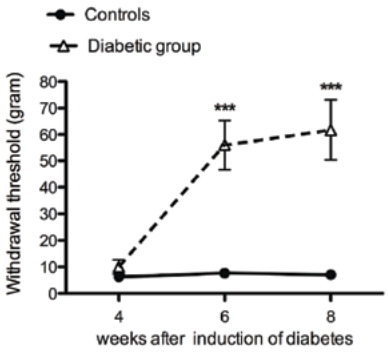

*Figure 6. Diabetic animals developed mechanical hyposensitivity. Increased mechanical withdrawal threshold was observed 6 and 8 weeks after induction of diabetes (dotted line) when compared to control (continuous line). Data is presented as mean ± SEM. *** p< 0.001 (two-way ANOVA with one repeated-measures factor 'time' with Bonferroni post-test).*

While the withdrawal latency for cold plate remained similar as control at all examined time points (Figure 7A), a significant decrease was seen in the withdrawal latency for the hot plate test at 4, 6 and 8 weeks after the induction of diabetes suggesting heat hypersensitivity (Figure 7B).

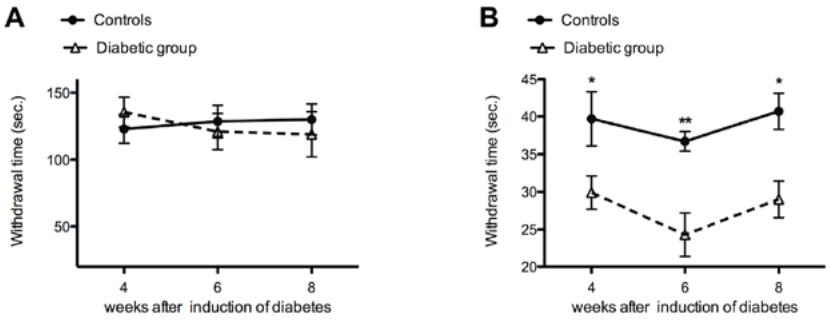

Figure 7. Heat hypersensitivity in diabetic animals.
A) No significant difference was observed between the diabetic animals (dotted line) and controls (continuous line) for the cold plate testing (5°C).
B) In contrast to the cold plate test, decreased withdrawal time was observed for the hot plate test (50°C) in diabetic animals (dotted line) when compared to control (continuous line) at all experimental time points.

IENFs were stained by the pan-neuronal protein gene product 9.5 (PGP9.5) marker. The average density of PGP9.5-IR nerve endings in the plantar skin was significantly lower in diabetic rats than in controls from 4 weeks onward (Figure 8B-D). This decreased skin innervation was accompanied by a significantly decreased epidermal thickness compared to controls (Figure 8A). Similar to the density of PGP9.5-IR nerve endings, significant decrease was observed in the average amplitude of evoked gastrocnemius muscle CMAPs in all diabetic groups (Control: 80.5 ± 2.2 mV vs. 4 weeks diabetes: 67.2 ± 2.7 mV; $p<0.05$, vs. 6 weeks diabetes: 62.6 ± 4.5 mV; $p<0.01$, and vs. 8 weeks diabetes: 60.5 ± 2.1 mV; $p<0.01$) (Figure 9A). However, the decrease in MNCV was seen later, 6 and 8 weeks after the induction of diabetes suggesting demyelination of motor nerves (Figure 9B).

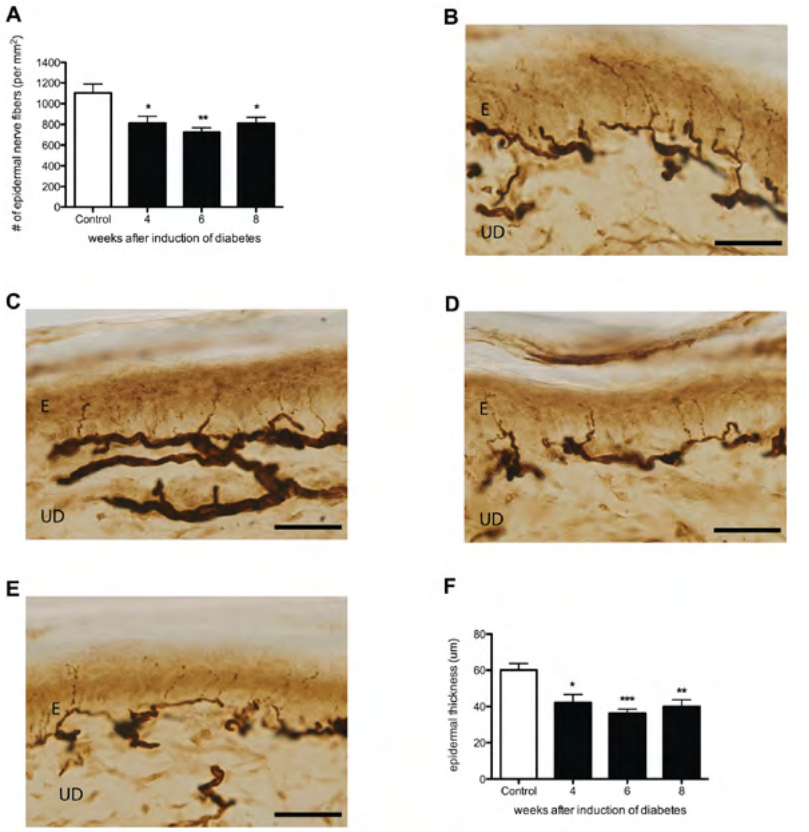

*Figure 8. Decreased innervation and decreased epidermal thickness in STZ diabetic rats. Decreased density PGP9.5-IR nerve fibers (A) and average epidermal thickness (F) was demonstrated in the plantar skin of diabetic animals 4, 6, and 8 weeks after induction of diabetes (black bars) when compared to control (white bar). This is illustrated by histological sections of plantar skin in controls (B), and 4 (C), 6 (D), and 8 (E) weeks after induction of diabetes. Data is presented as mean ± SEM. *p < 0.05; **p <0.01. (One-way ANOVA with Tukey post hoc test). E = epidermis, UD = upper dermis, scale bar = 100μm.*

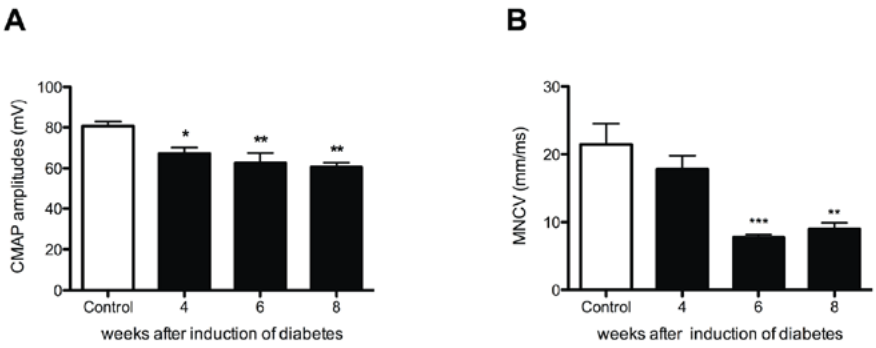

Figure 9. Electrophysiological changes in diabetic animals.
CMAPs amplitude decreased in all diabetic groups (black bars) when compared to controls (white bars) (A), while MNVC showed a significant decrease 6 and 8 weeks after induction of diabetes (B).

6.5.0. Discussion

The aim of our study was to investigate if the skin rewarming rate could serve as an early diagnostic tool for diabetic peripheral neuropathy in STZ diabetic rats as is shown in human diabetes (9). Although the STZ diabetic rat model has been used to study complications of diabetes for many years (26-30), there is no information available concerning the rewarming rate of the skin and its correlation to diabetic peripheral neuropathy in this model. In the present study, we quantified microvascular changes in the plantar skin of the rats' hind paw after the induction of diabetes and investigated whether these microvascular changes were associated with (the development of) diabetic peripheral neuropathy.

STZ is known to have toxic effects on beta cells in the Islets of Langerhans (31-33). In the current study, besides increased blood glucose, morphological changes were observed in the pancreatic tissue of the STZ diabetic rats confirming a normal progression of disease in our experimental animals.

6.5.1. Microvascular changes in diabetic rats

A decrease in the skin blood flow of the plantar hind paw was observed after the induction of diabetes at all measured time points. Analogous observations have been reported previously (34). However, in human diabetes, it has been found that early in the development of diabetic microvascular complications there is initially an increase in the skin blood flow before the blood flow decreases during progression of disease (35). Therefore, we performed additional blood flow measurements at 2 and 3 weeks after the induction of diabetes. Nevertheless, no significant difference was found in blood flow measurements of 2 and 3 weeks diabetic animals when compared to controls.

Interestingly, despite the decreased skin blood flow, initially no significant changes were seen in the skin oxygenation 4 weeks after the induction of diabetes. This finding suggests that the rats' circulation system maintained a normal oxygenation of the skin by a relative increase of CD31-positive endothelial cells in the upper dermis 4 weeks after the induction of diabetes. Although hypoxia is associated with angiogenesis, we were able to show a rise in CD31-positive cells as a response to the decrease in blood flow when oxygenation was comparable to control values (36). However, 6 and 8 weeks after the induction of diabetes, the relative significant increase in CD31-positive cells was no longer present, while the skin blood flow remained decreased, which resulted in hypoxia of the plantar skin. These findings suggest that the body was no longer able to compensate for the decreased skin blood flow from 6 weeks after the induction of diabetes.

The decreased skin blood flow was accompanied by a significant delay in the rewarming rate of the skin in diabetic rats compared to controls. These findings in STZ diabetic rats support the direct correlation between skin temperature and skin blood flow as is shown in human diabetes (37). Moreover, our diabetic animal model resembles skin rewarming rate of human diabetes. However, in human diabetes, a significant difference in the skin temperature was not observed until 10 minutes after cooling. In our study, significant differences in rewarming rate between the diabetic rats and the controls were already found after 120 seconds of monitoring. While human thermography studies use exposure to 14°C cold water, we observed in a pilot study that placement of STZ diabetic rats on a 14°C cold plate for 40 seconds was sufficient to detect differences in rewarming rate after 120 seconds (data not shown). Cold water exposure and longer monitoring of the plantar skin would have required administration of anesthesia, which is shown to have an effect on the blood flow and skin temperature and therefore was avoided in our study (38, 39).

6.5.2. Changes in skin innervations in diabetic rats

Four weeks after the induction of diabetes, no significant changes were observed in mechanical sensitivity, while more than 30% IENF loss was observed. These results demonstrate, similar to human diabetes that less innervation of the skin does not immediately lead to a measurable decrease in mechanical sensation (2). However, further decline in IENFs resulted in mechanical hyposensitivity 6 weeks after the induction of diabetes (40). From this finding we suggest that a threshold of the density of IENFs needs to be reached in order to cause changes in mechanical sensitivity: a similar phenomenon was also shown after peripheral nerve injury in rats (41). In addition, decreased density of IENFs in the plantar skin of diabetic rats was accompanied by a significantly decreased epidermal thickness. Decrease in epidermal thickness of the plantar foot is also observed in human diabetic neuropathy when compared to healthy controls (42) supporting the important role of IENFs in proliferation of keratinocytes in the epidermis (43).

In contrast to decreased sensitivity to mechanical stimuli, the diabetic animals demonstrated hypersensitivity to heat. This finding supports the previously suggested separate pathways for conducting mechanical and thermal information (44). However, further research identifying the subgroup of IENFs is required to confirm the modality-specific contribution of these sensory nerve fibers in diabetic peripheral neuropathy. Moreover, while hypersensitivity was observed for heat (50°C), no significant changes were observed for cold (5°C) temperature. This temperature-induced difference in hypersensitivity may be caused by changes in the expression of different thermo-sensitive transient receptor potential (TRP) channels expressed on IENFs that become activated at >42°C (TRPV1 channel) and <17°C (TRPA1 channel) involved in temperature signaling (45).

The CMAPs amplitude in the present study decreased prior to slowing of MNCV demonstrating the appearance of independent axonal degeneration followed by demyelination, which is in line with previous findings from electrophysiological studies performed in human diabetes and as well as in animal models of diabetes (4, 46).

The CMAPs amplitude was significantly decreased 4 weeks after induction of diabetes, a time point at which no changes were observed in mechanical sensitivity. This is consistent with findings in human diabetes, demonstrating that subclinical peripheral neuropathy can be early detected by electrophysiological tests (47, 48). Based on our results we conclude that the skin rewarming rate detects diabetic peripheral neuropathy in STZ diabetic rats, when loss of sensation measured by currently used monofilaments is not yet present. Therefore, our study supports the use of the skin rewarming rate as an early diagnostic tool for asymptomatic diabetic peripheral neuropathy in STZ diabetic rats. In addition, the current study has potential for translation to clinical practice in order to start a program of prevention in peripheral diabetic neuropathy. Major benefit of thermography for diabetic patients is the quick and non-invasive technique with which changes in rewarming rate in a large skin area are detectable. We therefore recommend performing thermography in all diabetic patients, especially diabetes type II, at the time of diagnosis to discover vascular changes in patients that are prone to develop peripheral diabetic neuropathy.

6.6.0. References

1. Ramsey SD, Newton K, Blough D, McCulloch DK, Sandhu N, Reiber GE, et al. Incidence, outcomes, and cost of foot ulcers in patients with diabetes. Diabetes Care. 1999 Mar;22(3):382-7.
2. Narayanaswamy H, Facer P, Misra VP, Timmers M, Byttebier G, Meert T, et al. A longitudinal study of sensory biomarkers of progression in patients with diabetic peripheral neuropathy using skin biopsies. J Clin Neurosci. 2012 Nov;19(11):1490-6.
3. Jin HY, Kang SM, Liu WJ, Song CH, Lee KA, Baek HS, et al. Comparison of peripheral nerve damages according to glucose control timing in experimental diabetes. Exp Clin Endocrinol Diabetes. 2012 Sep;120(8):451-9.
4. Tuncer S, Dalkilic N, Esen HH, Avunduk MC. An early diagnostic tool for diabetic neuropathy: conduction velocity distribution. Muscle Nerve. 2011 Feb;43(2):237-44.
5. Coppey LJ, Davidson EP, Dunlap JA, Lund DD, Yorek MA. Slowing of motor nerve conduction velocity in streptozotocin-induced diabetic rats is preceded by impaired vasodilation in arterioles that overlie the sciatic nerve. Int J Exp Diabetes Res. 2000;1(2):131-43.
6. Mori T, Nagase T, Takehara K, Oe M, Ohashi Y, Amemiya A, et al. Morphological pattern classification system for plantar thermography of patients with diabetes. J Diabetes Sci Technol. 2013 Sep;7(5):1102-12.
7. Sivanandam S, Anburajan M, Venkatraman B, Menaka M, Sharath D. Estimation of blood glucose by non-invasive infrared thermography for diagnosis of type 2 diabetes: an alternative for blood sample extraction. Mol Cell Endocrinol. 2013 Mar 10;367(1-2):57-63.
8. Mazilu G, Filos C, Popescu CD. [Cutaneous thermographic changes in diabetic polyneuropathy] Modificari termografice in polineuropatia diabetica. Rev Med Chir Soc Med Nat Iasi. 2011 Oct-Dec;115(4):1007-11.
9. Balbinot LF, Canani LH, Robinson CC, Achaval M, Zaro MA. Plantar thermography is useful in the early diagnosis of diabetic neuropathy. Clinics. 2012 Dec;67(12):1419-25.
10. Barriga ES, Chekh V, Carranza C, Burge MR, Edwards A, McGrew E, et al. Computational basis for risk stratification of peripheral neuropathy from thermal imaging. Conf Proc IEEE Eng Med Biol Soc. 2012;2012:1486-9.
11. Armstrong DG, Lavery LA, Liswood PJ, Todd WF, Tredwell JA. Infrared dermal thermometry for the high-risk diabetic foot. Phys Ther. 1997 Feb;77(2):169-75; discussion 76-7.
12. Weiss RB. Streptozocin: a review of its pharmacology, efficacy, and toxicity. Cancer Treat Rep. 1982 Mar;66(3):427-38.
13. Oltman CL, Davidson EP, Coppey LJ, Kleinschmidt TL, Dake B, Yorek MA. Role of the effect of inhibition of neutral endopeptidase on vascular and neural complications in streptozotocin-induced diabetic rats. Eur J Pharmacol. 2011 Jan 15;650(2-3):556-62.

14. Tong M, Tuk B, Shang P, Hekking IM, Fijneman EM, Guijt M, et al. Diabetes-impaired wound healing is improved by matrix therapy with heparan sulfate glycosaminoglycan mimetic OTR4120 in rats. Diabetes. 2012 Oct;61(10):2633-41.
15. Beckert S, Witte MB, Konigsrainer A, Coerper S. The impact of the Micro-Lightguide O2C for the quantification of tissue ischemia in diabetic foot ulcers. Diabetes Care. 2004 Dec;27(12):2863-7.
16. Rotter R, Kraemer R, Stratos I, Vogt P, Vollmar B, Mittlmeier T, et al. Compartmental and muscular response to closed soft tissue injury in rats investigated by oxygen-to-see and intravital fluorescence microscopy. J Trauma Acute Care Surg. 2012 Jul;73(1):73-9.
17. Jasmin L, Kohan L, Franssen M, Janni G, Goff JR. The cold plate as a test of nociceptive behaviors: description and application to the study of chronic neuropathic and inflammatory pain models. Pain. 1998 Apr;75(2-3):367-82.
18. Eddy NB, Leimbach D. Synthetic analgesics. II. Dithienylbutenyl- and dithienylbutylamines. J Pharmacol Exp Ther. 1953 Mar;107(3):385-93.
19. Smits ES, Duraku LS, Niehof SP, Daanen HA, Hovius SE, Selles RW, et al. Cold-induced vasodilatation in cold-intolerant rats after nerve injury. J Plast Reconstr Aesthet Surg. 2013 Sep;66(9):1279-86.
20. Werdin F, Grussinger H, Jaminet P, Kraus A, Manoli T, Danker T, et al. An improved electrophysiological method to study peripheral nerve regeneration in rats. J Neurosci Methods. 2009 Aug 30;182(1):71-7.
21. Kambiz S, Duraku SS, Baas M, Nijhuis THJ, Cosgun SG, Hovius SER, et al. Long term follow up of peptidergic and non-peptidergic re-innervation of the epidermis following sciatic nerve reconstruction in rats. Journal of Neurosurgery. 2014:in press.
22. Duraku LS, Hossaini M, Schuttenhelm BN, Holstege JC, Baas M, Ruigrok TJ, et al. Re-innervation patterns by peptidergic Substance-P, non-peptidergic P2X3, and myelinated NF-200 nerve fibers in epidermis and dermis of rats with neuropathic pain. Exp Neurol. 2013 Mar;241:13-24.
23. Kuhlmann WD, Peschke P. Glucose oxidase as label in histological immunoassays with enzyme-amplification in a two-step technique: coimmobilized horseradish peroxidase as secondary system enzyme for chromogen oxidation. Histochemistry. 1986;85(1):13-7.
24. Zylka MJ, Rice FL, Anderson DJ. Topographically distinct epidermal nociceptive circuits revealed by axonal tracers targeted to Mrgprd. Neuron. 2005 Jan 6;45(1):17-25.
25. Peleshok JC, Ribeiro-da-Silva A. Delayed reinnervation by nonpeptidergic nociceptive afferents of the glabrous skin of the rat hindpaw in a neuropathic pain model. J Comp Neurol. 2011 Jan 1;519(1):49-63.
26. Gong CY, Lu B, Hu QW, Ji LL. Streptozotocin induced diabetic retinopathy in rat and the expression of vascular endothelial growth factor and its receptor. Int J Ophthalmol. 2013;6(5):573-7.

27. Rondi S, Peddolla R, Venisetty RK. Neuro, cardio, and reno protective activities of rosuvastatin in streptozotocin-induced type 2 diabetic rats undergoing treatment with metformin and glimepiride. J Adv Pharm Technol Res. 2014 Apr;5(2):78-83.
28. Seyer-Hansen K. Renal hypertrophy in streptozotocin-diabetic rats. Clin Sci Mol Med. 1976 Dec;51(6):551-5.
29. D'Addio F, Maffi P, Vezzulli P, Vergani A, Mello A, Bassi R, et al. Islet transplantation stabilizes hemostatic abnormalities and cerebral metabolism in individuals with type 1 diabetes. Diabetes Care. 2014 Jan;37(1):267-76.
30. Fiorina P, Vezzulli P, Bassi R, Gremizzi C, Falautano M, D'Addio F, et al. Near normalization of metabolic and functional features of the central nervous system in type 1 diabetic patients with end-stage renal disease after kidney-pancreas transplantation. Diabetes Care. 2012 Feb;35(2):367-74.
31. Pisarev VB, Snigur GL, Spasov AA, Samokhina MP, Bulanov AE. Mechanisms of toxic effect of streptozotocin on beta-cells in the islets of langerhans. Bull Exp Biol Med. 2009 Dec;148(6):937-9.
32. Kleemann R, Rothe H, Kolb-Bachofen V, Xie QW, Nathan C, Martin S, et al. Transcription and translation of inducible nitric oxide synthase in the pancreas of prediabetic BB rats. FEBS Lett. 1993 Aug 9;328(1-2):9-12.
33. Muhammed SJ, Lundquist I, Salehi A. Pancreatic beta-cell dysfunction, expression of iNOS and the effect of phosphodiesterase inhibitors in human pancreatic islets of type 2 diabetes. Diabetes Obes Metab. 2012 Nov;14(11):1010-9.
34. Rendell MS, Kelly ST, Finney D, Luu T, Kahler K, McIntyre SF, et al. Decreased skin blood flow early in the course of streptozotocin-induced diabetes mellitus in the rat. Diabetologia. 1993 Oct;36(10):907-11.
35. Ditzel J, Standl E. The problem of tissue oxygenation in diabetes mellitus. I. Its relation to the early functional changes in the microcirculation of diabetic subjects. Acta Med Scand Suppl. 1975;578:49-58.
36. Pouyssegur J, Dayan F, Mazure NM. Hypoxia signalling in cancer and approaches to enforce tumour regression. Nature. 2006 May 25;441(7092):437-43.
37. Zotter H, Kerbl R, Gallistl S, Nitsche H, Borkenstein M. Rewarming index of the lower leg assessed by infrared thermography in adolescents with type 1 diabetes mellitus. Journal of pediatric endocrinology & metabolism : JPEM. 2003 Dec;16(9):1257-62.
38. Gonzalez de Zarate J, Olmos A, Alvarez JC, Ruiz N, de Andres B, Gonzalez-Fajardo JA. [Core and cutaneous thermal changes in the upper limb after anesthesia induction] Cambios termicos centrales y cutaneos en el miembro superior despues de la induccion anestesica. Rev Esp Anestesiol Reanim. 2000 Aug-Sep;47(7):287-92.
39. Gargiulo S, Gramanzini M, Liuzzi R, Greco A, Brunetti A, Vesce G. Effects of some anesthetic agents on skin microcirculation evaluated by laser Doppler perfusion imaging in mice. BMC Vet Res. 2013;9:255.

40. Marangoni MN, Brady ST, Chowdhury SA, Piano MR. The co-occurrence of myocardial dysfunction and peripheral insensate neuropathy in a streptozotocin-induced rat model of diabetes. Cardiovasc Diabetol. 2014;13(1):11.
41. Verdu E, Navarro X. Comparison of immunohistochemical and functional reinnervation of skin and muscle after peripheral nerve injury. Exp Neurol. 1997 Jul;146(1):187-98.
42. Chao CY, Zheng YP, Cheing GL. The association between skin blood flow and edema on epidermal thickness in the diabetic foot. Diabetes Technol Ther. 2012 Jul;14(7):602-9.
43. Huang IT, Lin WM, Shun CT, Hsieh ST. Influence of cutaneous nerves on keratinocyte proliferation and epidermal thickness in mice. Neuroscience. 1999;94(3):965-73.
44. Zhang J, Cavanaugh DJ, Nemenov MI, Basbaum AI. The modality-specific contribution of peptidergic and non-peptidergic nociceptors is manifest at the level of dorsal horn nociresponsive neurons. The Journal of physiology. 2013 Feb 15;591(Pt 4):1097-110.
45. Kambiz S, Duraku LS, Holstege JC, Hovius SE, Ruigrok TJ, Walbeehm ET. Thermo-sensitive TRP channels in peripheral nerve injury: A review of their role in cold intolerance. J Plast Reconstr Aesthet Surg. 2013 Dec 27.
46. Hasegawa O, Matsumoto S, Iino M, Mori I, Arita T, Baba Y. [Interrelationship among nerve conduction velocity, amplitudes of compound muscle and compound nerve action potentials in diabetic neuropathy]. No To Shinkei. 1999 Oct;51(10):863-6.
47. Liu MS, Hu BL, Cui LY, Tang XF, Du H, Li BH. [Clinical and neurophysiological features of 700 patients with diabetic peripheral neuropathy]. Zhonghua Nei Ke Za Zhi. 2005 Mar;44(3):173-6.
48. Holiner I, Haslinger V, Lutschg J, Muller G, Barbarini DS, Fussenegger J, et al. Validity of the neurological examination in diagnosing diabetic peripheral neuropathy. Pediatr Neurol. 2013 Sep;49(3):171-7.

Chapter 7

Acetyl-L-Carnitine prevents mechanical hyposensitivity and loss of epidermal non-peptidergic nerve fibers in Streptozotocin-induced diabetic rats

Shoista Kambiz, Saniye G. Cosgun, Johan W. van Neck, Steven E.R. Hovius, Jan C Holstege, Erik T. Walbeehm

Submitted

7.1.0 Abstract

Diabetic peripheral neuropathy is a common long-term complication of diabetes. A dietary supplement, Acetyl-L-Carnitine (ALCAR), has been shown to have positive effect on diabetic neuropathy. However, an extensive study examining the effect of ALCAR on subgroups of epidermal sensory nerve fibers after induction of diabetes is lacking. The aim of the current study was, therefore, to examine the effect of ALCAR on the development of diabetic peripheral neuropathy and the density of epidermal sensory nerve fibers in Streptozotocin (STZ)-induced diabetic rats. Peripheral neuropathy was determined by mechanical and thermal sensitivity in diabetic and ALCAR-treated diabetic rats during 12 weeks follow-up. In addition, the density of epidermal (peptidergic and non-peptidergic) nerve fibers were studied in the plantar skin of non-diabetic, diabetic and ALCAR-treated diabetic rats. The mechanical withdrawal threshold in the diabetic animals was at 60±sem gram, which was significantly increased compared to the non-diabetic animals at 10±sem gram and the ALCAR-treated diabetic animals at 18±sem gram. Moreover, the density of epidermal nerve fibers in diabetic animals was more than half decreased when compared to non-diabetic animals. Although the epidermal innervation in the ALCAR-treated diabetic animals was also reduced, it was significantly less decreased compared to the untreated diabetic animals.

Present study demonstrates a correlation between mechanical sensitivity and epidermal non-peptidergic nerve fibers. Moreover, the results of the current study strongly suggest a preventive role for ALCAR as a treatment basis for diabetic peripheral neuropathy.

7.2.0. Introduction

Diabetic peripheral neuropathy is the most common long-term complication of all types of diabetes affecting over 50% of the patients (1-3). Hyposensitivity accompanied by an inadequate wound healing is the leading cause of foot ulceration, diabetic foot, possibly leading to amputation of the lower limb in these patients (4). Some patients complain of mild to severe pain due to neurogenic changes caused by hyperglycemia. These complication results in a significantly reduced quality of life (3, 5).

QST studies and quantification of sensory nerve fibers in diabetic patients suggest an important role for epidermal nerve fibers in the development of diabetic peripheral neuropathy. Diabetic peripheral neuropathy is characterized by a decrease in the density of sensory epidermal nerve fibers in both human and animal models with diabetes (6, 7). Sensory epidermal nerve fibers can be subdivided in two functional distinct population of fibers. The peptidergic nerve fibers are sensitive for nerve growth factor (NGF) and express the neuropeptide calcitonin gene-related peptide (CGRP) while the non-peptidergic nerve fibers respond to glial cell line-derived neurotrophic factor (GDNF). The importance in distinction

between the subgroups of sensory epidermal nerve fibers has been shown in peripheral nerve injury studies that resulted in significant increase of specifically the peptidergic nerve fibers (8, 9). Moreover, in contrast to the non-peptidergic nerve fibers, the peptidergic nerve fibers have been correlated to thermal hypersensitivity (10). These studies suggest a modality specific contribution of the two subgroup of sensory epidermal nerve fibers.

At present, besides analgesics and blood glucose controlling medicaments, no additional therapy is available for the prevention or treatment of diabetic neuropathy. However, acetylated L-carnitine have been considered as a therapeutic agent for diabetic peripheral neuropathy, as pain relief and improvement of nerve conduction velocity were found in both diabetic rats and humans after supplementation of ALCAR (11-15). However, the effect of ALCAR on small fiber neuropathy, which is suggested to be the earliest detectable sign of peripheral neuropathy, is unknown. Moreover, the modality specific contribution of the two subgroup of sensory epidermal nerve fibers on ALCAR treated and untreated diabetic peripheral neuropathy is not examined yet. Therefore, for the first time, the effect of ALCAR on mechanical and thermal sensitivity and the density of both peptidergic and non-peptidergic epidermal nerve fibers was examined in STZ-induced diabetic rats as presented in the current study.

7.3.0. Materials and Methods

7.3.1. Animals

All experiments were performed on young adult female WAG/RijHsd rats (n=20, 8 weeks of age, weighing 130-150 grams) purchased from Harlan (Zeist, the Netherlands). The animals were pair-housed in hooded cages at room temperature on a 12-hour light/dark schedule, and were given water and food ad libitum. All experiments were approved by the Dutch Ethical Committee on Animal Welfare (DEC Erasmus MC, Rotterdam) according to the European guidelines for the care and use of laboratory animals (Council Directive 86/6009/EEC).

7.3.2. Induction of diabetes

Diabetes was induced in 14 rats by a single intra-peritoneal injection of Streptozotocin (Sigma-Aldrich, St. Louis, MO) at a dose of 50 mg/kg body weight in 0.05 mol/L sodium citrate buffer, pH 4.5. The rats were randomly assigned into two groups (n=7 in each group); untreated diabetic rats and ALCAR-treated diabetic rats (120 ± 10 mg/kg/day diluted in drinking water (16). ALCAR treatment was started immediately after STZ injection and both diabetic groups were euthanized 12 weeks after induction of diabetes. As controls to diabetic rats, 6 non-diabetic rats received a single intra-peritoneal injection with an equal volume of vehicle without Streptozotocin in citrate buffer (0.05 mol/L, pH 4.5). All

non-diabetic rats were followed for 4 weeks since previous studies did not show any significant difference in nociceptive thresholds in adult rats over 12 weeks. Blood glucose concentration from tail vein blood was measured by a glucometer (OneTouch, LifeScan, Milpitas, CA). Diabetes was diagnosed in rats, when blood glucose levels were higher than 20 mmol/L during the entire 4 weeks after the induction of diabetes.

7.3.3. Von Frey test

To determine the mechanical sensitivity threshold for nociception, each rat was placed in a chamber with a mesh plexiglas floor. Von Frey filaments ranging from 2 to 300 gram were applied 5 times on the plantar skin at maximum force (i.e. until bending of filament). A minimum of 3 paw flicks (the animal's reflex withdrawal response) was scored positive, as described previously (17).

7.3.4. Hot plate test

The hot plate test was performed in order to determine whether the animals developed hypersensitivity to heat. Rats were placed on an open-ended chamber with clear walls and a surface temperature of 50 ˚C (8). The time until withdrawal or licking of the hind paw was measured.

7.3.5. Compound Muscle Action Potentials (CMAPs)

Innervation of the gastrocnemius muscles was evaluated by recording evoked Compound Muscle Action Potentials (CMAPs) (18). At the appropriate survival time, the sciatic nerve was exposed, under 3% isoflurane anesthesia, through a gluteal muscle-splitting approach using a surgical microscope (Zeiss OP-MI 6-SD; Carl Zeiss, Goettingen, Germany). Subsequently, a monopolar needle stimulation electrode was placed 6-7 mm proximally from the nerve's trifurcation close to the nerve (19). For recordings, an active electrode was positioned on the medial gastrocnemius muscle with the reference electrode at the laterodistal end of the muscle. CMAP peak-peak amplitude was recorded and averaged over a batch of 20 responses.

7.3.6. Tissue preparation

At the appropriate survival time, animals were euthanized by an overdose pentobarbital (100mg/kg i.p.). The plantar skin of the hind paw was dissected and immersion-fixed in 2% paraformaldehyde-lysin-periodate (PLP) for 24 hours at 4˚C. The skin was then embedded in 10% gelatin, which was hardened in 10% formaldehyde for 2 hours, stored overnight in 30% sucrose and subsequently sectioned at 40 μm with a freezing microtome and collected in glycerol for long-term storage at –20 °C.

7.3.7. Immunohistochemistry

Immunohistochemistry was performed to quantify the density of sensory nerve fibers as described previously (8, 9). The sections were incubated in a cocktail of 2% BSA or milk powder containing the diluted primary antibody against the pan-neuronal marker protein gene product (PGP) 9.5 (1/5.000, anti-rabbit, Enzo), calcitonin gene related peptide (CGRP) (1/30.000, anti-rabbit, Calbiochem) or Purinergic P2X3 receptor (P2X3) (1/300, anti-rabbit, Sigma) at 4 ˚C for 48 hours. Subsequently, the sections were incubated with the biotinylated goat anti-rabbit antibody (1/200, Biotine) at room temperature for 90 minutes. Then, the 3, -3' diaminobenzidine (DAB), Nickel ($NiSO_4$) and Cobalt ($CoCl_2$) reaction was used to reveal the antigenic sites. Finally, the sections were mounted on slides, stained with 0.05% thionin, which discolored the epidermis blue, dehydrated using absolute ethanol (< 0.01% methanol), transferred to xylene and coverslipped with Permount (Fisher, Hampton, NH).

7.3.8. Analysis

Each skin section was scanned by Nanozoomer 2.0 series system (Hamamatzu, Japan). Four proximal and four distal skin samples of the plantar hind paw were quantified for epidermal nerve fibers (80.000 μm2) using 20x objective in ImageScope software (Aperio ImageScope v11.1.2.760). The mean labeled nerve fibers per mm was calculated for each rat and compared to control animals.

7.3.9. Statistical analysis

For determining statistical differences, the one way-ANOVA with a Tukey post hoc test or the two way-ANOVA with Bonferroni posttest was used for intergroup comparisons. Errors in variations were determined as standard error of the mean (SEM), and $p < 0.05$ was considered significant.

7.4.0. Results

All diabetic rats in both groups showed a six fold increase in blood glucose concentration in comparison to the non-diabetic rats during 12 weeks follow up (Figure 1A), with exception of two animals (one from each group), which recovered from diabetes during follow-up, due to unknown mechanisms. These two animals were excluded from the current study resulting in n=6 in each group. One week after the induction of diabetes, all diabetic rats demonstrated polydipsia, polyuria and absence of ketonurie (data not shown).

Both untreated and ALCAR-treated diabetic groups showed similar increase in weight over time. Although no significant difference was seen in the intake of drinking water between the untreated and ALCAR-treated animals, the

ALCAR-treated animals stayed behind in weight at 2 weeks after the induction of diabetes (Figure 1B).
All results in the present study are presented below as a comparison between the three groups as followed: untreated diabetes vs. non-diabetic controls, ALCAR-treated diabetes vs. non-diabetic controls, and untreated diabetes vs. ALCAR-treated diabetes.

From 9 weeks after the induction of diabetes, the untreated diabetic group showed a significant increase in withdrawal threshold to von Frey filaments compared to non-diabetic group indicating the presence of mechanical hyposensitivity (Figure 2). In contrast to the untreated diabetic group, the ALCAR-treated diabetic group showed similar mechanical sensitivity as non-diabetic group. This resulted in a significant difference between the untreated and ALCAR-treated diabetic groups at 9 and 12 weeks after induction of diabetes.

Significant decrease in withdrawal threshold for the hot plate test was observed in the untreated diabetic group already 5 weeks after the induction of diabetes when compared to non-diabetic group. Similar decrease in withdrawal threshold was seen in the ALCAR-treated group, which was significant only at 9 and 11 weeks after induction of diabetes. This result suggests a delay in heat hypersensitivity in the ALCAR-treated group (Figure 3). In contrast to mechanical hyposensitivity, no significant differences were seen in heat sensitivity between the untreated and ALCAR-treated diabetic groups.

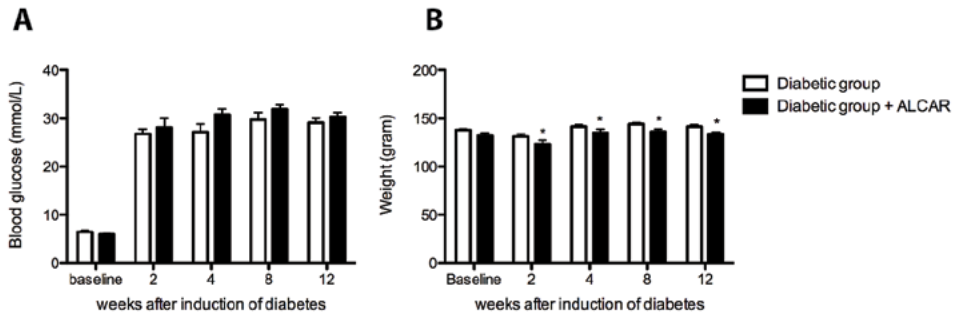

*Figure 1. Blood glucose levels and body weight of ALCAR treated diabetic animals compared to untreated diabetic animals during follow-up. Blood glucose (A) and body weight (B) were measured once a week in untreated (n=6, circle) and ALCAR treated diabetic rats (n=6, square). (A) After induction of diabetes, both experimental groups showed a six fold increase in blood glucose concentration when compared to baseline values. (B) Although the two diabetic groups showed similar increase in weight over time, at 2 weeks after development of diabetes the ALCAR treated animals stayed behind in weight. Each point represents the mean value ± SEM. ***p<0.001 untreated vs. ALCAR treated diabetic animals, Two-way ANOVA with Bonferroni posttest.*

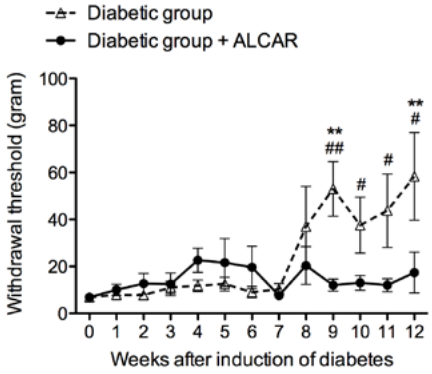

*Figure 2. Significantly higher mechanical withdrawal thresholds in untreated diabetic animals compared to ALCAR treated diabetic animals at the end of the follow-up period. Mechanical withdrawal thresholds of untreated (n=6, circle) and ALCAR treated (n=6, square) diabetic animals were measured once a week. The average mechanical withdrawal thresholds measured from the left and right paws are shown. Data is presented as mean ± SEM. **p<0.01, untreated vs. ALCAR treated diabetic animals, Two-way ANOVA with Bonferroni posttest. #p<0.05; ##p<0.01; untreated diabetic animals vs. baseline, One-way ANOVA with Tukey posttest.*

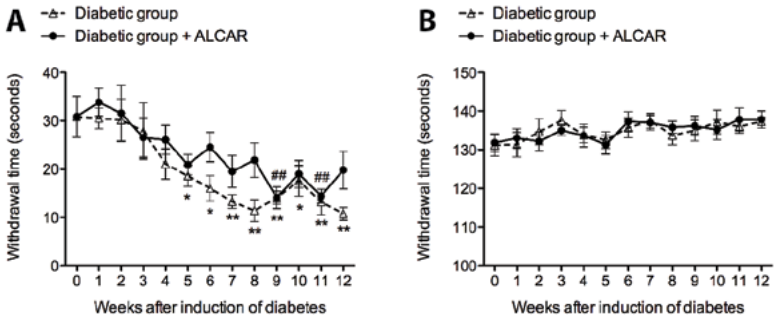

*Figure 3. Significantly decreased thermal withdrawal thresholds in untreated and ALCAR treated diabetic animals compared to baseline. Thermal withdrawal thresholds of untreated (n=6, circle) and ALCAR treated (n=6, square) diabetic animals were measured once a week. Untreated diabetic animals show significant decrease in mean thermal withdrawal thresholds for hot plate compared to baseline values starting at week 9 after induction of diabetes until the end of the experiment. The ALCAR treated diabetic animals also show a significant decrease of mean thermal withdrawal thresholds compared to baseline but only in week 9 and 11 after induction of diabetes. No significant difference is present between the ALCAR treated and untreated diabetic animals. Each point represents the mean value ± SEM. Two-way ANOVA with Bonferroni posttest. *p<0.05; **p<0.01; untreated diabetic animals vs. baseline, One-way ANOVA with Tukey posttest. ##p<0.01; ALCAR treated diabetic animals vs. baseline, One-way ANOVA with Tukey posttest.*

Mechanical hyposensitivity in the untreated diabetic animals, present at 12 weeks after the induction of diabetes, was accompanied by a significant decrease of more than half in the density of epidermal PGP9.5-immuno reactive (IR) nerve fibers when compared to the non-diabetic group (Figure 4A). Although less than in the untreated diabetic group, the density of epidermal PGP9.5-IR nerve fibers was also decreased in the ALCAR-treated diabetic group compared to the non-diabetic group. This resulted in a significantly lesser reduction in the epidermal PGP9.5-IR nerve fibers in the ALCAR-treated diabetic group when compared to the untreated diabetic group. In accordance with the decrease in PGP9.5-IR nerve fibers, a significant decrease was also seen in the epidermal CGRP-IR (peptidergic) nerve fibers in both untreated and ALCAR-treated diabetic groups compared to non-diabetic group (Figure 4B). However, no significant difference was present in the density of epidermal CGRP-IR nerve fibers between the untreated and ALCAR-treated diabetic groups, suggesting no effect of ALCAR on peptidergic nerve fibers.

Similar to PGP9.5-IR and CGRP-IR nerve fibers, the density of P2X3-IR (non-peptidergic) nerve fibers was significantly decreased in both the untreated diabetic group and ALCAR-treated diabetic group when compared to the non-diabetic group (Figure 4C). However, the ALCAR-treated diabetic group showed less reduction in the density of P2X3-IR nerve fibers when compared to untreated diabetic animals resulting in a significant difference in the density of P2X3-IR nerve fibers between the untreated and ALCAR-treated diabetic group.

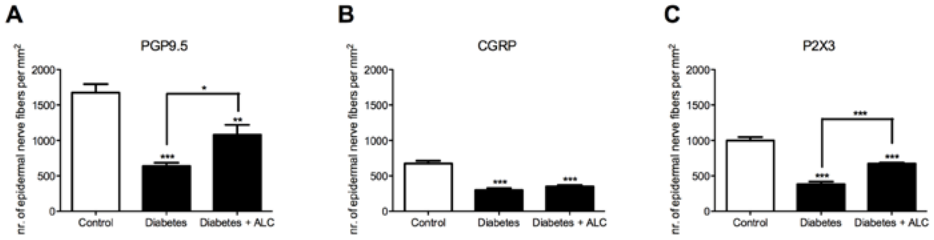

*Figure 4. Epidermal nerve fibers in the plantar skin of ALCAR treated diabetic animals compared to untreated diabetic animals. The histograms show the mean density of epidermal PGP 9.5-IR nerve fibers (A), CGRP-IR fibers (B) and P2X3-IR fibers (C)per square millimeter for all experimental groups (n=6 per group). Significant decrease is seen in the density of epidermal nerve fibers in the plantar skin of both ALCAR treated and untreated diabetic animals. Data is presented as means ± SEM. *p<0.05, **p<0.01, ***p<0.001, One-way ANOVA with Tukey posttest.*

Besides sensory modalities, the average CMAP amplitude, which is an indirect measure of the number of functional motor axons in the stimulated nerve, was determined in the current study. In contrast to the ALCAR-treated diabetic animals, the CMAP amplitude in the untreated diabetic group was significantly decreased when compared to the non-diabetic group. However, these changes did not result in a significant difference in CMAP amplitude between the untreated and ALCAR-treated group (Figure 5).

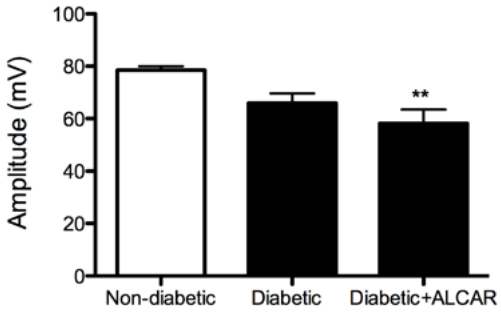

*Figure 5. Significantly lower evoked Compound Muscle Action Potential amplitudes of the gastrocnemius muscle of untreated diabetic animals compared to control animals. Histograms showing the average evoked compound muscle action potential (CMAP) amplitudes of the gastrocnemius muscle in mV of control (n=6, Control), untreated diabetic (n=6, Diabetic) and ALCAR treated (n=6, Diabetic+ALC) diabetic animals measured at the end of the experiment. Data is presented as means ± SEM. **p<0.01 untreated diabetic animals vs control, One-way ANOVA with Tukey posttest.*

7.5.0. Discussion

The aim of this study was to examine the effect of ALCAR on symptoms of diabetic peripheral neuropathy and the density of epidermal sensory nerve fibers in STZ-induced diabetic rats. This model is widely used to study diabetic peripheral neuropathy (20), and has recently been shown to mimic diabetic peripheral neuropathy in human diabetes in many aspects, especially in Wag/RIJ rats (21).

All untreated diabetic animals, in this study, showed heat hypersensitivity prior to mechanical hyposensitivity at 5 and 9 weeks after the induction of diabetes, respectively. Changes in mechanical and thermal sensitivity, induced by diabetes, are well known (3). Moreover, pain followed by loss of sensibility, as presented in the current study, is also seen in human diabetes. In the current study, ALCAR treatment showed a delay in the appearance of heat hypersensitivity, and, even more importantly, ALCAR prevented mechanical hyposensitivity in the plantar hind paw of STZ-induced diabetic rats.

As expected, the mechanical hyposensitivity in the untreated diabetic animals was accompanied by decreased epidermal innervation. Although normal mechanical sensitivity was observed in the ALCAR-treated animals, the epidermal innervation was also decreased in this group. However, the decrease in the epidermal innervation by PGP9.5-IR nerve fibers was significantly less in the ALCAR-treated animals when compared to the untreated diabetic animals, suggesting a protective role by ALCAR in the neurodegenerative process of diabetic peripheral neuropathy. In addition, these results propose that a possible threshold for the density of epidermal nerve fibers needs to be reached to cause changes in mechanical sensation. The same phenomenon was previously observed in nerve regeneration models (10, 22).

It is reported that PGP9.5-IR staining covers two distinct population of sensory nerve fibers; the peptidergic and non-peptidergic nerve fibers. Although, an 10% co-localization between these two subgroup of sensory nerve fibers was reported(23), the sum of the density of peptidergic and non-peptidergic nerve fibers was not significantly different when compared to the density of PGP9.5-IR nerve fibers in the current study (data not shown). From this we can conclude that the staining of sensory nerve fibers is performed correctly.

In contrast to findings from peripheral nerve injury models, showing an increase in the peptidergic nerve fibers and a decrease in the non-peptidergic fibers (9), the untreated diabetic group showed a decrease in both subtypes of epidermal nerve fibers, leading to similar absolute numbers of fibers in both groups, 12 weeks post-diabetic induction. However, ALCAR treatment showed a lesser reduction in specifically the epidermal non-peptidergic nerve fibers. These results support the previously reported alleviation of mechanical hypersensitivity by administration of P2X3 receptor antagonist (24). From these findings, we suggest a correlation between the epidermal non-peptidergic nerve fibers and mechanical sensitivity. However, in the present study, the density of epidermal peptiderig nerve fibers was similar between the untreated and ALCAR-treated diabetic animals. In addition, heat hypersensitivity developed in both untreated and ALCAR-treated animals, supporting the previously made correlation between the peptidergic skin innervation and thermal sensitivity (10). However, while an increased number of epidermal peptidergic nerve fibers was related to thermal hypersensitivity in the nerve injury model (10), our diabetic animals demonstrated a loss of epidermal peptidergic nerve fibers accompanied by thermal hypersensitivity. This discrepancy may be explained by two different mechanisms: increased expression of temperature sensitive transient receptor potential (TRP) channels and/or a lower activation-threshold of the TRP channels on epidermal peptidergic nerve fibers in the diabetic rat model. From these results and previously reported electrophysiological findings (25), we conclude that the peptidergic and the non-peptidergic nerve fibers have modality specific contribution in behavioral responses to heat and mechanical stimuli, respectively. This finding is of major importance since ALCAR treatment affects specifically the non-peptidergic and therefore the mechanical induced hyposensitivity.

Furthermore, CMAPs amplitude of the gastrocnemius muscle was recorded in the current study. Consistent with studies in human diabetes (26), the amplitude of CMAP was considerably decreased in the untreated diabetic animals. However, no changes were seen in the CMAPs amplitude of ALCAR treated animals. This finding suggests that besides sensory nerve protection also the motor nerve fibers are to some extent protected by ALCAR.

In conclusion, our study shows for the first time that a continuous treatment with ALCAR prevents mechanical hyposensitivity and has a neuro-protective effect on specifically the epidermal non-peptidergic nerve fibers in STZ-induced diabetic rats. This is a fundamental finding showing a) the modality specificity be-

tween the peptidergic and the non-peptidergic fibers and b) new potential therapy for diabetic peripheral neuropathy the risk of developing a diabetic foot is very high in diabetic patients with sensory loss (3). Our study and previous reports clearly indicate the prophylactic or therapeutic potential of ALCAR on diabetic neuropathies. However, in order to introduce ALCAR as a therapeutic option for diabetic peripheral neuropathy, extensive clinical trials are needed focusing on the effect of ALCAR treatment on hyposensitivity in diabetic patients.
Loss of sensibility in the lower extremities is a major complication of peripheral diabetic neuropathy. It puts patients at risk for insensitive foot lesions, which could lead to limb amputations.

7.6.0. References

1. Dyck PJ, Kratz KM, Karnes JL, Litchy WJ, Klein R, Pach JM, et al. The prevalence by staged severity of various types of diabetic neuropathy, retinopathy, and nephropathy in a population-based cohort: the Rochester Diabetic Neuropathy Study. Neurology. 1993 Apr;43(4):817-24.
2. Young MJ, Boulton AJ, MacLeod AF, Williams DR, Sonksen PH. A multicentre study of the prevalence of diabetic peripheral neuropathy in the United Kingdom hospital clinic population. Diabetologia. 1993 Feb;36(2):150-4.
3. Boulton AJ, Vinik AI, Arezzo JC, Bril V, Feldman EL, Freeman R, et al. Diabetic neuropathies: a statement by the American Diabetes Association. Diabetes Care. 2005 Apr;28(4):956-62.
4. Boulton AJ, Malik RA, Arezzo JC, Sosenko JM. Diabetic somatic neuropathies. Diabetes Care. 2004 Jun;27(6):1458-86.
5. Sinnreich M, Taylor BV, Dyck PJ. Diabetic neuropathies. Classification, clinical features, and pathophysiological basis. Neurologist. 2005 Mar;11(2):63-79.
6. Narayanaswamy H, Facer P, Misra VP, Timmers M, Byttebier G, Meert T, et al. A longitudinal study of sensory biomarkers of progression in patients with diabetic peripheral neuropathy using skin biopsies. J Clin Neurosci. 2012 Nov;19(11):1490-6.
7. Jin Y, Kanamori A, Ito S, Matoba K, Miyakawa M, Kaneshige H, et al. Cross-sectional survey of diabetic neuropathy in Kanagawa and clinical significance of a touch test using tissue paper. J Diabetes Investig. 2012 Jun 6;3(3):252-8.
8. Duraku LS, Hossaini M, Hoendervangers S, Falke LL, Kambiz S, Mudera VC, et al. Spatiotemporal dynamics of re-innervation and hyperinnervation patterns by uninjured CGRP fibers in the rat foot sole epidermis after nerve injury. Mol Pain. 2012;8:61.
9. Duraku LS, Hossaini M, Schuttenhelm BN, Holstege JC, Baas M, Ruigrok TJ, et al. Re-innervation patterns by peptidergic Substance-P, non-peptidergic P2X3, and myelinated NF-200 nerve fibers in epidermis and dermis of rats with neuropathic pain. Exp Neurol. 2013 Mar;241:13-24.
10. Kambiz S, Duraku LS, Baas M, Nijhuis TH, Cosgun SG, Hovius SE, et al. Long-term follow-up of peptidergic and nonpeptidergic reinnervation of the epidermis following sciatic nerve reconstruction in rats. J Neurosurg. 2015 Jul;123(1):254-69.
11. Ido Y, McHowat J, Chang KC, Arrigoni-Martelli E, Orfalian Z, Kilo C, et al. Neural dysfunction and metabolic imbalances in diabetic rats. Prevention by acetyl-L-carnitine. Diabetes. 1994 Dec;43(12):1469-77.
12. Sima AA, Ristic H, Merry A, Kamijo M, Lattimer SA, Stevens MJ, et al. Primary preventive and secondary interventionary effects of acetyl-L-carnitine on diabetic neuropathy in the bio-breeding Worcester rat. J Clin Invest. 1996 Apr 15;97(8):1900-7.
13. Sima AA, Calvani M, Mehra M, Amato A, Acetyl LCSG. Acetyl-L-carnitine improves pain, nerve regeneration, and vibratory perception in patients with chronic diabetic neuropathy: an analysis of two randomized placebo-controlled

trials. Diabetes Care. 2005 Jan;28(1):89-94.
14. De Grandis D, Minardi C. Acetyl-L-carnitine (levacecarnine) in the treatment of diabetic neuropathy. A long-term, randomised, double-blind, placebo-controlled study. Drugs R D. 2002;3(4):223-31.
15. Wilson AD, Hart A, Brannstrom T, Wiberg M, Terenghi G. Delayed acetyl-L-carnitine administration and its effect on sensory neuronal rescue after peripheral nerve injury. J Plast Reconstr Aesthet Surg. 2007;60(2):114-8.
16. Pesce V, Fracasso F, Cassano P, Lezza AM, Cantatore P, Gadaleta MN. Acetyl-L-carnitine supplementation to old rats partially reverts the age-related mitochondrial decay of soleus muscle by activating peroxisome proliferator-activated receptor gamma coactivator-1alpha-dependent mitochondrial biogenesis. Rejuvenation Res. 2010 Apr-Jun;13(2-3):148-51.
17. Smits ES, Duraku LS, Niehof SP, Daanen HA, Hovius SE, Selles RW, et al. Cold-induced vasodilatation in cold-intolerant rats after nerve injury. J Plast Reconstr Aesthet Surg. 2013 Sep;66(9):1279-86.
18. Werdin F, Grussinger H, Jaminet P, Kraus A, Manoli T, Danker T, et al. An improved electrophysiological method to study peripheral nerve regeneration in rats. J Neurosci Methods. 2009 Aug 30;182(1):71-7.
19. Nijhuis TH, Smits ES, van Neck JW, Visser GH, Walbeehm ET, Blok JH, et al. Ultrasound-guided needle positioning near the sciatic nerve to elicit compound muscle action potentials from the gastrocnemius muscle of the rat. J Neurosci Methods. 2011 Jan 15;194(2):283-6.
20. Calcutt NA, Freshwater JD, Mizisin AP. Prevention of sensory disorders in diabetic Sprague-Dawley rats by aldose reductase inhibition or treatment with ciliary neurotrophic factor. Diabetologia. 2004 Apr;47(4):718-24.
21. Kambiz S, van Neck JW, Cosgun SG, van Velzen MH, Janssen JA, Avazverdi N, et al. An early diagnostic tool for diabetic peripheral neuropathy in rats. PLoS One. 2015;10(5):e0126892.
22. Verdu E, Navarro X. Comparison of immunohistochemical and functional reinnervation of skin and muscle after peripheral nerve injury. Exp Neurol. 1997 Jul;146(1):187-98.
23. Zylka MJ, Rice FL, Anderson DJ. Topographically distinct epidermal nociceptive circuits revealed by axonal tracers targeted to Mrgprd. Neuron. 2005 Jan 6;45(1):17-25.
24. Dai Y, Fukuoka T, Wang H, Yamanaka H, Obata K, Tokunaga A, et al. Contribution of sensitized P2X receptors in inflamed tissue to the mechanical hypersensitivity revealed by phosphorylated ERK in DRG neurons. Pain. 2004 Apr;108(3):258-66.
25. Zhang J, Cavanaugh DJ, Nemenov MI, Basbaum AI. The modality-specific contribution of peptidergic and non-peptidergic nociceptors is manifest at the level of dorsal horn nociresponsive neurons. J Physiol. 2013 Feb 15;591(Pt 4):1097-110.
26. Bagai K, Wilson JR, Khanna M, Song Y, Wang L, Fisher MA. Electrophysiological patterns of diabetic polyneuropathy. Electromyogr Clin Neurophysiol. 2008 Apr-May;48(3-4):139-45.

Chapter 8

Discussion

Damage to the peripheral nerves has major consequences for epidermal innervation. The most common pathologies of peripheral nerves are injury and diabetic neuropathy (1). The important communality among these disorders is the requirement of axon regeneration to restore motor and sensory function. While the lesions of diabetic neuropathies usually are not as abrupt and permanent as a traumatic nerve transection, they can be widespread, proximal, and eventually destroy entire axon populations within the nerve trunk. The aim of this thesis is to elucidate the dynamics in epidermal innervation in both types of neuropathology using well-designed experimental models.

8.1.0. Importance of well-defined skin innervation regions

A number of animal models, mainly in rats, have been developed to study human peripheral neuropathology based on procedures at or near the sciatic nerve (2, 3). The sciatic nerve is due to plexus formation supplied by multiple spinal nerves: L4, L5 and L6 (4-7). It has three branches, namely the tibial nerve, the peroneal and the sural nerve. As skin biopsies for neurodiagnostic purposes have become increasingly important, accurate defined mapping of skin innervation in the rat hind paw is crucial when examining epidermal innervation following peripheral neuropathology in experimental studies (8). The Evans Blue extravasation technique was previously used to map the skin innervation in rats (9). However, these studies have several disadvantages. The analysis is either based on subjective interpretation, possible overestimation of the results or unreliable analysis of overlapping areas (10). Therefore, in an attempt to quantify the analysis, the Evans blue technique was combined with full 360 degrees circle Optical Surface Mapping (OSM), and computer-assisted surgical anatomy mapping (CASAM) technology (11), to improve objectivity and quantification of the innervation regions of individual nerves. The extensive analysis resulted in detailed mapping of different innervation areas, overlapping areas and variability of the innervation pattern of the skin. However, this comprehensive analysis requires time. Therefore, further research on digitalization of anatomical landmarks and analysis is required.

Consistent with electrophysiological studies, we were able to demonstrate that the skin demarcated by Evans Blue technique corresponds histologically with its innervation area. While electrical stimulation of the undamaged saphenous nerve showed blue coloring of the innervated skin, the denervated skin due to the sciatic nerve lesion remained non-extravasated. Therefore, we believe that the Evans Blue extravasation technique combined with an image evaluation method is an excellent tool to examine in detail the origin of the nerves that supply the skin. Using this methodology, we demonstrated that the three branches of the sciatic nerve (tibial nerve, sural nerve and peroneal nerve) together with the saphenous nerve, supply the innervation of almost the entire hind paw of the rat. The tibial nerve innervates exclusively the plantar hind paw, whereas the peroneal nerve supplies almost the entire dorsal hind paw and the sural nerve the lateral side of

both the plantar and dorsal hind paw. The saphenous nerve originating from L3 innervates the medial side of the hind paw.

The necessity for accurately defined innervation areas of the rat hind paw became apparent when comparing different studies of plantar innervation: in various studies a considerably larger area of the plantar skin has been assumed to be supplied by the saphenous nerve and the sural nerve when compared to the initial described innervation pattern of the hind paw by Swett and Woolf (12, 13). Using the Evans Blue extravasation technique, we were able to confirm that the initial electrophysiological study by Swett and Woolf, in our view, demonstrates the correct plantar extent of innervation pattern and other studies should be interpreted with caution. Correct innervation pattern of rats' hind paw is crucial as all behavioral and most histological studies are validated on the plantar skin of rats' hind paw (14, 15). Therefore, only the innervation of the plantar hind paw is histologically evaluated. However, Evans Blue extravasation revealed larger overlap areas in skin innervation on the dorsal part of the hind paw when compared to the plantar side. Future study needs to examine whether the larger observed overlap areas on the dorsal hind paw are accompanied by higher density of epidermal nerve fibers. Moreover, it is unknown whether this phenomenon has any implications for the regeneration processes of the relevant nerve. Therefore, it would be more interesting to also study the dynamics of the dorsal skin innervation with a main focus on the regeneration pattern and the density of epidermal nerve fibers after peripheral nerve injury.

8.2.0. Experimental models for peripheral nerve injury

Experimental neuropathic pain models include the chronic constriction injury (CCI), which is a loose ligation of the sciatic nerve, a tight ligation of a partial sciatic nerve (PSL), a tight ligation followed by distal cut of the spinal nerves (SNL), and a tight ligation followed by distal cut of the peroneal and sural nerve in which the tibial nerve is spared (SNI), amongst others (13, 16, 17). All animals in these models show behavioral signs of ongoing and evoked hypersensitivity for mechanical and thermal stimuli and are therefore considered to be useful models for neuropathic pain. Recently, an interesting review was published that provides the pros and cons of each neuropathic pain model (18).

In contrast to the CCI and the PSL, the SNL and the SNI do not allow regeneration of the damaged nerve resulting in highly reproducible models that show less variation in pain behavior and are therefore more suitable to study changes in skin innervation. To better evaluate neuropathic pain outcomes after end-to-end reconstruction, which is the golden standard therapy for transacted nerves, it seems rational to substitute the ligation in the validated neuropathic pain model by an end-to-end reconstruction. However, an end-to-end reconstruction in the SNL model would not necessary result in denervation followed by re-innervation of a specific region in the skin due to plexus formation. This may lead

to potentially undetectable changes in sensibility. In case of the SNI model, end-to-end reconstruction would be performed in the peroneal and the sural nerve. As the peroneal nerve innervates the dorsal hind paw it would not enable us to monitor the sensory re-innervation pattern using the validated behavioral experiments. In addition, it is known that peripheral nerve injuries cause central propagation via retrograde signaling (19, 20). It is therefore more likely to find non-specific results not necessarily related to the end-to-end reconstruction, but rather due to retrograde changes in the uninjured branch of the sciatic nerve. Moreover, as shown in chapter two, the three branches of the sciatic nerve demonstrate considerable overlap in innervation area of the skin (21). This could result in misinterpretation of behavioral data due to absence of denervation after nerve injury.

Since the lateral part of the hind paw is known to be exclusively innervated by the sciatic nerve, in our opinion an end-to-end reconstruction of the entire sciatic nerve proximal from its trifurcation, leaving the saphenous nerve undamaged, is a reliable method to study changes in skin innervation. Future studies performing end-to-end reconstruction of the saphenous nerve, leaving the sciatic nerve undamaged, may give additional information about the consistency of the nerve regeneration pattern and appearance of neuropathic pain features as found in our study.

8.3.0. Communication of adjacent nerve fibers after nerve injury

The re-designed Evans Blue technique, as described in chapter two, was applied in the uninjured adjacent saphenous nerve following end-to-end reconstruction of the whole sciatic nerve. It resulted in a temporary increase of up to two times of the extravasation area of the skin by the saphenous nerve as compared to the original surface area. This phenomenon is known as collateral sprouting and is described for the first time in human subjects by Theriault et al. in 1988 (22).
For the last decade, many researches made a positive correlation between collateral sprouting and neuropathic pain features (23, 24). Moreover, a recent study showed that specifically the peptidergic nerve fibers involved in collateral sprouting might play a major role in the development of neuropathic pain (25). Although we confirmed in chapter three that these newly formed collaterals consisted mainly of peptidergic nerve fibers, no correlation could be observed between the temporary proliferation of these collaterals and neuropathic pain features. Besides collateral sprouting, also the density of PGP9.5-positive Langerhans Cells (LCs) has been suggested to correlate with the occurrence of neuropathic pain (26, 27). However, this notion was based on chronic models of neuropathic pain after peripheral nerve injury. Therefore, it could not be established to what extent neuropathic pain was correlated to collateral sprouting by undamaged fibers and to what extent to regeneration of damaged fibers. Our end-to-end reconstruction model resulted only in transient neuropathic pain features and therefore presents an additional and interesting model to study these correlations. Although we observed

enhanced density of LCs in skin areas that showed most dramatic denervation after end-to-end reconstruction, no correlation was found with neuropathic pain features. In addition, LCs were absent in diabetic animals that showed neuropathic pain features. Combining these observations together with the lack of collateral sprouting in animals with neuropathic pain features, suggests a role for LCs and collateral sprouting in regeneration rather than in induction or maintenance of pain.

It is demonstrated that the central as well as the peripheral nervous system play a role in the development of neuropathic pain after nerve injury. Studies revealing the importance of the central nervous system showed changes in the expression of signaling pathways of the central nervous system (28). Others emphasized the important role of the peripheral nervous system by local changes at the site of the nerve injury causing retrograde transport of transcription factors leading to nerve regeneration and neuropathic pain features (29). Involvement of the peripheral nervous system in the development of neuropathic pain features is confirmed in the present thesis by demonstrating changes in the densities of epidermal innervation in the rat plantar hind paw following peripheral nerve injury. Furthermore, after unilateral peripheral nerve injury, mechanical and thermal sensitivity along with changes in the epidermal innervation were observed on the non-injured hind paw. This phenomenon is known as 'mirror image pain'. The most prominent changes in the non-injured epidermal innervation density involve the central and lateral part of the contralateral plantar hind paw. These regions are innervated by the sciatic nerve as shown in chapter two. Therefore, our results are indicative of mirror image pain due to sciatic nerve injury rather than a systemic effect.

8.4.0. Changes in innervation density

One of the strengths of this thesis is the quantification of epidermal innervation at different (central, medial and lateral) regions in both the proximal and the distal part of the plantar hind paw. This enabled us to draw conclusions about plantar skin innervation in the rat hind paw. In addition, we used two different models to study skin innervation. We observed disparity between the density of skin innervation and mechanical sensitivity in both the end-to-end reconstruction model (chapter 2) and in the diabetic peripheral neuropathy animals (chapter 6 and 7). More than 30% and even more than 75% loss of innervation in rats' hind paw was demonstrated in diabetic animals and in animals following end-to-end reconstruction of the nerve, respectively. However, no obvious sensory deficits were observed in either model. Although it may be argued that if comparison between local changes by nerve reconstruction and systematic changes by diabetes induction is justified, we suggest that a possible threshold for the density of skin innervation needs to be reached to cause changes in sensitivity. This phenomenon was partly shown by Verdu et al (30).

We also found a discrepancy in the innervation threshold that results in detectable sensory changes in these neuropathological conditions. While a decrease of more than 60% in the density of epidermal nerve fibers was accompanied with detectable mechanical hyposensitivity in our diabetic animals, it took about 90% loss of innervation in the end-to-end reconstruction model to cause hyposensitivity. We therefore conclude that besides loss in the number of epidermal nerve fibers, induction of a systematic disease such as diabetes may also lead to other changes in electrophysiological factors. This was confirmed by showing a decreased number of functional axons in diabetic animals by compound muscle axon potential recordings.

8.5.0. Innervation by peptidergic and non-peptidergic nerve fibers after peripheral neuropathology

Thermal hypersensitivity was observed simultaneously with hyperinnervation of peptidergic nerve fibers after end-to-end reconstruction of the nerve. This finding supports the previously shown expression of thermo-sensitive transient receptor potential (TRP) channel expression on peptidergic nerve fibers. Moreover, reduced thermal hyperalgesia is seen when specific TRP channels were silenced in an experimental model (31). Therefore, we propose that an increased density of peptidergic nerve fibers results in thermal hypersensitivity; a phenomenon that is described in chapter 5.

In contrast to our end-to-end reconstruction model, we observed only hypersensitivity to high temperature (50^{0}C), which was accompanied by a decrease in both peptidergic and non-peptidergic epidermal nerve fibers in diabetic animals (chapter 7). This finding contradicts the previously made correlation between thermal hypersensitivity and an increase in the peptidergic nerve fibers. The temperature induced hypersensitivity in our diabetic animals could be ascribed to increased expression of specific TRPV1 (transient receptor potential vanilloid 1) channels that become activated at temperatures above 42^{0}C, while TRP (transient receptor potential ankyrin 1) channels involved in cold temperatures sensation may not be affected (32, 33). However, further immunohistological and electrophysiological research in thermo-sensitive TRP channels is required to ascertain the contribution of TRP channels in the detected thermal hypersensitivity in our animal models.

Remarkably, the density of the non-peptidergic nerve fibers remained significantly diminished after both end-to-end reconstruction and after induction of diabetic peripheral neuropathy model thereby contrasting the dynamics of the peptidergic nerve fibers. These findings are in line with the decreased expression of neurotrophic factor GDNF that promotes non-peptidergic nerve fibers in diabetic rats and after peripheral nerve injury (34-36). Moreover, application of GDNF has proven to be beneficial for both peripheral nerve regeneration and diabetic neuropathy (37-40). These results suggest that non-peptidergic nerve fibers are

more vulnerable in peripheral nerve injury and diabetes than peptidergic fibers. The observed changes in the non-peptidergic nerve fiber population were independent from that of the peptidergic nerve fibers in our studies. Our findings together with the previously shown anatomical and functional differences in these two subgroups of sensory fibers in the dorsal root ganglion (DRG) suggest two separate pathways and possibly a more vulnerable or a slower regeneration of the non-peptidergic nerve fibers following peripheral neuropathologies. Given the potent effects of GDNF on survival and repair of injured peripheral neurons, we propose that targeting this pathway may yield therapeutic tools to treat peripheral nerve injury and neuropathies.

8.6.0. Diabetic peripheral neuropathy

Peripheral neuropathy is a common complication of diabetes caused by chronic hyperglycemia. Symptoms of diabetic neuropathy are variable, but mostly involve distal peripheral nerves and include abnormal touch, temperature, pain, and pressure sensation. Multiple factors contribute to the pathogenesis of diabetic neuropathy, including reduced blood supply, axonal loss, segmental demyelination, and defective neurotrophic factors (41-43). We observed many of these factors in our streptozotocin (STZ) induced diabetic rats, which therefore may be considered as an attractive animal model for diabetes. Peripheral vascular changes are shown by reduced skin blood flow, decreased skin oxygenation and delayed rewarming rate of the skin. Changes in peripheral sensory nerve fibers were observed by a loss of epidermal innervation accompanied with decreased mechanical sensation, additionally, thermal pain was also present in our diabetic animals. Moreover, a reduced motor nerve conduction velocity was observed suggesting demyelination of motor nerves. All these findings indicate that our STZ-induced diabetic rats are a reliable model to study diabetic vascular changes and the development of diabetic peripheral neuropathy.

Although the STZ diabetic rat model has been used to study complications of diabetes for many years, only limited information is available concerning the rewarming rate of the skin and its correlation to diabetic peripheral neuropathy in this model. We showed for the first time that the decreased skin blood flow is accompanied by lower skin temperature and a significant delay in the rewarming rate of the skin in diabetic rats compared to controls, which further increases the similarity between the STZ model and human diabetes. Indeed our results demonstrate that there is a correlation between the skin temperature and skin blood flow. Moreover, we showed that the skin rewarming rate could serve as an early diagnostic tool for diabetic peripheral neuropathy in diabetic rats when no changes were yet observed in behavioral outcomes. With these findings, we confirm that vascular deformities may be present prior to the development of overt diabetic peripheral neuropathy in diabetic rats.

The rewarming rate of the skin has many advantages when compared to skin biopsies as a diagnostic tool for diabetic peripheral neuropathy. Thermographic assessment of vascular properties is a non-invasive method to determine diabetic peripheral neuropathy. In contrast to skin biopsies, the rewarming rate of the skin includes the entire affected area of the skin. Moreover, impairment of the small unmyelinated fibers, which are shown to be the first affected in the course of diabetic
peripheral neuropathy, is detected using this method. Therefore, early diagnosis of diabetic peripheral neuropathies by monitoring the skin rewarming rate may be a valuable tool to reduce the development of diabetic complications such as foot ulcers, diabetic foot and amputations.

The absence of the toe spread response and decreased CMAPs amplitudes suggests that the motor function of the nerves was affected in our diabetic rats. Decreased CMAPs amplitude along with muscle weakness have also been demonstrated in diabetic subjects with diabetic peripheral neuropathy (29; 30). Similar to electrophysiological studies in human and animal diabetes, the CMAP amplitude in our study, described in chapter six, decreased prior to slowing of MNCV demonstrating early appearance of independent axonal degeneration followed by demyelination. However, CMAPs amplitudes do not evaluate small fiber neuropathy, which are suggested to be the earliest detectable sign of neuropathy (1). Therefore, von Frey monofilaments and the density of epidermal nerve fibers (31) were measured to determine small fiber neuropathy in chapter six and seven. Several studies applying von Frey filaments have demonstrated mechanical hypersensitivity in diabetic rats (31; 32), while others determined mechanical hyposensitivity (33). Although there was a difference in the concentration (ranging between 45-70mg/kg) and administration (intravenous, intra-peritoneal, intra-muscular, subcutaneous) of STZ-injections, all Wistar (31; 34-38) and Sprague-Dawley rats (32; 39-42) showed mechanical hypersensitivity after STZ-injection, while those in the Fisher study (33) and, in chapter 6 and 7, the WagRij strain demonstrated mechanical hyposensitivity. Despite the differences in mechanical sensitivity, all studies showed increased plasma glucose after STZ-injection meeting the criteria of diabetes in animal studies and used comparable methodology when collecting behavioral data. This suggests, a rodent strain difference in mechanical sensitivity. However, diabetic human subjects present more often with complications of peripheral hyposensitivity rather than mechanical hypersensitivity leading to unnoticed skin damage and ulcers. In our diabetes studies mechanical hyposensitivity is seen after inducing diabetes, which makes use of WagRij strain of rats a more comparable model for human diabetes when examining diabetic peripheral neuropathy.

8.7.0. ALCAR

It is shown that ALCAR administration results in pain relief and improvement of nerve conduction velocity in both diabetic rats and humans. In chapter 7, we were able to show for the first time an absence of changes in mechanical sensation accompanied with a reduced loss of epidermal nerve fibers in ALCAR-treated diabetic animals. These findings, together with delayed thermal hypersensitivity after ALCAR administration supports the neuro-protective role of ALCAR in diabetic animals. The aim of our study in chapter 7 was to examine the effect of ALCAR on subgroup of epidermal sensory nerve fibers after induction of diabetes. It has been shown that ALCAR normalizes peripheral and central alterations of GDNF, which is the promoter of non-peptidergic nerve fibers. Consistent with these findings, we found significantly less reduction in non-peptidergic nerve fibers after ALCAR treatment in diabetic animals when compared to non-treated diabetic animals. However, the peptidergic nerve fibers were reduced in both ALCAR treated and not ALCAR treated diabetic animals. From this we conclude that ALCAR specifically protects non-peptidergic nerve fibers and emphasizes the previously described two separate sensory pathways by the peptidergic and the non-peptidergic nerve fibers.

8.8.0. Future perspectives

Skin biopsies have become increasingly important for neurodiagnostic purposes in peripheral neuropathology studies. In the clinic, the total density of epidermal innervation is analysed without distinction between its subgroups: the peptidergic and the non-peptidergic nerve fibers. However, the present thesis demonstrated that the subtypes of sensory nerve fiber show different responses to peripheral neuropathologies. Furthermore, these peptidergic and non-peptidergic nerve fibers seem to be involved in different sensory modules supporting the previously described theory that the two nerve fiber types make use of two separate signalling pathways.

Many researchers have attempted to find an effective therapy for the invalidating neuropathic pain symptoms caused by different neuropathologies such as peripheral nerve injury and diabetic neuropathy. Therapeutic approaches from first-line analgesic treatments, antidepressants (tricyclic agents and serotonin-norepinephrine reuptake inhibitors), anticonvulsants (gabapentin and pregabalin) to chronic motor cortex stimulation by implanted epidural electrodes have been studied. Unfortunately, no evidential progress has been made in this field in the past decade.

Based on our results, we believe that future therapeutic advancement in neuropathic pain are likely to benefit from improved understanding in subtype of sensory nerve fibers. Moreover, TRP channels could serve as a potential therapeutic target for cold intolerance. Advancement in neuropathic pain caused by peripheral neuropathology is likely to benefit from improved understanding of TRP channels expressed on these sensory nerve fibers.

8.9.0. References

1. Burnett MG, Zager EL. Pathophysiology of peripheral nerve injury: a brief review. Neurosurg Focus. [Review]. 2004 May 15;16(5):E1.
2. Yang CC, Wang J, Chen SC, Jan YM, Hsieh YL. Enhanced functional recovery from sciatic nerve crush injury through a combined treatment of cold-water swimming and mesenchymal stem cell transplantation. Neurol Res. 2015 Jun 4:1743132815Y0000000060.
3. Geuna S. The sciatic nerve injury model in pre-clinical research. Journal of neuroscience methods. [Research Support, Non-U.S. Gov't Review]. 2015 Mar 30;243:39-46.
4. Wessels WJ, Feirabend HK, Marani E. The rostrocaudal organization in the dorsal root ganglia of the rat: a consequence of plexus formation? Anat Embryol (Berl). [Review]. 1994 Jul;190(1):1-11.
5. Wessels WJ, Marani E. A rostrocaudal somatotopic organization in the brachial dorsal root ganglia of neonatal rats. Clin Neurol Neurosurg. [Research Support, Non-U.S. Gov't]. 1993;95 Suppl:S3-11.
6. Puigdellivol-Sanchez A, Forcada-Calvet P, Prats-Galino A, Molander C. Contribution of femoral and proximal sciatic nerve branches to the sensory innervation of hindlimb digits in the rat. Anat Rec. [Research Support, Non-U.S. Gov't]. 2000 Oct 1;260(2):180-8.
7. Greene EC. Anatomy of the rat. New York: Hafner; 1955.
8. Buonocore M. Unilateral peripheral neuropathic pain: The role of neurodiagnostic skin biopsy. World J Clin Cases. [Review]. 2014 Feb 16;2(2):27-31.
9. Brenan A, Jones L, Owain NR. The demonstration of the cutaneous distribution of saphenous nerve C-fibres using a plasma extravasation technique in the normal rat and following nerve injury. J Anat. [Research Support, Non-U.S. Gov't]. 1988 Apr;157:57-66.
10. Gonzalez HL, Carmichael N, Dostrovsky JO, Charlton MP. Evaluation of the time course of plasma extravasation in the skin by digital image analysis. The journal of pain : official journal of the American Pain Society. [Research Support, Non-U.S. Gov't]. 2005 Oct;6(10):681-8.
11. Kerver AL, van der Ham AC, Theeuwes HP, Eilers PH, Poublon AR, Kerver AJ, et al. The surgical anatomy of the small saphenous vein and adjacent nerves in relation to endovenous thermal ablation. Journal of vascular surgery. 2012 Jul;56(1):181-8.
12. Swett JE, Woolf CJ. The somatotopic organization of primary afferent terminals in the superficial laminae of the dorsal horn of the rat spinal cord. The Journal of comparative neurology. [Research Support, Non-U.S. Gov't Research Support, U.S. Gov't, P.H.S.]. 1985 Jan 1;231(1):66-77.
13. Decosterd I, Woolf CJ. Spared nerve injury: an animal model of persistent peripheral neuropathic pain. Pain. [Research Support, Non-U.S. Gov't Research Support, U.S. Gov't, P.H.S.]. 2000 Aug;87(2):149-58.

14. Jasmin L, Kohan L, Franssen M, Janni G, Goff JR. The cold plate as a test of nociceptive behaviors: description and application to the study of chronic neuropathic and inflammatory pain models. Pain. [Research Support, Non-U.S. Gov't Research Support, U.S. Gov't, P.H.S.]. 1998 Apr;75(2-3):367-82.
15. Boric M, Skopljanac I, Ferhatovic L, Jelicic Kadic A, Banozic A, Puljak L. Reduced epidermal thickness, nerve degeneration and increased pain-related behavior in rats with diabetes type 1 and 2. J Chem Neuroanat. [Research Support, Non-U.S. Gov't]. 2013 Nov;53:33-40.
16. Bennett GJ, Xie YK. A peripheral mononeuropathy in rat that produces disorders of pain sensation like those seen in man. Pain. [Research Support, Non-U.S. Gov't Research Support, U.S. Gov't, P.H.S.]. 1988 Apr;33(1):87-107.
17. Kim SH, Chung JM. An experimental model for peripheral neuropathy produced by segmental spinal nerve ligation in the rat. Pain. [Research Support, Non-U.S. Gov't Research Support, U.S. Gov't, P.H.S.]. 1992 Sep;50(3):355-63.
18. Challa SR. Surgical animal models of neuropathic pain: Pros and Cons. Int J Neurosci. 2015 Mar;125(3):170-4.
19. Richardson PM, Miao T, Wu D, Zhang Y, Yeh J, Bo X. Responses of the nerve cell body to axotomy. Neurosurgery. [Review]. 2009 Oct;65(4 Suppl):A74-9.
20. Carcamo CR. Mirror-image pain is mediated by nerve growth factor produced from tumor necrosis factor-alpha-activated satellite glia after peripheral nerve injury. Pain. [Comment Letter]. 2014 Aug;155(8):1675.
21. Kambiz S, Baas M, Duraku LS, Kerver AL, Koning AH, Walbeehm ET, et al. Innervation mapping of the hind paw of the rat using Evans Blue extravasation, Optical Surface Mapping and CASAM. Journal of neuroscience methods. 2014 May 30;229:15-27.
22. Theriault E, Diamond J. Nociceptive cutaneous stimuli evoke localized contractions in a skeletal muscle. J Neurophysiol. [Research Support, Non-U.S. Gov't]. 1988 Aug;60(2):446-62.
23. Kim HJ, Na HS, Sung B, Nam HJ, Chung YJ, Hong SK. Is sympathetic sprouting in the dorsal root ganglia responsible for the production of neuropathic pain in a rat model? Neurosci Lett. [Research Support, Non-U.S. Gov't]. 1999 Jul 9;269(2):103-6.
24. Zhang JM, Strong JA. Recent evidence for activity-dependent initiation of sympathetic sprouting and neuropathic pain. Sheng Li Xue Bao. [Review]. 2008 Oct 25;60(5):617-27.
25. Duraku LS, Hossaini M, Hoendervangers S, Falke LL, Kambiz S, Mudera VC, et al. Spatiotemporal dynamics of re-innervation and hyperinnervation patterns by uninjured CGRP fibers in the rat foot sole epidermis after nerve injury. Mol Pain. 2012;8:61.
26. Duraku LS, Hossaini M, Schuttenhelm BN, Holstege JC, Baas M, Ruigrok TJ, et al. Re-innervation patterns by peptidergic Substance-P, non-peptidergic P2X3, and myelinated NF-200 nerve fibers in epidermis and dermis of rats with neuropathic pain. Experimental neurology. 2013 Mar;241:13-24.

27. Lindenlaub T, Sommer C. Epidermal innervation density after partial sciatic nerve lesion and pain-related behavior in the rat. Acta Neuropathol. [Research Support, Non-U.S. Gov't]. 2002 Aug;104(2):137-43.
28. Xie K, Jia Y, Hu Y, Sun Y, Hou L, Wang G. Activation of notch signaling mediates the induction and maintenance of mechanical allodynia in a rat model of neuropathic pain. Mol Med Rep. [Research Support, Non-U.S. Gov't]. 2015 Jul;12(1):639-44.
29. Cheng CF, Cheng JK, Chen CY, Lien CC, Chu D, Wang SY, et al. Mirror-image pain is mediated by nerve growth factor produced from tumor necrosis factor alpha-activated satellite glia after peripheral nerve injury. Pain. [Research Support, Non-U.S. Gov't]. 2014 May;155(5):906-20.
30. Verdu E, Navarro X. Comparison of immunohistochemical and functional reinnervation of skin and muscle after peripheral nerve injury. Exp Neurol. 1997 Jul;146(1):187-98.
31. Christoph T, Grunweller A, Mika J, Schafer MK, Wade EJ, Weihe E, et al. Silencing of vanilloid receptor TRPV1 by RNAi reduces neuropathic and visceral pain in vivo. Biochem Biophys Res Commun. 2006 Nov 10;350(1):238-43.
32. Caterina MJ, Julius D. The vanilloid receptor: a molecular gateway to the pain pathway. Annu Rev Neurosci. [Review]. 2001;24:487-517.
33. Story GM, Peier AM, Reeve AJ, Eid SR, Mosbacher J, Hricik TR, et al. ANKTM1, a TRP-like channel expressed in nociceptive neurons, is activated by cold temperatures. Cell. [Comparative Study Research Support, Non-U.S. Gov't Research Support, U.S. Gov't, P.H.S.]. 2003 Mar 21;112(6):819-29.
34. Liu GS, Shi JY, Lai CL, Hong YR, Shin SJ, Huang HT, et al. Peripheral gene transfer of glial cell-derived neurotrophic factor ameliorates neuropathic deficits in diabetic rats. Hum Gene Ther. 2009 Jul;20(7):715-27.
35. Nagano M, Sakai A, Takahashi N, Umino M, Yoshioka K, Suzuki H. Decreased expression of glial cell line-derived neurotrophic factor signaling in rat models of neuropathic pain. Br J Pharmacol. 2003 Dec;140(7):1252-60.
36. Vivoli E, Di Cesare Mannelli L, Salvicchi A, Bartolini A, Koverech A, Nicolai R, et al. Acetyl-L-carnitine increases artemin level and prevents neurotrophic factor alterations during neuropathy. Neuroscience. 2010 Jun 2;167(4):1168-74.
37. Blesch A, Tuszynski MH. Cellular GDNF delivery promotes growth of motor and dorsal column sensory axons after partial and complete spinal cord transections and induces remyelination. J Comp Neurol. 2003 Dec 15;467(3):403-17.
38. Chen ZY, Chai YF, Cao L, Lu CL, He C. Glial cell line-derived neurotrophic factor enhances axonal regeneration following sciatic nerve transection in adult rats. Brain Res. 2001 Jun 1;902(2):272-6.
39. Anitha M, Gondha C, Sutliff R, Parsadanian A, Mwangi S, Sitaraman SV, et al. GDNF rescues hyperglycemia-induced diabetic enteric neuropathy through activation of the PI3K/Akt pathway. J Clin Invest. 2006 Feb;116(2):344-56.

40. Akkina SK, Patterson CL, Wright DE. GDNF rescues nonpeptidergic unmyelinated primary afferents in streptozotocin-treated diabetic mice. Exp Neurol. 2001 Jan;167(1):173-82.
41. Vinik AI, Park TS, Stansberry KB, Pittenger GL. Diabetic neuropathies. Diabetologia. 2000 Aug;43(8):957-73.
42. Apfel SC. Nerve growth factor for the treatment of diabetic neuropathy: what went wrong, what went right, and what does the future hold? Int Rev Neurobiol. 2002;50:393-413.
43. Siemionow M, Demir Y. Diabetic neuropathy: pathogenesis and treatment. J Reconstr Microsurg. 2004 Apr;20(3):241-52.

Chapter 9

Summary/Samenvatting

9.1.0 Summary

In the present thesis the two most common peripheral nerve pathologies, peripheral nerve injury and diabetic peripheral neuropathy, were examined using preclinical animal models. Both nerve pathologies commonly lead to neuropathic pain, which is defined as pain caused by lesion or disease of the somatosensory nervous system. Manifestations of neuropathic pain features were analysed using quantitative sensory testing, electrophysiology, and skin biopsy with a focus on dynamics of epidermal innervation.

The epidermis, the outermost layer of the skin, is innervated by fast conducting thinly myelinated Aδ-fibers and slow conducting unmyelinated C-fibers. All Aδ and C-fibers use the fast excitatory neurotransmitter glutamate for signalling. However, a subpopulation may also contain various neuropeptides, resulting in a subdivision of epidermal nerve fibers into peptidergic and non-peptidergic. The peptidergic nerve fibers express Substance P (SubP) on C-fibers and Calcitonin Gene-Related Peptide (CGRP) on both C-fibers and Aδ-fibers. The non-peptidergic nerve fibers express P2X3 receptor on C-fibers.

In the first part of this thesis we mapped the epidermal innervation of the rats' hind paw in control animals, as all behavioral and most histological studies concerning peripheral nerve pathologies were validated on the plantar skin of rats' hind paw (**chapter 2**). The Evans Blue extravasation technique was combined with full 360 degrees circle Optical Surface Mapping (OSM), and computer-assisted surgical anatomy mapping (CASAM) technology to improve the objectivity and quantification of the innervation regions of individual nerves. This extensive analysis resulted in detailed mapping of different innervation areas, overlapping areas, and variability of the innervation pattern of the skin.

In **chapter 3** the redesigned Evans Blue technique was used to demonstrate collateral sprouting by adjacent uninjured saphenous nerve fibers supplying the denervated skin after transection and immediate end-to-end reconstruction of the sciatic nerve. In recent years, collateral sprouting has been implicated in the development of neuropathic pain features. However, this notion was based on chronic models of neuropathic pain after peripheral nerve injury. Therefore, it could not be established to what extent neuropathic pain was correlated to collateral sprouting by undamaged fibers and to what extent to regeneration of damaged fibers. Our end-to-end reconstruction model resulted only in transient neuropathic pain features and therefore presents an additional and interesting model to study these correlations. Based on the results described in **chapter 3,** no correlation was found between collateral sprouting and neuropathic pain features. Importantly, as the sciatic nerve repopulated the rats' hind paw, the saphenous nerve withdrew to its original territory, illustrating the dynamic behaviour of peripheral nerves after nerve injury. Therefore, we conclude that collateral sprouting is more involved in nerve regeneration than in the induction of neuropathic pain. Furthermore, an increased density of peptidergic nerve fibers was found in the injured plantar

hind paw simultaneously with thermal hypersensitivity after unilateral end-to-end reconstruction of the sciatic nerve. These findings together with the known expression of specific temperature sensitive transient receptor potential (TRP) channels on peptidergic fibers (**chapter 5**), point to a potential role for peptidergic nerve fibers in thermal hypersensitivity. However, while the peptidergic nerve fibers recovered to control values, the non-peptidergic nerve fibers remained decreased at all experimental time points (up to 20 weeks after end-to-end reconstruction) showing to be the more vulnerable aspect of this subgroup of epidermal nerve fibers.

In **chapter 4**, it was shown that similar to the injured hind paw, the uninjured plantar hind paw demonstrated a transient increase in the density of peptidergic nerve fibers that was accompanied with thermal hypersensitivity after unilateral end-to-end reconstruction of the sciatic nerve. This phenomenon is known as 'mirror image pain' and supports the previously described retrograde signalling that induces changes in the dorsal root ganglion (DRG) contralateral to the injury. Furthermore, these findings warn against using the uninjured side as a control in examining behavioral changes or in evaluating the skin innervation.

In the second part of this thesis, we examined diabetic peripheral neuropathy. Diabetic peripheral neuropathy is a nerve disorder with one of the fastest growing incidence rates, frequently leads to foot ulcers and occasionally may necessitate partial or complete foot amputation. Streptozotocin(STZ)-induced diabetic rats are widely used as a model to study complications caused by diabetes. In **chapter 6**, the effect of STZ-induced diabetes on the appearance of neuropathic pain features in correlation with epidermal innervation was examined. Furthermore, the skin rewarming rate of diabetic patients is used as a diagnostic tool for early diagnosis of diabetic neuropathy. Therefore, we also studied whether the skin rewarming rate in diabetic rats is related to microvascular changes and whether this is correlated to changes observed in classical diagnostic methods for diabetic peripheral neuropathy.

We demonstrated that loss of epidermal nerve fibers was accompanied with decreased mechanical sensation and thermal hypersensitivity in our diabetic animals. In addition, our thermography results revealed decreased skin temperatures prior to detectable peripheral neuropathy suggesting that signs of microvascular disease are already present prior to the development of clinically overt diabetic peripheral neuropathy. Therefore, we show that the changes in skin innervation and in microvascular modalities are similar between our STZ-induced diabetic rat model and human diabetes, increasing our confidence in this diabetes model.

At present, no additional therapy is available for the prevention or treatment of diabetic neuropathy besides analgesics and blood glucose controlling medicaments. However, acetylated L-carnitine (ALCAR) has been proposed as a therapeutic agent for diabetic peripheral neuropathy, as pain relief and

improvement of nerve conduction velocity were found in both diabetic rats and humans after supplementation with ALCAR.

In **chapter 7** of the present thesis, ALCAR administration in STZ-diabetic rats resulted in mechanical sensitivity comparable to non-diabetic animals and a significantly smaller reduction in non-peptidergic nerve fibers. As non-peptidergic nerve fibers are exclusively expressed on C-fibers, which are known to be involved in mechanoreception, we suggest a correlation between the density of non-peptidergic nerve fibers and mechanical sensitivity. Furthermore, the results of this thesis strongly suggest a preventive role for ALCAR as a treatment basis for diabetic peripheral neuropathy.

9.2.0. Samenvatting

Perifeer zenuwletsel en diabetische neuropathie zijn de twee meest voorkomende perifere zenuwpathologieën. Beide ziektebeelden zijn in dit proefschrift bestudeerd, waarbij gebruikgemaakt wordt van preklinische diermodellen. De overeenkomst tussen deze zenuwpathologieën is de ontwikkeling van neuropathische pijn die gedefinieerd wordt als letsel of ziekte van het somatosensorische zenuwstelsel. Manifestatie van kenmerken die passen bij neuropathische pijn zijn geanalyseerd met behulp van kwantitatieve sensorische testen, elektrofysiologie en huidbiopsie met de focus op de dynamiek van epidermale innervatie.

De epidermis, de opperhuid, wordt geïnnerveerd door snel geleidende, dun gemyeliniseerde Aδ-vezels en langzaam geleidende, niet-gemyeliniseerde C-vezels. Alle Aδ- en C-vezels gebruiken de snel excitatoire neurotransmitter glutamaat voor signaaltransductie. Een subpopulatie hiervan bevat verschillende neuropeptiden resulterend in onderverdeling van de epidermale zenuwvezels in peptiderge en niet-peptiderge zenuwvezels. De peptiderge zenuwvezels brengen substance P (SubP) tot expressie op C-vezels en calcitonin gene-related peptide (CGRP) op zowel C-vezels als Aδ-vezels. De niet-peptiderge vezels brengen P2X3-receptoren tot expressie op C-vezels.

Het merendeel van sensorische testen en histologische zenuwkleuringen in de experimentele studies is gevalideerd op de plantaire achterpoten van ratten. Daarom hebben we in het eerste deel van dit proefschrift de epidermale innervatie in de achterpoot van controleratten in kaart gebracht (**hoofdstuk 2**). De Evans Blue-extravasatietechniek werd gecombineerd met een 360 graden optical surface mapping (OSM) en computer-assisted surgical anatomy mapping (CASAM)-technologie. Hiermee verkregen we een verbeterde methodologie voor het objectiveren en kwantificeren van individuele innervatiegebieden per zenuw, overlap in innervatiegebieden en variabiliteit in innervatiepatroon in de achterpoot van de rat.

In **hoofdstuk 3** is de vernieuwde Evans Blue-techniek gebruikt om collateral sprouting aan te tonen, re-innervatie van gedenerveerde huid door aangrenzende intacte zenuwvezels, na transsectie en end-to-end-reconstructie van de zenuw. De afgelopen jaren is de veronderstelling ontstaan dat collateral sprouting een rol speelt bij de ontwikkeling van neuropathische pijn. Deze veronderstelling is echter gebaseerd op onderzoeken betreffende chronischepijnmodellen het ontstaan van perifeer zenuwletsel. Hierdoor is het moeilijk te achterhalen of de neuropathische pijn gecorreleerd is aan collateral sprouting dan wel aan regeneratieve zenuwvezels, afkomstig van de beschadigde zenuw. Ons end-to-end gereconstrueerde model vertoont voorbijgaande symptomen van neuropathische pijn, waardoor het een interessant model is om deze specifieke correlaties te bestuderen. Gebaseerd op onze resultaten, zoals beschreven in **hoofdstuk 3**, hebben we geen correlaties kunnen vinden tussen collateral sprouting en kenmerken van neuropathische pijn. Een belangrijke bevinding is dat de collateral sprouting,

afkomstig van de niet-aangedane nervus saphenous, zich terugtrekt nadat de gereconstrueerde nervus ischiadicus regenereert naar zijn eigen territorium. Deze resultaten illustreren het dynamische gedrag van perifere zenuwen na het ontstaan van zenuwletsel. We concluderen daarom dat het aannemelijker is dat collateral sprouting betrokken is bij zenuwregeneratie dan bij inductie of handhaving van neuropathische pijn. Tevens hebben we, na zenuwreconstructie, verhoogde densiteit van peptiderge zenuwvezels gekwantificeerd in de plantaire achterpoten van de dieren. Dit gaat gepaard met hypersensitiviteit voor temperatuur. Deze bevindingen, samen met de kennis dat temperatuur sensitieve transient receptor potential (TRP)-kanalen op peptiderge zenuwvezels tot expressie komen (**hoofdstuk 5**), wijzen op een potentiële rol voor de peptiderge zenuwvezels in thermale hypersensitiviteit. Na verloop van tijd bereikt de densiteit van de peptiderge zenuwvezels controlewaardes, terwijl de non-peptiderge vezels tot het laatste experimentele tijdspunt (twintig weken na zenuwreconstructie) significant verlaagd blijven Hieruit kunnen we concluderen dat de non-peptiderge zenuwvezels mogelijk kwetsbaarder zijn voor zenuwletsel.

In **hoofdstuk 4** is aangetoond dat de niet-aangedane achterpoot, vergelijkbaar met de aangedane zijde, tijdelijke toename laat zien in de densiteit van peptiderge zenuwvezels gepaard gaand met thermale hypersensitiviteit. Dit fenomeen staat bekend als 'mirror image pain' en ondersteunt de eerder beschreven retrograde signaaltransductie, die veranderingen veroorzaakt in de dorsale ganglia (DRG) aan de niet-aangedane zijde. Gebaseerd op onze resultaten concluderen wij dat de niet- aangedane zijde niet gebruikt kan worden als een betrouwbare controle om gedragsexperimenten dan wel de huidinnervatie te onderzoeken.

In het tweede deel van dit proefschrift hebben we diabetische perifere neuropathie bestudeerd. Diabetische perifere neuropathie is een groeiende zenuwaandoening die frequent leidt tot voetulceraties en dit kan amputatie van ledematen tot gevolg hebben. De streptozotocin (STZ)-geïnduceerde diabetische rat is een veelgebruikt model om complicaties van diabetes te onderzoeken. In **hoofdstuk 6** hebben we het effect van STZ-geïnduceerde diabetes onderzocht op het voorkomen van neuropathische pijn in relatie tot epidermale innervatie. Naast kwantificatie van epidermale zenuwvezels wordt tegenwoordig met behulp van thermografie ook de snelheid waarmee de huid verwarmt als een diagnostisch middel gebruikt om diabetische perifere neuropathie vast te stellen in de kliniek. Daarom hebben we ook thermografische data verzameld en deze gerelateerd aan mogelijke veranderingen in de microvasculaire modaliteiten en epidermale innervatie. We hebben aangetoond dat verlies van mechanische sensatie en hypersensitiviteit voor temperatuur gepaard gaan met verlaagde densiteit van epidermale zenuwvezels in de dieren met STZ-geïnduceerde diabetes. Tevens laten onze thermografische data vertraagde verwarming van de huid zien voordat klinisch detecteerbare symptomen van diabetische perifere neuropathie ontstaan. Hieruit concluderen wij dat de veranderingen in epidermale innervatie en in microvasculaire modaliteiten, zoals

gezien in dieren met STZ-geïnduceerde diabetes, het aantal overeenkomsten tussen dit diabetische diermodel en humane diabetes vergroten.

Naast pijnstillers en bloedglucose controlerende medicatie bestaat er tot op heden geen effectieve therapie ter preventie of behandeling van diabetische perifere neuropathie. Het is aangetoond dat geacetyleerd L-carnitine (ALCAR) een pijnstillende werking heeft en verbetering vertoont in zenuwgeleiding van zowel diabetische dieren als mensen. Daarom wordt ALCAR overwogen als een therapeutisch middel voor diabetische perifere neuropathie. In **hoofdstuk 7** hebben we ALCAR toegediend aan dieren met STZ-geïnduceerde diabetes, wat resulteert in het behouden van mechanische sensitiviteit. Tegelijkertijd vinden we significant minder verlies in de densiteit van non-peptiderge epidermale zenuwvezels in vergelijking tot de diabetische dieren zonder ALCAR-toediening. Gebaseerd op onze bevindingen en de kennis dat non-peptiderge zenuwvezels uitsluitend tot expressie komen op C-vezels, die betrokken zijn bij mechanoreceptie, suggereren we een correlatie tussen de densiteit van non-peptiderge zenuwvezels en mechanische sensitiviteit. Bovendien duiden de resultaten van dit proefschrift sterk op een rol voor ALCAR in profylactische behandeling van diabetische perifere neuropathie.

Chapter 10

Appendices

Abbreviations
PhD portofolio
List of publications
Acknowledgements/Dankwoord
About the Author

Abbreviations

ALCAR: Acetyl-L-Carnitine

CASAM: Computer Assisted Surgical Anatomy Mapping

CGRP: Calcitonin Gene Related Peptide

CMAPs: Compound Muscle Action Potentials

DRG: Dorsal Root Ganglion

GDNF: Glial cell Derived Neurotrophic Factor

GMI: Gastrocnemius Muscle Index

IASP: International Association for the Study of Pain

IB4: Isolectin B4

IENFs: Intraepidermal Nerve Fibers

NF200: Neurofilament 200

NGF: Nerve Growth Factor

OPT: Optical Projection Tomography

OSM: Optical Surface Mapping

P2X3: Purinogenic 2X3

PGP9.5: Protein Gene Product 9.5

STZ: Streptozotocin

SubP: Substance P

TNF-α: Tumor Necrosis Factor-α

TRP: Transient Receptor Potential

PhD portfolio

Name PhD student:	Shoista Kambiz
Erasmus MC department:	Plastic, Reconstructive and Hand Surgery
PhD period:	August 2011 – November 2015
Title PhD thesis:	Dynamics of epidermal innervation: role of the peptidergic and non-peptidergic nerve fibers in relation to peripheral nerve pathology
Promotor:	Prof. S.E.R. Hovius
Copromotors:	Dr. E.T. Walbeehm, Dr. T.J.H. Ruigrok

PhD training	Year	ECTS
Research Master of Neuroscience	2010-2012	
General courses		
-Biomedical English Writing Erasmus Medical Center, Rotterdam	2011	0.4
-Scientific English Writing Center for British English, Rotterdam	2012	2.5
-Animal Ethics Course (art.9) Erasmus Medical Center, Rotterdam	2013	0.5
-Statistics SPSS6 for PhD students Erasmus Medical Center, Rotterdam	2013	0.5
-Integrity course for PhD students Erasmus Medical Center, Rotterdam	2014	0.3
Specific courses		
-Microsurgery course by Mrs. J.M. Hekking Skillslab, Erasmus Medical Center, Rotterdam	2010-2015	9.5

PhD training	Year	ECTS
Seminars		
-Neural mechanism for rapid perceptual decision Speaker: Zach Mainen Erasmus Medical Center, Rotterdam	2011	0.1
-Reverse engineering the brain: which tools do we need? Speaker: Winfried Denk Erasmus Medical Center, Rotterdam	2011	0.1
-Defining the neuronal circuitry of fear Speaker: Andreas Luthi Erasmus Medical Center, Rotterdam	2011	0.1
-Journal Club Immunohistochemistry Speaker: Dr. Dick Jaarsma and Dr. J.C. Holstege Erasmus Medical Center, Rotterdam	2011	2.5
-Interweaving neural substrates for perception and motivation Speaker: Cyriel Pennartz Erasmus Medical Center, Rotterdam	2012	0.1
Workshops		
-Nerve reconstruction Skillslab Erasmus Medical Center, Rotterdam	2011-2014	0.4
-Tendon reconstruction Skillslab Erasmus Medical Center, Rotterdam	2011-2014	0.4
-Local flaps Skillslab Erasmus Medical Center, Rotterdam	2013	0.2
-Anatomy and Zoo Erasmus Medical Center, Rotterdam	2013	0.3

PhD training	Year	ECTS
National conferences		
- Seminar at the department of plastic surgery Oral presentation in Rotterdam	2011	0.1
- Seminar at the department of plastic Surgery Oral presentation in Rotterdam	2011	0.1
-21st Esser Course 'Wide Awake, A Live Surgery Event' Attendance in Rotterdam	2013	0.3
-Annual meeting of the Dutch Society for Hand Surgery (NVvH) Oral presentation in Leiden	2013	0.7
-Annual meeting of the Dutch Society for Plastic Surgery (NVPC) Oral presentation in Amsterdam	2014	0.7
-Annual meeting of the Dutch Society for Plastic Surgery (NVPC) Oral presentation in Tilburg	2014	0.7
-22nd Esser Course 'What's New in Breast Surgery' Attendance in Rotterdam	2014	0.3
-Annual meeting of the Dutch Society for Plastic Surgery (NVPC) Attendance in Maastricht	2015	0.4

PhD training	Year	ECTS
International conferences		
-15th European Conference of Scientists and Plastic Surgeons Oral presentation in Pamplona, Spain	2011	1.2
-Federation of European Societies for Surgery of the Hand (FESSH) Oral presentation in Antalya, Turkey	2013	1.2
-International Federation of Societies for Hand Surgery of the Hand Oral presentation in New Delhi, India	2013	2.4
-Federation of European Societies for Surgery of the Hand (FESSH) Poster presentation in Paris, France	2014	1.2
-Annual meeting of European Society for Peripheral Nerve Surgery Oral presentation in Vienna, Austria	2014	1.2
-Federation of European Societies for Surgery of the Hand (FESSH) Poster presentation in Milan, Italy	2015	1.2
Teaching and lecturing		
-Anatomy of the hand Course for medical students Erasmus Medical Center, Rotterdam	2013	0.5
-Microsurgery course Clinical application of microsurgery Practical hands-on microsurgery course on rodents Erasmus Medical Center, Rotterdam	2010-2014	1.4

PhD training	Year	ECTS
-Suture techniques Course for medical students Erasmus Medical Center, Rotterdam	2013	0.5
-Anatomy and pathology of the brain Neuro-anatomy class for medical students Erasmus Medical Center, Rotterdam	2012	0.2
-'Swollen joints' (pathology of the hand) Course for medical students Erasmus Medical Center, Rotterdam	2012	0.2
-Minor in hand surgery Course for medical students Erasmus Medical Center, Rotterdam	2012-2014	1.3
Supervising medical/master thesis		
-3D cell culture of the skin by Elise Brakkee, Master of Neuroscience, Erasmus Medical Center, Rotterdam	2012-2014	12
-Skin innervation in diabetic peripheral neuropathy by Gokce Goskun, Master student of Neuroscience Erasmus Medical Center, Rotterdam	2012-2014	24
-Skin rewarming rate using UV thermographic video Naim Avazverdi, Master student of Medicine Erasmus Medical Center, Rotterdam	2013	5
-Evans Blue technology Martijn Baas, Master student of Medicine Erasmus Medical Center, Rotterdam	2013	9

PhD training	Year	ECTS
Other		
-Organizing Annual Plastic Surgery Social Program Erasmus Medical Center, Rotterdam	2012-2014	2.5
-Organizing Annual Dutch Society for Hand Surgery (NVVH) Program Rijnstate Hospital, Arnhem	2013	0.4
-Organizing Esser Course 'Neuropathic Pain' Erasmus Medical Center, Rotterdam	2013	1.5
-Organizing Esser Course 'Carpometacarpal 1' Erasmus Medical Center, Rotterdam	2013	2.0
-Peer reviewer Acta Orthopaedica et Traumatologica Turcica	2013-currently	2
Grants		
-Co-applicant Nuts-Ohra Foundation (€196.000)	2012	1.5
-Koninkelijke Nederlandse Akademie van Wetenschappen (KNAW), van Walree (€1.000)	2013	0.1
-Trustfonds, 2014 (€1.500)	2014	0.1

List of publications

1. L. S. Duraku, M. Hossaini, S. Hoendervangers, L.L. Falke, **S. Kambiz**, V.C. Mudera, J.C. Holstege, E.T. Walbeehm, T.J.H. Ruigrok. Spatiotemporal dynamics of re-innervation and hyperinnervation patterns by uninjured CGRP fibers in the rat foot sole epidermis after nerve injury.
   Molecular pain 2012; 30;8:61

2. **S. Kambiz**, M. Baas, L.S. Duraku, A.L. Kerver, A.H.J. Koning, E.T. Walbeehm, T.J.H. Ruigrok. Innervation mapping of the hind paw of the rat using Evans Blue extravasation, Optical Surface Mapping and CASAM.
   Journal of Neuroscience Methods 2014; (229):15-27.

3. **S. Kambiz**, L.S. Duraku, J.C. Holstege, S.E.R. Hovius, T.J.H. Ruigrok, E.T. Walbeehm. Thermo-sensitive TRP channels in peripheral nerve injury: a review of their role in cold intolerance.
   Journal of Plastic, Reconstructive & Aesthetic Surgery 2014; 67(5):591-599.

4. **S. Kambiz**, L.S. Duraku, T.H.J. Nijhuis, S.G. Cosgun, S.E.R. Hovius, T.J.H. Ruigrok, E.T. Walbeehm. Long term follow up of peptidergic and non-peptidergic re-innervation of the epidermis following sciatic nerve reconstruction in rats.
   Journal of Neurosurgery 2015; 123(1):254-269.

5. **S. Kambiz**, E.M. Brakkee, L.S. Duraku, S.E.R. Hovius, T.J.H. Ruigrok, E.T. Walbeehm. Mirror-image pain after nerve reconstruction in rats is related to enhanced density of epidermal peptidergic nerve fibers.
   Experimenral Neurology 2015; 267:87-94.

6. **S. Kambiz**, J.W. van Neck, S.G. Cosgun, M.H.N. van Velzen, J.A.M.J.L. Janssen, N. Avazverdi, T.J.H. Ruigrok, E.T. Walbeehm.
   An early diagnostic tool for diabetic peripheral neuropathy in rats.
   PLoS One 2015; 10 (5).

7. **S. Kambiz**, S. G. Cosgun, J.W. van Neck, S.E.R. Hovius, J.C Holstege, E.T. Walbeehm. Acetyl-L-Carnitine prevents mechanical hyposensitivity and loss of epidermal non-peptidergic nerve fibers in Streptozotocin-induced diabetic rats.
   Submitted for publication.

8. E.M. Brakkee, E. van den Bogaard, T.J.H. Ruigrok, J.W. van Neck, **S. Kambiz**, J.B. Phillips, J. Schalkwijk, E.T. Walbeehm. An innovative 3D-model: in-vitro skin innervation.
   To be submitted.

Acknowledgements/Dankwoord

Vier jaar geleden heb ik ervoor gekozen om het pad van een promotietraject te bewandelen. De hindernissen in dit parcour heb ik als uitdaging beleefd en de behaalde doelen als succes. Eenmaal aangekomen bij het laatste hoofdstuk van dit proefschrift, kan ik met blijdschap vertellen dat het zien van de finishlijn aanvoelt als een overwinning. Deze mijlpaal had ik niet kunnen behalen zonder de hulp, inspiratie en motivatie van personen die ik via deze weg wil bedanken.

Mijn promotor, **prof. dr. S.E.R. Hovius**. Geachte professor Hovius, ik ben u zeer erkentelijk voor het vertrouwen dat u in mij heeft gehad tijdens mijn promotieonderzoek en voor de gelegenheid die u mij heeft geboden om veelzijdige ervaring op te doen binnen de afdeling Plastische Chirurgie. Door uw integere wijze van begeleiden wist u mij telkens weer te motiveren en intellectueel uit te dagen. U wist altijd de rode draad van het stuk op te pakken als ik het overzicht dreigde kwijt te raken. Ook buiten de muren van het Erasmus MC heeft u mij veel bijgeleerd. Ik kijk met veel plezier terug op onze deelname aan diverse (inter) nationale congressen waarbij u mijn presentaties aanzienlijk wist te verbeteren met uw waardevolle commentaar.

Mijn copromotoren, **dr. E.T. Walbeehm en dr. T.J.H. Ruigrok**, wil ik hartelijk danken voor alle tijd en energie die zij in mijn proefschrift hebben gestoken. Jullie hebben aan de basis gestaan van mijn wetenschappelijke carrière.
Beste Erik, ik voelde mij niet alleen je promovenda maar ik maakte ook deel uit van de 'periferezenuwfamilie'. Dank voor je gastvrijheid en de mogelijkheid die je mij geboden hebt om met andere onderzoekers bij je over de vloer te komen om onder het genot van een kop koffie of thee van gedachten te wisselen over onze nieuwe ideeën. Bij ieder nieuw plan bleef je mij kritische vragen stellen, waarbij je mij hebt geleerd om geen genoegen te nemen met andermans hypotheses. Jouw ongekende enthousiasme voor wetenschappelijk onderzoek heeft mij gemotiveerd om mijn masteronderzoek voort te zetten in een promotieonderzoek. Ondanks je verhuizing naar Nijmegen ben je de afgelopen jaren altijd betrokken gebleven bij mijn onderzoek. Ik ben je hier enorm dankbaar voor.
Beste Tom, ik ben de tel kwijt hoe vaak ik bij je heb aangeklopt met de vraag 'heb je even tijd?' Ondanks alle drukte gaf je mij altijd de gelegenheid om mijn verhaal te doen. De ene keer was ik blij dat mijn kleuring gelukt was, de andere keer kwam ik vertellen dat ik baalde van een niet-significant resultaat. Tot mijn grote verbazing wist je telkens weer een wijze raad te geven en liep ik met een glimlach en vol goede moed jouw kamer uit. Ik waardeer jouw bereidwilligheid om samen te werken met de afdeling Plastische Chirurgie en jouw enorme belangstelling voor het huidonderzoek dat buiten je eigen vakgebied ligt. Tegenwoordig heb je je ook deze discipline eigen gemaakt. Dank voor je betrokkenheid, inzet en kritische blik. Jouw constructieve opmerkingen en feedback hebben mijn stukken aanzienlijk verbeterd.

De leden van de promotiecommissie, **prof. dr. P.A. van Doorn**, **prof. dr. F.J.P.M. Huygen**, **prof. dr. A. Dahan** en **prof. dr. G.J. Kleinrensink**, wil ik bedanken voor het beoordelen van mijn proefschrift en voor de bereidheid zitting te nemen in mijn promotiecommissie.
Prof. dr. A.M. Hart, I appreciate your willingness to review my thesis and for being a member of the doctorate committee. Thank you very much for travelling from Glasgow (UK) to Rotterdam for my public defense.

Dr. J.C. Holstege. Beste Joan, we hebben samen mijn eerste artikel geschreven over TRP-kanalen waarbij ik veel van je heb geleerd. Bedankt dat ik altijd met mijn vragen bij je terecht kon en voor de prettige samenwerking.
Dr. J.A.M.J.L. Janssen. Beste dr. Janssen, bedankt voor de leerzame en inspirerende samenwerking gedurende het schrijven van het hoofdstuk over diabetische neuropathie. Daar waar ik te langdradig werd, vatte u het perfect samen en bleef u één woord herhalen dat mij altijd bij zal blijven: staccato.
Alle overige coauteurs en afdelingen (Neurowetenschappen, Bio-informatica, Anesthesiologie en Anatomie) die betrokken zijn geweest bij het onderzoek wil ik bedanken voor hun waardevolle feedback en de prettige samenwerking.
Dr. L.S. Duraku. Beste Liron, door jou werd ik aangespoord om het huidonderzoek voort te zetten. Als medeoprichter van deze onderzoekslijn heb je een waardevolle bijdrage geleverd aan mijn artikelen. Je hebt mij altijd geïnspireerd en gemotiveerd met je enorme toewijding aan wetenschappelijk onderzoek. Bedankt dat je in mij hebt geloofd en dat je op deze bijzondere dag mijn paranimf wilt zijn. Terwijl ik dit schrijf hoor ik je vol overtuiging roepen: "Shoista, jij kunt dit!"
Dr. T.H.J. Nijhuis, Beste Tim, bedankt voor de prettige samenwerking en je hulp tijdens de EMG metingen.
Dr. L.N.M. van Adrichem. Beste dr. Van Adrichem, bedankt dat ik u altijd laagdrempelig heb mogen benaderen en dat ik volgend jaar als anios op de afdeling Plastische Chirurgie mag starten. Ik hoop in deze periode en in de toekomst veel van u te mogen leren.
J.M. Hekking. Beste Ineke, je betrokkenheid en inzet gedurende mijn onderzoek was werkelijk uniek. Ik zal niet snel vergeten hoe hard wij geworsteld hebben om de Evans Blue-extravasatie aan het werk te krijgen. Ik heb je nog nooit zo blij gezien met een blauw verkleurd rattenpootje. Dank dat je altijd voor mij klaarstond en mij wist te inspireren met je talloze talenten. Ik heb onze lange gesprekken, waarin je mij zonder oordeel en etiket advies wist te geven, zeer gewaardeerd.
E.M.G. Fijneman. Beste Esther, ook jij hebt mij altijd bijgestaan, voornamelijk als de dieren mij in de steek dreigden te laten. Jouw oplossing om de dieren warmer te krijgen met een constructie van warmtelampen was geweldig bedacht. Ook wist je ze allemaal aardig diabeet te krijgen. Dankjewel voor de prettige samenwerking, je hulp en vertrouwen.
Dr. J.W. van Neck. Beste Han, bedankt voor je kritische blik en het spelen van de 'advocaat van de duivel', waarmee je mij bleef aansporen om alert te blijven en alles tot in de details na te kijken.

Carin Oostdijk. Beste Carin, je bent als secretaresse van professor Hovius het gezicht van de afdeling. Een gezicht dat altijd lacht. Bedankt voor je hulp en inspanning tijdens de laatste loodjes van mijn promotie.
Ik wil de collega-promovendi van de toren, **Caroline, Michelle, Bianca, Robert, Evelien, Bart, Willem, Martijn, Kim** en **Chao,** bedanken voor de leuke gesprekken, adviezen, geweldige skireis, borrels en onze ongekende lol tijdens de congressen. Ik wens jullie veel succes met het afronden van jullie promotieonderzoek en kijk uit naar jullie proefschriften.
Beste kamergenootjes, **Bas** en **Linda**, bedankt voor jullie gezelschap en de leuke tijd op kamer Ee1593. Bas, dank voor alle praktische hulp rondom het werk op het lab en in het bijzonder bij de bediening en dataverwerking van het mysterieuze O2C-apparaat.

Graag wil ik de medische staf van de afdeling Plastische Chirurgie bedanken voor de leerzame patiëntendemonstraties en journalclubs op de donderdagmiddagen. Jullie klinische blik en input tijdens mijn presentaties op de refereeravonden hielpen mij om de resultaten van mijn dierexperimenteel onderzoek te kunnen extrapoleren naar de kliniek. Tevens wil ik jullie bedanken voor de memorabele momenten tijdens het maken van de stranddagfilmpjes en natuurlijk op de stranddag zelf.

Beste **Elize** en **Erika**, zelfs in de late uren waren jullie bereid om mij uit de brand te helpen tijdens mijn immunohistologische kleuringen op het lab. Bedankt voor jullie suggesties en hulp.
Dear **Malik**, merci beaucoup for your help and company during my histology adventures at the lab.
Martijn, Elise, Gokce en **Naim**, ik heb jullie met veel plezier mogen begeleiden tijdens jullie keuze- of masteronderzoek. Dank voor jullie buitengewone inzet en veel succes met jullie verdere loopbaan.

Mijn lieve vriendinnetjes, **Wieying**, **Genesis**, **Tanaz**, **Dianta**, **Florance**, **Linda** en **Hanna,** bedankt voor de ontspanning, afleiding en het plezier in verschillende vormen en maten. Maar in het bijzonder wil ik jullie stuk voor stuk bedanken voor jullie steun in de afgelopen jaren. Dear **Olesya**, you are one of my few friends who know the exact content of this thesis. Thank you very much for your revisions, and therefore tremendous contribution to my thesis.

Mijn lieve schoonfamilie, vanaf dag één hebben jullie mij met open armen verwelkomd binnen jullie gezin. Ik prijs mij gelukkig met jullie liefde, steun en de vanzelfsprekenheid waarmee jullie mij altijd bijstaan met alle belangrijke en minder belangrijke momenten in mijn leven. Jullie waardering en interesse voor de ontwikkelingen rondom mijn proefschrift waren van onschatbare waarde. Bedankt dat jullie mij tijdens de verdediging van mijn proefschrift bij willen staan *vanaf de eerste rij*. Ik hou van jullie.

My dear family in Afghanistan, Tajikistan, the United States, the United Kingdom and the Netherlands, thank you for your support and unconditional love. Although we live oceans apart, our love would make oceans flood. My dearest uncle **Dastagir Kambiz**, thank you for your encouragement every step of the way during my career. I love you and miss you all.

Mijn lieve zusje en broertje, **Niloufar** en **Nabi**, ik heb goed nieuws: ik ben weer aanspreekbaar als ik achter mijn laptop(**s**) zit. Mijn proefschrift is definitief klaar mede dankzij jullie ongekende steun. Lieve Nilo, mijn fashion icon, bedankt voor je zorgzaamheid en dat je altijd voor me klaar staat. Lieve Naab, bedankt voor al je technische hulp aan een niet zo technisch georiënteerde zus. Ik hou ontzettend veel van jullie en wil jullie bedanken voor jullie geduld en vertrouwen. Ik wens jullie veel succes met jullie opleiding. Mijn zus en vriendin voor het leven, **Fara**, ik kan jou niet genoeg bedanken voor je medeleven bij elke nieuwe stap in mijn leven. Hoe onbegrijpelijk mijn onderzoek ook was, je bleef me altijd vragen stellen en interesse tonen. Ik wens jou veel geluk en liefde met je lieve gezin. **Zabi** jaan, bedankt dat je de rol van oudere broer op je hebt genomen en me altijd hebt bijgestaan. Mijn lieve nichtje en neefje, **Medina** en **Zaid**, jullie zijn mijn kleine hartendiefjes en jullie overweldigen mij altijd met jullie positieve energie. Ik hou van jullie.

Lieve **papa** en **mama**, jullie hebben me altijd het gevoel gegeven dat ik alles aankan en dat ik al mijn dromen vol passie en liefde moet najagen. Dankzij jullie rotsvaste vertrouwen ben ik zo ver gekomen. Lieve mama, ik heb enorm veel bewondering voor je onuitputtelijke energie. Je staat voor al je kinderen dag en nacht klaar. Naast een zorgzame moeder ben je ook mijn vriendin met wie ik tot in de late uurtjes kan kletsen. Bedankt, mam, voor je vertrouwen en je steun: "Aga tura nagiran kira bigiran?" Lieve papa, bedankt dat wij voor jou altijd op de eerste plaats komen. Jij bent een wereldvader die niet alleen heerlijk kan koken, maar ook bij iedere stap in ons leven met ons meeleeft. Met je technische trucjes krijg je het altijd voor elkaar om het thuis zo comfortabel mogelijk te maken. Pap en mam, bedankt voor jullie onvoorwaardelijke liefde en begrip in tijden waarin ik er door de drukte niet altijd was. Bedankt dat jullie ons altijd een warme thuisbasis hebben gegeven. Jullie zijn mijn alles en ik hou zielsveel van jullie. Mede dankzij jullie steun ben ik zo ver gekomen en daarom draag ik dit proefschrift aan jullie op.

De rest van jullie leven hand in hand als één.

Tenslotte een speciaal woord van dank aan mijn allerliefste, **Meelad**. Jij weet mij altijd op te vrolijken met je geweldige gevoel voor humor en positieve levensinstelling. Je hebt mij gesteund en hebt, waar je mogelijkheden zag, een praktische bijdrage geleverd. Ze zeggen dat de laatste loodjes het zwaarst wegen, maar dankzij jouw hulp en vertrouwen heb ik vooral kunnen genieten van de laatste fase van mijn promotietraject. Dank dat je altijd achter me hebt gestaan en ik vind het bijzonder dat je als paranimf nu letterlijk achter me wilt staan. Ik hou ontzettend veel van je en kijk uit naar de rest van ons leven samen.

Shoista

About the author

Shoista Kambiz was born in Kabul, Afghanistan on December 19th, 1988. At the age of eight, she moved to the Netherlands, together with her parents, sisters, and brother. After graduating from secondary school (Willem van Oranje College) in Waalwijk, she started medical school in 2007 at the Erasmus University in Rotterdam.

During her second year of medical school, Shoista served as the supervisor of the student assistant team of the department of Cardiology of the Erasmus Medical Center. In her 4th year of medical training, she was selected to participate in the extracurricular research master's program in Neuroscience at Erasmus Medical Center. While pursuing this program, she developed a strong interest in fundamental research and started a project in collaboration with the department of Plastic and Reconstructive Surgery and Neuroscience. She received her MSc degree in Neuroscience in 2012 and was offered the opportunity to continue her research in a PhD program (Promotor: Prof. S.E.R. Hovius, Copromotors: Dr. E.T. Walbeehm, and Dr. T.J.H. Ruigrok).

Shoista received a grant from the NutsOhra foundation in 2012 to conduct research in the field of epidermal innervation. She has published her work in several peer-reviewed international journals and has presented her findings at several national and international conferences. While pursuing her doctorate degree, Shoista was also involved in overseeing medical and graduate students' research projects and participated in microsurgery courses to enhance her surgical skills.

Since August 2014, Shoista has been conducting her clinical clerkships. She successfully enrolled an elective clerkship at the department of Plastic and Reconstructive Surgery of the John Radcliffe Hospital (Oxford, UK) for the period of November 30 to December 24, 2015. After graduating medical school in August 2016, she will start as a resident (ANIOS) at the Department of Plastic and Reconstructive Surgery (Erasmus Medical Center, Rotterdam, The Netherlands). Shoista has a strong desire to become a plastic surgeon and also continue her academic interests by performing research in the field of hand and peripheral nerve injuries.